Light Limits on Dark Matter

by

Jonathan Christopher McDowell

Churchill College, Cambridge
and
Institute of Astronomy, Cambridge

March 1986

A dissertation submitted to the University of Cambridge
for the degree of Doctor of Philosophy

Declaration

I declare that this dissertation is my own work and includes nothing which is the outcome of work done in collaboration. Chapter 4 is a revised version of work published in a paper by B.J. Carr, the author, and H. Sato (Nature, vol. 306, p. 666, 1983). Parts of Chapters 7 and 8 have been published in Monthly Notices of the Royal Astronomical Society (J. McDowell, MNRAS, vol 217, p 77, 1985). Parts of Chapters 2, 3, and 5 have been submitted as a paper to MNRAS.

I declare that this thesis is not substantially the same as any that I have submitted for a degree or diploma or other qualification at any other University. No part of this thesis has been or is being submitted for any such qualification.

Acknowledgements

Working at the Institute over the past few years has been an enjoyable and stimulating experience, and it would be impossible to give individual thanks to all those who have made these years so memorable. Bernard Carr, my supervisor, has never failed to inspire with wide ranging insights, and has been careful to gently prod me when my enthusiasm has flagged. Martin Rees has always been ready to answer questions and guide me to see my errors, and stood in as supervisor during Bernard's absence. I thank H.Sato for his help with Chapter 4, and the CUAS coffee morning for helping me with eq. 7.5.2. Rick Shafer taught me theoretical flaming and cookery, and I also thank him for many enjoyable discussions on astrophysics. Alison Campbell lent me her expertise on massive stars, Janet Drew her knowledge of nebular processes, and I also acknowledge useful discussions with Donald Lynden-Bell, Gerry Gilmore, Bob Carswell, Rachel Webster, Peter Thomas, Claire Craig, Dick Bond, John Negroponte, Bozena Czerny, and my first-year office-mates Sue Stepney, Elena Terlevich, Mary Sakellariadou, and Sanjiv Kumar who all made the way easier for me. Paul Hewett has often been prevailed upon to give advice on astrophysics and computing ever since my days as a vac student at ROE, and I'm sure he'll be glad to finally see the back of me. Keith Taylor and Dave Axon introduced me to astronomical research when I was a summer student at RGO, and Dave metaphorically held my hand on my first observing trip five years later. The SERC, Cambridge Philosophical Society, my parents, Churchill College, and other sources all provided financial support. John Webb saved me from homelessness at the last minute. Andrea Prestwich has been a constant source of support and encouragement throughout the past four years. Finally, thanks particularly to Andrea and to Sue Edmundson for their support and friendship during various stages of the final traumatic eight months of the preparation of this thesis.

Thanks to you all.

Jonathan McDowell

Contents

1 Introduction

1.1 The Dark Matter Problem

For over 50 years one of the outstanding problems in astrophysics has been the dark matter problem (formerly known as the missing mass problem). It appears that most of the mass in the universe is in a form which is so far undetected except through its gravitational influence. The first hint of this astonishing discovery came in 1933, when Zwicky (1933) studied the dynamics of the Coma cluster of galaxies and found that the apparently visible mass failed to provide the gravitational potential needed to explain the velocity dispersion of the galaxies in the cluster by a large factor. This 'virial discrepancy' has since been reduced but is still significant (Kent and Gunn 1982). Meanwhile, similar discrepancies between the visible (and inferred) mass and the dynamics have cropped up on every scale from the solar neighbourhood to the Hubble flow (Faber and Gallagher 1979).

In retrospect the existence of dark matter should not be so surprising. All the forms of matter astronomers are familiar with are luminous at least to some extent, because it is by their light that astronomical objects are detected. It is true that interstellar dust was first detected in absorption in the visible rather than by its infrared emission, but by and large astronomers have studied luminous matter simply because of the observational selection effect to end all such effects: observability, at whatever flux level in whichever waveband. We now realize that nature has no need to produce only luminous matter, and indeed there is no *a priori* reason why there should not be as many different kinds of dark matter as there are luminous matter. For this reason I do not feel that the 'Occam's razor' argument in favour of trying to explain all dark matter problems by a single 'dark matter candidate' holds much weight.

We can now identify 4 different dark matter problems: The local or 'Oort limit' matter; the dark matter in galactic halos; the dark matter on scales of

clusters, which seems to make up one tenth of the closure density; and the aesthetic dark matter, required to make the universe exactly flat, for which there is little observational evidence as yet.

What observational evidence there is for dark matter is all of the same basic form. In principle dark matter (mass-energy not emitting electromagnetic radiation) might interact with the universe in a number of ways that we might detect, for instance by the emission of neutrinos, or it may be completely inert. All matter must, however, be detectable by its gravitation. Gravitation causes test particles to fall towards matter of mass M which is a distance R away at a speed V which depends on the initial conditions but in general is of an order given by

$$M = V^2 R/G \tag{1.1.1}$$

where G is the Newtonian gravitational constant. The equation is exact for a test particle in circular orbit around a central Newtonian mass, but all other methods of measuring mass basically boil down to (1.1.1) with appropriate generalizations of V and R. For a cluster of stars or galaxies the individual gravitating objects are also the test particles, and the virial theorem is used with the adoption of appropriately weighted mean cluster radius and velocity dispersion (Heisler, Tremaine and Bahcall 1985). For the disk of a galaxy the mass interior to radius R may be measured by the velocity of gas orbiting at that radius; the gas atoms are treated as test particles. If the potential is not spherical, the formula is only true exactly in the large R limit, and the exact formula for a finite disk has been derived by Lynden-Bell and Pineault (1978).

The evidence for the local dark matter problem comes from estimates of the acceleration of stars in the direction perpendicular to the galactic disk. This is referred to as 'Oort's limit' on the local dark matter, after the paper (Oort 1960) in which he claimed evidence of a large mass density by analysing the 'K_z' (vertical force) law for a sample of stars. The 'K_z' formalism gives an estimator of R in

(1.1.1) as

$$R = -\frac{1}{4\pi V^2}\frac{\partial}{\partial z}\frac{1}{n}\frac{\partial}{\partial z}(nV^2) \qquad (1.1.2)$$

where V in this case is the vertical velocity dispersion and n is the number density of the stellar population being used as a mass tracer. Early attempts to measure the galaxy's local gravitational field in this way ran into many problems, and if some of the data were interpreted by simple models a negative mass density could be derived for part of the disk! (See Radford's (1976) discussion of his analysis of Upgren's data using Oort's method, and alternative methods which give a physically reasonable answer.) However when care is taken to select uniform samples of test stars, and to treat the stellar hydrodynamics in a self-consistent manner, it appears that the measured value of the local mass density (Bahcall 1984) is twice that estimated from adding up the locally observed stars and gas. The mass density is about $0.1 M_{\odot} \mathrm{pc}^{-3}$. For some time it was thought that very faint main sequence stars might make up the difference, but the work of Reid and Gilmore (1982,1984) constraining the low mass end of the main sequence excludes this possibility (but see Hawkins (1986)). It remains possible that there is a further peak in the stellar initial mass function at low initial masses, but despite the discovery of the brown dwarf candidate VB8B (McCarthy et al 1985) searches for such 'Brown dwarfs' have yielded little evidence for such objects (Probst 1983, Tyson et al 1985, Gilmore and Hewett 1983). Hegyi and Olive (1983) show that low mass stars cannot make up the local dark matter if their IMF is a simple power law extending up to normal masses. Hegyi (1981) and Boughn, Saulson and Seldner (1981) set limits on the number of low mass stars in the halo of NGC 4565 by photometric observations in the near infrared. Low mass stars and 'Jupiters' cannot be excluded if their initial mass function is independent of the IMF of luminous stars. In some galaxies dark matter may be produced by formation of low mass stars in cooling flows (Fabian, Arnaud and Thomas 1985). Larson (1985) proposes a bimodal star formation model in which there would be

an extra peak in the IMF above 1 $M_{\odot}$at early times, leading to the production of burnt-out white dwarfs which could explain the local dark matter.

The best evidence for dark matter on galactic scales comes mainly from measurements of the neutral hydrogen rotation curves of spiral galaxies (Freeman 1970, Bosma 1978, Rubin et al 1980, Burstein et al 1982). The rotation velocity of the gas in spirals appears to remain constant out to radii well beyond the optical extent of the galaxy, whereas, if the mass traced the light, the velocity should drop off slowly with radius. Recently attempts have been made to analyse the rotation curves to determine the distribution of matter in the disk, bulge, and dark halo components of the galaxy (Carnigan and Freeman 1985). The results indicate that most such galaxies do indeed have dark halos, although their importance relative to the luminous component may vary considerably. These decompositions give some freedom to vary the relative importance of disk and dark halo to explain a given curve but many galaxies require at least some halo component. Polar ring galaxies (Katz and Richstone 1984, Sparke 1985) allow the potential to be probed well out of the plane and show that the potential is more spherical than flat.

Clearly this dark matter is distributed in a different manner from the luminous stellar populations; its origin is therefore presumably different from that of these populations. The evidence for a dark halo of our own galaxy is weaker and rests largely on the velocities of distant globular clusters (Hartwick and Sargent 1978, Frenk and White 1982) and dwarf galaxy satellites; the observational uncertainties are sometimes quite large (Lynden-Bell *et al.* 1983) although they are being reduced by ongoing projects (Peterson 1985, McDowell and Godwin 1986). Similarly, the evidence for dark matter in elliptical and dwarf galaxies is still tentative (Lin and Faber 1983), but growing. Aaronson and Olszewski (1985) report new measurements of Draco and Ursa Minor, indicating that dark matter does exist in these dwarf galaxies, which provides a severe constraint on some dark matter models.

The original dark matter problem, that of clusters of galaxies, remains beset with uncertainties. Problems of the definition of cluster membership and uncertainty as to whether the clusters have reached virial equilibrium or still show the effects of earlier substructure in their dynamics mean that estimates of cluster gravitational masses are often controversial (Valtonen et al 1985). Re-estimates of the masses of individual galaxies and the discovery in some clusters of large amounts of hot X-ray-emitting gas have reduced the discrepancies, but in many cases they remain substantial (Rood 1981, Kent and Gunn 1982.) The discovery of the X-ray gas allows an improved probe of the potential (Fabricant and Gorenstein 1983). Cooling flows onto central cluster galaxies indicate that dark matter may still be being formed in these objects as mass drops out of the flow and remains invisible. Low mass stars might explain this form of dark matter (Fabian et al 1982).

In recent years estimates of the mass density of the universe on very large scales, in terms of the density parameter Ω_0 (the ratio of the density of the universe to the critical density for recollapse), have been made by analysing redshift surveys to detect deviations from the uniform Hubble flow, both by studying infall toward Virgo within the local supercluster, and Hubble flow deviations on larger scales. Most of these analyses give $\Omega_0 = 0.1 - 0.3$ (Peebles 1984). The only evidence for larger values of Ω_0 come from analysis of IRAS galaxy distributions (Yahil, Walker and Rowan-Robinson 1985) which now give an estimate of $\Omega_0 = 1.0$.

Another candidate for the dark matter clustered on scales larger than galaxies is hot X-ray emitting gas, which could in principle be responsible for the X-ray background. Guilbert and Fabian (1985) show that such a fit requires $\Omega_{gas} > 0.2$.

The most popular candidates for the dark matter on scales larger than galaxy haloes are various varieties of non-baryonic particle, particularly weakly interacting massive particles. None of the currently proposed candidates has yet been shown to exist even in a laboratory context, much less in the cosmological con-

text. Much of their appeal comes from their ability to provide the aesthetic dark matter, for which baryonic matter seems ruled out by the constraints on light element nucleosynthesis in the Big Bang. To put these constraints in context I now summarize the contribution to the cosmological density parameter inferred for each of the dark matter problems. The visible material and the local dark matter each contribute Ω=0.01. The halo dark matter has $\Omega = 0.1$, and most estimates of the matter in clusters range from $\Omega = 0.1$ to 0.3. The closure density is $\Omega = 1$. The hot big bang nucleosynthesis calculations (Yang et al 1984) suggest that the contribution from baryons to the mean mass density of the universe is $\Omega_b = 0.12 h_{50}^{-2}$, where h_{50} is the Hubble parameter in units of 50 km/s/Mpc. If we believe h_{50} is unity, then we must associate the mass in halos and possibly clusters with dark baryons. In this case there may not be any nonbaryonic matter, except if the universe does have $\Omega = 1$, when such particles must be involved. If $h_{50} = 2$, however, then only the local dark matter is baryonic, and the matter in halos and on larger scales must be nonbaryonic if the nucleosynthesis limits apply (Rees (1984) discusses some ways to avoid the nucleosynthesis limits).

The inflationary cosmological scenario (Guth 1981, Linde 1982) which has motivated much recent work on the very early universe predicts that $\Omega_0 = 1$ to a high degree of accuracy. This has reinforced the view long held by many cosmologists on more metaphysical grounds that this is the natural value for Ω_0 to have. Recent theoretical work in particle physics (grand unification, supergravity) has also predicted the existence of many new elementary particles. If any of these are found to exist, they will contribute to the energy density of the universe. Among the candidates that have been discussed are massive neutrinos, photinos, axions, higgsinos, gravitinos, etc. Fortunately, considering the rapidity with which new candidates are suggested, Bond and Szalay (1983) pointed out that the relevant property of any of these candidates is the epoch at which they become non-relativistic, which determines the mass scale which collapses first. Particles

are divided into 'hot' and 'cold' according to whether their temperature is high enough to smear out small scale fluctuations in the early universe or not. For fast, 'hot' particles such as massive neutrinos, the effective free streaming mass is large and clusters can form easily, but the neutrinos cannot cool enough to settle in the halos of individual galaxies. For 'cold' particles smaller fluctuations form first (Davis et al 1985).

Limits can be set on particles which decay into photons (Silk and Stebbins 1983, Bond,Carr, and Hogan (1986), Steckel 1986) by comparing the expected flux of redshifted photons with observed background light limits in the same way as I do for pregalactic starlight in Chapters 3 and 5 of this thesis; however, I do not consider these decaying-particle 'light limits on dark matter', as I restrict my investigation to astrophysical (as opposed to particle-physics) candidates for the dark matter.

The simplest remaining candidate for the local or halo dark matter is the remnants of previously luminous stars. However, if the stars were of ordinary mass, they would have produced too high a metallicity in the succeding generations of stars to be consistent with the known chemical history of the galaxy if current models of stellar and galactic evolution are correct. Stars of sufficiently high mass might leave most of their nucleosynthesis products in their remnants and thus escape the nucleosynthetic constraint. Such stars could also explain the missing mass discrepancy on all scales except where they would be inconsistent with the Big Bang limit on baryon density. The remnants of these stars would be massive black holes.

1.2 The Population III Hypothesis

The galaxy contains two main populations of stars - the modern Population I, with a metallicity (metal fraction by mass) of 10^{-2}, of which our Sun is an example, and Population II, an older generation of stars with metallicity a hundred times lower, forming the bulge and halo of our galaxy. In fact there is a continuum of ages from the youngest extreme Population I stars to the oldest and most metal-poor Population II stars, but no star is known with a metallicity less than about $Z = 10^{-5}$ (Bond 1981). If the standard hot big bang model of the universe is correct, the first stars to form would have had no CNO metals at all, so there must have been precursors to the Population II stars. This hypothetical first generation of stars has been given the name Population III . There have been many theoretical studies which have investigated star formation in a metal-free environment; the main feature is that the collapsing cloud cannot cool as efficiently, due to the absence of metal line cooling. The main cooling effect is that of molecular hydrogen. It has been pointed out (Tohline 1980, Silk 1983) that the low cooling and the possible absence of substructure in the Population III clouds will make it easier for stars of high mass to form. If the Population III initial mass function were biased to higher than normal masses, then the zero-metal stars could have been very numerous in the past despite their complete absence today, since they would by now all have completed their evolution. The formation of stars at high redshift is likely if the spectrum of the density fluctuations in the early universe that gave rise to galaxies continued to smaller scales. Bound regions of a few million solar masses would then form naturally (Peebles 1974, Fall 1979). Carr and Rees (1984a) discuss why the first pregalactic objects might have masses in the range $10^2 - 10^6 M_\odot$.

In order to explain the early nucleosynthetic history of the galaxy, Schwarzchild and Spitzer (1953) suggested that the earliest stars were more massive than typical stars at the present time. Schmidt (1963) developed this idea in a detailed model

for the galactic star formation history. Truran and Cameron (1971) suggested that these Population III stars could also provide the dark matter. This requires large numbers of very massive stars which just provide dark remnants in addition to the massive stars which provide the initial enrichment.

Pregalactic stars have also been invoked to produce the microwave background (Layzer and Hively 1972, Rees 1978) or to produce distortions in it (Puget and Heyvaerts 1980, Rowan-Robinson, Negroponte, and Silk 1979, Negroponte, Rowan-Robinson and Silk 1981), or explain the dark haloes of galaxies (White and Rees 1978). Galaxy formation triggered by Population III stars has been discussed by Ostriker and Cowie (1981), Ikeuchi (1981), and Carr and Rees (1984a).

The properties of an early generation of metal-free very massive stars have been studied by Ezer and Cameron (1971), Ober, El Eid and Fricke (1982), and Bond, Arnett and Carr (1984, hereafter BAC). I will use the BAC models of Population III VMO (Very Massive Object) structure as the starting point of my calculations, and expand upon the studies of the consequences of Population III stars in the universe in Carr, Bond and Arnett (1984,CBA). The background radiation from pregalactic and protogalactic stars has previously been considered by Peebles and Partridge (1967), Thorstensen and Partridge (1975), Eichler and Solinger (1976), Hartquist and Cameron (1977) and CBA.

The fate of a massive star depends on both its composition and its angular momentum. A non-rotating metal-free star will collapse if its oxygen core is more massive than $100M_{\odot}$(BAC) but suffiecient rotation can stabilize it against collapse, resulting in explosions for stars as massive as $10^4 M_{\odot}$(Glatzel et al 1986). Non-rotating supermassive stars with mass of order $10^6 M_{\odot}$collapse if they have Population III metallicities, but Population II stars of the same mass explode (Fuller et al 1986).

Population III massive stars solve the orginal problem for which they were created, producing an initial galactic nucleosynthetic enrichment, so well as to be

positively embarrassing. Tarbet and Rowan-Robinson (1982) study the constraints on production of heavy elements by Population III stars assuming a power-law initial mass function. Carr and Glatzel (1985) show that $\Omega_* < 10^{-4}$ for exploding VMOs from the constraint that the minimum Population I abundance is $Z=10^{-3}$. Collapsing VMOs will return some of their mass to space via mass loss prior to collapse. If the mass loss rate is low, slower than the rate at which the outer layers of the star are enriched, then the stars will produce far too much helium to be consistent with both the present abundance and the hot big bang nucleosythesis calculations. This problem can be turned to advantage, as it turns out that in the context of a cold (low entropy per baryon) universe (Carr 1977) the Population III stars can produce all the helium (Talbot and Arnett 1971, Bond et al 1983) and the appropriate amounts of light elements (Ramadurai and Rees, 1985). In this model the radiation produced by the stars would be the microwave background itself and so the limits presented in Chapter 5 of this thesis would not apply, although the limits on nearby remnants (Chapter 7) would.

1.3 Black Holes in Astrophysics

The Newtonian black hole was first discussed by Michell (1784) and Laplace (1795, 1799). The general theory of relativity (Einstein 1916) also predicts the existence of black holes; a non-rotating black hole is one of the simplest solutions to Einstein's equations, the geometry due to a point mass at the origin in a spherically symmetric empty spacetime (Schwarzchild 1916). More realistic rotating solutions were found by Kerr (1963). However the idea that such objects might actually occur in nature was initially met with fierce resistance. When Chandrasekhar (1931) discovered the maximum stable mass for a star supported by electron degeneracy pressure against its own weight, the possibility of catastrophic stellar collapse had to be addressed seriously (Oppenheimer and Snyder, 1939). But it was not until the reawakening of interest in GR in the 1960's that the black hole was studied in the astrophysical context (Wheeler 1968).

How might black holes arise in nature? The most obvious way is through the collapse of a massive star. Most massive stars are believed to leave neutron star remnants after losing much of their mass in a supernova explosion. If the mass left in the collapsing core is too large, however, neutron degeneracy pressure will not be sufficient to halt the collapse and the core will continue collapsing until after it is within its event horizon - a black hole will have formed. While it is true that the heaviest stars lose large amounts of their mass during their evolution, it seems unlikely that all stars will lose enough mass to avoid leaving a remnant massive enough to become a black hole. It was thought that the minimum initial mass above which all stars would leave black hole remnants might be as low as 10 solar masses, but many recent authors suggest that a much higher mass is likely (see chapter 8). While such black holes will exist, the rarity of such massive stars today means that they will be very rare unless the star formation initial mass function was very different in the past.

In 1970 the American X-ray astronomy satellite Uhuru was launched and

made the first extended studies of celestial X-ray sources. This mission revealed the existence of energetic sources of radiation variable on short timescales, leading to the realization that many of the X-ray sources were compact objects. Most are now believed to be neutron stars, but some are candidate black holes. The first and most famous black hole candidate was Cygnus X-1, a strong X-ray source orbiting the star HDE 228668. Other black hole candidates are Cir X-1 (Toor 1977) and LMC X-3 (Forman et al 1976).

More massive black holes may arise more easily, if enough mass can be collected together in a small space. This would be possible either through the coalescence of smaller objects, for instance by the dynamical evolution of massive star clusters, or simply by primordial collapse; 'protostars' of mass above $10^6 M_\odot$ will collapse directly to a black hole via the GR stellar instability without ever igniting their central fuel (Fowler 1966).

The standard model of active galactic nuclei claims that such massive (10^6 to 10^8 $M_\odot$) black holes are indeed present in the nuclei of galaxies. The 'evidence' that the central engines of AGN are massive black holes is basically indirect. There seems to be no plausible way of generating such large luminosities - both radiative and kinetic (as in the bulk relativisitic flows in at least some radio sources) - apart from the use of a very deep gravitational potential well. All the plausible non-black-hole models of this type seem liable to evolve rapidly into black holes anyway. (Rees 1985)

It is even possible that there might be entire 'black galaxies' which would form primordially given appropriate initial fluctuations. This idea has recently gained some support from the observation (Turner 1985) that many gravitationally lensed galaxies seem to have no visible lens associated with them. If the missing lenses are indeed 'big black lumps' this could have important implications for the dark matter on the largest scales.

At the other end of the mass range, primordial black holes of very low mass

(Hawking 1971) might have been produced at very early stages in the expansion of the universe, when the horizon mass scale was comparable to their mass. The best limits on such objects come from the non-observation of gamma radiation that would be produced when such holes evaporated by the Hawking process (Carr 1978). This limit only constrains holes of mass below 10^{17}g. Since any baryons going into these primordial holes would have been lost to the Universe prior to nucleosynthesis, the usual constraints on baryonic matter do not apply in this case. I will not consider primordial holes in this thesis.

1.4 Light Limits on Stars and Black Holes

In Chapter 2 I will describe the models I will use for Population III VMOs, and discuss the likely spectrum from these objects. I will also extend the work of CBA by discussing the effect of the VMOs on their environment, and calculate the emergent spectrum in the case of an optically thick nebula surrounding the VMO.

Chapter 3 discusses the evolution of the background light produced by pregalactic or protogalactic sources like the Population III stars. Extragalactic background radiation may be our only way of inferring the conditions in the pregalactic 'dark ages' of the universe between the last scattering of the microwave background and the recent era which we can observe directly. Any astrophysical processes occurring at high redshift are likely to have been accompanied by some energy release, so research into the extragalactic background holds out great promise of containing clues to the origin of the structure we observe in the universe today. Section 3.1 reviews the theory of the evolution of radiation in the expanding universe and casts it in a form appropriate for the Population III context. Section 3.2 discusses analytically the effects of the radiation on the thermal history of the intergalactic medium, and the absorbing effects of the intergalactic medium on the background. I also discuss the likely contribution to the dust opacity from galaxies along the line of sight. In 3.3, I describe a numerical code I have developed to model the evolution of the background spectrum under a variety of assumptions and to compare the predicted spectrum with observational limits. In 3.4, I present the results of running this code for a representative variety of models.

Chapter 4 illustrates the problem by considering the interpretation of one particular possible background radiation. Although the near-infrared background discussed in this chapter has not been confirmed, it demonstrates how one could interpret such a background if confirmed, or how one might interpret a far-IR background in one should be discovered. The conclusions of this study were that

to explain the postulated near-IR background as redshifted starlight one would have to invoke a closure density of stars at a moderate redshift.

Chapter 5 discusses the current status of observational constraints on the extragalactic background light, and confronts the predicted models of Chapter 3 with these observations. I hence derive constraints on the dark matter presented as a series of curves of allowed density parameter in VMOs as a function of redshift. I deduce that current limits exclude the Population III hypothesis unless either there is a dense dusty intergalactic medium, or the stars formed at high redshifts (more than 40). In section 5.3 I briefly discuss limits on radiation generated by the accreting black hole remnants of the Population III stars.

In Chapter 6, I repeat the calculations of Chapters 3 and 5 for stars with conventional mass and spectra with temperatures appropriate to Population II stars. This extends the results of Thorstensen and Partridge (1975).

Chapter 5 discussed limits on background light from the stellar precursors of black holes; in Chapter 7 I study the limits on the non-observation of discrete black hole sources. If black holes solve any of the the dark matter problems, they should be present within a few hundred parsecs (depending somewhat on their mass), and will be faint sources of optical and infrared radiation as they accrete from interstellar clouds. In section 7.1, I review the expected frequency of local black holes, and, in 7.2, I summarize a model for the local interstellar medium. Section 7.3 discusses black hole accretion from the interstellar medium. Section 7.4 discusses the spectrum generated by accreting black holes with thin disks and holes accreting spherically and radiating by the mechanisms described by Ipser and Price (1982). In 7.5, I calculate the corresponding predicted brightness of the nearest black holes, for the cases when they make up the halo dark matter and the disk dark matter. I deduce the maximum mass such holes could have without contravening observations. The halo dark matter holes must have mass less than 100 $M_{\odot}$, while the disk dark matter holes must have mass less than 10

$M_{\odot}$. These constraints unfortunately cannot be regarded as conclusive since they depend on the uncertain details of the accretion spectrum.

In section 7.6 I use the accretion models discussed in Chapter 7 to investigate the likely brightness of the nearest black holes which are 'certain' to exist - the remnants of ordinary massive Population I stars. The limit thus set on the minimum initial stellar mass for black hole formation is rather low and somewhat uncertain, but it may be possible to improve this limit in the future.

Chapter 8 summarizes the conclusions of the thesis and discusses how future observational and theoretical work could improve the results discussed here.

1.5 Cosmological Assumptions

I will assume that spacetime is described by the standard matter-dominated Friedmann-Robertson-Walker model with zero cosmological constant, which can be parameterized by the Hubble constant H_0 and the density parameter Ω_0 . I will set $H_0 = 50h_{50}$ km/s/Mpc. Ω_0 is equal to the mass(-energy) density of the universe divided by the critical density

$$\rho_c = 4.7 \times 10^{-27} h_{50}^2 \text{kg m}^{-3} \qquad 1.5.1$$

When, as in chapter 3, I make analytical estimates of timescales in the expanding universe I adopt an approximate time-redshift relationship

$$t = \frac{2}{3} H_0^{-1} \Omega_0^{-\frac{1}{2}} (1+z)^{-3/2} \qquad (1.5.2)$$

which is valid for $1 + z \gtrsim \Omega_0^{-1}$, and exact for Ω_0 =1. In numerical calculations I consider the two extreme cases Ω_0 =0.1, as implied by some actual measurements, and Ω_0 =1, which has theoretical appeal, especially in inflationary scenarios.

I assume that the universe contains the presently visible galaxies with density Ω_{gal} in units of the critical density, gas with comoving density $\Omega_g(t)$, Population III stars with comoving density $\Omega_*(t)$, and a possible further non-baryonic dark matter component Ω_{nb}, which can make up Ω_0 =1 in cases where $\Omega_* < 0.1$ to conform to the nucleosynthesis limits. There is no compelling reason to suppose that the dark matter on the largest scales is the same as that making up galaxy haloes; As pointed out in section 1.1, while Occam's razor suggests we should avoid multiplying our hypotheses, there may in principle be as many forms of dark matter as of luminous matter, and more than one form may provide a significant contribution to Ω_0 (Carr 1985). In this thesis I attempt to constrain only the contribution from stellar remnants, without specifying whether or not there is additional non-baryonic dark matter making up the principal contribution to the mass density.

2. Population III Very Massive Objects and Their Environment

2.1 Models of Population III VMOs

Bond, Arnett and Carr (1984, BAC) study the structure and evolution of Very Massive Objects, which they define as stars which go unstable to the creation of electron-positron pairs during oxygen core burning. Here I review their results and calculate a set of models to illustrate the properties of the VMOs.

The VMO mass range covers stars between 100 and 10^5 $M_\odot$. It was originally thought that stars of such high mass would be unstable to disruptive oscillations powered by thermonuclear burning, but nonlinear calculations show that these oscillations are of finite amplitude and should not disrupt the star. There is no question, however, that the rate of mass loss from the outer layers of the atmosphere would be very large; it is not known how to estimate how large, although crude extrapolations from the MO (Massive Object, or 10-100 $M_\odot$ stars) range, where observational data exists, indicate that it will crucially affect the evolution of the star. If the mass loss is severe enough to reduce the total mass of a star of arbitrarily large initial mass to masses less than 100 $M_\odot$ on a timescale shorter than its evolutionary timescale, then VMOs cannot exist. I will assume that there is an initial mass range for which the mass at the end of the main sequence lifetime is still well within the VMO range. Since the material lost prior to this stage is returned unprocessed to space, I will use M as the main sequence rather than the intial mass M_i of the objects I discuss in connection with the dark matter problems. If $M_i \gg M$ this means that many stellar generations will be required to put most of the universe's mass into remnants.

Elementary stellar structure theory suggests that VMOs will have electron scattering as the main source of atmospheric opacity, and radiation pressure will dominate gas pressure. This means that the luminosity will be roughly equal to the Eddington luminosity at which gravity just balances radiation pressure (so

that the star remains bound),

$$L_{Edd} = 4\pi GMm_p c/\sigma_T, \tag{2.1.1}$$

which in turn implies that the lifetime $t_{ms} \sim \epsilon Mc^2/L$ is independent of mass and depends only on the efficiency ϵ with which the rest mass of the star is converted into radiant energy. This efficiency depends on the initial composition and the fraction of hydrogen burnt.

As pointed out by BAC, since the specific entropy of the star is roughly constant, the Eddington standard n=3 polytrope model is a good first approximation to the structure giving analytic expressions for the luminosity and radius. Their more accurate approximation is a 'point source model' in which an extended atmosphere is matched on to an n=3 polytrope exterior. This gives rise to correction factors to the polytropic formulae which are expressed as functions of the entropy parameter $\sigma = s_\gamma/4Y_T$ of the central polytrope, where s_γ is the photon entropy and Y_T is the number of particles per baryon. Y_T is related to the hydrogen abundance Y_p by $Y_T = (3 - 5Y_p)/4$.

I now summarize the BAC equations giving the relevant stellar parameters. σ is given implicitly in terms of the mass by

$$M(\sigma) = F_M(\sigma)1.1s^2(1+\sigma^{-1})^{3/2}M_\odot \tag{2.1.2}$$

where F_M is the polytropic mass correction factor. An approximate solution of this equation is

$$\sigma(M) = 0.24Y_T^{-1}M^{1/2} - 0.61 \tag{2.1.3}$$

but I have used the exact analytic form of F_M given in BAC Appendix C. The luminosity is given by

$$L/L_{Edd} = F_L(\sigma)(1+\sigma^{-1})^{-1} \tag{2.1.4}$$

and the main sequence time by

$$t_{ms} = 1.7 \times 10^6(1+\sigma^{-1})F_L^{-1}Y_p(1+Y_p/2)(1-5.6Y_T^2/M)yr \tag{2.1.5}$$

The radius of the star is

$$r_* = F_R(M)30.4Y_T\sigma^{1/2}/T_C(\sigma)R_\odot \tag{2.1.6}$$

which depends on the central temperature T_C (in keV). An accurate approximation to this is

$$T_C(\sigma) = 11.3(\sigma^2/1+\sigma)^{0.087}(Z/10^{-9})^{-0.079}\text{keV} \tag{2.1.7}$$

From these fundamental parameters we derive three more useful quantities. We define the stellar 'effective temperature' T_E by the relation

$$L = 4\pi r_*^2 \sigma_R T_E^4 \tag{2.1.8}$$

where σ_R is Stefan's radiation constant. The surface gravity is given by

$$g = GM/r_*^2 \tag{2.1.9}$$

and the efficiency of the star is defined as the fraction of its mass M turned into radiant energy,

$$\epsilon = Lt_{ms}/Mc^2 \tag{2.1.10}$$

This last parameter is independent of the uncertain quantity F_L which appears in both the luminosity and the lifetime.

Table 2.1 gives the solution of these equations for a variety of parameter choices. As our reference configuration we take a VMO model with parameters chosen in the limit of large mass, and with an initial CNO element abundance of $Z = 10^{-9}$. This abundance corresponds to that generated by the stars themselves on their approach to the main sequence (Bond, Arnett and Carr 1984). We then parameterize other stellar models in terms of this model and mass (and composition) dependent correction factors denoted by f(M), as follows:

$$\begin{aligned} L &= f_L(M)L_{Edd} = 1.4\times 10^{33} f_L(M)M_2 \quad \text{W} \\ r_* &= 6.2 f_R(M)M_2^{1/2}R_\odot \end{aligned} \tag{2.1.11}$$

$$T_E = 10^5 f_T(M)\mathrm{K}$$
$$t_{ms} = 1.75 f_t(M)\mathrm{Myr}$$
$$\epsilon = 0.0041 f_\epsilon$$
$$g = 1.5 \times 10^3 f_g \ \mathrm{ms}^{-2}$$

where $M_2 = M/10^2 M_\odot$ These factors are not independent and are related by

$$\begin{aligned} f_L &= f_\epsilon / f_t \\ f_R &= f_\epsilon^{\frac{1}{2}} f_t^{\frac{1}{2}} f_T^{-2} \\ f_g &= f_R^{-2} \end{aligned} \tag{2.1.12}$$

i.e. , there are three independent quantities. Table 2.2 recasts the information of Table 2.1 in terms of these factors. All these correction factors are slowly varying with mass, so we may generally consider VMOs as being stars radiating at a large fraction of the Eddington luminosity at an effective temperature of 10^5K; they have surface gravities given by $\log(g/1 \text{ cm s}^{-2}) = 5.2$. We shall adopt these parameters to choose an appropriate model atmosphere spectrum. I choose to adopt f_ϵ, f_t, and f_T as the basic parameters to describe the stellar properties, rather than mass, radius and luminosity. This choice is motivated by the fact that the intensity of the background depends basically on ϵ.

Previous authors have considered modelling the stellar spectrum as a pure blackbody; in fact the electron-scattering dominated atmosphere will mean that the atmosphere is more transparent at higher frequencies, because of the frequency dependence of the free-free opacity. The higher the frequency, the lower the optical depth, so escaping photons come from deeper in the star where the temperature is hotter than at the nominal photosphere. They are scattered out of the beam since the opacity is scattering dominated, so the emergent flux is diluted relative to a blackbody at the hotter temperature of the deeper material. At low frequencies, the opacity is absorption dominated and the emergent flux is

blackbody at a frequency dependent temperature which decreases with decreasing frequency. This results in a harder 'modified black body' spectrum; accurate model atmosphere calculations have not been done for such stars with log g =5, but a pure hydrogen model atmosphere for a star of somewhat higher surface gravity ($\log g = 6$) has been calculated, (Wesemael *et al.* 1980) which I shall refer to as the H model. In Fig. 2.1 I plot appropriate blackbody, modified blackbody, and H model atmosphere spectra for comparison. The 'modified blackbody' model used to fit the model atmosphere is a simple homogeneous slab model (Felten and Rees 1972, Shapiro and Teukolsky 1983) with a density of $10^{15}\mathrm{cm}^{-3}$ and temperature 2.6×10^{5}K, which reproduces the correct total flux. It is intended simply as a crude indication that the origin of the harder spectrum of the H model atmosphere arises from the fact that electron scattering rather than free-free absorption begins to dominate the opacity at high frequencies. The Lyman limit is in the frequency regime where the absorption is greater than scattering, and the opacity increase due to photoionization means that the flux is smaller on the high frequency side of the Lyman jump. This model atmosphere should be a better representation than the blackbody for our stars; if the stars actually have a normal helium abundance, the spectrum will have a large jump at the helium edge and will contain little flux beyond this point.

Husfeld *et al.* (1983) calculate low gravity non-LTE hydrogen-helium atmospheres with helium abundance by number $Y_{He} = 0.1$ and show that the details of the spectrum close to the helium ionization edge are strongly gravity dependent. Fortunately our models have almost constant surface gravity; they lie in the region of the (log g, T_{eff}) plane where Husfeld *et al.* predict that the helium edge is in emission. In the layers of the stellar atmosphere in which this part of the spectrum is formed, there is less singly ionized helium than one would expect if the gas there were in LTE. This is because the He^{+} is being photoionized to He^{++} by radiation from deeper in the star. Thus the He^{+} continuum is more transparent

and so in turn the continuum radiation that escapes from the star comes from deeper, hotter layers than an LTE calculation would suggest. We adopt one of the Husfeld *et al.* models (log g=5.0, T-eff = 10^5K) and will refer to it as the He model. It is similar to the H model at lower frequencies, but the high-frequency flux has been redistributed to give a helium emission edge and a steeper cutoff. The BB (blackbody), H and He model atmospheres are plotted for comparison in Fig 2.2.

I parameterize the number of ionizing photons in the spectrum by

$$\dot{N} = 2.6 \times 10^{50} f_N f_L M_{2S}{}^{-1}. \tag{2.1.13}$$

This definition gives $f_N = 1$ for the blackbody, $f_N = 0.73$ for the H model stellar atmosphere, and $f_N = 0.83$ for the He model.

Table 2.1 VMO properties

M ($M_\odot$)	L/L_{Edd}	t (Myr)	R ($R_\odot$)	T_e (K)	log(g) (g in cm/s^2)	
100	0.32	4.6	4.3	92000	5.17	0.0034
200	0.44	3.7	6.2	99000	5.15	0.0038
300	0.51	3.2	7.8	102000	5.13	0.0039
400	0.57	3.0	9.1	103000	5.12	0.0040
500	0.62	2.8	10.3	105000	5.11	0.0040
10^3	0.79	2.2	15.6	107000	5.05	0.0041
10^4	0.93	1.9	51.1	110000	5.02	0.0041
10^5	0.98	1.8	146.0	117000	5.11	0.0041

Table 2.2 VMO propeties: the 'f' parameters

M_2	f_L	f_t	f_R	f_T	f_g	f_ϵ
1	0.32	2.6	1.00	0.92	1.00	0.83
2	0.44	2.1	1.02	0.99	0.96	0.93
3	0.51	1.8	1.04	1.02	0.92	0.95
4	0.57	1.7	1.04	1.03	0.92	0.98
5	0.62	1.6	1.06	1.05	0.89	0.98
10	0.79	1.2	1.14	1.07	0.77	1.00
100	0.93	1.1	1.17	1.10	0.73	1.00
1000	0.98	1.0	1.06	1.17	0.89	1.00

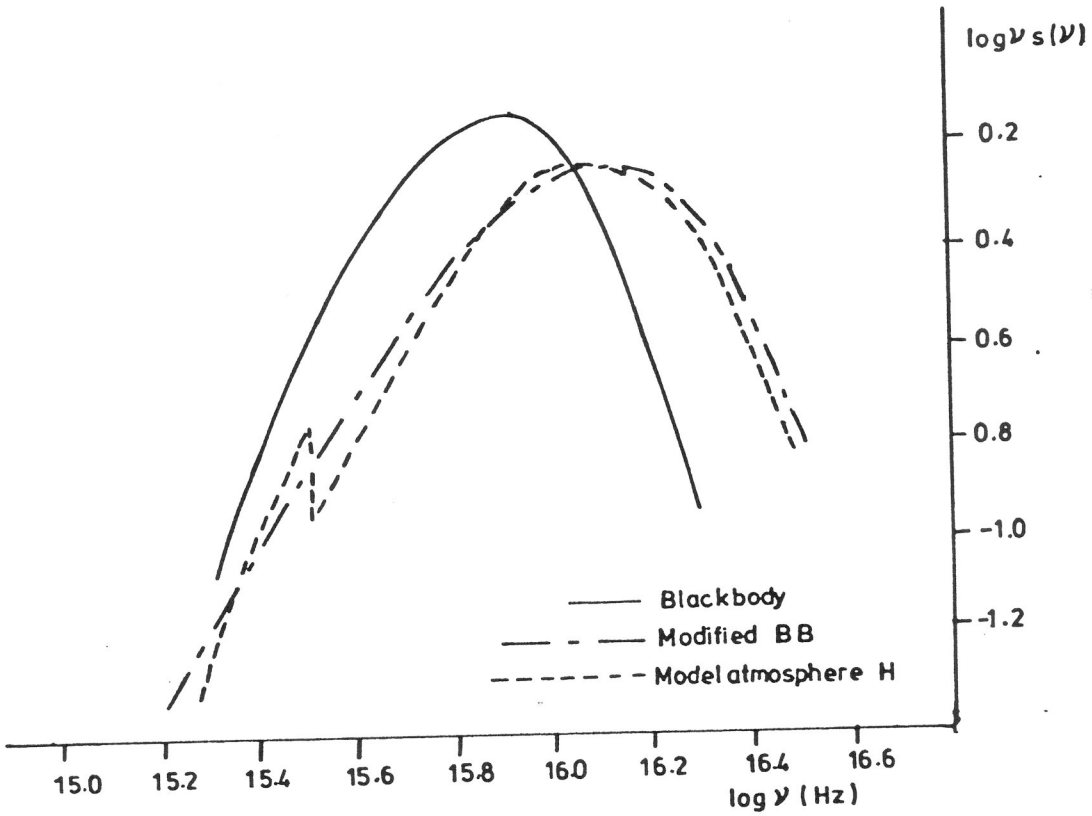

Fig 2.1 Fit to H model atmosphere

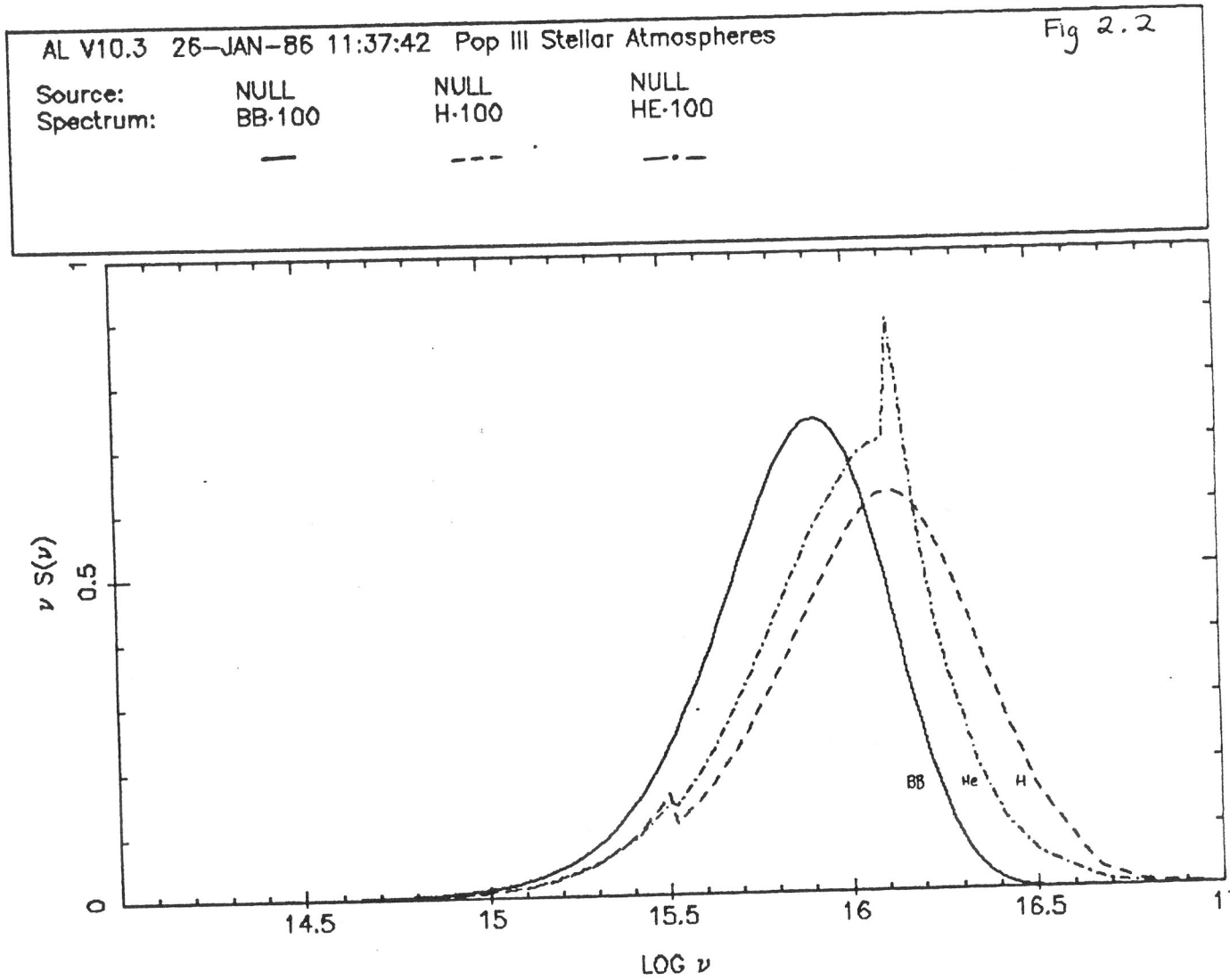
AL V10.3 26-JAN-86 11:37:42 Pop III Stellar Atmospheres
Source: NULL NULL NULL
Spectrum: BB-100 H-100 HE-100
ν S(ν)
1
0.5
0
14.5
15
15.5
16
16.5
17
LOG ν
BB
He
H

Fig 2.2

2.2 Ionization of HII regions by VMOs

Whether the Population III stars are pregalactic or form within protogalaxies, it is likely that there would be a substantial amount of gas in their vicinity. Ordinary massive stars form in dense gaseous environments, which absorb their extreme ultraviolet radiation in a region of ionized hydrogen (HII region) around the stars. The enormous amounts of ionizing radiation emitted by VMOs may be sufficient to ionize not just the surrounding gas but the entire rest of the universe (if a sustantial fraction of the mass of the universe is in VMOs) and so affect the universe's thermal history. In fact Couchman (1985) and CBA have shown that even for small abundances of VMOs the universe may be re-ionized. I now study the possible environments of the VMOs to attempt to quantify the likely effects of VMOs on the universe.

Consider a nebula of density profile n(r) surrounding the star, or a group of the stars. Let the number of hydrogen atoms in the cloud per star be $\beta Y_H M/m_H$, so as to make ratio of the mass in the clouds to the mass in the stars β where the hydrogen abundance is Y_H. In 2.2.1 I consider the cloud to be the star's mass loss atmosphere, and in 2.2.2 the cloud in question is a constant density nebula around the stars. In each case β is used to denote the ratio of gas mass in the relevant cloud to the mass in stars. Note that this fraction β may be large, but if the sources make up the dark matter it will be less than 1 at a typical time in the Population III era, unless the holes accrete most of their mass subsequently. For a given volume of gas, we now determine the density that the nebula must have in order to absorb all the incoming radiation. As a simple approximation, we consider a one-zone model with a single temperature, and balance ionizations caused by the star with those recombinations which do not involve the production of ionizing photons. This is the 'on-the-spot' approximation in which ionizing photons produced in the cooling of the gas are reabsorbed immediately. If α_{eff} is the effective recombination rate (i.e. excluding reionizing recombinations), then

equating the rate of production of stellar ionizing photons to the effective number of recombinations in the nebula gives

$$\dot{N} = \int \alpha_{eff} n^2 dV \tag{2.2.1}$$

We will temporarily ignore reionizations caused by free-free photons and n≥2 recombination continuum photons. $\alpha_{\rm eff}$ is then simply the recombination coefficient to all levels excluding the ground state, $\alpha_{\rm eff} = 3.7 \times 10^{-20} T_5^{-0.8}$ $\rm m^3 s^{-1}$, (Kaplan and Pikel'ner 1970) which depends on the nebular temperature $T = 10^5 T_5$ K. The intense stellar flux will maintain T_5 close to 1 in spite of cooling due to hydrogen and helium, in contrast to the normal metallicity case where line cooling by oxygen and other metals would lower T_5 to 0.1 or so. If the nebula is very thin, Compton cooling by the microwave background photons may be an important effect, but we shall see that the nebula must be very dense to affect the outgoing radiation. Detailed calculations, discussed in the next section, show that inelastic collisions reduce the temperature to $T_5 = 0.3$.

In addition the gas may contain dust; in the true first generation of stars there will of course be no dust, but in succeeding generations of stars there may be a small abundance. If the dust mass fraction is χ, the Lyman limit optical depth is

$$\tau_0 = \kappa_0 m_H \chi \int n dr \tag{2.2.2}$$

where κ_0 is the dust opacity at the Lyman limit, so $\kappa_0 m_H \chi$ is the dust optical depth per unit hydrogen column; a rough fit to the dust extinction in our own galaxy is that the cross section of cosmic dust varies approximately linearly with frequency from the IR to the far UV. Using this approximation we adopt a fit to the data of Howarth (1983) with $\kappa_0 m_H \chi = 2.7 \times 10^{-25} \rm m^2$ for the interstellar medium in our own galaxy. It is believed that $\chi \sim 0.01$ in our galaxy, so if the Population III era dust had the same properties, $\kappa_0 = 1.6 \times 10^4 \rm m^2 kg^{-1}$. This is the only reasonable assumption we can make but of course the size and composition of Population III grains might be quite different.

2.2.1 The Mass Loss Atmosphere

Now consider the star's mass loss atmosphere. I assume the nebula to contain the total mass lost in the main sequence phase, which is a fraction β of the stellar mass M. Hence the mass loss rate is $\dot{M} = \beta M/t_{ms}$. Following Hoyle et al.(1973), we consider an r-independent wind velocity $v = 10^3 v_3$ km/s giving a density profile for the hydrogen number density of

$$4\pi v m_H r^2 n = \beta Y_H M/t_{ms} \tag{2.2.3}$$

where Y_H is the hydrogen mass fraction. The ratio of ionizations to recombinations in the gas is then

$$\frac{\dot{N}}{4\pi\alpha n_0^2 r_0^3} = 80 M_2^{-\frac{1}{2}} T_5^{0.8} (\beta Y_H)^{-2} v_3^2 (r_0/r_*) f_N f_t^{\frac{1}{2}} f_\epsilon^{\frac{3}{2}} f_T^{-2} \tag{2.2.4}$$

where n_0 is the density at the inner edge r_0 of the $1/r^2$ nebula and the stellar radius is given by eq. (2.1.11)

Even if β is of order unity, as is likely for such radiation pressure dominated stars, this means that the condition (2.2.1) cannot be easily satisfied and the envelope will be highly ionized. The main source of opacity will then be dust. The optical depth is just $\tau = n_0 \kappa_0 m_H \chi r_0$, or

$$\tau = 1.0 \times 10^6 \chi M_2^{\frac{1}{2}} \beta Y_H (r_0/r_*)^{-1} f_t^{-\frac{1}{2}} f_\epsilon^{-\frac{1}{2}} f_T^2 \tag{2.2.5}$$

at the Lyman limit. Hence the stars can only be infrared objects if they have such a mass-loss atmosphere with $\chi\beta$ greater than about 10^{-6}. The first generation Population III stars will have smaller abundances than this if their nucleosynthesis products are not well mixed into the atmosphere. If there is enough dust, the spectrum will be redshifted to the present epoch without further modification unless the intergalactic dust abundance is very high (see next section). For the remainder of this section we assume that there is insufficient dust produced in the star's atmosphere to make it opaque, and consider the case where the star is an ultraviolet source.

2.2.2 The Local Nebula

We now consider a constant density region around the star (or a group of the stars). The minimum density required to absorb all the ionizing radiation is from (2.2.1)

$$n = \left(\frac{\dot{N} m_H}{\beta Y_H \alpha_{\rm eff} M}\right) \qquad (2.2.6)$$
$$= 5.9 \times 10^{10} T_5^{0.8} (\beta Y_H)^{-1} f_N f_\epsilon f_t^{-1} \quad \mathrm{m}^{-3}$$

This corresponds to a Stromgren radius of

$$R_S = 0.25 M_2^{1/3} T_5^{-0.3} (\beta Y_H)^{2/3} \left(\frac{f_t}{f_N f_\epsilon}\right)^{1/3} \mathrm{pc} \qquad (2.2.7)$$

This HII region will expand in order to achieve pressure balance with the surrounding gas. The standard analysis (see Spitzer 1978 for details) gives

$$R/R_S = (1 + t/t_1)^{4/7} \qquad (2.2.8)$$

where

$$t_1 = 4R_S/7(2kT/m_p)^{1/2} \qquad (2.2.9)$$
$$= 3 \times 10^3 M_2^{1/3} T_5^{-0.8} (\beta Y_H)^{2/3} (f_N f_\epsilon / f_t)^{-1/3} \mathrm{yr}$$

which is essentially the Stromgren sphere sound crossing time. The ratio of the stellar lifetime to this timescale is

$$t_{ms}/t_1 = 5 \times 10^2 M_2^{-1/3} T_5^{0.8} (\beta Y_H)^{-2/3} f_t^{2/3} f_N^{1/3} f_\epsilon^{1/3} \qquad (2.2.10)$$

so the expansion will be unimportant only for large masses and cases where the gas to star mass ratio is large. Eq. (2.2.8) remains valid until pressure equlibrium has been attained, or until the star turns off. In the scenario we are considering the stellar life is always less than the time to reach pressure equilibrium.

For a pregalactic uniformly distributed Population III of 200 $M_\odot$ stars with roughly half the stars burning at the same time, so the gas mass can be comparable to the star mass, we have $\beta = 1$ and $M_2 = 2$, so $t_{ms}/t_1 = 240$ (taking $T_5 = 0.3$). In this case we must therefore allow for the expansion; at the end of the stellar life the radius of the ionized zone is

$$R = 9M_2^{1/7}T_5^{0.2}(\beta Y_H)^{2/7}f_t^{8/21}(f_N f_\epsilon)^{1/5}\text{pc} \qquad (2.2.11)$$

and the mass of gas in the zone has increased by a factor

$$\delta M/M = 200M_2^{-2/7}T_5^{0.7}(\beta Y_H)^{-4/7}f_t^{4/7}(f_N f_\epsilon)^{2/7}, \qquad (2.2.12)$$

which for our example is equal to 100. Hence for the final ratio of gas mass to star mass to be β', the initial density must be

$$n = 1.4 \times 10^{16}M_2^{-2/3}T_5^{2.4}\beta'^{-7/3}Y_H^{-7/3}f_t^{1/3}(f_N f_\epsilon)^{5/3} \quad \text{m}^{-3} \qquad (2.2.13)$$

and final radius

$$R = 0.25M_2^{1/3}T_5^{-0.3}(\beta' Y_H)^{2/3}\text{pc} \qquad (2.2.14)$$

For the parameters above, we have $n = 1.2 \times 10^9\text{cm}^{-3}$ and $R = 0.5$pc, which sems implausible as it is much higher than the densities encountered in regions of ordinary massive star formation. We conclude that if the stars are uniformly distributed pregalactic objects they will probably ionize the gas in their vicinity without running out of UV photons. In other words, as discussed below, they will ionize the universe (since the total mass of gas in the IGM will be less than the mass in stars.)

At the other extreme we consider a protogalaxy of mass $10^{10}M_\odot$. If all the mass eventually goes into VMOs, then the fraction in VMOs at any one time must be greater than the ratio of the stellar lifetime to the Hubble time, or 10^{-4}. Consider the galaxy as a common HII region for a cluster of VMOs of total mass $10^6M_\odot$; then the expansion is negligible and the density required to absorb the

UV is 1 cm^{-3}, which is typical for a galaxy. Hence in this scenario the galaxy can just contain the UV radiation. One might worry that the ionization would prevent further star formation but, even in this low density case, the recombination time is short compared with a stellar generation, and will be even shorter in low density regions. The other potential problem with extending the Population III era over so many stellar generations is that pollution by earlier generations will probably establish Population II conditions before all the mass is processed into VMOs.

An intermediate scenario is one in which the Population III objects are star clusters of total mass $10^6 M_\odot$, (whether this is made up of 100 $10^4 M_\odot$ stars or 10^4 $100 M_\odot$ stars is immaterial due to the slow variation of the 'f parameters'). There are many ways in which such objects might arise in the early universe (Carr and Rees 1984a). To give a large gas mass we suppose that star formation is sufficiently inefficient that only 1% of the mass is in stellar form at any time, so $\beta = 100$ and $M_2 = 100$. 100 stellar generations corresponds to an expansion time at $z = 16 h_{50}^{-2/3}$, so there is enough time for all the cluster to go through the Population III phase. Then the expansion of the HII region is marginally important, and we find that $n = 400$ $cm^{-3}$and $R = 40$ pc is required to contain the ionizing flux. This seems a plausible Population III scenario, so I conclude that the nebular-reprocessed spectrum is a viable possibility for the light from Population III stars.

For dust absorption, $\tau_0 = n \kappa_0 m_H \chi r$. Since we can find r in terms of n and β from $4\pi n r^3/3 = \beta M/m_H$, $\tau_0 > 1$ if

$$n > 4 \times 10^4 (\beta Y_H)^{-\frac{1}{2}} \chi^{-\frac{3}{2}} M_2^{-\frac{1}{2}} \quad \mathrm{m}^{-3} \qquad (2.2.15)$$

This is always less important than neutral hydrogen absorption providing that the dust abundance is poorer than Population II.

In the cosmological context it is useful to express the above results in terms of the corresponding cosmological density parameters and the overdensity compared to the background gas density. In this way we determine whether the condition

for ionization derived in eq (2.2.6) implies that the stars will ionize all the gas in the universe, so that their ionizing ultraviolet flux is not all absorbed.

Assume that the mean number of stars per unit volume is n_*, and that each is surrounded by a nebula of volume V_N and gas density n_g . The stars may be grouped in clusters of N_* objects, in which case the total volume of the surrounding nebula is taken to be $N_* V_N$. Then the clumping factor of the nebulae δ, defined by the inverse of their volume filling factor in the universe, is given by

$$\delta = \frac{n_*^{-1}}{V_N/N_*} = \frac{nm_H}{\beta Y_H M n_*} \tag{2.2.16}$$

Let the cosmological density parameters for the stars and nebulae be Ω_* and $\Omega_g = \beta\Omega_*$ respectively. The corresponding coordinate number densities are

$$\begin{aligned} n_* &= \Omega_* \rho_c (1+z)^3 / M \qquad (2.2.17a) \\ &= 2.4 \times 10^{-59} \Omega_* h_{50}^2 z^3 M_2^{-1} \quad \mathrm{m}^{-3} \\ n_g &= \Omega_g \rho_c (1+z)^3 Y_H \delta / m_H \qquad (2.2.17b) \\ &= 2.8 \Omega_g h_{50}^2 Y_H \delta z^3 \quad \mathrm{m}^{-3} \end{aligned}$$

so to avoid ionizing the universe we require, substituting (2.2.16) in (2.2.6),

$$\delta > \left(\frac{\dot{N}}{\alpha n_*}\right)\left(\frac{m_H}{\beta Y_H M}\right)^2 = 2.0 \times 10^{10} T_5^{0.8} f_N f_\epsilon f_t^{-1} \beta^{-2} Y_H^{-2} \Omega_*^{-1} h_{50}^{-2} z^{-3} \tag{2.2.18}$$

For the unclumped background gas, δ is unity. If equation 2.2.18 is to be satisfied in this case, we must choose not only large z but also large β. Assuming that we believe that the total density parameter is at most unity, this means that Ω_* must be small. Even at z=100 the background gas will be ionized unless Ω_* is roughly as small as 10^{-4} or so. At lower redshifts it is even easier to ionize the gas. We are interested in the case in which Ω_* is the major baryonic contributor to Ω_0, and so $\beta < 1$. We therefore conclude that a substantial amount of matter is required in dense, clumped ($\delta \gg 1$) regions, or the Lyman continuum will not be absorbed

(Carr,Bond and Arnett 1984). In section 5.3 I show that the remnants of the stars will not accrete a significant amount of mass if the gas is unclumped.

Equation (2.2.18) may be satisfied for high redshift sources ($z \sim 100$) in the case of parent gas clouds of $10^6 M_\odot$ collapsing shortly after recombination and forming clusters of Population III objects at a later epoch. Such density perturbations would collapse, turning round when their density relative to the background gas is 5.5. The clouds collapse and virialize at some epoch z_1, increasing their density relaitve to the background gas by a further factor of 30. Assume they then form stars at a redshift z_2, when the overdensity relative to the bakground is $\delta = 200(z_1/z_2)^3$. This satisfies eq. (2.2.18) if $z_1 > 450$ which is comfortably after recombination in the standard model. Hence in this scenario the ionizing radiation might be absorbed. I note that the implied gas density is quite large; clumps of normal galactic densities would be insufficient to absorb the radiation but the densities found in dense molecular cloud cores would be adequate. The opacity from dust is similar to the hydrogen opacity if the gas-to-dust ratio is 1 per cent of galactic, corresponding to Population II metallicities.

The results of this section can be summarized by saying that very dense gas is required to stop the VMOs ionizing the universe. In section 3.2 I will show that even if the universe is ionized initially, the radiation may be absorbed later. In the next section I calculate the likely spectrum if the radiation is indeed absorbed by hydrogen.

2.3. Modelling the Stellar and Nebular Spectrum

The spectrum of a pure hydrogen nebula photoionized by a VMO will be largely recombination continuum and Lyman line radiation. We take into account free-bound and free-free processes, but we ignore collisional excitations and photoionizations from excited states. We start by omitting collisional ionization and excitation entirely, to get a first approximation to the problem, and then include these processes.

In the actual spectrum calculated we approximate the line spectrum by assuming that an electron recombining to an excited level falls one level at a time to the ground state, producing $L\alpha, H\alpha, P\alpha$, etc., photons. This gives the correct total energy and corresponds to the standard 'Case B' approximation in which the optical depth is large in the Lyman lines. We also assume that Lα line photons will be scattered out of the high optical depth line core before they are degraded.

The electron temperature of the nebula is calculated by modifying the hydrogen nebula equation of Baker, Menzel and Aller (1938) to include the on-the-spot approximation. Suppose that in a region of the nebula with emission measure $W = n^2V$ the gas absorbs N stellar ionizing photons per unit time corresponding to absorbed energy L per unit time. Then the total number of recombinations must be equal to N plus the number of ionizing photons created in recombination and free-free processes. Hence the effective recombination rate is equal to the recombination coefficient for non-ionizing photons minus the production rate of ionizing free-free photons. Similarly, L must be equal to the emitted luminosity from non-ionizing recombination and free-free radiation. In fact, if we adopt as temperature parameter $x_0 = R/kT$, where $R = \frac{1}{2}\alpha^2 mc^2$ and define a characteristic recombination coefficient

$$A_0 = 64\pi^2(3\pi)^{-\frac{3}{2}}\alpha^2(\hbar/mc)^2 c = 5.20 \times 10^{-20}\mathrm{m^3 s^{-1}}, \qquad (2.3.1)$$

then

$$N/W = A_0 x_0^{\frac{3}{2}} f(x_0) \qquad (2.3.2)$$

$$L/W = RA_0 x_0^{\frac{8}{3}} g(x_0)$$

and

$$L/NR = g(x_0)/f(x_0) = \epsilon(x_0) \tag{2.3.3}$$

where $\epsilon(x_0)$ is a completely determined function of temperature which is derived below. Choosing to express all quantities in terms of A_0 allows me to express the standard equations for the radiative processes in a particularly simple form, avoiding the usual proliferation of dimensional constants. Hence for a given value of L/NR, since $\epsilon(x_0)$ is monotonic in the range of interest, the temperature of the zone can be determined and the spectrum calculated. L and N are both proportional to the neutral fraction, so this unknown factor cancels out and the ionization does not need to be known before the temperature. It turns out that a simple one-zone model reproduces the spectrum and the value of W required to absorb all the ionizing radiation to good accuracy when compared with more detailed zoned ionization models run with a variety of parameters. The derived electron temperature is close to that of the input stellar spectrum.

I now derive the function $\epsilon(x_0)$. Introducing $x = h\nu/kT = h\nu x_0/R$ as a dimensionless frequency variable, the recombination coefficient to level n is

$$\alpha_n(x, x_0) = A_0 x_0^{3/2} \frac{\exp(x_0/n^2)}{n^3} \left(\frac{\exp(-x)}{x}\right) \tag{2.3.4}$$

for $x > x_0/n^2$. Hence the total recombination coefficient to levels n=2 and above, excluding recombinations which produce ionizing photons (so the frequency integral is cut off at $x = x_0$) is

$$\alpha_{\text{non-ionizing}}(x_0) = A_0 x_0^{3/2} \sum_{n=2}^{\infty} \frac{1}{n^3} e^{x_0/n^2} (E_1(x_0/n^2) - E_1(x_0)) \tag{2.3.5}$$

where E_1 is the first exponential integral, $E_1(y) = \int_y^\infty e^{-y}/y dy$. The energy emitted for each of these recombinations consists of a continuum photon of energy

xR/x_0 and line photons of total energy $R(1-1/n^2)/x_0$, the energy level difference between level n and the ground state. The frequency-integrated emission coefficient is therefore

$$j_{cont} = RA_0 x_0^{3/2} \sum_{n=2}^{\infty} \frac{1}{n^3} x_0^{-1}(1 - e^{-x_0(1-1/n^2)}) \tag{2.3.6}$$

for the recombination continuum, and

$$j_{line} = RA_0 x_0^{3/2} \sum_{n=2}^{\infty} \frac{1}{n^3}(1 - \frac{1}{n^2}) e^{x_0/n^2} E_1(x_0/n^2) \tag{2.3.7}$$

for the lines.

The free-free radiation has emission coefficient

$$j_{ff}(x) = \frac{1}{2} RA_0 x_0^{-\frac{1}{2}} e^{-x} \tag{2.3.8}$$

and hence the ionization coefficient due to ionizing free-free photons is

$$\alpha_{ff} = \frac{1}{2} A_0 x_0^{\frac{1}{2}} E_1(x_0) \tag{2.3.9}$$

and the emission coefficient from the non-ionizing free-free radiation is

$$j_{ff} = \frac{1}{2} RA_0 x_0^{-\frac{1}{2}}(1 - e^{-x_0}) \tag{2.3.10}.$$

Therefore

$$\epsilon(x_0) = \frac{\sum_{n=2}^{\infty} \frac{1}{n^3}((1-\frac{1}{n^2})e^{x_0/n^2} E_1(x_0/n^2) + x_0^{-1}(1 - e^{-x_0(1-1/n^2)})) + \frac{1}{2}x_0^{-2}(1-e^{-x_0})}{\sum_{n=2}^{\infty} \frac{1}{n^3} e^{x_0/n^2}(E_1(x_0/n^2) - E_1(x_0)) - \frac{1}{2}x_0^{-1}E_1(x_0)} \tag{2.3.11}$$

The value of α_{eff} calculated for the blackbody VMO spectrum is $1.4 \times 10^{-20} m^3 s^{-1}$, corresponding to $W = 5.8 \times 10^{69}$ m^{-3} . This corresponds to $T_5 = 3.3$ in eq (2.2.6), although the actual temperature is only of order 1×10^5K. The resulting spectrum is plotted in Fig 2.3. As with all the other spectra used in the numerical studies, it is stored as $\nu S(\nu)$ in bins 0.02 wide in log ν. Lines are assumed to be less than one bin in width. For this model, 50 per cent of the flux

is in the Lyman line. When the model atmosphere spectrum is used as the input stellar spectrum rather than a blackbody, the result is very similar.

I now consider a more accurate model for the spectrum, including inelastic collisions with the ground level and 2-photon emission. Let the ionized fraction be f, the incoming spectrum be $L_0 s(\nu)$, where L_0 is the total luminosity and s gives the spectral dependence, and the hydrogen cross-section be $a(\nu) = a_H(R/h\nu)^3 g(\nu)$, where a_H is the cross-section at threshhold and g is a Gaunt factor for which an analytic expression is given in Osterbrock (1974). Then in a spherical shell of radius r-dr to r, and volume Adr, the total energy absorbed is

$$L = (1-f)na_H dr L_0 S_1 \tag{2.3.12}$$

where S_1 is the dimensionless integral

$$S_1 = \int_{R/h}^{\infty} s(\nu)(R/h\nu)^{-3} g(\nu) d\nu \tag{2.3.13}$$

and the total number of stellar photons absorbed per unit time is

$$N = (1-f)na_H dr(L_0/R)S_2 \tag{2.3.14}$$

where S_2 is another dimensionless integral

$$S_2 = \int_{R/h}^{\infty} s(\nu)(R/h\nu)^{-4} g(\nu) d\nu \tag{2.3.15}$$

The effective radiative recombination coefficient is

$$\alpha_{eff} = \alpha_{\text{non-ionising}} - \alpha_{ff} \tag{2.3.16}$$

and the radiation emitted in radiative processes is

$$j_{rad} = j_{cont} + j_{line} + j_{ff} \tag{2.3.17}$$

The energy and ionization balance are then

$$\frac{(1-f)nS_1 La_H}{4\pi r^2} = f(1-f)n^2 j_{coll} + f^2 n^2 j_{rad} \tag{2.3.18}$$

and

$$\frac{(1-f)nS_2La_H}{4\pi r^2 R} = -f(1-f)n^2\alpha_{coll} + f^2n^2\alpha_{eff} \qquad (2.3.19)$$

Approximations to the functions j_{coll} and α_{coll} are given by Kaplan and Pikel'ner (1970) as

$$j_{coll}(x_0) = \sum_{n>2} q_n x_0^{-1/8}(1-1/n^2)^{-1/8}\exp(-x_0(1-1/n^2)) \qquad (2.3.20)$$

and

$$\alpha_{coll}(x_0) = q_i x_0^{-\frac{1}{2}}\exp(-x_0) \qquad (2.3.21)$$

where $q_i = 4\times10^5 A_0$ and the q_n are of similar magnitude.

The simultaneous equations (2.3.18, 2.3.19) determine the temperature and ionization of the zone, and are solved with an iterative numerical code. The spectrum emitted by the zone is now determined except for the fact that some transitions from level 2 to level 1 occur by 2-photon emission from 2s to 1s rather than by Lyman alpha emission from 2p to 1s. The ratio of 2-photon to Lyman alpha is discussed by Cox and Matthews (1969) and Osterbrock (1974). It is given by

$$f_{2\gamma} = S(x_0)/(1.+fnr(x_0)) \qquad (2.3.22)$$

where S and r are slowly varying functions of temperature whose values are approximately S=0.34 and r=6×10^{-5}cm^3. This normalises the 2-photon spectrum. To describe its spectral dependence I have fitted the data of Osterbrock (1974) by

$$j_{2\gamma}(\nu) \sim (1-8\mathrm{abs}(h\nu/0.75R-0.5)^3) \qquad (2.3.23)$$

where the function abs denotes the absolute value of its argument.

2.3.1 Description of the numerical code

The input to the NEBULA code is the adopted stellar spectral model (BB, H or He) and the adopted stellar parameters chosen from table 2.2. The program requests a value of the gas number density and an upper limit to the number of

radial zones to be calculated. An option also exists to select an inverse square density profile. The results from using this option will not be illustrated here as they confirm the analysis of section 2.2 that such a nebula will be transparent within the assumptions of our scenario.

In each zone of thickness dr the code calculates the effective flux, which I define to be the luminosity divided by an effective area of the zone

$$A = (\text{zone volume})/dr = 4\pi r^2(1 - \left(\frac{dr}{r}\right) + \frac{1}{3}\left(\frac{dr}{r}\right)^2) \qquad (2.3.24)$$

This is the quantity required to balance the energy per unit volume emitted in a zone of finite radial extent and allows a consistent (albeit approximate) treatment of the innermost zones. This number, together with data from the previous zone on temperature, ionization, and the spectrum at that radius, are passed to the central routine, IONIZE, which uses the old data as a first approximation to the conditions in the next zone.

IONIZE calculates the integrals $S1$ and $S2$ and stores the integrand of $S1$ at each frequency point in an array; since the neutral fraction is as yet unknown the absorbed flux cannot yet be subtracted (eq. 2.3.12). The temperature and ionization are now found by an iterative procedure. The quantities α_{eff} and α_{coll} are calculated for the current value of the temperature parameter x_0, and then (2.3.19) is solved for f. The right hand side of (2.3.18) is then evaluated and compared with $S1$ to yield an new estimate of x_0 and the above procedure is repeated until the energy balance equation (2.3.18) is satisfied to within a tenth of a percent. A maximum of 20 iterations is allowed, and if the procedure has not converged by then a message is logged giving the size of the error. In practice this occasionally occurs in the last few zones where there is very little ionizing flux, and so the total effect on the emergent spectrum is small. Now that the ionization is known, the optical depth is calculated and the absorbed ionizing flux is removed from the spectrum. Important errors would be introduced at this point if the optical depth at any frequency were greater than 1. This is avoided by choosing

size of the next zone to have small optical depth at the highest frequency at ich there is still flux in the spectrum. The optical depth expected in the next ıe is calculated on the basis of the neutral fraction just calculated for the current ne, and set to be 0.1. This would lead to the zones becoming infinitely small at e edge of the nebula, and to avoid this two alterations are made to the scheme. rstly, when the normalized spectral intensity $\nu s(\nu)$ becomes less than 0.5% in ıy bin it is set to zero. This ensures that the zones are appropriately sized to ɔsorb the bulk of the flux. Secondly, the outer NEBULA routine adjusts the ɔne size returned by IONIZE to be always at least 0.2% of the radial coordinate , thus avoiding infinitely thin zones. This scheme leads to absorption of all the ɔnizing flux in between 100 and 200 zones.

The final stage of the IONIZE routine consists of calling another routine (EMIT) which adds the emitted nebular spectrum to the spectrum array. The ɜmission is normalized using (2.3.18) and the spectral dependence of the recombination and free-free continua is proportional to $\nu \exp(-h\nu/kT)$.

To start the routine off the temperature and ionization of the innermost zone is first calculated ignoring the effect of collisions, using (2.3.11) and (2.3.19) with α_{coll} set to zero. The normal iteration procedure is then entered with this as a starting point.

The stability of the routine has been checked by setting the collisional terms to zero and comparing the results with a simple single-zone calculation based on eqs. (2.2.6), (2.3.2), and (2.3.11). The derived size of the nebula and the effective recombination coefficient are in very close agreement. It is not clear how one could treat the collisional effects in a one-zone model.

On the following pages (Fig. 2.4- 2.6) I display the computed spectra from the NEBULA program for a variety of values of the gas density n: $n = 10^2, 10^4,$ and $10^6 \mathrm{cm}^{-3}$. The input spectrum in all cases is the blackbody model for a VMO with $M_2 = 1$. The normalized spectra are very similar for other choices of

source parameters and spectral inputs. The displayed spectra show most 2-photon emission for the lowest densities (cf. (2.3.22)) and practically none for the high density case. In the n=10^4cm^{-3}model, the 2-photon emission basically cancels the extra collisional line flux relative to the simpler model presented in Fig. 2.2.

The results of running the code for a variety of parameters are summarized in Table 2.3. The parameters which define the model are M_2, the gas density n, and the input spectral shape (BB, H, or He referring to the models discussed in section 2.1). Output results tabulated are L, the fraction of the total flux predicted to be in the Lyman alpha line, R, the computed radius of the Stromgren sphere, and $n\beta$, the ratio of gas mass within the sphere to stellar mass multiplied by the gas density (this quantity is proportional to the variable W introduced at the beginning of section 2.3). From this I have derived α, the effective recombination coefficient, and hence T5(eff), the corresponding value of T_5 for use in the equations of section (2.2). Also tabulated is T5(1/2), the actual value of T_5 at the radius where half the ionizing flux has been absorbed. The results confirm that the combination $n\beta$ is roughly constant for a given mass VMO. The run of temperature with radius is plotted for several of the models in Fig 2.7.

The numerical results predict a spectrum which has about half its flux in the Lyman line and half in the recombination continua, with a weak dependence on density. The conditions in the nebula are summarized by the equations of section 2.2 with the variable T_5 approximately equal to 0.5, although the actual temperature in the nebula is only 20000 – 30000 K because of the collisional cooling not taken into account in section 2.2.

M_2	Sp	log n ($n/1\,cm^{-3}$)	L	R (pc)	n Beta (cm^{-3})	Alpha ($10^{-20} m^3 s^{-1}$)	T5(eff)	T5(1/2)
1	BB	2	0.46	9.0	7500	9.3	0.32	0.20
	H	2	0.50	9.0	7700	6.6	0.48	0.17
	He	2	0.50	9.3	8300	7.0	0.45	0.18
	BB	4	0.53	0.44	8800	8.0	0.38	0.25
	H	4	0.59	0.41	7200	7.1	0.44	0.21
	He	4	0.57	0.42	7700	7.5	0.41	0.23
	BB	6	0.66	0.022	11200	6.3	0.52	0.33
	H	6	0.73	0.020	8200	6.2	0.52	0.27
	He	6	0.72	0.021	9400	6.2	0.53	0.30
1000	H	2	0.48	122	19000	8.5	0.36	0.25
	H	4	0.55	6.2	25000	6.5	0.50	0.34
	H	6	0.67	0.32	34000	4.7	0.76	0.48

Table 2.3

Results from the NEBULA program.
The input consists of M_2, the mass in units of 100 solar masses, Sp, the spectral model as described in section 2. , and the number density of the gas, n, in cm^{-3}.

L is the fraction of the emiited flux that is in the Lyman alpha line. R is the radius in parsecs of the ionized region. n Beta is the ratio of gas mass to stellar mass multiplied by ($n/1\ cm^{-3}$) to keep the value approximately constant for a given stellar mass (see eq. 2.2.6). Alpha is the corresponding effective recombination coefficient for the whole nebula (total number of recombinations needed to balance photoionizations by the stellar radiation field) and T5(eff) is the corresponding effective value of T5 based on the approximation $\alpha = 3.7\times10^{-20} T_5^{-0.9} m^3 s^{-1}$. It is this value of T5 which should be substituted into the equations of section 2.2. T5(1/2) is the actual value of the nebular temperature T5 at the point in the nebula where half the stellar flux has been absorbed.

Fig 2.3 One-zone radiative recombination model

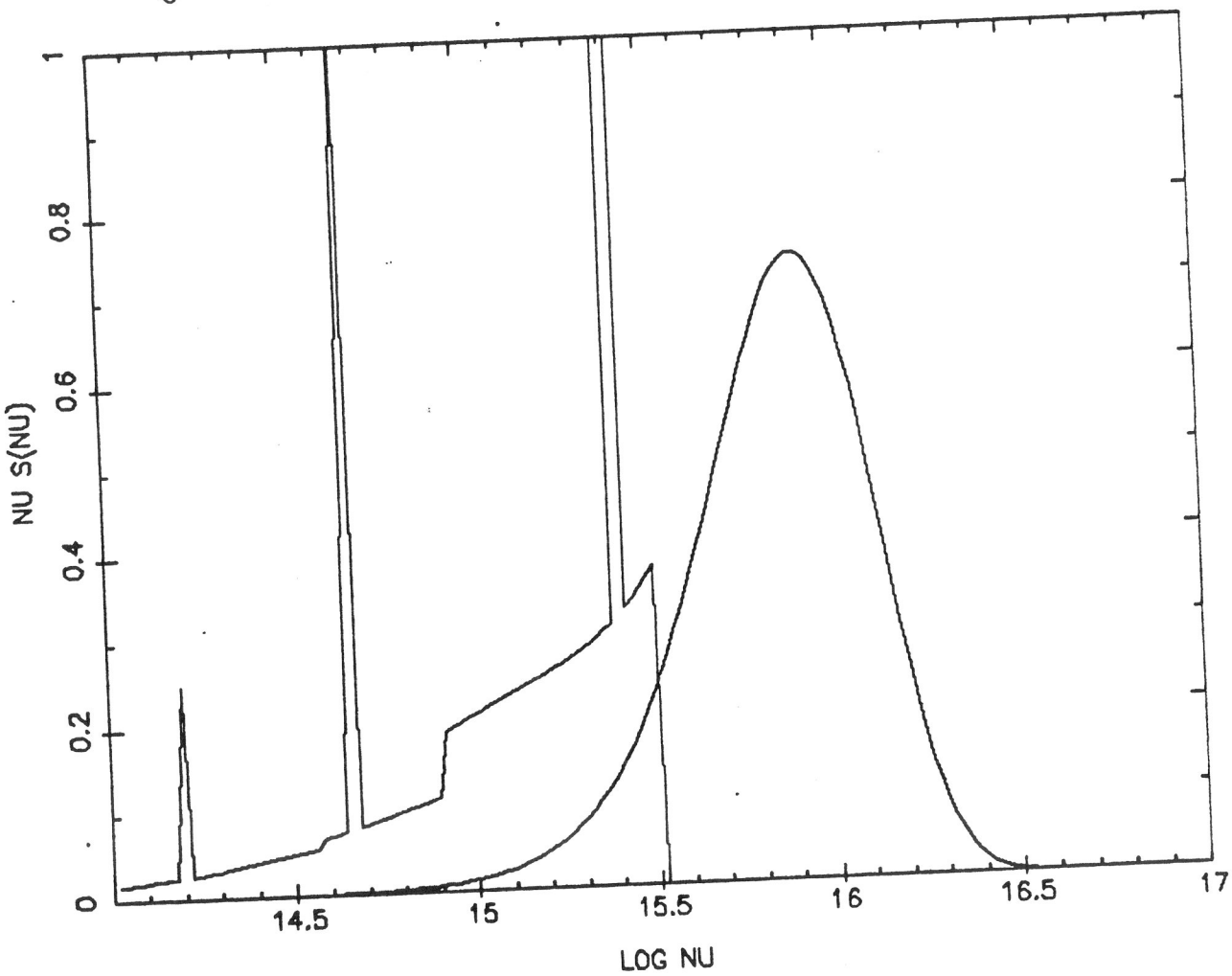

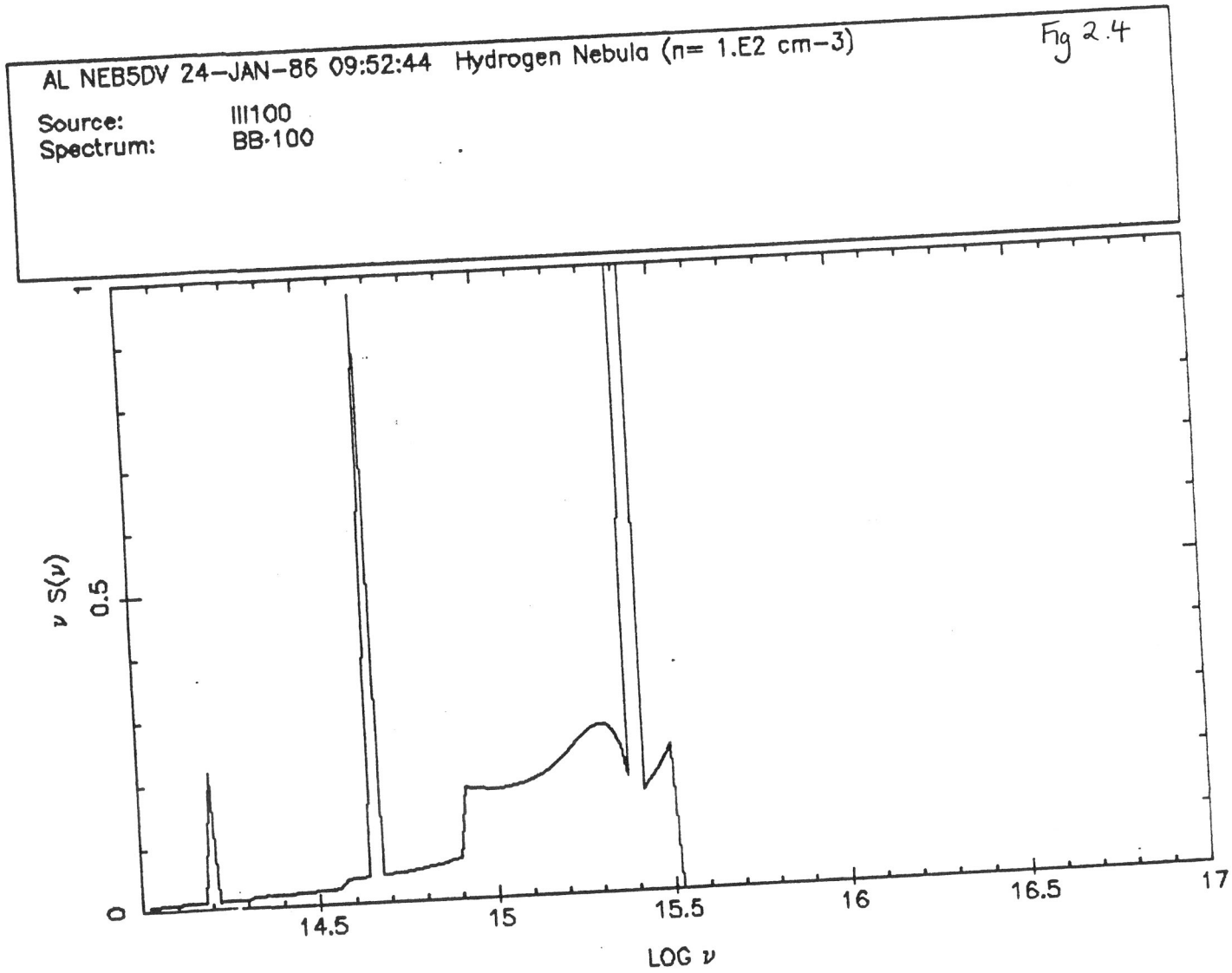
AL NEB5DV 24-JAN-86 09:52:44 Hydrogen Nebula (n= 1.E2 cm-3)
Source: III100
Spectrum: BB·100
ν S(ν)
1
0.5
0
14.5
15
15.5
16
16.5
17
LOG ν

Fig 2.4

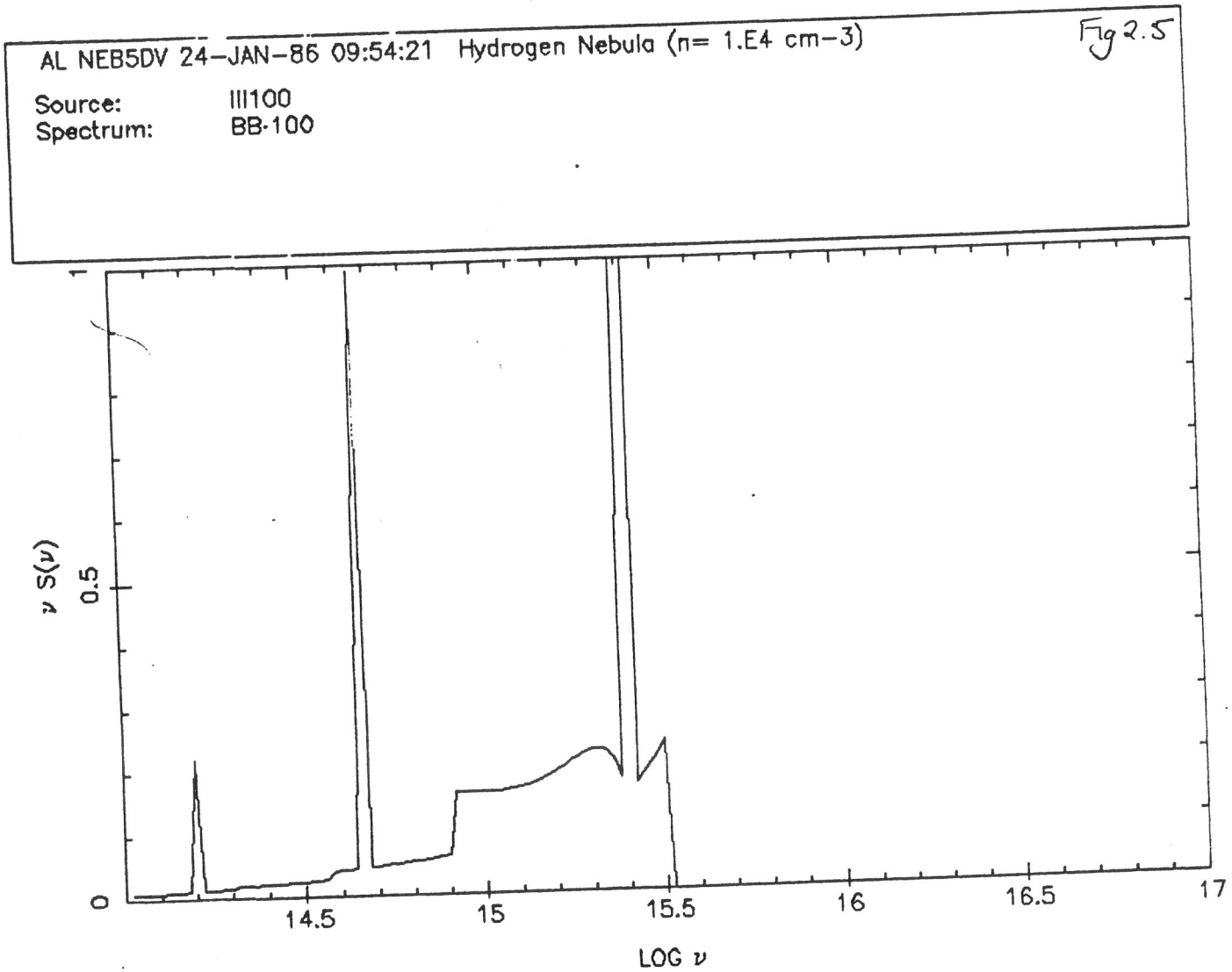
AL NEB5DV 24-JAN-86 09:54:21 Hydrogen Nebula (n= 1.E4 cm-3)
Source: III100
Spectrum: BB-100
ν S(ν)
0
0.5
14.5
15
15.5
16
16.5
17
LOG ν

Fig 2.5

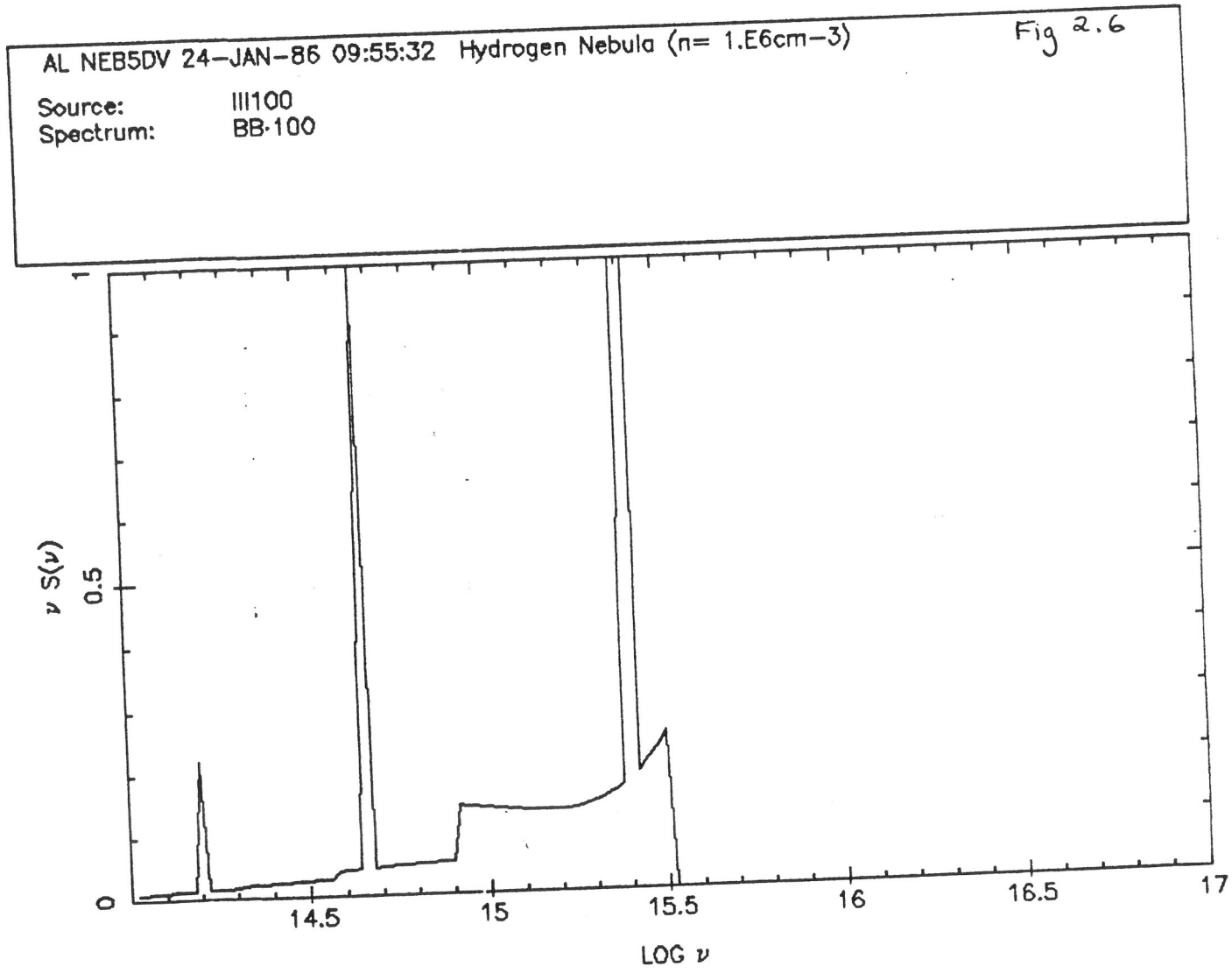
AL NEB5DV 24-JAN-86 09:55:32 Hydrogen Nebula (n= 1.E6cm-3)
Source: III100
Spectrum: BB·100
ν S(ν)
1
0.5
0
14.5
15
15.5
16
16.5
17
LOG ν

Fig 2.6

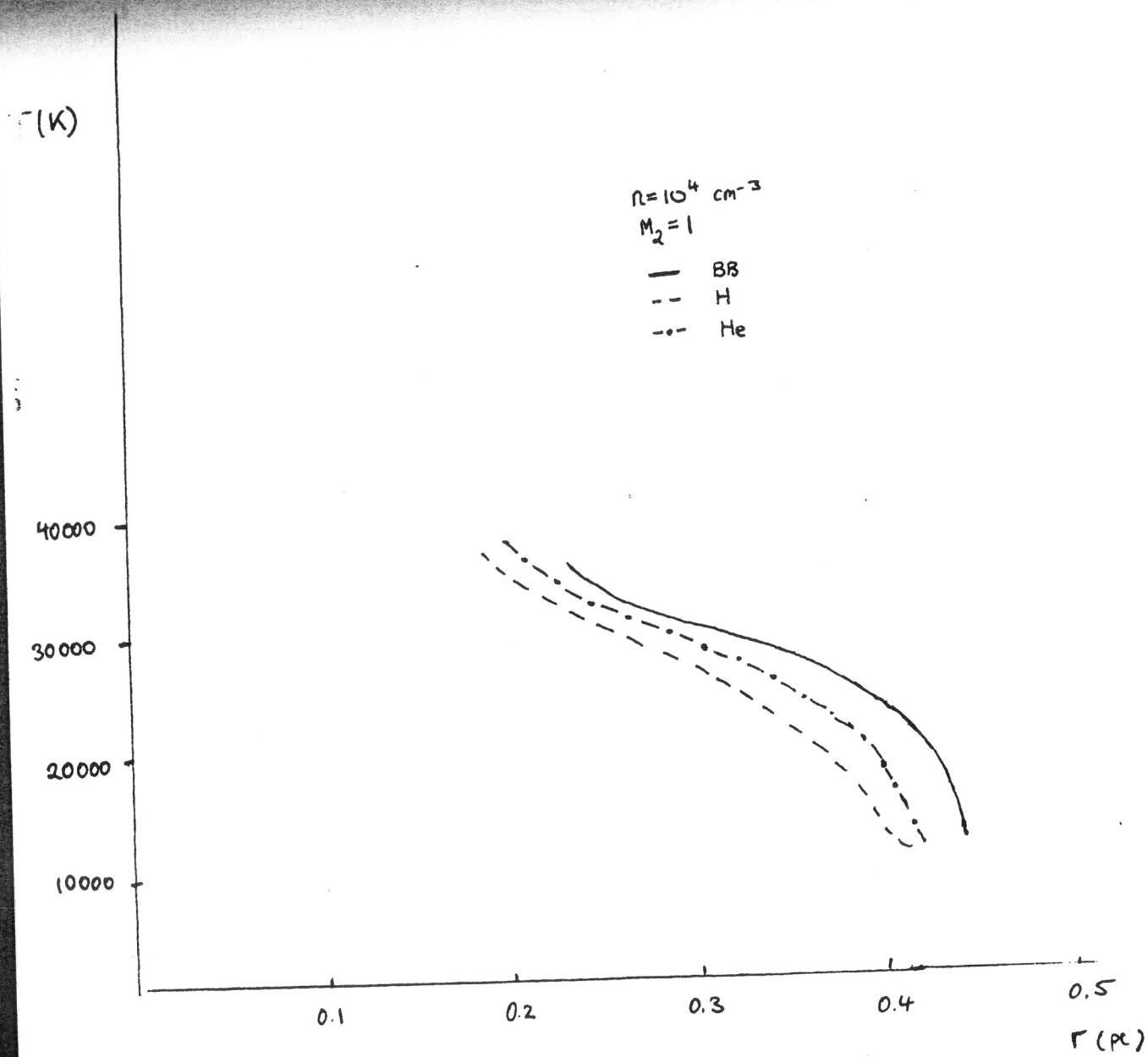

Fig 2.7 Nebular Temperatur

3. Evolution of Cosmological Background Radiation

3.1 The Spectrum of the Background Radiation

If there was a generation of stars which formed at high redshift, the radiation which they produced would be present in the universe today. It is simple to calculate the total energy density of this radiation in terms of the efficiency of the sources. Suppose that sources with density parameter Ω_* (after mass loss) converted a fraction ϵ of their rest mass to energy at a redshift z. The number density of the sources at redshift z is $\Omega_* \rho_c (1+z)^3 / Mc^2$, and the energy density falls off as the fourth power of the expansion factor, so the present energy density of the radiation in units of the critical energy density $\rho_c c^2$ is

$$\Omega_R = \frac{\epsilon \Omega_*}{1+z} \tag{3.1.1}$$

This assumes that the lifetime of the sources is small compared with an expansion time,

$$z < 390 f_t^{-2/3} \Omega_0{}^{-1/3} h_{50}^{-2/3} \tag{3.1.2}$$

It is important to notice that, if any high redshift stars existed, this energy density must be present in the extragalactic background at some wavelength, whatever sources of opacity intervene. However, if the universe is full of dust, the radiation may be reprocessed to the far infrared where our observational knowledge is very limited at present. This point has been emphasized by Bond, Carr, and Hogan (1985).

We can derive predictions which are more directly tied to observation by adopting a specific spectral model for the sources and explicitly considering extinction in the intervening medium. We denote by $s(\nu)d\nu$ the fraction of the luminosity between frequencies ν and $\nu + d\nu$ coming from each individual source (after modification by its local environment if appropriate.) The intensity of the

background produced locally is

$$i(\nu) = \epsilon M c^2 n_* s(\nu)/4\pi \tag{3.1.3}$$

for a population of sources of mass M and number density n_*. We represent the radiation field energy density by the dimensionless parameter

$$\begin{aligned} \omega(\nu, z) &= \frac{4\pi\nu i(\nu)}{\rho_c c^3} \\ &= \epsilon\Omega_*(1+z)^3 \nu s(\nu) \end{aligned} \tag{3.1.4}$$

where ρ_c is always the present critical density (not that at redshift z). The time evolution of the energy density in the expanding universe is given by

$$\partial f/\partial z = 0 \tag{3.1.5}$$

in the absence of sources, where the comoving occupation number f is related to the energy density by

$$\omega(\nu) = \frac{8\pi h}{c^3}\frac{\nu^4 f(\nu)}{\rho_c c^2} \tag{3.1.6}$$

To enable us to work in comoving frequency we define

$$\begin{aligned} \omega_0(\nu, z) &= \omega(\nu(1+z), z)(1+z)^{-4} \\ &= \frac{8\pi h}{\rho_c c^5}\nu^4 f(\nu(1+z), z) \end{aligned} \tag{3.1.7}$$

Since ν is independent of redshift, the quantity ω_0 is essentially just f times factors and is conserved in the absence of sources. Its use will simplify the equations when I consider sources and sinks of radiation in section 3.3. At present we consider simple models where the background radiation is produced at redshift z and evolves without modification as the universe expands, so

$$\begin{aligned} \omega(\nu, 0) &= \omega_0(\nu, z) \\ &= \epsilon\Omega_*\nu s(\nu(1+z)) \end{aligned} \tag{3.1.8}$$

ω is also related to the total cosmological density parameter of the radiation by

$$\Omega_R = \int \omega(\nu) d(\ln \nu) \qquad (3.1.9)$$

For comparison, the value of Ω_R for the microwave background is $10^{-4} h_{50}^{-2}$. If the present value of $\omega(\nu)$ is identified with an observed background, adoption of a model $s(\nu)$ immediately leads to Ω_*, the mass in VMOs. In practice attempts to detect and measure extragalactic background light are very difficult indeed, and all observations will be treated as upper limits, yielding upper limits for the maximum possible mass in an early generation of very massive stars (see Chapter 5).

I consider the four simple models for $s(\nu)$ described in section 2.1: the black-body (BB) model, the pure hydrogen stellar atmosphere model (H), the H/He stellar atmosphere model (He), and one of the models discussed in section 2.3, which I shall call the 'Recombination' or R model. The R model is the one plotted in Fig 2.5. Illustrative predicted background radiation spectra for the BB model are plotted in Fig. 3.1 for several different redshifts (z= 5,20,100); the spectra have been normalised by setting Ω_* =0.1 and the microwave background is included on the plot for comparison. The VMO model adopted is the one for $10^5 M_\odot$ which approaches the limiting values of the f parameters define in chapter 2. This model is labelled IIIVMO in the 'Source' field of the diagram headers. Fig 3.2 illustrates the spectra obtained by using the R model; obviously the flux is at lower frequency for a given redshift. Consequently, at a given frequency, the corresponding redshift of any Population III background radiation is lower for the R model than the BB model and hence the value of Ω_* needed to account for a given flux is lower, except insofar as this effect is mitigated by the smaller continuum flux of the R model.

Fig 3.3 shows the effect of changing the source parameters from those of the IIIVMO model (dotted line) to those of a 100 $M_\odot$ VMO (solid line), keeping the value of Ω_* constant. The BB spectral model has been used. The change in the

'f parameters' introduces only neglible changes in the resulting spectrum. This important result means that our results are insensitive to the mass spectrum and typical mass of the VMOs and only depend on their total mass density as measured by the parameter Ω_* . I will henceforth adopt the $10^5 M_\odot$ IIIVMO model for all the remaining Population III background calculations in this chapter.

Fig 3.4 compares the four different spectral models, all plotted for Ω_* =0.1, and $z_* = 20$. Note that this plot is log-log while Fig 2.2, which illustrates the normalized spectral models is linear-log. The low frequency cutoff in the R model is arbitrary and unphysical, but the high frequency cutoff occurs at the Lyman limit. This plot well illustrates the enormous amount of ionizing flux produced by the other three models.

Fig 3.1

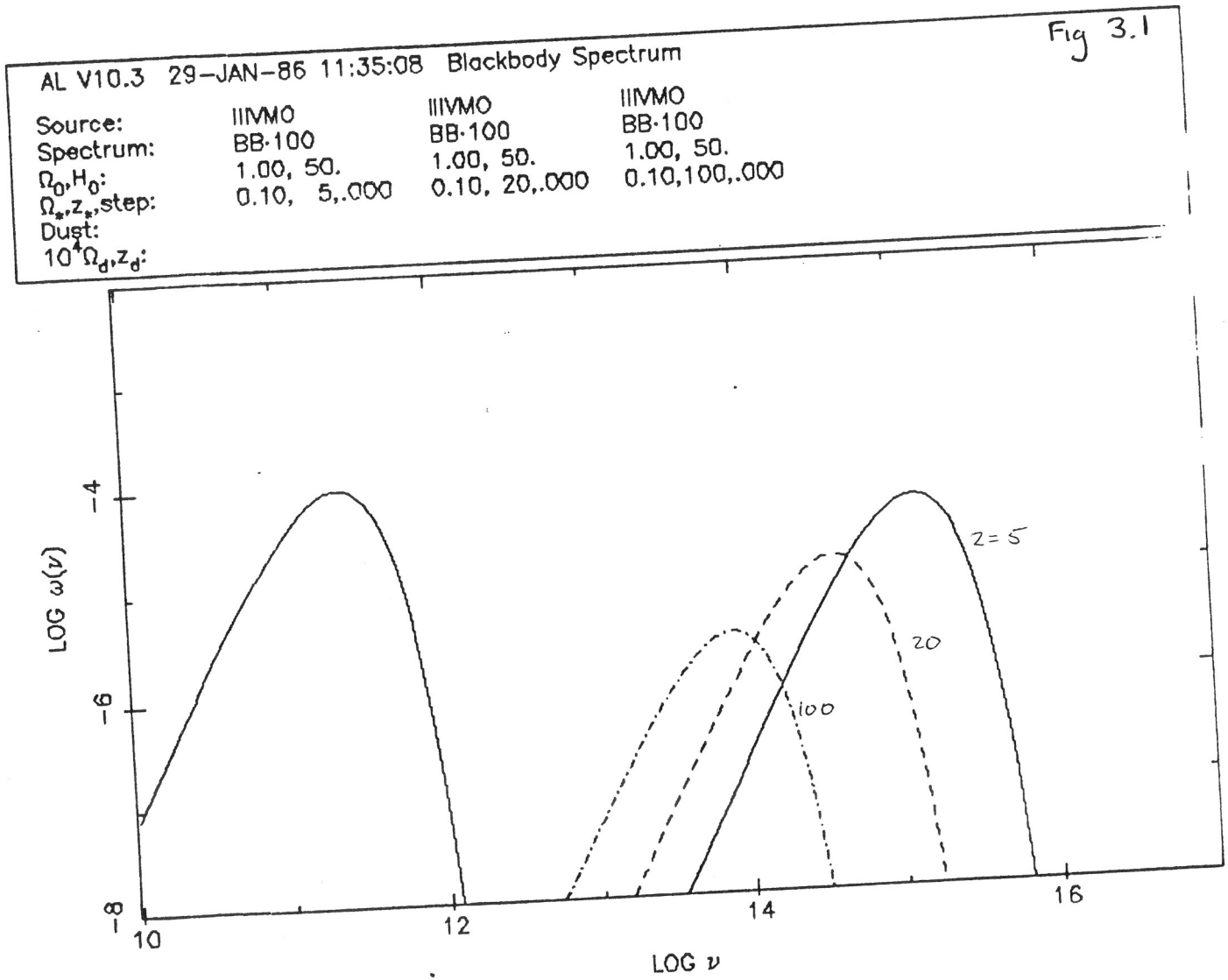
AL V10.3 29-JAN-86 11:35:08 Blackbody Spectrum
Source: IIIVMO IIIVMO IIIVMO
Spectrum: BB·100 BB·100 BB·100
Ω0,H0: 1.00, 50. 1.00, 50. 1.00, 50.
Ω*,z*,step: 0.10, 5,.000 0.10, 20,.000 0.10,100,.000
Dust:
10^4Ωd,zd:
LOG ω(ν)
-4
-6
-8
10
12
14
16
LOG ν
z=5
20
100

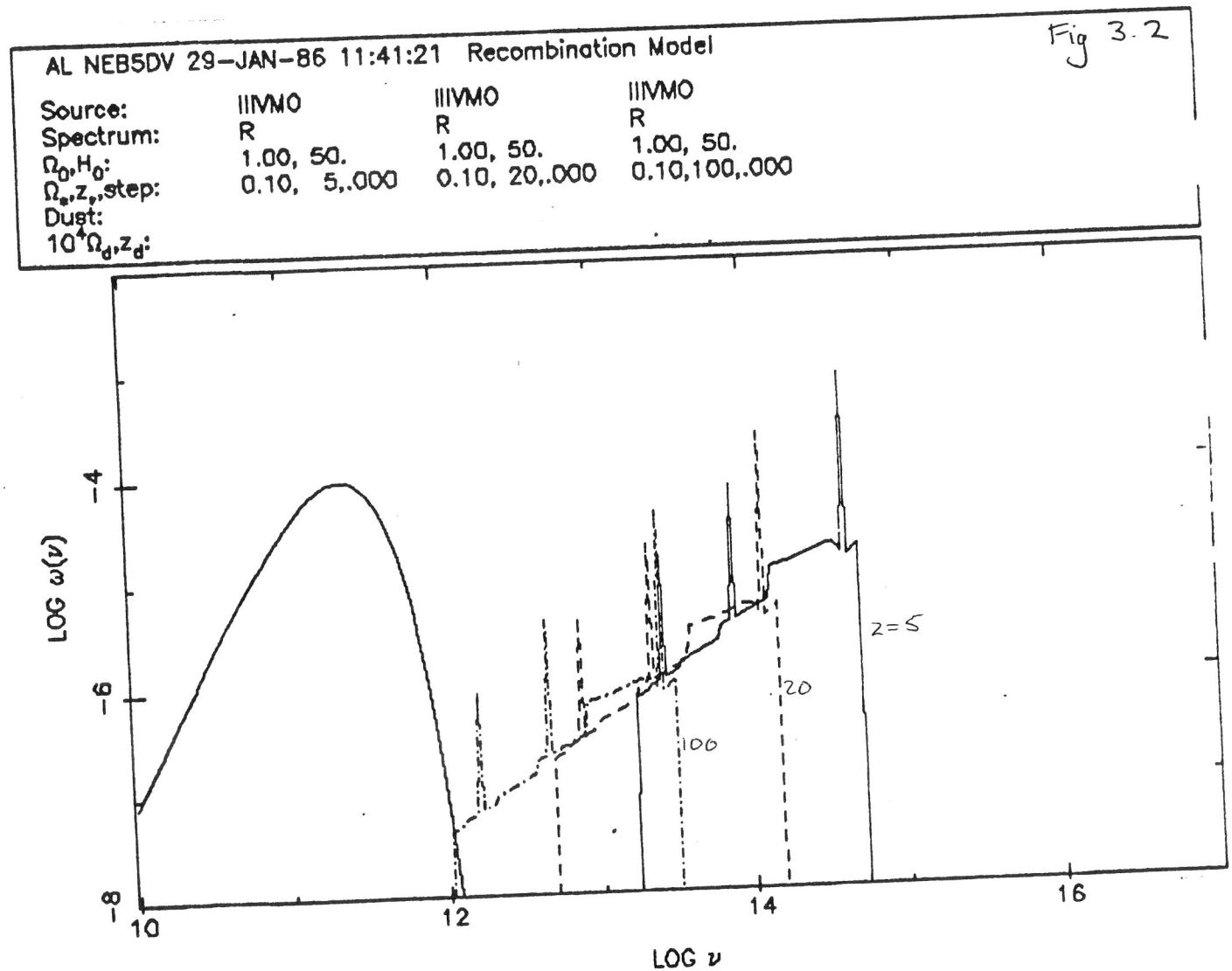
AL NEB5DV 29-JAN-86 11:41:21 Recombination Model
Source: IIIVMO IIIVMO IIIVMO
Spectrum: R R R
Ω_0, H_0: 1.00, 50. 1.00, 50. 1.00, 50.
Ω_*, z_*, step: 0.10, 5,.000 0.10, 20,.000 0.10,100,.000
Dust:
$10^4\Omega_d, z_d$:
LOG ω(ν)
-4
-6
-8
10
12
14
16
LOG ν
z=5
20
100

Fig 3.2

Fig 3.3

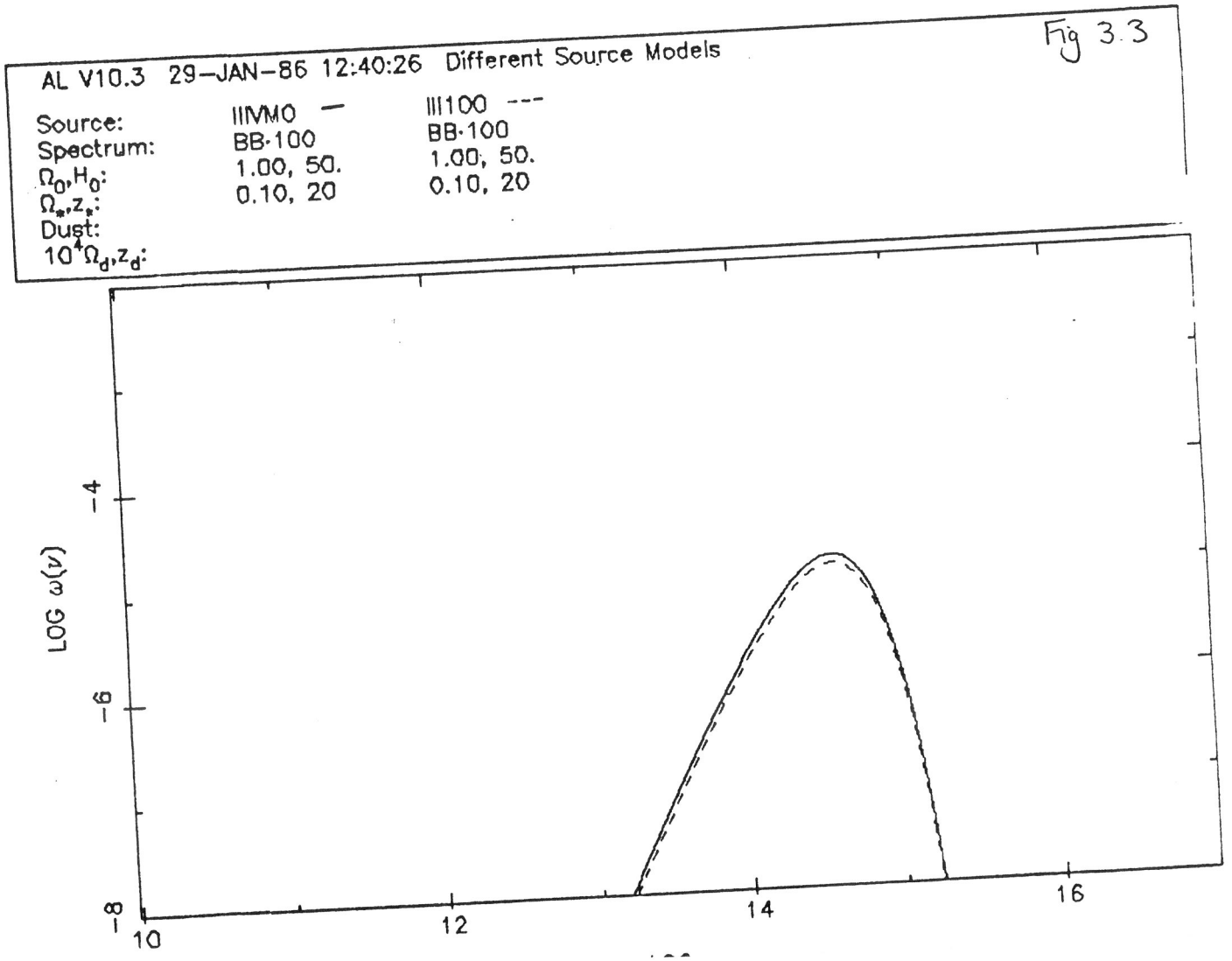
AL V10.3 29-JAN-86 12:40:26 Different Source Models
Source: IIIVM0 — III100 ---
Spectrum: BB·100 BB·100
Ω_0, H_0: 1.00, 50. 1.00, 50.
Ω_*, z_*: 0.10, 20 0.10, 20
Dust:
$10^4\Omega_d, z_d$:
LOG ω(ν)
-4
-6
-8
10
12
14
16

Fig 3.4

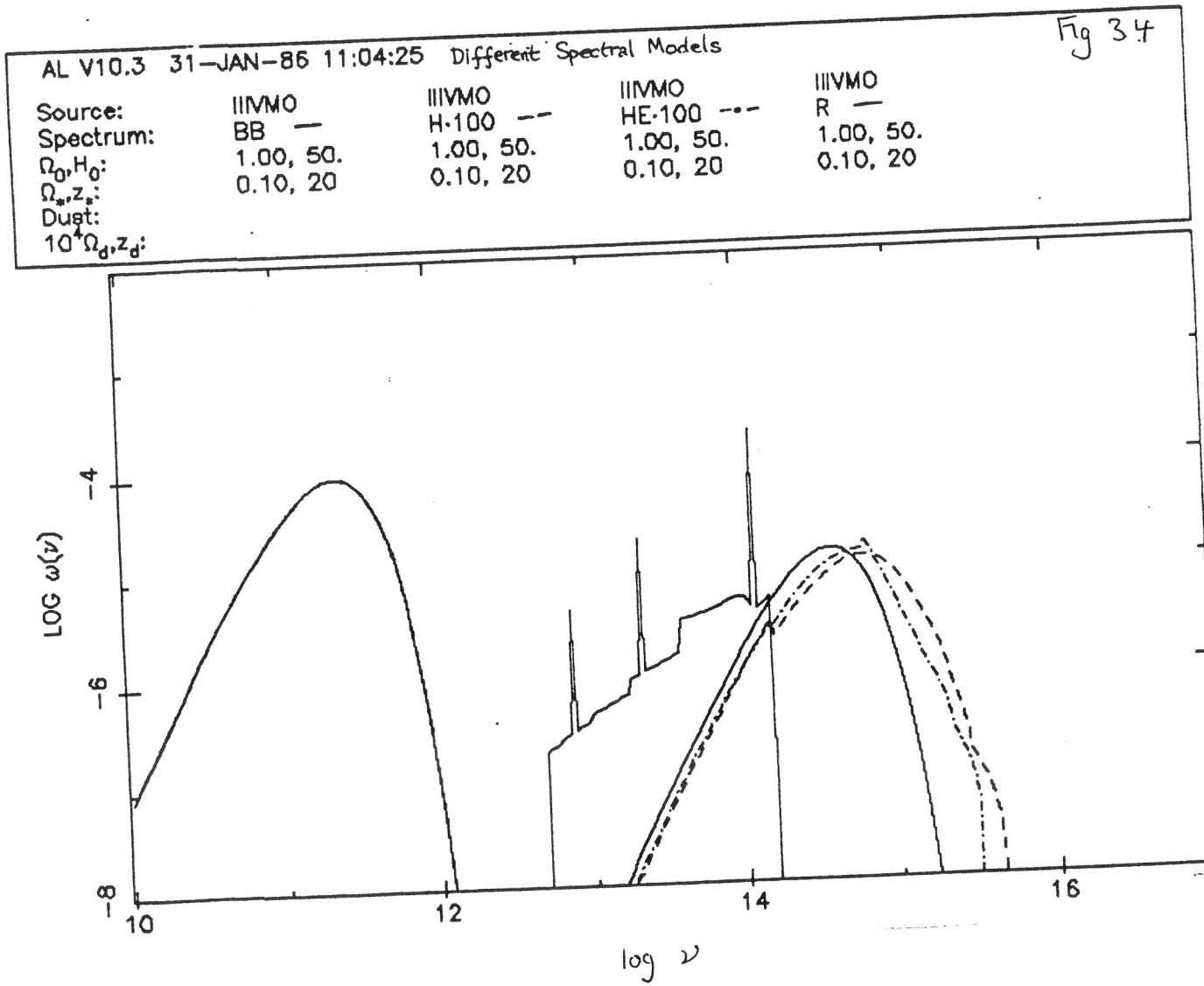
AL V10.3 31-JAN-86 11:04:25 Different Spectral Models
Source: IIIVMO
Spectrum: BB —
Ω0,H0: 1.00, 50.
Ω*,z*: 0.10, 20
Dust:
10⁴Ωd,zd:
IIIVMO
H·100 --
1.00, 50.
0.10, 20
IIIVMO
HE·100 -·-
1.00, 50.
0.10, 20
IIIVMO
R —
1.00, 50.
0.10, 20
LOG ω(ν)
-4
-6
-8
10
12
14
16
log ν

3.2 Opacity of the Universe at high redshift

In chapter 2 we considered the effects of diffuse material on the individual spectra of each of the sources. We now consider the effect of more widely distributed diffuse material on the evolution of the background radiation as a whole.

3.2.1 Absorption by neutral hydrogen in the Universe

We extend the calculation of section 2.2 using the same notation, with $\beta = \Omega_g/\Omega_*$. If the condition (2.2.18) is not satisfied for the gas surrounding the VMOs, the ionizing radiation from the VMOs will ionize the universe completely. However, even though the recombination time is not short enough for the hydrogen to absorb all the photons within the lifetime of the stars, they may still be absorbed after the sources have turned off. Since the stars emit a total of $\dot{N}t_{ms}$ photons, the universe will be filled with a photon number density $\dot{N}t_{ms}n_*$. A photon travelling through clumps of density n with a volume filling factor δ^{-1} will spend a fraction $1/\delta$ of its time in clumps, so in a time t its path length through the dense gas is ct/δ and the optical depth is

$$\tau = (1-x)n\sigma_H ct/\delta \tag{3.2.1}$$

where x is the ionized fraction. There are $\tau\dot{N}t_{ms}n_*/t$ ionizations per unit volume per unit time in the gas . Equating this to the number of recombinations in the gas gives a total photon optical depth for time t

$$\tau = \left(\frac{\alpha n^2/\delta}{\dot{N}n_*}\right)\frac{t}{t_{ms}}, \tag{3.2.2}$$

so $\tau > 1$ if

$$\delta \geq (\dot{N}/\alpha n_*)(m_H/\beta Y_H M)^2(t_{ms}/t), \tag{3.2.3}$$

If $t = t_{ms}$, we recover the previous analysis. This condition can also be expressed by saying that each atom must recombine at least as many times within the main sequence time as the total number of ionizing photons emitted per atom in the gas. If t is the expansion time, we obtain instead

$$\delta > 2.2 \times 10^6 T_5^{0.8}(\beta Y_H)^{-2}(\Omega_* h_{50}^2)^{-1}(\Omega_0 h_{50}^2)^{\frac{1}{2}}(1+z)^{-\frac{3}{2}} f_N f_t^{-1} \tag{3.2.4}$$

as the condition that the photons will be absorbed within an expansion time. If the photons cannot be absorbed within a time of order the expansion time, the bulk of the photons will be redshifted below the Lyman limit without being absorbed. Hence the spectrum may reach us largely unaltered if the gas associated with the VMOs is not so highly clumped that its recombination time is very short, the clumpiness being given by δ above. The ionization of the clumps is found to be given by

$$1 - x = \left(\frac{\alpha}{\dot{N}\sigma c t_{ms}}\right)\left(\frac{\beta Y_H M}{m_H}\right)\delta \qquad (3.2.5)$$
$$= 2 \times 10^{-12}\delta(T_5^{-0.8}\beta Y_H f_N^{-1} f_t^{-1})$$

If we identify the clumps with the mass in galaxies now, then $\beta = 0.1$ at most, so for $\Omega_* = 0.1$ we get $\delta = 10^9(1+z)^{-1.5}$, which is much higher than the overdensity of gas in galaxies relative to the background at any redshift. If the gas is not associated with galaxies, then δ could be as small as 10^2 at z=100, for large β, and this is just plausible. In Fig 3.5 I plot the (z,Ω_*) regimes in which the universe is ionized for an assumed amount of gas $\Omega_g = 0.1$ and clumpiness factor δ. I also indicate the regime in which the absorption occurs in the locality of the sources. This diagram has been plotted assuming $T_5 = 0.1$ and is valid providing $\Omega_* / \Omega_g > 3 \times 10^{-6}$, which is always true if we are trying to provide the dark matter with Ω_* . If the latter condition is not satisfied, then $t_{rec} > t_{ms}$ and there are not enough photons produced by the star over its lifetime to ionize all the atoms around it and the ionizing flux is all absorbed locally (Couchman 1985). The dotted lines in Fig 3.5 indicate where this constraint lies for different values of δ. Below these dotted lines the flux is always absorbed locally.

3.2.2 Dust absorption in the Universe

Now let us consider the effects of dust in the universe, as the photons are redshifted to the present epoch. There will be absorption due to both any dust in a uniform intergalactic medium, and to dust in galaxies along the line of sight. As

pointed out by Ostriker and Heisler (1984), the patchiness of this latter effect may allow it to obscure high redshift objects without the revealing presence of partially obscured objects at lower redshifts. The obscuration is uncertain due to our lack of knowledge of the evolution of dust content in galaxies, and of the size of the absorbing region in a typical galaxy. Ostriker and Heisler pointed out that in an exponential disk galaxy the radius corresponding to a given optical depth through the disk will increase (due to the increase in dust opacity with the frequency of the photon) at high redshift. This leads to very high effective cross sections for high redshift galaxies, and a high covering factor of the galaxies on the sky at a given redshift. However it is not clear that the gas and dust distribution in galaxies follows the light distribution in this way. In fact, modern observations indicate (Blitz, Fich and Kulkarni 1983) that the hydrogen surface density in our galaxy is fairly constant out to a radius of 20 kpc and then cuts off sharply. Of course, it may just be that the hydrogen is ionized beyond this point, but the warping and scalloping of the disc in this region suggests that the galaxy may have a recognizable edge rather than just going on for ever. This density profile, provided that the dust-to-gas ratio does not increase with galactocentric radius, will result in a galaxy effective radius that is constant with redshift (although the optical depth through it will still increase, the covering factor due to galaxies will not be so large). At high redshifts, more of the mass of a galaxy may be in diffuse form, but the dust-to-gas ratio may be smaller, and the size of the dusty region may be smaller if infall and collapse are not complete. We therefore believe that the covering factor calculated below is a not unreasonable estimate. At the Lyman edge, neutral hydrogen absorption will be more important than dust (at a normal dust-to-gas ratio of order 10^{-2}) provided the neutral fraction is more than 5×10^{-4}. Within an expansion time of the Population III era, when the universe might be filled with large numbers of ionizing photons, the neutral fraction could be significantly less than this, so dust might still be the most important opacity

source even at those high frequencies.

We adopt representative values of galaxy radius r =20 kpc, area $A_G = \pi r^2$, disc thickness H= 200 pc, optical depth through the disk $\tau_G(\nu) = \kappa(\nu) m_H \chi n H$ or $\tau_G(\nu) = 0.5(\chi/0.01)(\nu_{15})$, where $\nu = 10^{15}\nu_{15}$Hz and comoving galaxy number density $n_G = 0.01$ Mpc^{-3}.

Consider a disk galaxy at an angle θ to the line of sight; it has projected area $A_G cos\theta$, and there are $n_G d(cos\theta)$ such galaxies per unit volume, each with optical depth along the line of sight $\tau_G(\nu) sec\theta$. The covering factor is then

$$\begin{aligned} N =& \frac{1}{2} n_G A_G c H_0^{-1} \int_0^z (1+z)^{\frac{1}{2}} dz \\ =& 0.025 h_{50}^{-1} ((1+z)^{1.5} - 1) \end{aligned} \tag{3.2.6}$$

and the optical depth along the line of sight at comoving frequency $\nu_0 = 10^{15}\nu_{15}$Hz is

$$\begin{aligned} \tau(\nu_0, z) =& n_G A_G \tau_G(\nu_0) c H_0^{-1} \int_0^z (1+z)^{1.5} dz \\ =& 0.015 \nu_{15} (\chi/0.01) h_{50}^{-1} ((1+z)^{2.5} - 1) \end{aligned} \tag{3.2.7}$$

assuming that z is large enough that there are always several galaxies along the line of sight, i.e. $N > 1$ or $z > 11$ (in agreement with Bond, Carr, and Hogan (1986)).

For the uniform intergalactic medium the optical depth may be quite large. Limits from reddening in QSOs (Wright 1981) suggest that any intergalactic dust has $\Omega_d < 1.2 \times 10^{-4}$. Assuming this maximum amount gives

$$\tau(\nu, z) = 0.24 \nu_{15} \frac{\Omega_d}{10^{-4}} h_{50}^{-1} ((1+z)^{2.5} - 1) \tag{3.2.8}$$

(see section 3.4). Hence the maximum possible optical depth due to a dusty IGM could be substantially larger than that due to galaxies. At high redshifts such an obscuration would be of great importance. The Lyman limit is at a comoving frequency of $\nu_{15} = 3.3(1+z)^{-1}$, corresponding to an optical depth from eq. (3.2.8)

of $0.6z^{1.5}$ at large z. This would completely obscure sources at high redshifts. However, this assumes that the dust existed at these redshifts. If the Population III objects form well before galaxy formation, the upper limit in the integral should probably be the redshift of galaxy formation rather than that of the sources.

In summary, galactic absorption must exist but may not cover the sky; uniform dust would be important but may not exist. It appears impossible to resolve the issue of the importance of dust absorption at present. In later sections we present results assuming no dust, dust forming at z=3, and dust forming at the same epoch as the stars, to illustrate the likely range of effects. In Fig 3.6 I plot the (z,Ω_d) regimes in which the universe is opaque according to this calculation as dotted lines. Fig 3.6(a) gives lines corresponding to $\tau(\nu) = 1$ at observed frequencies $\log\nu$ =12, 13, 14, 15, and 16. For a given Ω_d the graph gives the redshift out to which the universe is transparent at a given observed frequency. The lines in Fig 3.6(b) correspond to unit optical depth at constant comoving frequency, allowing one to estimate the redshift beyond which a source peaking at that frequency will be obscured. The solid lines in Fig 3.6 are discussed in section 3.4 and refer to an alternative model for the opacity law.

Fig 3.5 Hydrogen Absorption

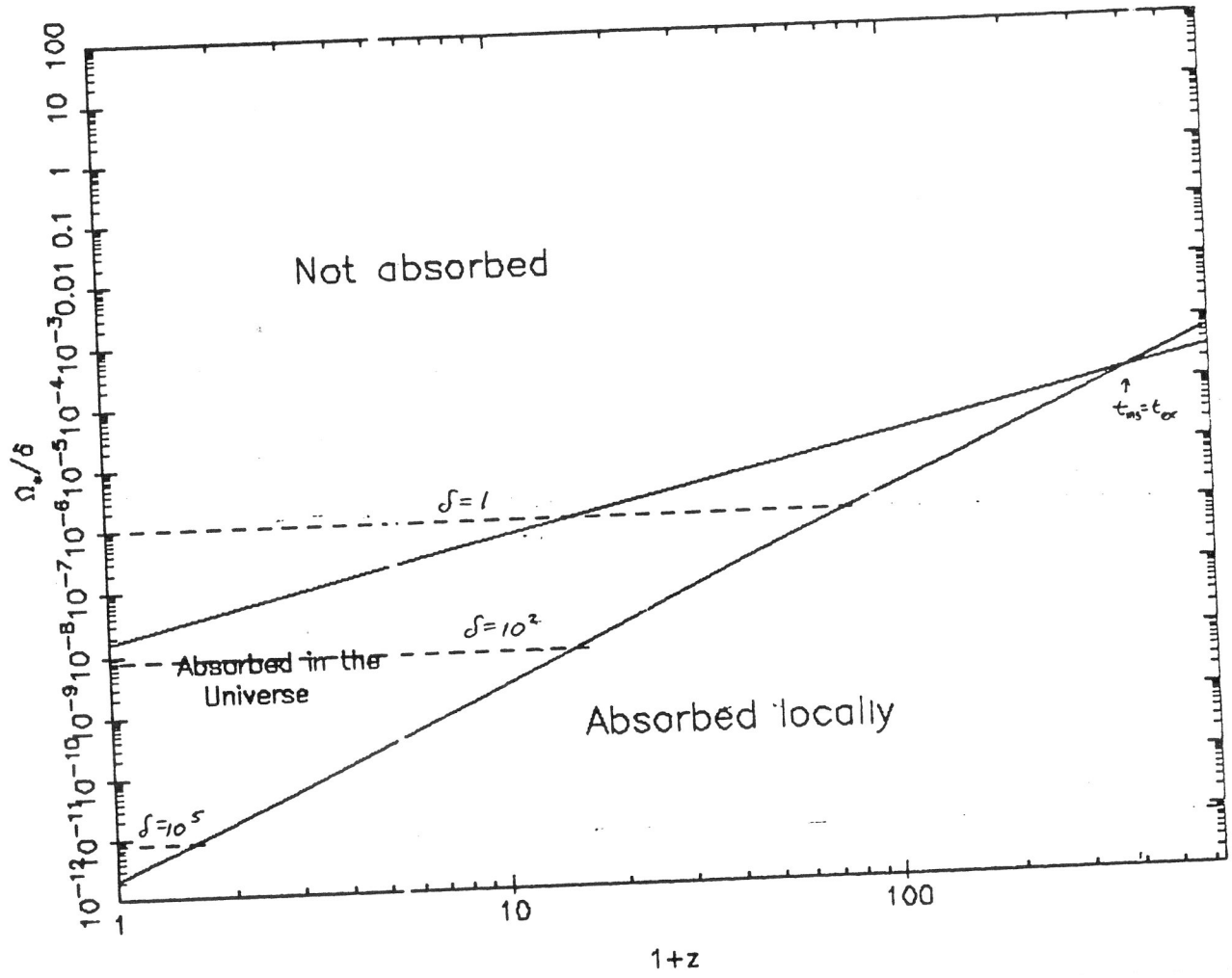

Fig 3.6 (a) Dust Absorption (Observed ν)

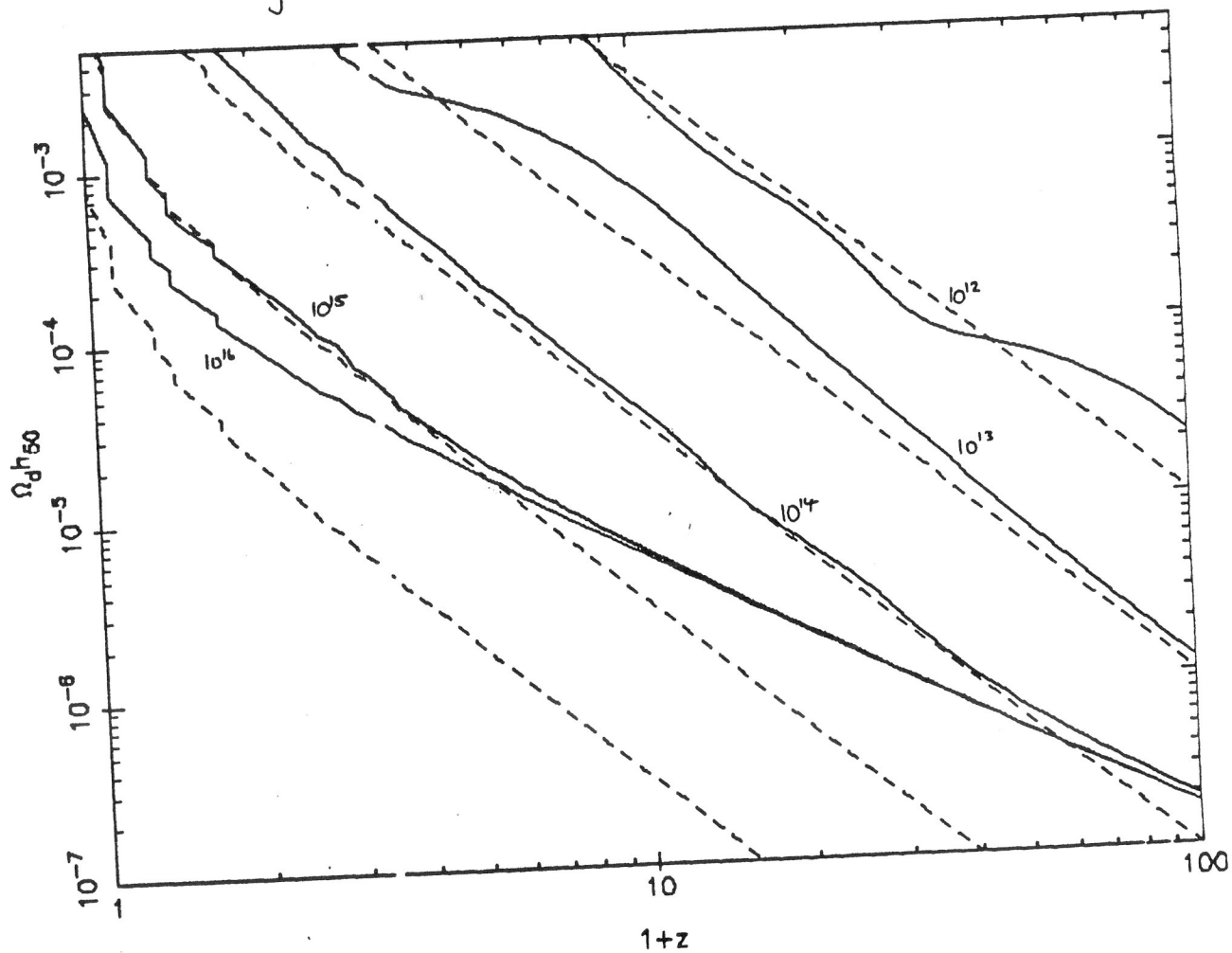

Fig 3.6(b) Dust Absorption (Comoving ν)

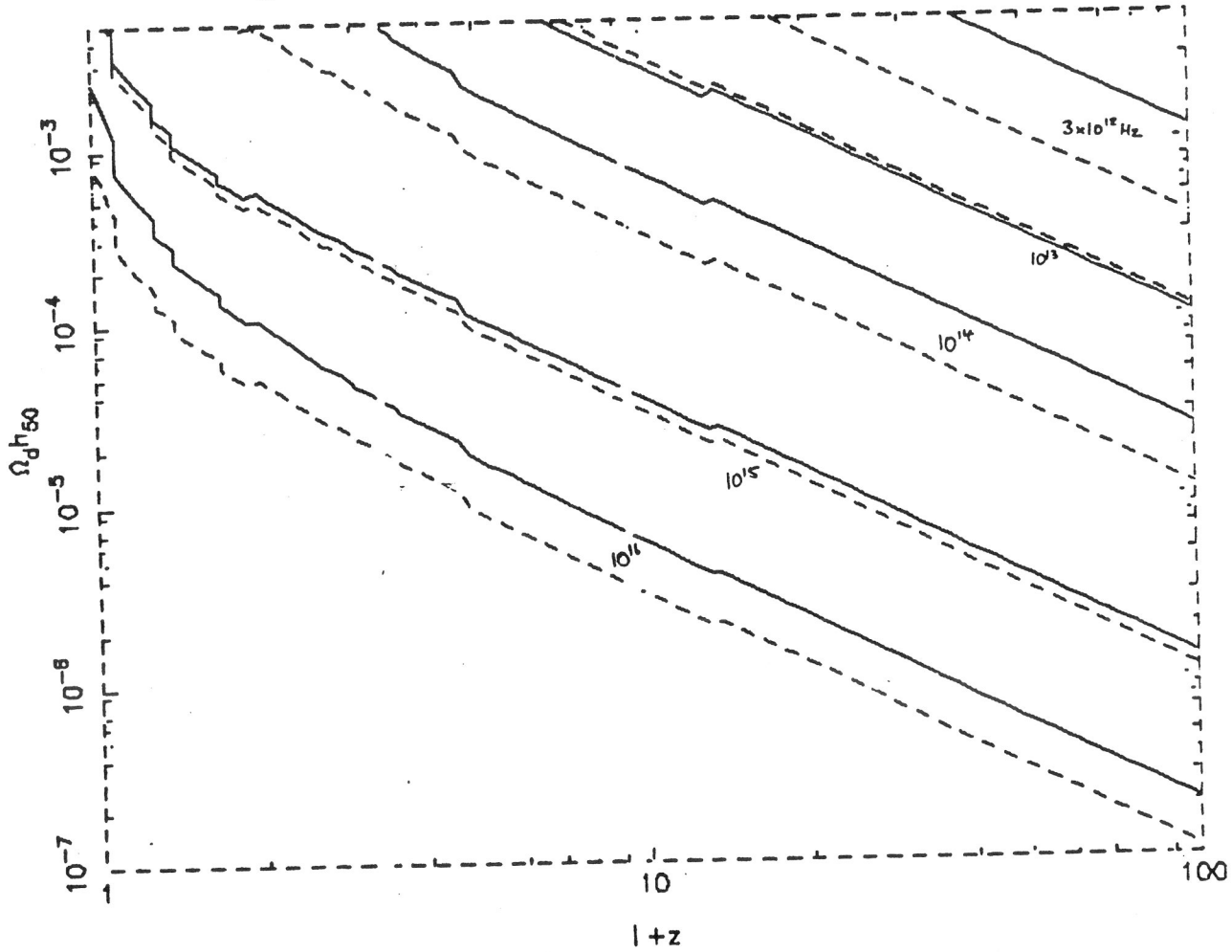

3.3 Modelling the Spectrum in a Dusty Universe

If we take into account the absorption due to the intergalactic medium, or consider Population III star formation over an extended redshift range, we must solve the radiative transfer problem. Since the neutral hydrogen in the IGM cannot have a large optical depth (eq (2.2.18) with $\delta = 1$), we only consider the absorbing effects of dust, which is assumed to reach a steady state on timescales much shorter than the expansion time. If the epochs of Population III and dust formation are t_* and t_d respectively, t_0 is the present, then

$$\omega(\nu, 0) = \omega_0(\nu, z(t_*)) + \int_{t_*}^{t_0} (F_*(\nu, t) + F_d(\nu, t))dt \tag{3.3.1}$$

and the source terms are

$$F_*(\nu, t) = \epsilon\Omega_*\nu s(\nu(1+z))/t_{ms} \tag{3.3.2}$$

for $t_* < t < t_* + t_{ms}$, and

$$F_d(\nu, t) = \Omega_d\rho_c(1+z)^3\kappa(\nu(1+z))\chi c(\omega_{eq}(T, \nu(1+z))(1+z)^{-4} - \omega_0(\nu, z)) \tag{3.3.3}$$

for $t > t_d$; here the dust temperature T is found from

$$\int_0^\infty F_d(\nu)d(\ln\nu) = 0 \tag{3.3.4}$$

and the dust emission follows a Planck distribution

$$\omega_{eq}(T, \nu) = \frac{8\pi h}{\rho_c c^5}\frac{\nu^4}{\exp(h\nu/kT) - 1} \tag{3.3.5}$$

modified by the dust cross-section as shown in eq.(3.3.3).

In general equations (3.3.1) and (3.3.4) must be solved numerically. In order to adequately test the numerical code, it is crucial to find an analytic solution to the equations, although this need not be based on a physical model. In fact an approximate analytical solution may be found with a simple and physically quite

reasonable model, involving blackbody input spectra and a linear dust opacity law.

First, as in chapter 2, we adopt the approximation that $\kappa(\nu) = (\nu/\nu_0)\kappa_0$. Then

$$\int \kappa(\nu(1+z))\omega_{eq}(T,\nu(1+z))(1+z)^{-4}d(\ln\nu) = 4!\zeta(5)\frac{8\pi h}{\rho_c c^5}\left(\frac{kT}{h(1+z)}\right)^5(\kappa_0/\nu_0)(1+z) \tag{3.3.6}$$

which allows us to find T explicitly in terms of the incident spectrum,

$$T^5 = 0.04(h/k)^5\left(\frac{\rho_c c^5}{8\pi h}\right)\int \omega_0(\nu,z)d\nu \tag{3.3.7}$$

Next adopt the blackbody model for the source spectrum, and omit the cosmic microwave background for simplicity. We choose $z_* \geq z_d$ and assume $t_{ms} \ll t_*$ so that after z_d there is no further contribution from the stars. Then

$$\omega_0(\nu,z_d) = \frac{\epsilon\Omega_*}{1+z_*}\frac{15}{\pi^4}\frac{y^4}{e^y-1} \tag{3.3.8}$$

where

$$y(\nu) = \frac{h\nu(1+z_*)}{kT_*} \tag{3.3.9}$$

The radiative transfer equation (3.3.1) can be written

$$\frac{\partial\omega_0(\nu)}{\partial\tau(\nu,z)} = \omega_{eq}(T/(1+z),\nu) - \omega_0(\nu,z) \tag{3.3.10}$$

where the optical depth between z_* and z is

$$\begin{aligned}\tau(\nu,z) &= \Omega_d\rho_c c\int_z^{z_d}\kappa(\nu(1+z))(1+z)^3\frac{dt}{dz}dz \qquad (3.3.11)\\ &= \frac{2}{5}\Omega_d\rho_c c\Omega_0{}^{-\frac{1}{2}}H_0^{-1}(\kappa_0/\nu_0)\frac{kT_*(1+z_*)^{-1}}{h}((1+z_d)^{2.5}-(1+z)^{2.5})y\\ &= \lambda(z)y\end{aligned}$$

where the approximate cosmology of section 1.5 has been used and $y(\nu)$ is defined in eq.(3.3.9).

If we assume that the stellar radiation and dust emission do not overlap in frequency, then above some comoving frequency ν_1

$$\omega_0(\nu, z) = \omega_0(\nu, z_d)e^{-\tau(\nu,z)}. \tag{3.3.12}$$

For the moment we treat the case where the universe is optically thin to the dust emission, so τ is small for $\nu < \nu_1$. In this case we can write

$$\int_0^\infty \kappa(\nu(1+z))\omega_0(\nu, z)d(\ln \nu) = \frac{15}{\pi^4}\frac{\epsilon\Omega_*}{1+z_*}\frac{kT_*}{h(1+z_*)}(1+z)I(\lambda(z)) \tag{3.3.12}$$

where the integral

$$I(\lambda) = \int_0^\infty \frac{y^4 e^{-\lambda y}dy}{e^y - 1} \tag{3.3.13}$$

can be expressed in terms of the hexagamma function $\psi^{(4)}(x)$ (Abramowicz and Stegun 1965),

$$I(\lambda) = -4!\psi^{(4)}(1+\lambda) = 4!\sum_{k=0}^{\infty}(\lambda + k)^{-5} \tag{3.3.14}$$

Note that $I(0) = 4!\varsigma(5)$ as expected. Fig 3.7 shows $(I(\lambda)/4!)^{1/5}$ as a function of λ.

Combining equations (3.3.6) and (3.3.12) we now derive an expression for the dust temperature,

$$\left(\frac{T}{(1+z)}\right)^5 = \frac{15}{8\pi^5}\frac{\rho_c c^5 h^3}{k^4}\frac{\epsilon\Omega_* T_*}{(1+z)^2}\frac{1}{\varsigma(5)}\sum_{k=0}^{\infty}(\lambda(z)+k)^{-5} \tag{3.3.15}$$

Substituting in numerical values,

$$\frac{T}{1+z} = 45(\Omega_*\, h_{50}^2 f_\epsilon f_T)^{\frac{1}{5}}(1+z_*)^{-\frac{2}{5}}\left(\frac{1}{\varsigma(5)}\sum_{k=0}^{\infty}(\lambda(z)+k)^{-5}\right)^{\frac{1}{5}} \text{K} \tag{3.3.16}$$

As the stellar radiation is absorbed, $T/(1+z)$ slowly falls from its initial value. To solve for the spectrum we can take $T/(1+z) = T_1$ =constant as a reasonable first approximation. Then the solution of (3.3.10) is

$$\omega_0(\nu, z) = (1 - e^{-\tau(\nu,z)})\omega_{eq}(T/(1+z), \nu) + e^{-\tau(\nu,z)}\omega_0(\nu, z_d) \tag{3.3.17}$$

Adopting this approximation we can account for reabsorption by the dust of its own emission. Define

$$\theta = (T_1(1+z_*)/T_*)\lambda(z) \tag{3.3.18}$$

so that $\tau = (\theta)(h\nu(1+z)/kT)$. Then the absorption of the dust emission becomes important when $I(\theta)$ departs from unity. If T_1 is the temperature derived without reabsorption then a first approximation can be obtained by iterating

$$(T^5)' = (1 - I(\theta)/I(0))T^5 + T_1^5 \tag{3.3.19}$$

which is the integral of (3.3.17) over frequency. With our linear opacity model the spectrum is effectively thermalised except at wavelengths short of the peak, and in high optical depth cases the dust temperature quickly drops to the thermal equilibrium value. With the more accurate opacity law of section 3.4, the spectrum is not so smooth but the dust temperature shows the same behaviour. Fig 3.13 shows the calculated spectrum for such a case compared with the microwave background spectrum (see end of section 3.4).

At low redshifts the universe is optically thin and so the value of $T/(1+z)$ tends to a constant in all cases. Of course, the microwave background should be included in the initial spectrum $\omega_0(\nu, z(t_*))$; the dust temperature then never drops below 3(1+z)K.

If the stars form over an extended redshift range, then in general the most recent epoch will dominate due to the (1+z) falloff in energy. However for the recombination spectrum model we can make a useful approximation; if we consider just the Lyman α line (which contains half of the flux in our simple model) then the intensity of the background at a particular frequency is simply proportional to the star formation rate per unit redshift, $\phi(z)$, evaluated at the redshift at which the line has that comoving frequency. Thus an observed set of limits as a function of frequency can be directly inverted to give a limit on $\phi(z)$ (Chapter 4).

Fig. 3.7 The hexagamma function

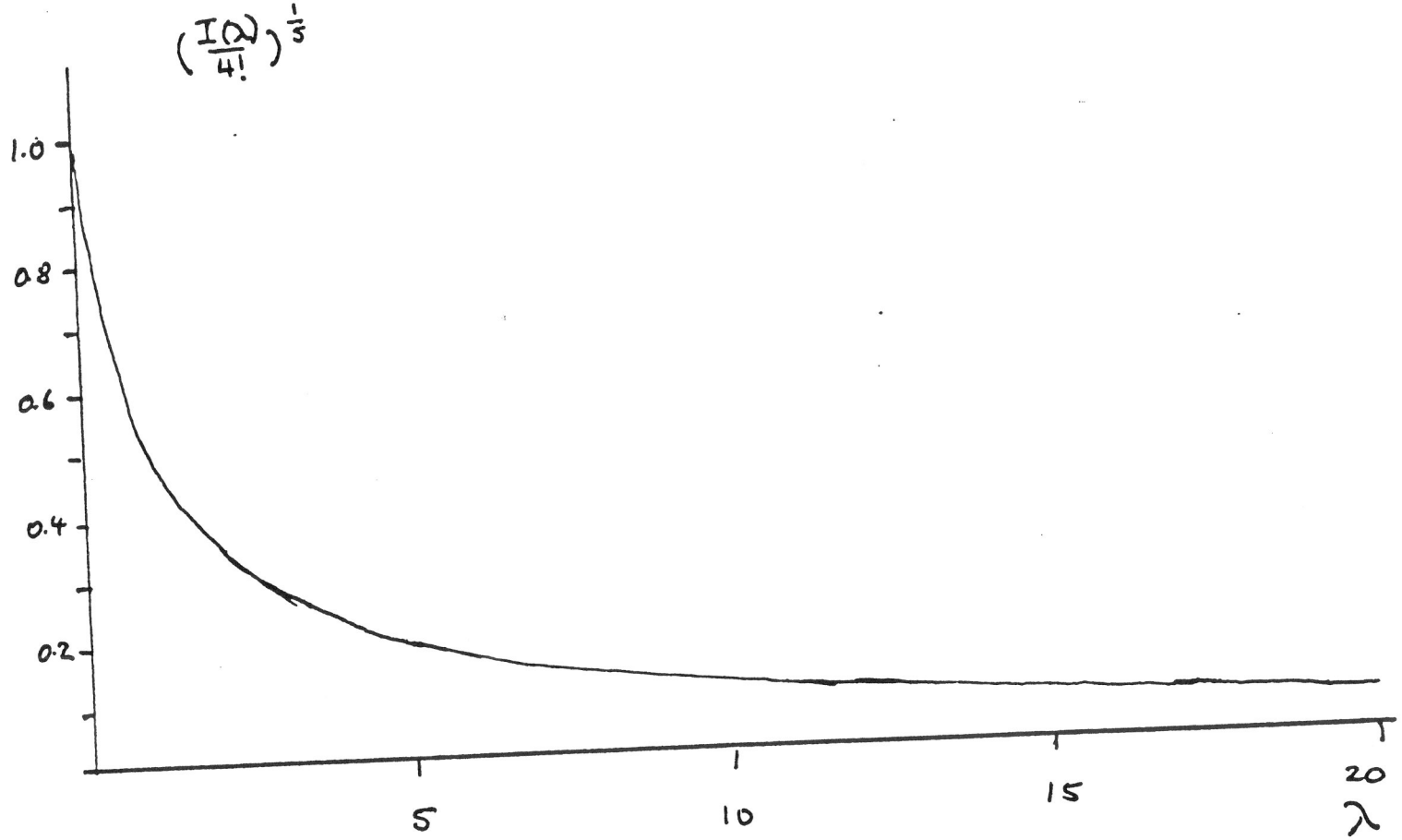

3.4 The predicted form of the background

3.4.1 The code

In this section I describe the numerical code to solve equations (3.3.1) and (3.3.4). I have since found out that Negroponte (1986) has written a similar code to solve the same problem. I developed my code independently as the natural extension to the work I had already carried out on background radiation as described in sections 3.1 and 3.2, and chapters 4 and 5, which predates the results of Negroponte for the dust-free case. His results for the evolution of the spectrum in a universe with dust were, however, obtained well before mine although his preprint was not released until after my calculations were complete. My code incorporates a background spectrum covering any given frequency range, but I have used a spectrum covering the range $\nu = 10^{10}$ Hz to 10^{17} Hz in comoving frequency. The values of $\omega_0(\nu, z)$ are stored in an array with bin size equal to 0.02 in $\log\nu$. The redshift evolution in frequency is treated simply by altering the origin of the array index at each redshift step.

The inputs to the code include the input source spectrum model, which for this discussion is one of the Population III models discussed in Chapter 2, but in principle could be the normalized spectrum of any supposed radiation source. The parameters of the source are defined by specifying its lifetime and efficiency ϵ. The cosmological model is specified by Ω_0 and H_0 to describe the overall Friedmann universe, Ω_* and z_* to define the density parameter and formation redshift of the sources, Ω_d and z_d to define the density parameter and formation redshift of the dust. The dust opacity law can also be selected, and is discussed below. Finally an initial integration step size is chosen; the redshift parameter used is

$$\varsigma = \log(1+z) \tag{3.4.1}$$

and the step size for the first part of the run is a constant increment in ς.

Before running the code the spectrum is initialized and a 3K blackbody can optionally be added to the spectrum to represent the microwave background. The

code evolves the spectrum from the initial value of $\varsigma = \log(1 + z_*)$ to $\varsigma = 0$. The cosmological time t is evaluated at each step by solving the exact solution to Friedmann's equation,

$$H_0 t = \frac{1}{2}\frac{\Omega_0}{(1-\Omega_0)^{3/2}}(\sinh\phi - \phi) \qquad (3.4.2)$$
$$(1+z)^{-1} = \frac{1}{2}\frac{\Omega_0}{(1-\Omega_0)}(\cosh\phi - 1);$$

this has been used unless $2(1-\Omega_0)\Omega_0{}^{-1}(1+z)^{-1} < 0.01$, when the solution

$$H_0 t = \frac{2}{3}\Omega_0{}^{-\frac{1}{2}}(1+z)^{-\frac{3}{2}} \qquad (3.4.3)$$

has been used.

The size of the integration step in time, dt, is also evaluated. In each step the contribution from the stellar radiation is added in provided $t + dt < t_* + t_{ms}$. If the stars expire within a particular step their contribution within that step is reduced by the appropriate proportion. In this way the code can treat stars which have lifetimes longer than the expansion time, and we are not restricted to the instantaneous approximation used earlier.

If $z < z_d$ the step size for the zone is changed so that the optical depth to the dust is only 0.1 for the zone, at the highest frequency at which the flux in the background is non-zero. The code now calculates the dust absorption and emission.

3.4.2 The Dust Opacity

The observationally determined parameters needed to normalise our dust opacity law are: firstly, the dust optical depth at V per unit hydrogen column in our galaxy, found from the optical depth per unit distance C_V compared with the mean hydrogen density n; secondly, the dust-to-gas mass ratio in our galaxy, χ_{gal}; and finally, the variation of optical depth with frequency. This is traditionally expressed in terms of the selective extinction A_λ/E_{B-V}, the ratio of total extinction at λ to the selective extinction of B relative to V. We normalize the

optical depth to the value of the extinction optical depth at a fiducial frequency $\nu_P = 10^{15}$Hz, denoting this dimensionless cross-section by $\sigma(\nu) = \tau(\nu)/\tau(\nu_P)$, and convert from selective extinction using the ratio $R = A_V/E_{B-V}$. To obtain the absorption optical depth relevant to the background light calculation, where scattering has no net effect, we must multiply the extinction value by $(1 - F_\nu)$, where F_ν is the frequency-dependent dust albedo. Hence the value of σ as I have defined it is not 1 at ν_P in this case. These quantities enable us to calculate the dust optical depth for a given dust mass column assuming that the nature of the dust particles is the same as in our galaxy. We have

$$d\tau(\nu) = (1 - F_\nu)\frac{A_\lambda}{RE_{B-V}}\frac{C_V}{n\chi_{gal}m_H}\rho_d dr = \kappa_P \rho_d dr \qquad (3.4.4)$$

for intergalactic dust of density ρ_d over coordinate path length dr.

We adopt (Spitzer 1978) $R = 3.2$, $C_V = 1.9$ mag/kpc, n=1.2 cm^{-3}, $\chi_{gal} = 0.01$, and $A_P/E_{B-V} = 5.8$; then $\kappa_P = 5700$ m^2/kg and

$$d\tau(\nu) = 4.9 \times 10^3 \Omega_d h_{50}(1+z)^3 \sigma(\nu(1+z))\frac{d(H_0 t)}{dz} \qquad (3.4.5)$$

for an element of look-back time dt, giving a total optical depth

$$\tau(\nu) = 4.9 \times 10^3 \Omega_d h_{50} \int (1+z)^3 \frac{d(H_0 t)}{dz}\sigma(\nu(1+z))dz \qquad (3.4.6)$$

Fig 3.4.5 has been used to calculate the solid lines in Fig 3.6, which give unit optical depth for the D2 model for given Ω_d,z,ν. The dotted lines give the corresponding curves for the linear model and were discussed at the end of section 3.2. The main difference is that the universe is more transparent at high frequencies because the Lyman continuum cross section is taken to be constant rather than increasing. Also, the universe is more transparent at comoving far infrared frequencies corresponding to the peak in the dust emission.

For the frequency dependence of the absorption I have adopted the extinction law calculated by Draine and Lee (1984) for a graphite and silicate mixture. In

the optical and ultraviolet I have used the values for the extinction tabulated by Savage and Mathis (1979) rather than the curve calculated by Draine and Lee to fit those values, but I have used Draine and Lee's estimate of the albedo at all frequencies to estimate the absorption from the extinction. The extinction in the extreme UV is completely uncertain; it must flatten off at some wavelength of the order of the smallest grain size but it is still rising at 1000Å . I adopt two extreme cases to explore the sensitivity of my results to this uncertainty; model D3 is linear in the extreme UV, while model D2 is linear up to the Lyman limit at 3.3 PHz and set to be constant beyond this value. At low frequencies ($\nu < 0.01$PHz) I have adopted a ν^2 law in agreement with the Draine and Lee model. The value of $\sigma(\nu)$ versus ν is plotted for model D2 in Fig. 3.8

To evaluate the dust temperature in each redshift zone, I evaluate the absorbed energy

$$\rho_A = \int \sigma(\nu) f(\nu) d(\nu) \tag{3.4.7}$$

where f is the spectral energy density (in J m^{-3}), and compare it with a look-up table of $\rho_E(T_d)$, the energy emitted (the same integral evaluated with a Planck distribution at temperature T_d). The dust temperature is always at least 3K because of the microwave background, and cannot exceed some melting point T_{melt}. The appropriate value of T_{melt} is unclear but I arbitrarily adopt T_{melt} = 2000K (The dust is never this hot in practice) and evaluate 200 values of ρ_E equally spaced in $\log T_d$ between these temperature limits. Linearly interpolating between these values to find T_d for a given ρ_A gives energy conservation to sufficient accuracy at each step to ensure that the total energy remains constant to one per cent in the whole integration.

The same routine can be used for putting dust into the nebular problem by setting a scaling variable. In this case the dust melting point is an important issue.

3.4.3 Results

In this section I present the predicted spectral form and intensity of the extragalactic background light observable at the present epoch which would result from a Population III generation of very massive stars. The results for a dust free universe, when the effects of finite stellar lifetime are included, are indistinguishable from the simple models of section 3.1.

First I present the effect of varying the dust opacity law in a given cosmological situation. I choose a low redshift Population III with the dust and stars at the same epoch to maximize the importance of the high frequency opacity, with Ω_* =1, $\Omega_d = 10^{-4}$, $z_* = z_d = 5$. In fact, the predicted spectra (Fig 3.9(a)) from models D2 and D3 are quite similar, and much closer to each other than to the linear absorption law model D0A. The D3 model has a hotter dust temperature at first (see Fig 3.9(b) which plots $T_d/(1+z)$ versus z) but both have the same present (zero redshift) temperature; the latter is hotter than that predicted for the linear case. From now on I shall adopt the D2 law unless explicitly stated.

Next I present a sequence of models with gradually increasing dust abundance at fixed redshifts z_* and z_d, showing the predicted background spectra and the redshift evoultion of the redshifted dust temperature. Fig. 3.10 is for $z_* = 50$, $z_d = 5$ which represents a Population III background being absorbed by dust produced in galaxies forming later; Fig 3.11 is for $z_* = z_d = 5$, dust and stars having the same origin. Fig 3.12 has $z_* = z_d = 20$. The dust abundances chosen are $\Omega_d = 0, 10^{-5}, 5 \times 10^{-5}$, and 10^{-4}. The results show that dust abundances of about $\Omega_d = 10^{-5}$ or greater are required before the effects of absorption become significant.

Fig 3.13 illustrates a case which is optically thick to the reemitted dust emission. The parameters have been chosen to give a spectrum which is optically thick at the frequencies corresponding to the original dust temperature, and has the same total energy density as the microwave background. Finally, Fig 3.14 shows

the dependence of the results on the density parameter of the universe and on Hubble's constant. This dependence only comes in through the relation between optical depth and redshift, which involves the time-redshift relationship.

Negroponte (1986) has performed similar calculations to the ones I have described in this section. Detailed quantitative comparison with his results is difficult due to the different opacity laws which he uses, as can be seen from Fig 3.9(b), but the spectra he obtains are quite similar and the temperature - redshift relation shows the same range of behaviour.

Fig 3.8 (a) **D·2** Dust opacity model

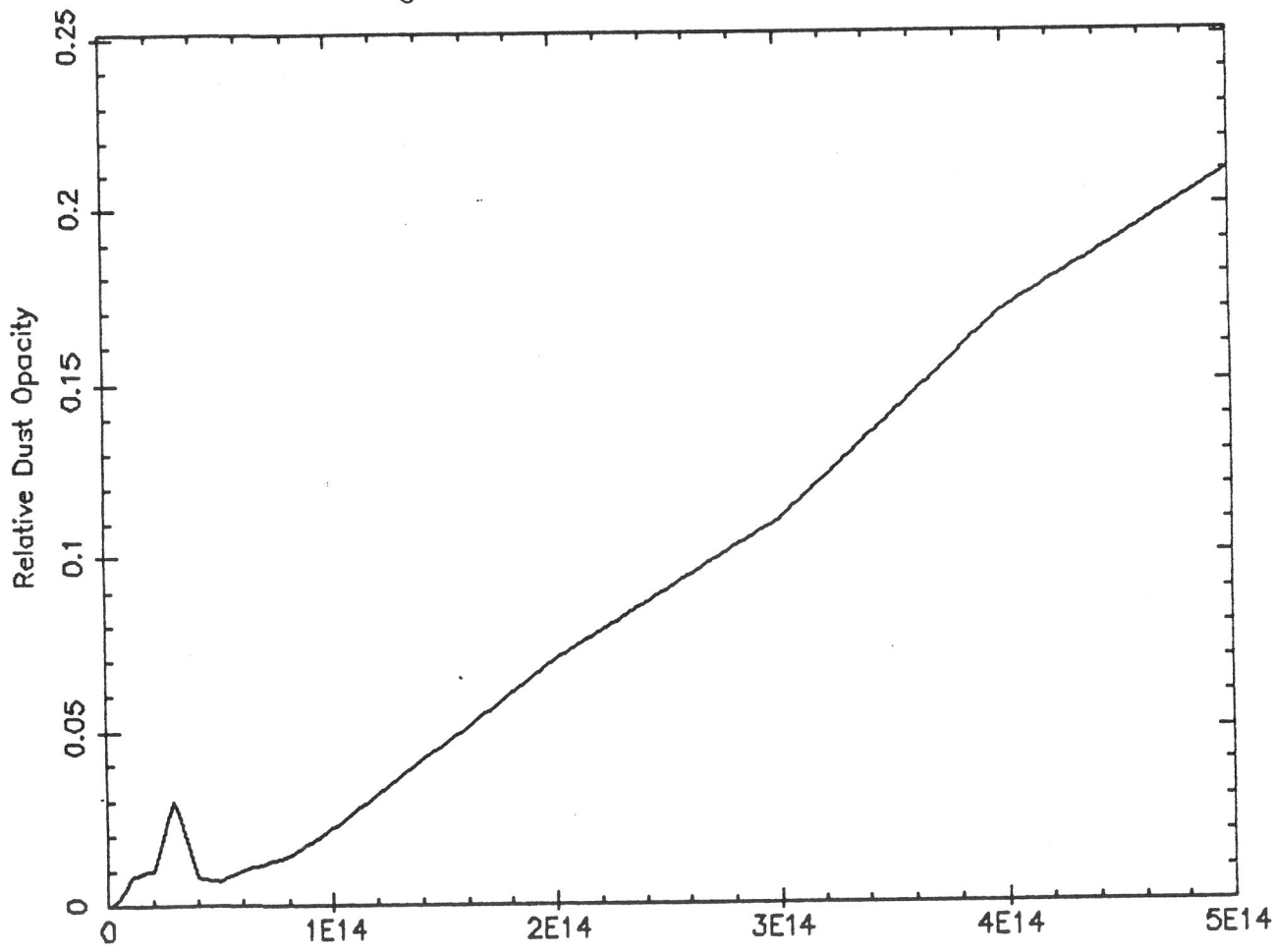

Fig 3.8 (b) D·2 Dust Opacity model

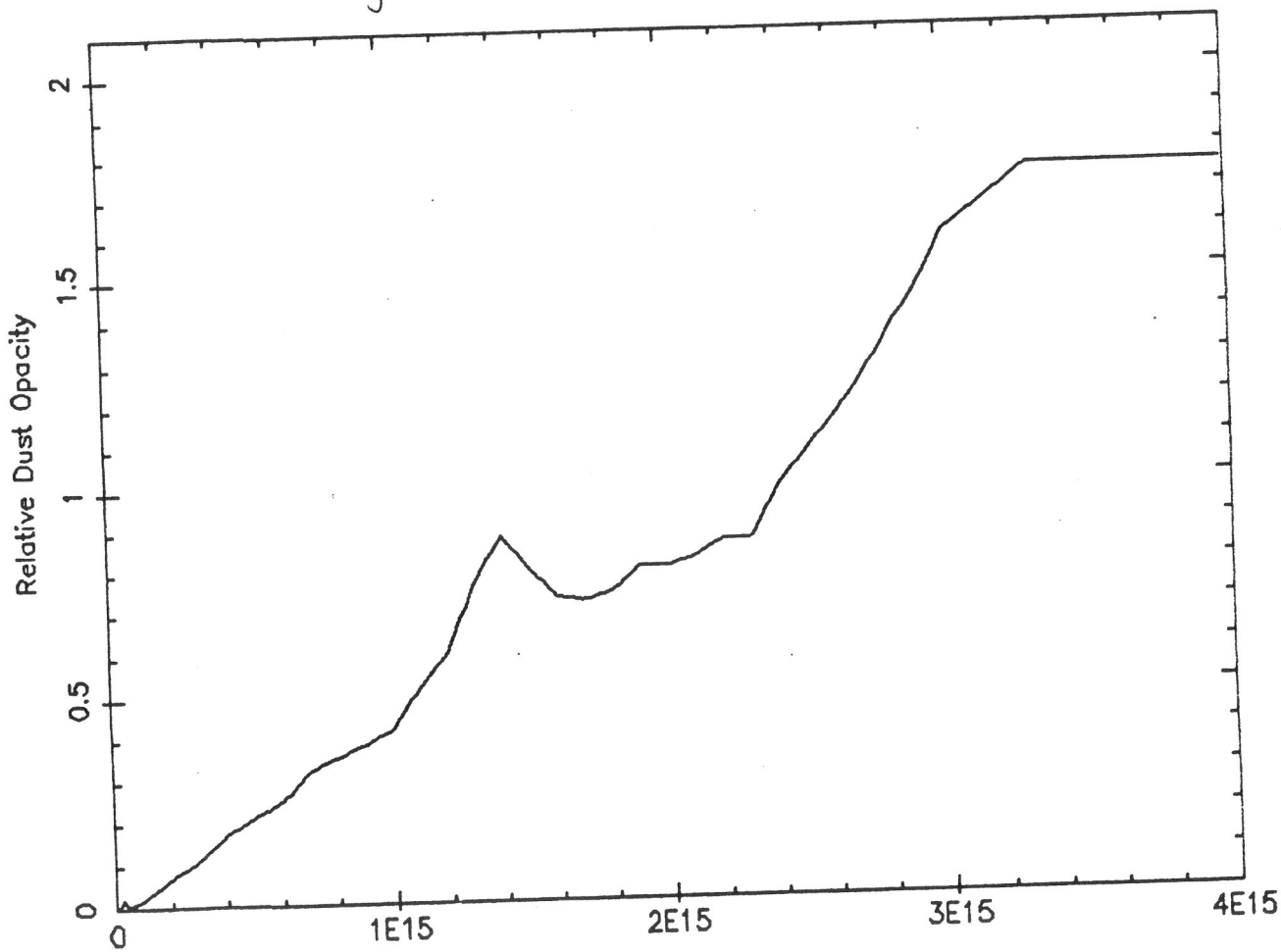

log ν

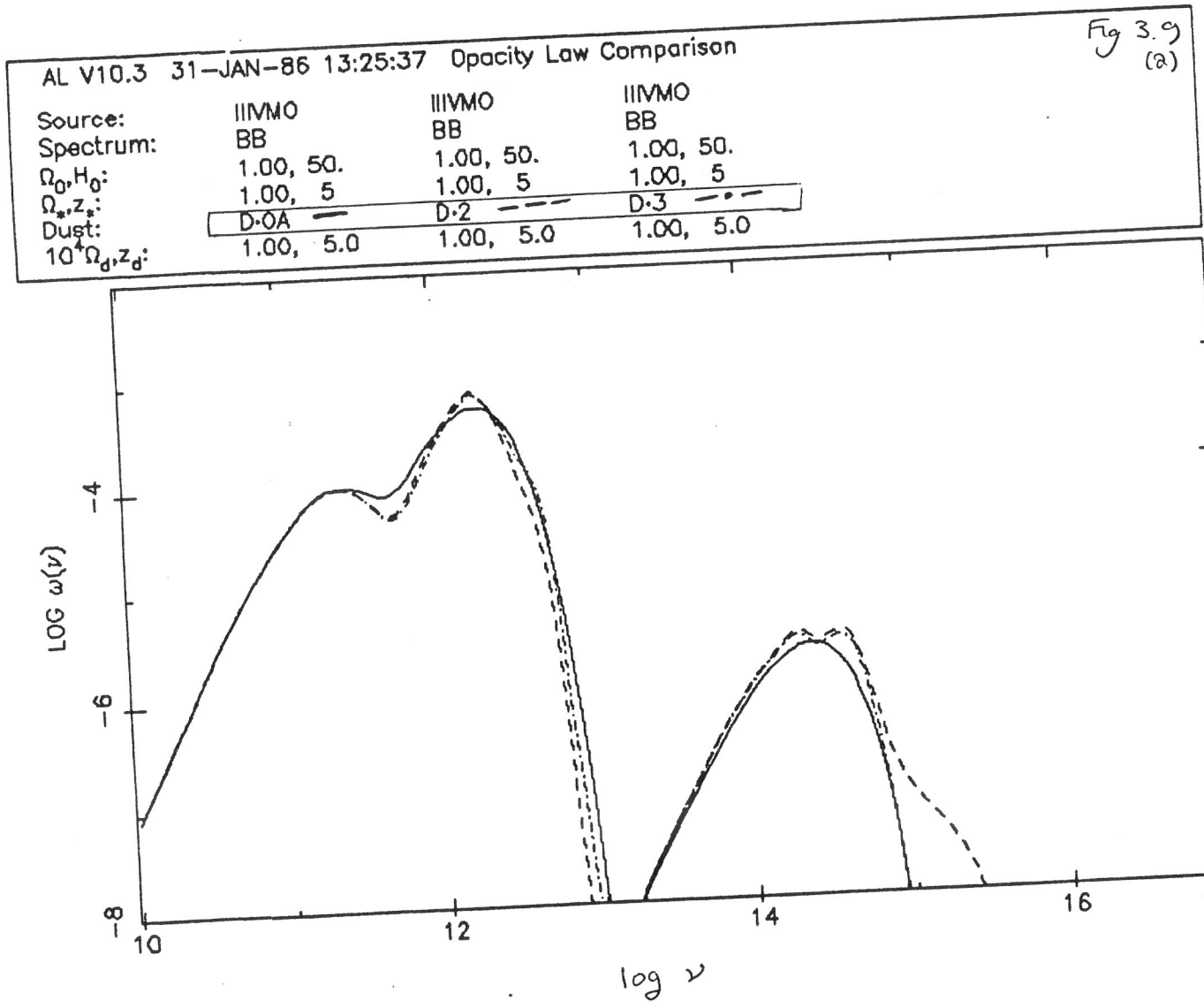
AL V10.3 31-JAN-86 13:25:37 Opacity Law Comparison
Source: IIIVMO IIIVMO IIIVMO
Spectrum: BB BB BB
Ω0,H0: 1.00, 50. 1.00, 50. 1.00, 50.
Ω*,z*: 1.00, 5 1.00, 5 1.00, 5
Dust: D·0A D·2 D·3
10⁴Ωd,zd: 1.00, 5.0 1.00, 5.0 1.00, 5.0
LOG ω(ν)
-4
-6
-8
10
12
14
16
log ν

Fig 3.9 (2)

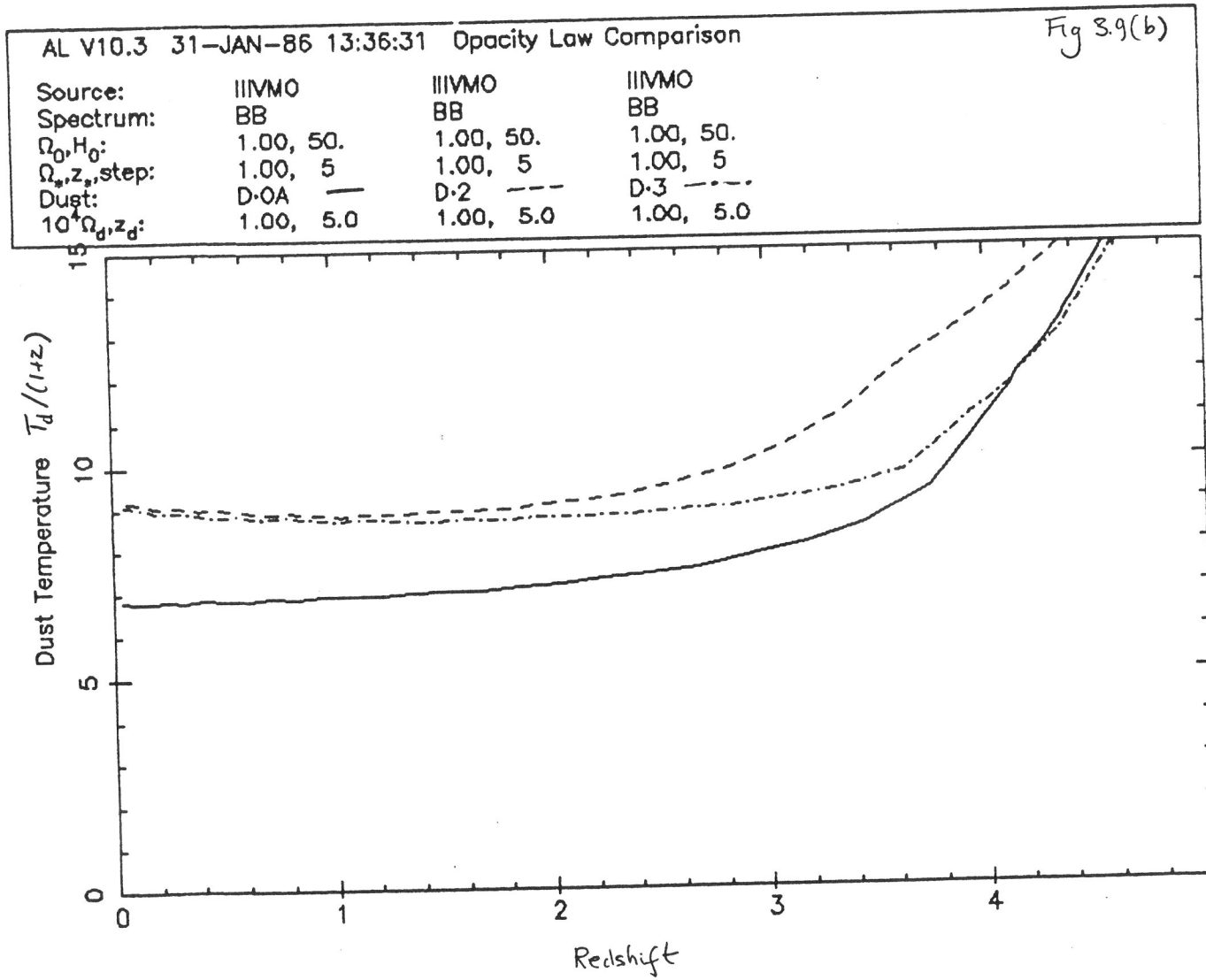
AL V10.3 31-JAN-86 13:36:31 Opacity Law Comparison
Source: IIIVMO IIIVMO IIIVMO
Spectrum: BB BB BB
Ω_0, H_0: 1.00, 50. 1.00, 50. 1.00, 50.
Ω_*, z_*, step: 1.00, 5 1.00, 5 1.00, 5
Dust: D·0A — D·2 --- D·3 -·-·-
$10^4\Omega_d, z_d$: 1.00, 5.0 1.00, 5.0 1.00, 5.0
Dust Temperature $T_d/(1+z)$
0
5
10
15
0
1
2
3
4
5
Redshift

Fig 3.9(b)

Fig 3.10(2)

AL V10.4 4-FEB-86 21:07:27 Changing Dust Abundance

Source:	IIIVMO	IIIVMO	IIIVMO	IIIVMO
Spectrum:	BB	BB	BB	BB
Ω_0, H_0:	1.00, 50.	1.00, 50.	1.00, 50.	1.00, 50.
Ω_*, z_*:	1.00, 50	1.00, 50	1.00, 50	1.00, 50
Dust:	D·2	D·2	D·2	D·2
$10^4\Omega_d, z_d$:	0.00, 5.0	0.10, 5.0	0.50, 5.0	1.00, 5.0

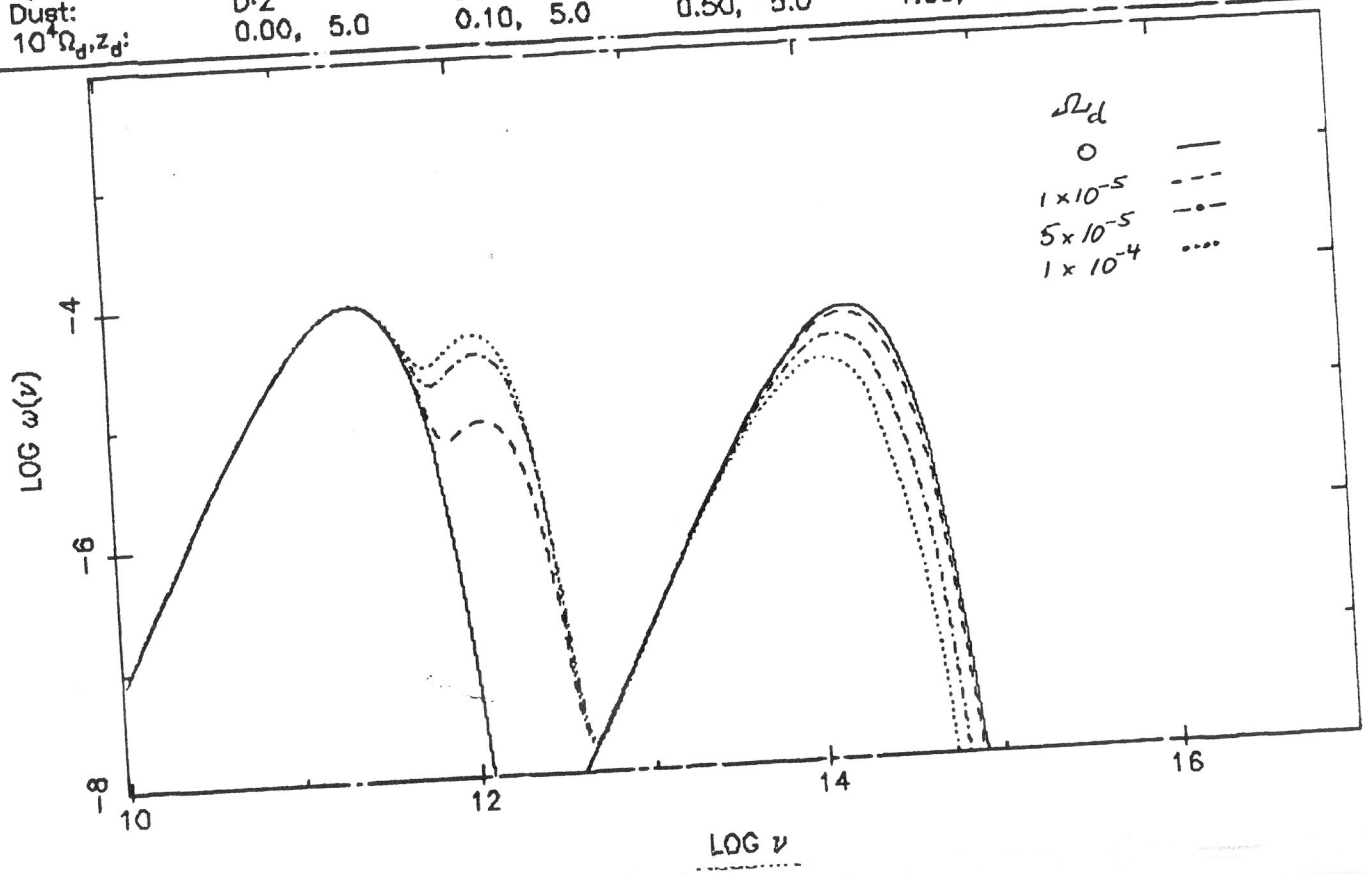

Fig 3.10 (b)

AL V10.4 4-FEB-86 21:07:39 Changing Dust Abundance

Source:	IIIVMO	IIIVMO	IIIVMO
Spectrum:	BB	BB	BB
Ω_0, H_0:	1.00, 50.	1.00, 50.	1.00, 50.
Ω_*, z_*, step:	1.00, 50	1.00, 50	1.00, 50
Dust:	D·2	D·2	D·2
$10^4\Omega_d, z_d$:	0.10, 5.0	0.50, 5.0	1.00, 5.0

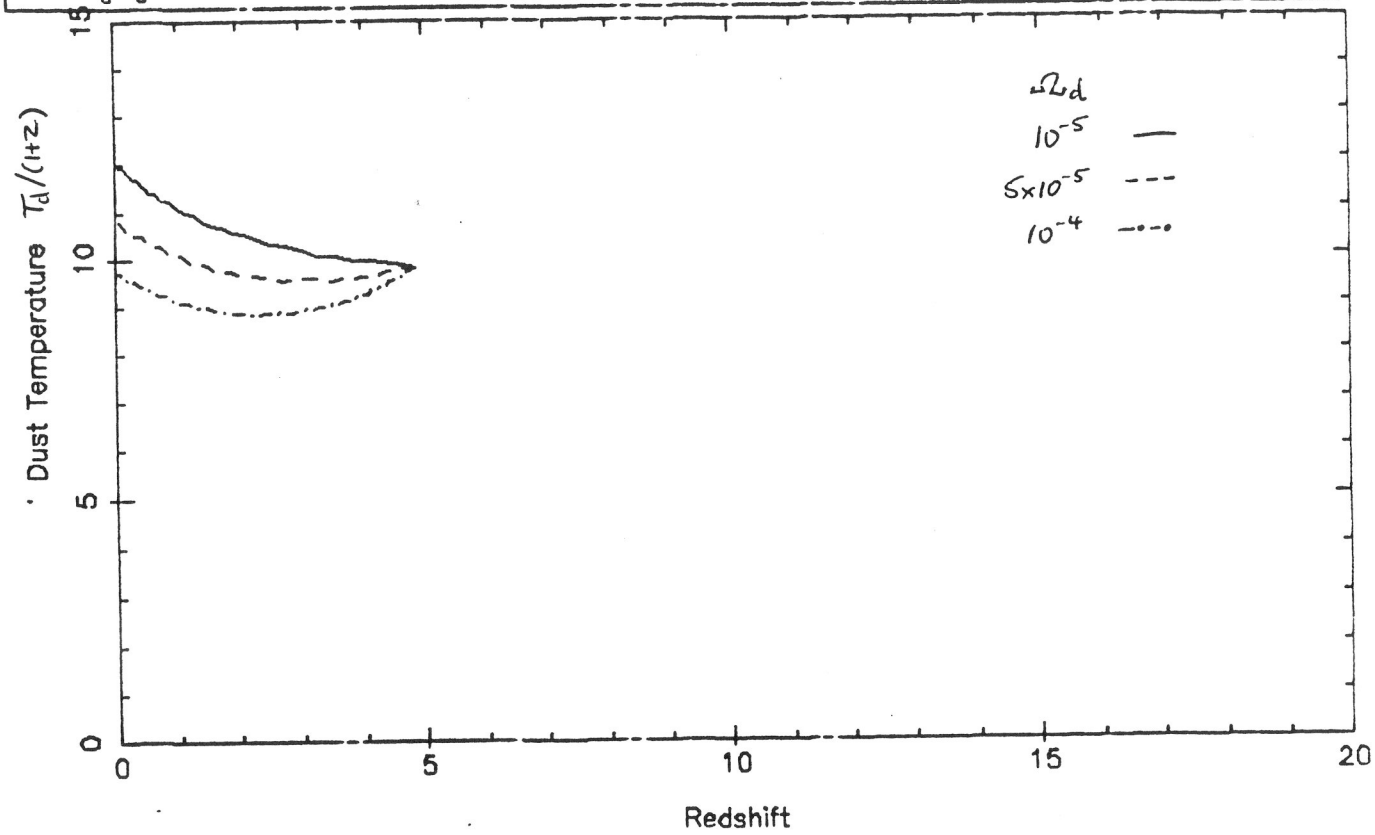

Fig 3.11(a)

AL V10.3 31-JAN-86 14:06:59 Changing Dust Abundance

Source:	IIIVMO	IIIVMO	IIIVMO
Spectrum:	BB	BB	BB
Ω_0, H_0:	1.00, 50.	1.00, 50.	1.00, 50.
Ω_*, z_*:	1.00, 5	1.00, 5	1.00, 5
Dust:	D-2	D-2	D-2
$10^4\Omega_d, z_d$:	0.10, 5.0	0.50, 5.0	1.00, 5.0

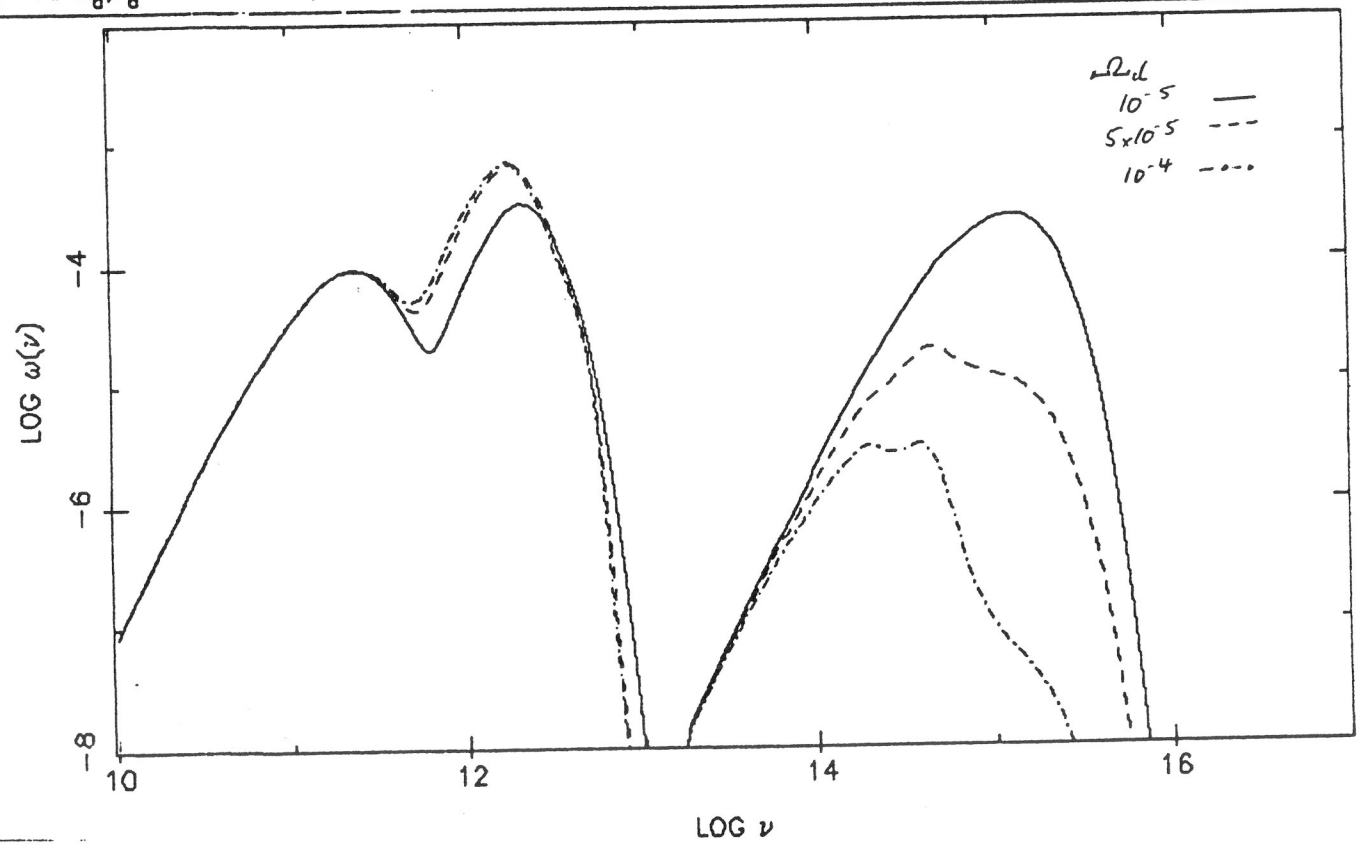

Fig 3.11 (6)

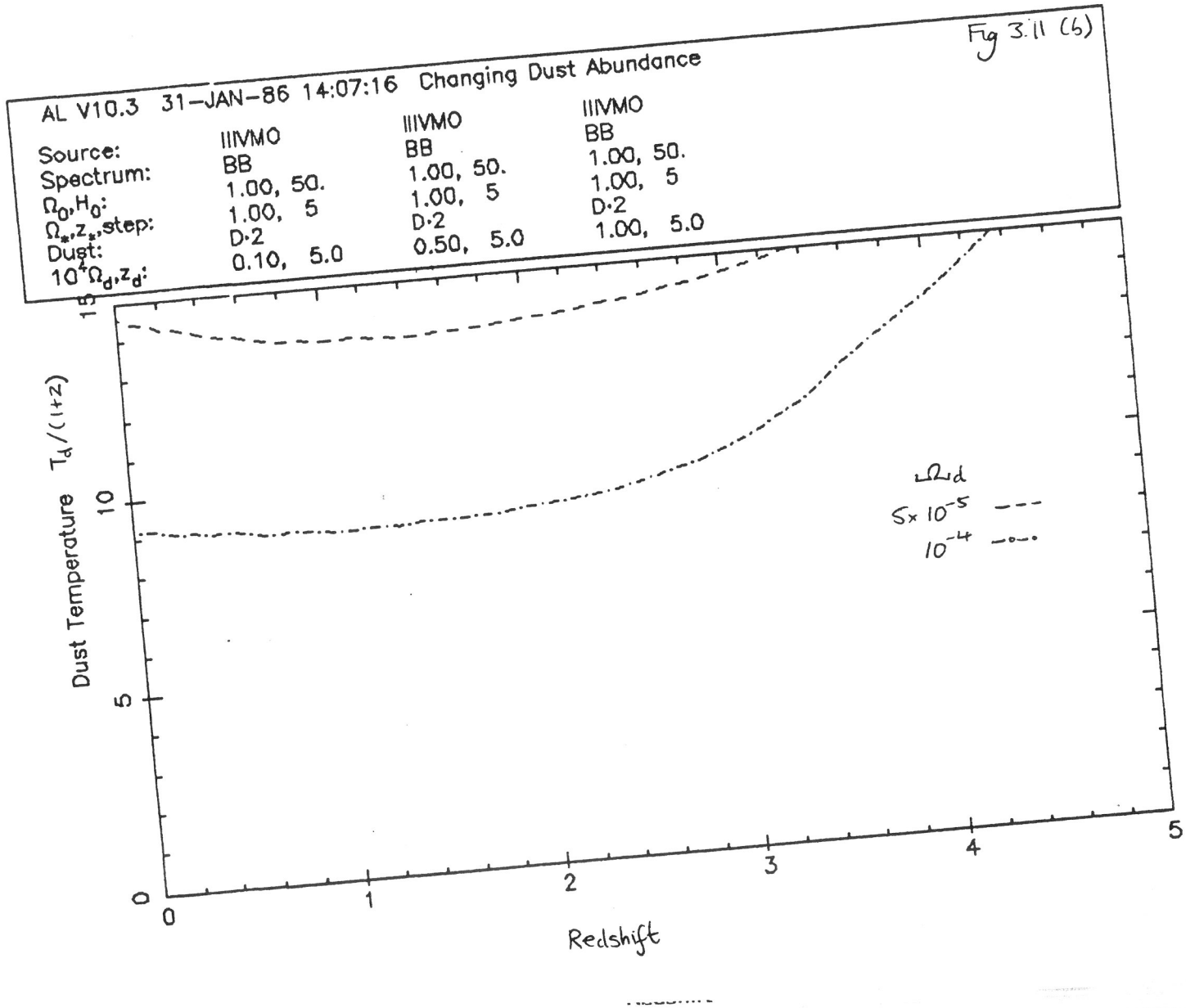
AL V10.3 31-JAN-86 14:07:16 Changing Dust Abundance
Source: IIIVMO IIIVMO IIIVMO
Spectrum: BB BB BB
Ω_0, H_0: 1.00, 50. 1.00, 50. 1.00, 50.
Ω_*, z_*, step: 1.00, 5 1.00, 5 1.00, 5
Dust: D·2 D·2 D·2
$10^4\Omega_d, z_d$: 0.10, 5.0 0.50, 5.0 1.00, 5.0
Dust Temperature $T_d/(1+z)$
0
5
10
15
0
1
2
3
4
5
Redshift
Ω_d
5×10^{-5}
10^{-4}

Fig 3.12(a)

AL V10.3 31-JAN-86 16:24:51 Changing Dust Abundance

Source:	IIIVMO	IIIVMO	IIIVMO	IIIVMO
Spectrum:	BB	BB	BB	BB
Ω_0, H_0:	1.00, 50.	1.00, 50.	1.00, 50.	1.00, 50.
Ω_*, z_*:	1.00, 20	1.00, 20	1.00, 20	1.00, 20
Dust:	D·2	D·2	D·2	D·2
$10^4\Omega_d, z_d$:	0.00, 20.0	0.10, 20.0	0.50, 20.0	1.00, 20.0

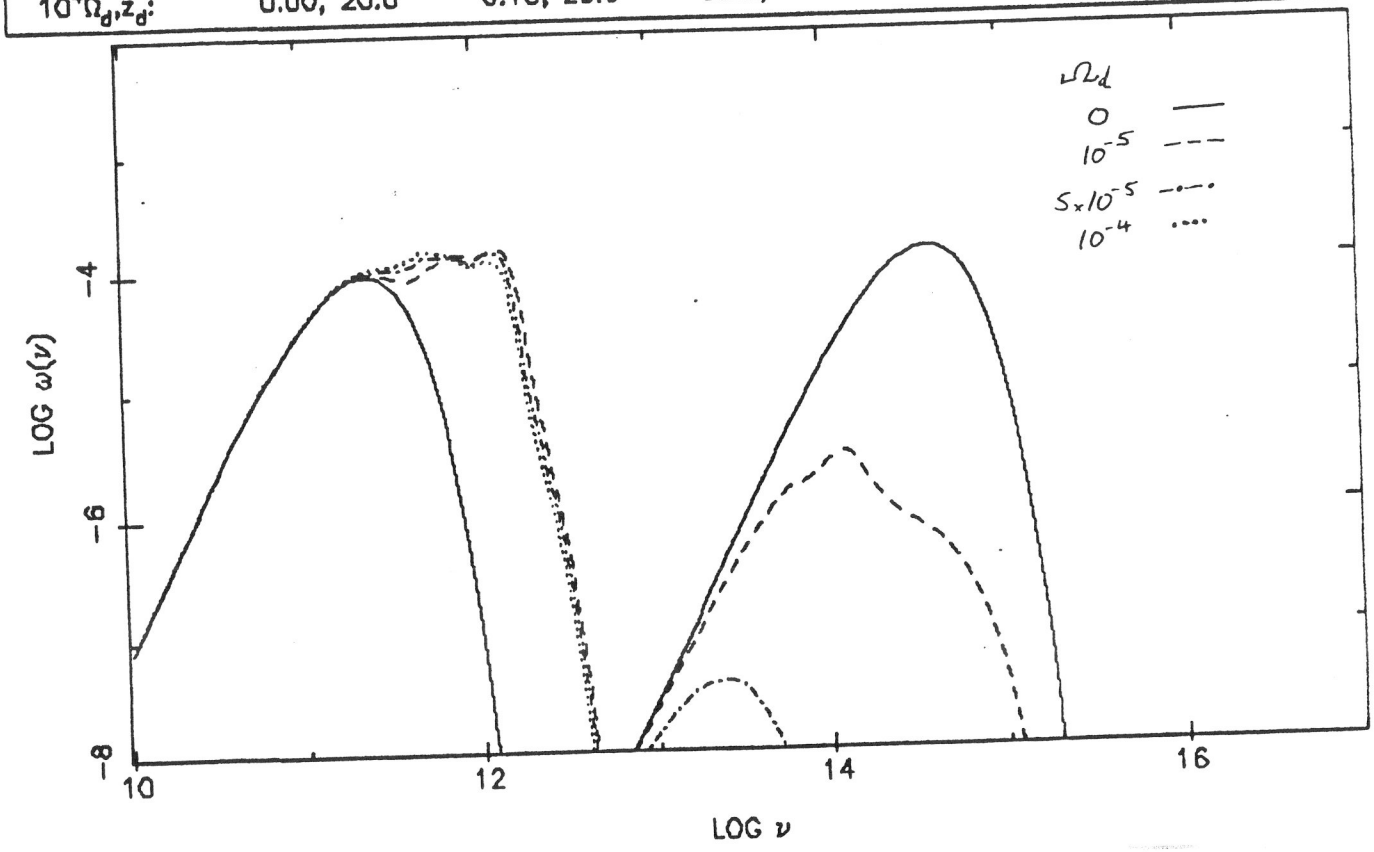

Fig 3.12(6)

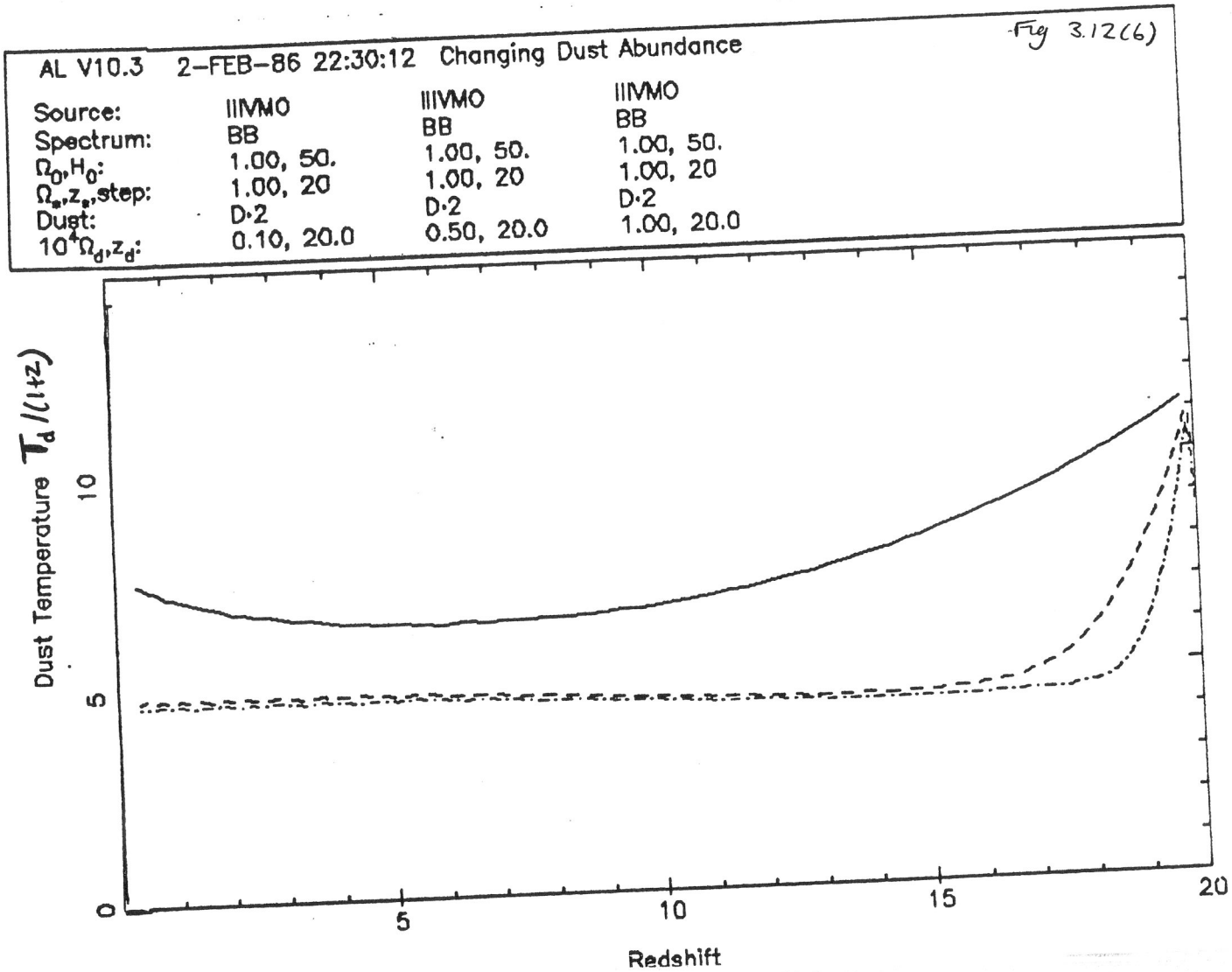
AL V10.3 2-FEB-86 22:30:12 Changing Dust Abundance
Source: IIIVMO IIIVMO IIIVMO
Spectrum: BB BB BB
Ω_0, H_0: 1.00, 50. 1.00, 50. 1.00, 50.
Ω_e, z_e, step: 1.00, 20 1.00, 20 1.00, 20
Dust: D·2 D·2 D·2
$10^4\Omega_d, z_d$: 0.10, 20.0 0.50, 20.0 1.00, 20.0
Dust Temperature $T_d/(1+z)$
0
5
10
5
10
15
20
Redshift

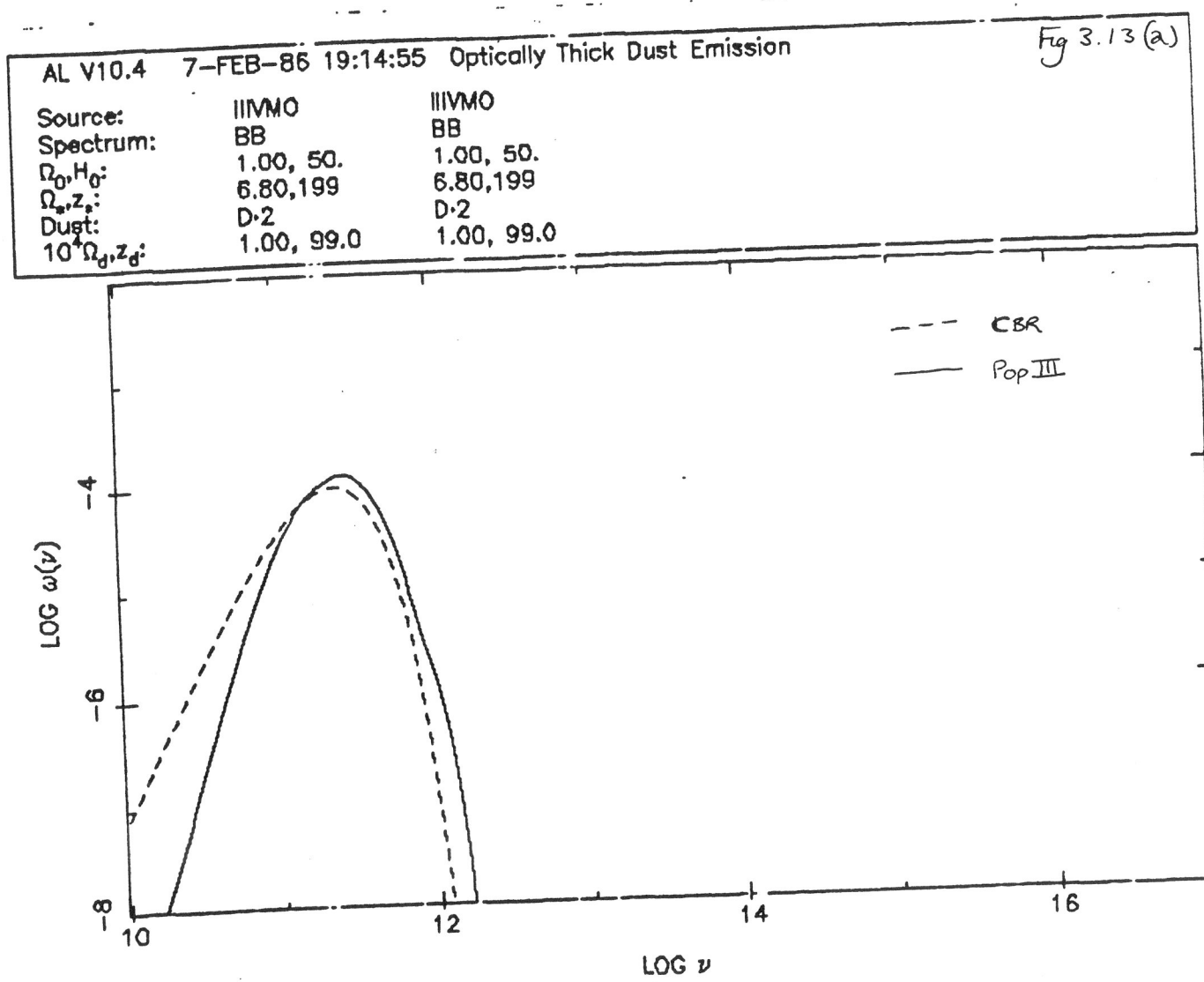
AL V10.4 7-FEB-86 19:14:55 Optically Thick Dust Emission
Source: IIIVMO IIIVMO
Spectrum: BB BB
Ω_0, H_0: 1.00, 50. 1.00, 50.
Ω_*, z_*: 6.80,199 6.80,199
Dust: D·2 D·2
$10^4\Omega_d, z_d$: 1.00, 99.0 1.00, 99.0
CBR
Pop III
LOG ω(ν)
-4
-6
-8
10
12
14
16
LOG ν

Fig 3.13 (a)

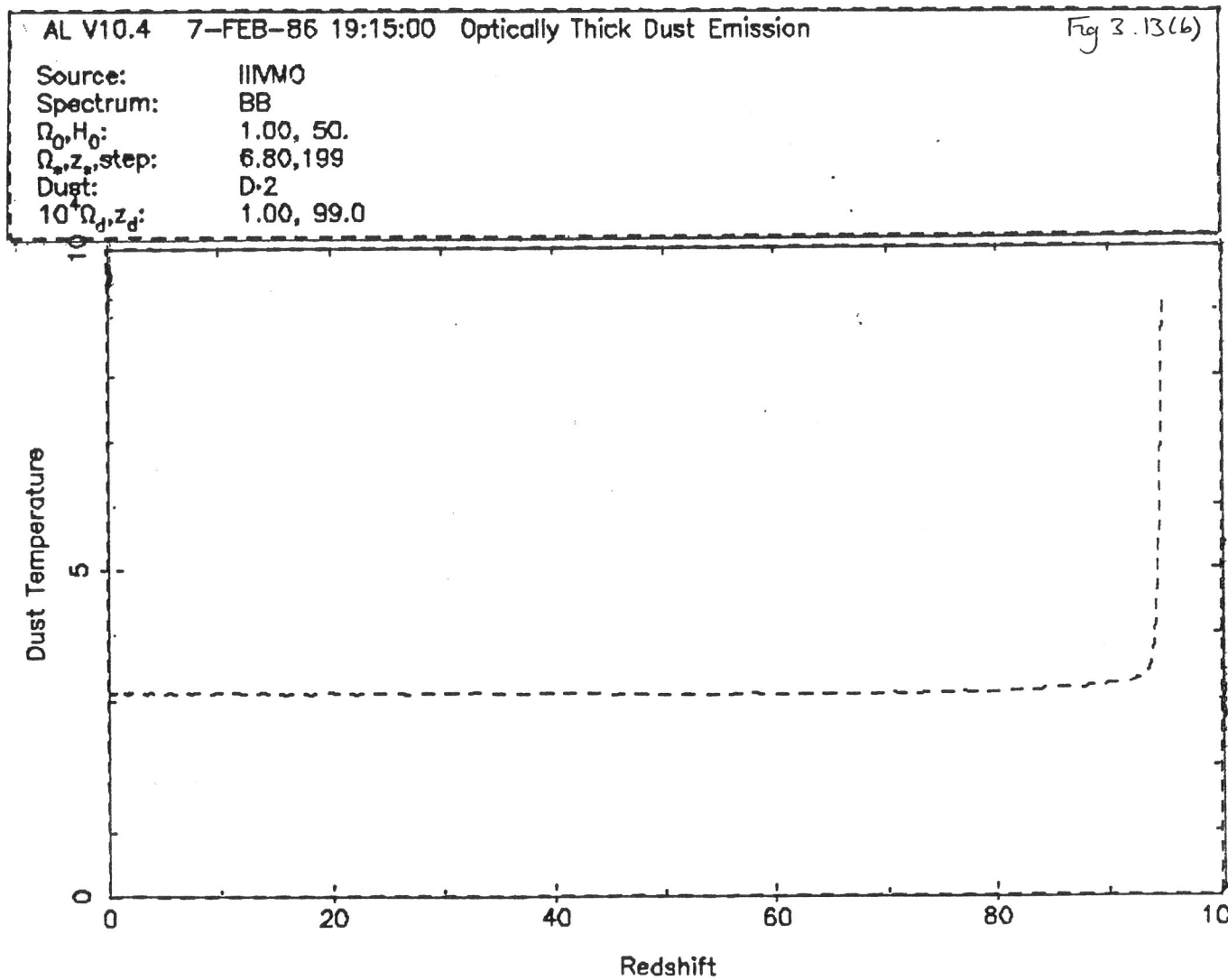
AL V10.4 7-FEB-86 19:15:00 Optically Thick Dust Emission
Fig 3.13(b)
Source: IIMMO
Spectrum: BB
Ω_0, H_0: 1.00, 50.
Ω_*, z_*, step: 6.80, 199
Dust: D·2
$10^4\Omega_d, z_d$: 1.00, 99.0
Dust Temperature
0
5
10
0
20
40
60
80
100
Redshift

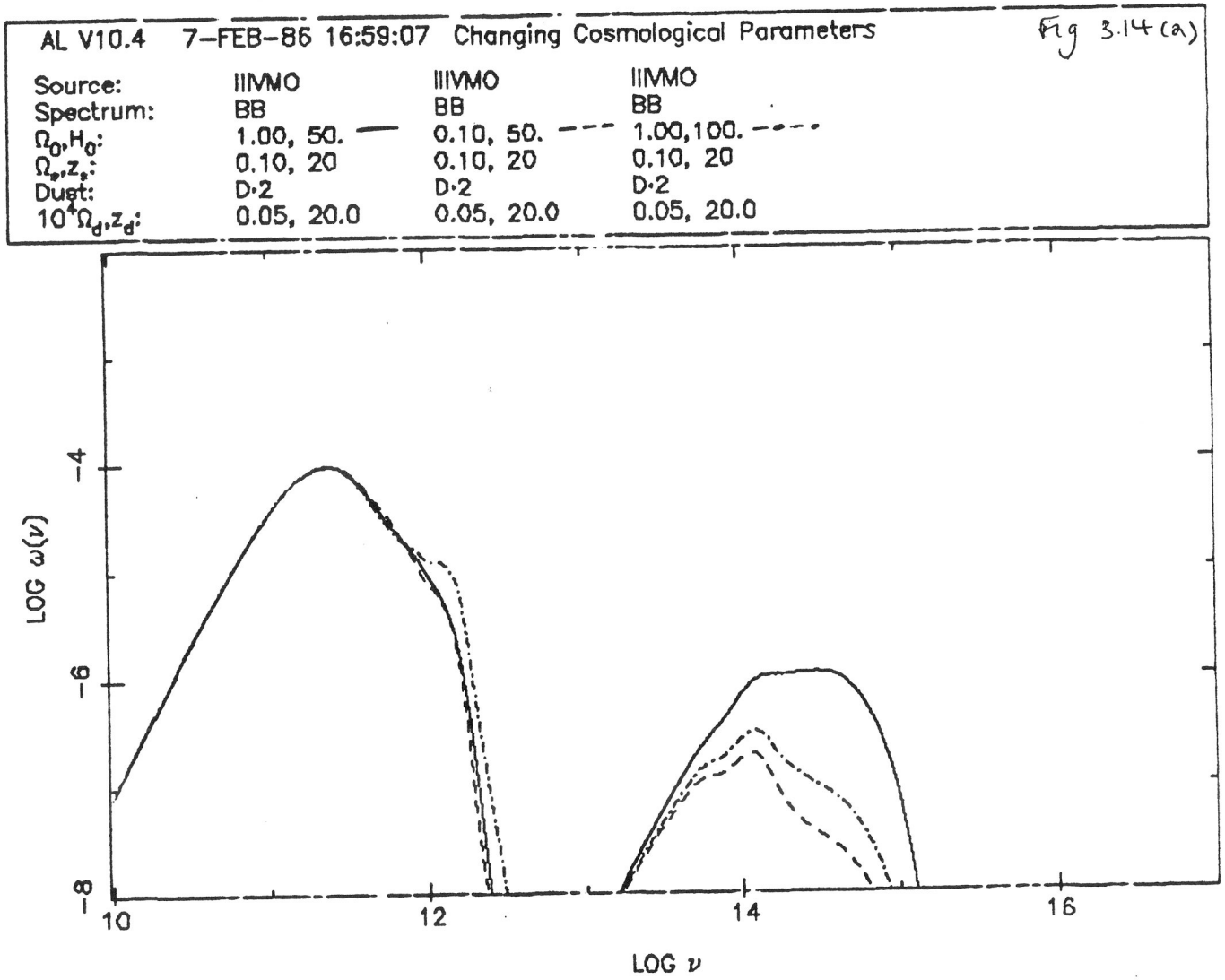
AL V10.4 7-FEB-86 16:59:07 Changing Cosmological Parameters
Source: IIIVMO IIIVMO IIIVMO
Spectrum: BB BB BB
Ω_0, H_0: 1.00, 50. — 0.10, 50. - - - 1.00,100. - - -
Ω_s, z_s: 0.10, 20 0.10, 20 0.10, 20
Dust: D·2 D·2 D·2
$10^4\Omega_d, z_d$: 0.05, 20.0 0.05, 20.0 0.05, 20.0
LOG $\omega(\nu)$
-4
-6
-8
10
12
14
16
LOG ν

Fig 3.14 (a)

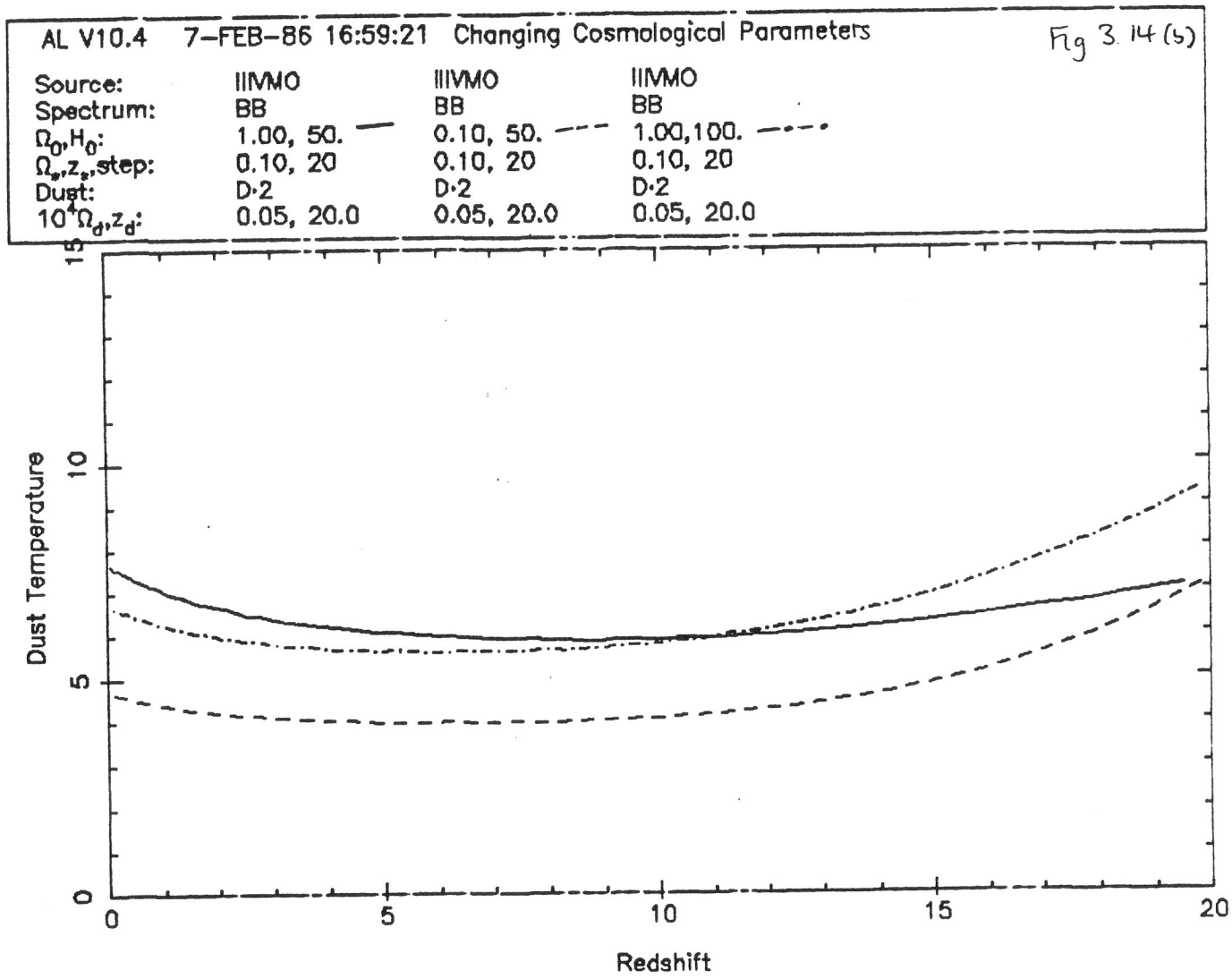
AL V10.4 7-FEB-86 16:59:21 Changing Cosmological Parameters
Source: IIMMO IIIVMO IIMMO
Spectrum: BB BB BB
Ω_0, H_0: 1.00, 50. 0.10, 50. 1.00,100.
Ω_*, z_*, step: 0.10, 20 0.10, 20 0.10, 20
Dust: D·2 D·2 D·2
$10^4\Omega_d, z_d$: 0.05, 20.0 0.05, 20.0 0.05, 20.0
Dust Temperature
0
5
10
15
20
Redshift

Fig 3.14 (b)

4. The Near Infrared Background

4.1 The Observations

In 1983 Matsumoto, Akiba and Murakami reported the detection of a near infrared background radiation with photometers operating in the 1.4 to 5 micron range on a sounding rocket. They argued that the intensity was too high to be explained by atmospheric, planetary or galactic sources, and claimed that any contribution due to the rocket stage could be ruled out due to lack of time variation. (Such a contribution was detected in the early part of the flight.) They also suggested that the radiation might best be explained as being of cosmological origin. This interesting experimental result has not been confirmed, and it may be that the contributions from stellar radiation and interplanetary dust were underestimated. It is however useful to consider the interpretation of this reported background as redshifted Population III light to illustrate what might be deduced from a confirmed detection of extragalactic background light; since the observations can at least be taken as upper limits, they serve as a detailed example of the more general results presented in the next chapter.

The observational data are presented in Fig 4.1 and summarized in Table 4.1. The five bandpasses used were the standard ground-based photometric bands H, K, L, and M, and an extra band A between L and M. The rocket was launched in Sept 1982 from Kagoshima Space Center in Japan and reached an altitude of 322 km. 200 seconds of observations were carried out from the rocket during the ascending phase, as the rocket's 5 degree precession cone carried the field of view in a small circle around the region $l = 60^o$, $b = -20^o$. However, in this phase the signals show a time dependence which the experimenters interpreted as being due to emission from the final stage of the rocket, and may be unreliable. Near apogee the rocket was despun to increase its precession cone angle to 21 degrees in radius, with the centre of the observed region in the region at approximately $l = 45^o$,

$b = -5^{o}$, in the Aquila - Delphinus region. This observation lasted 220 s and was free of the time dependence (in the sense that the signals repeated after one precession period) until the rocket descended through 250 km, when atmospheric emission began to affect the data. The photometers were calibrated by observing standard stars for the H, K, and L bands, and, by fitting a model to the galactic plane emission, this calibration was extended to the two long wavelength bands.

Matsumoto *et al.* claim that stray light from the Earth gave a negligible contribution to the signal. They subtracted off galactic starlight which they modelled as a function of galactic latitude, and estimated the contribution from interplanetary dust and zodiacal light. The total subtractions from the observed signal amounted to about 60% of the signal at H, where starlight is the main contribution, dropping to less than 10% of the signal at M, where interplanetary dust was the main contribution to the subtraction. The residual background has an integrated energy density of about $\Omega_R h_{50}^2 = 10^{-4}$, comparable to the cosmic microwave background.

Table 4.1

Band	Eff. wavelength (μ)	Bandwidth (μ)	$\log \omega(\nu)$ max	min
H	1.6	0.3	-4.14	-4.57
K	2.2	0.4	-4.19	-4.48
L	3.8	0.7	-4.10	-4.24
L'	4.2	0.7	-4.17	-4.42
M	4.7	0.6	-3.92	-4.21

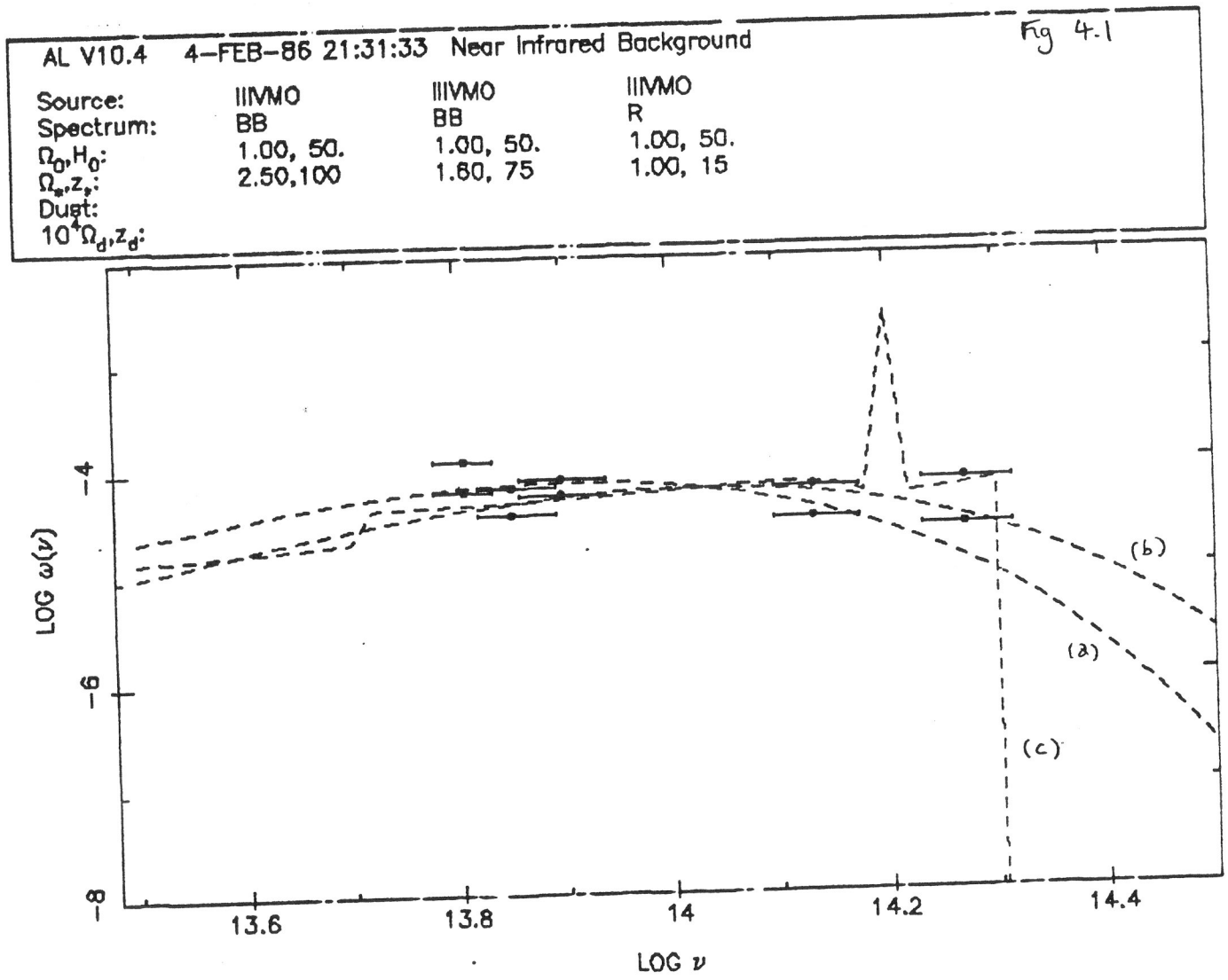
AL V10.4 4-FEB-86 21:31:33 Near Infrared Background
Source: IIIVMO IIIVMO IIIVMO
Spectrum: BB BB R
Ω_0, H_0: 1.00, 50. 1.00, 50. 1.00, 50.
Ω_*, z_*: 2.50,100 1.60, 75 1.00, 15
Dust:
$10^4\Omega_d, z_d$:
LOG $\omega(\nu)$
-4
-6
-8
13.6
13.8
14
14.2
14.4
LOG ν
(a)
(b)
(c)

Fig 4.1

4.2 Population III Stars and the Infrared background

We first assume that the radiation comes from stars with masses in the VMO range with luminosity $L = 1.3 \times 10^{31} f_L (M/M_\odot)$ W and surface temperatures $T = 10^5 f_T$ K in the notation of chapter 2. Again we assume that they all form at the same redshift z_* and that their radiation all comes from that epoch, which restricts us to $z_* < 390 f_t^{-2/3} \Omega_0{}^{-1/3} h_{50}^{-2/3}$ from eq (3.1.2). If the universe is transparent to the radiation the present background radiation spectrum should just be a diluted blackbody with temperature $T_{obs} = T(1+z_*)^{-1}$K. The integrated energy density of the background is then

$$\Omega_R = 0.004 f_\epsilon \Omega_* (1+z)^{-1} \tag{4.2.1}$$

in units of the critical density. The predicted spectrum is (Carr, McDowell and Sato 1983)

$$\omega(\nu) = 6.5 \times 10^{-4} f_\epsilon \left(\frac{\Omega_*}{1+z_*}\right)\left(\frac{x^4}{e^x - 1}\right) \tag{4.2.2}$$

where $x = h\nu(1+z_*)/kT$; this spectrum peaks at $\nu = 8.1 \times 10^{15}(1+z_*)^{-1}$ Hz, corresponding to a wavelength $\lambda = 370(1+z_*)$Å .

We now fit the data 'by eye', assuming $f_T = f_\epsilon = 1$. A more formal fitting procedure is not warranted, given the size of the error bars on the data. The dotted curve (a) in Fig 4.1 is a representative fit which has $z_* = 100$ and $\Omega_* = 2.5 h_{50}^{-2}$. This fit does not pass through the $2-\mu$m point; if one includes that point but neglects the $5-\mu$m point (which is the most dubious since it could be contaminated by interplanetary dust emission) the best 'fit by eye' to the points is shown by curve (b) and requires $z_* = 75$ and $\Omega_* = 1.6 h_{50}^{-2}$. More generally, one might demand that the spectrum should peak between 2 and 5 μm , the range spanned by the data; the first limit is also necessary if the spectrum is to fall sufficiently to go below the optical limit (chapter 5) at 0.5 μm . This corresponds to redshifts $50 < z_* < 140$, which implies that the stars almost certainly need to be pregalactic, since the redshift of galaxy formation is usually thought to be around 10 or even less. The

value of Ω_* required is necessarily close to 1. This may not conflict with the upper limit permitted by measurements of the cosmological deceleration parameter (Sandage 1972), and it would certainly suffice to explain the dark matter problem. However, it would be too large to be consistent with the observed dueterium abundance if this results from cosmological nucleosynthesis.

If M is allowed to fall below 200 $M_\odot$, despite the enrichment constraints, the value required for z_* decreases in proportion to the stellar temperature T. The value required for Ω_* first increases slightly due to the lower stellar efficiency and then decreases when M falls below 20 $M_\odot$ due to the lower redshift required. However, it will be shown in chapter 6 that stars in some mass ranges would contravene the optical background light limits. The spectrum of the radiation can be made broader by extending the period of formation, the lifetime or the mass spectrum of the stars, and all the data points could thereby be included, but this does not alleviate the energetic problem. Note that objects of mass above $10^5 M_\odot$ do not produce appreciable starlight since such SMOs, if they contain no heavy elements, collapse due to relativistic instabilities before burning their nuclear fuel (Fricke 1973).

We now consider the 'recombination' model discussed in sections 2.3 and 3.2.1, where the stellar spectrum is reprocessed by neutral hydrogen absorption in either the vicinity of the source or by diffuse or clumped gas in the background universe. In this case, the bulk of the radiation is predicted to be in the form of a fairly narrow Lyman α line at $\lambda = 0.12(1 + z_*)\mu$m , with the spectrum completely cut off above $\lambda = 0.09(1 + z_*)\mu$m . The hypothesis of a single formation redshift z_* then leads to higher required values of Ω_* , because of the lower continuum flux. At most one observational point would be boosted by the Lyman α emission. The curve (c) in Fig 4.1 illustrates a fit to the data with Ω_* =1 and z_* = 15. The R model used in these calculations is an improvement on the simple model of Carr, McDowell and Sato (1983) and allows a better fit to the data.

On the other hand, if the stars form over an extended redshift range, the Lyman α line radiation is spread over a wide frequency interval and can be used to fit the spectrum. In this section we will model the recombination spectrum simplistically by considering it to consist purely of the Lyman line. The Lyman α density at observed frequency ν is related to the star formation rate per unit redshift interval, $\phi(z)$ expressed in units of the critical density, by

$$\omega_\alpha(\nu) = \epsilon L \phi(z_\nu) \tag{4.2.3}$$

where L is the fraction of the flux in Lyman alpha. Since the intensity at a given frequency ν depends only on the star formation rate at one particular redshift, $z_\nu = \nu_\alpha/\nu - 1$, any desired spectrum can be reproduced with an appropriately chosen *ad hoc* form of $\phi(z)$. Even if the continuum contribution is included, it is still true that the intensity at ν is dominated by the value of ϕ at z_ν. I fit the data to two frequency segments using the simple model $\phi(z) = A + B(1+z)^{-1}$ which allows eq. (4.2.3) to be integrated easily. A fit to the upper ends of the error bars (maximum energetic requirement) gives the total star density to be $\Omega_* = 0.55/L$ and a fit to the lower ends of the error bars gives $\Omega_* = 0.28/L$. Using the R model spectrum and adjusting A and B interactively for the same frequency ranges, the fit obtained is $\Omega_* = 1.0$ for the maximum and $\Omega_* = 0.4$ for the minimum energetic requirements, respectively. This suggests that an approximate way to allow for the effects of the continuum is to set L=0.6 in eq. (4.2.3). The fitted spectra using the R model are displayed in Fig. 4.2. The redshift range implied for the star formation is from $z = 11$ to $z = 41$, so the stars would still be pregalactic.

All these calculations assume that the opacity due to grains is negligible; any dust absorption would increase the required Ω_* . Conversely, confirmation of such a near-IR background as being due to redshifted starlight, coupled with the assumption that Ω_* can be at most 1, in conformity with inflationary cosmological theories now in vogue, would impose a severe restriction on the cosmic dust abundance.

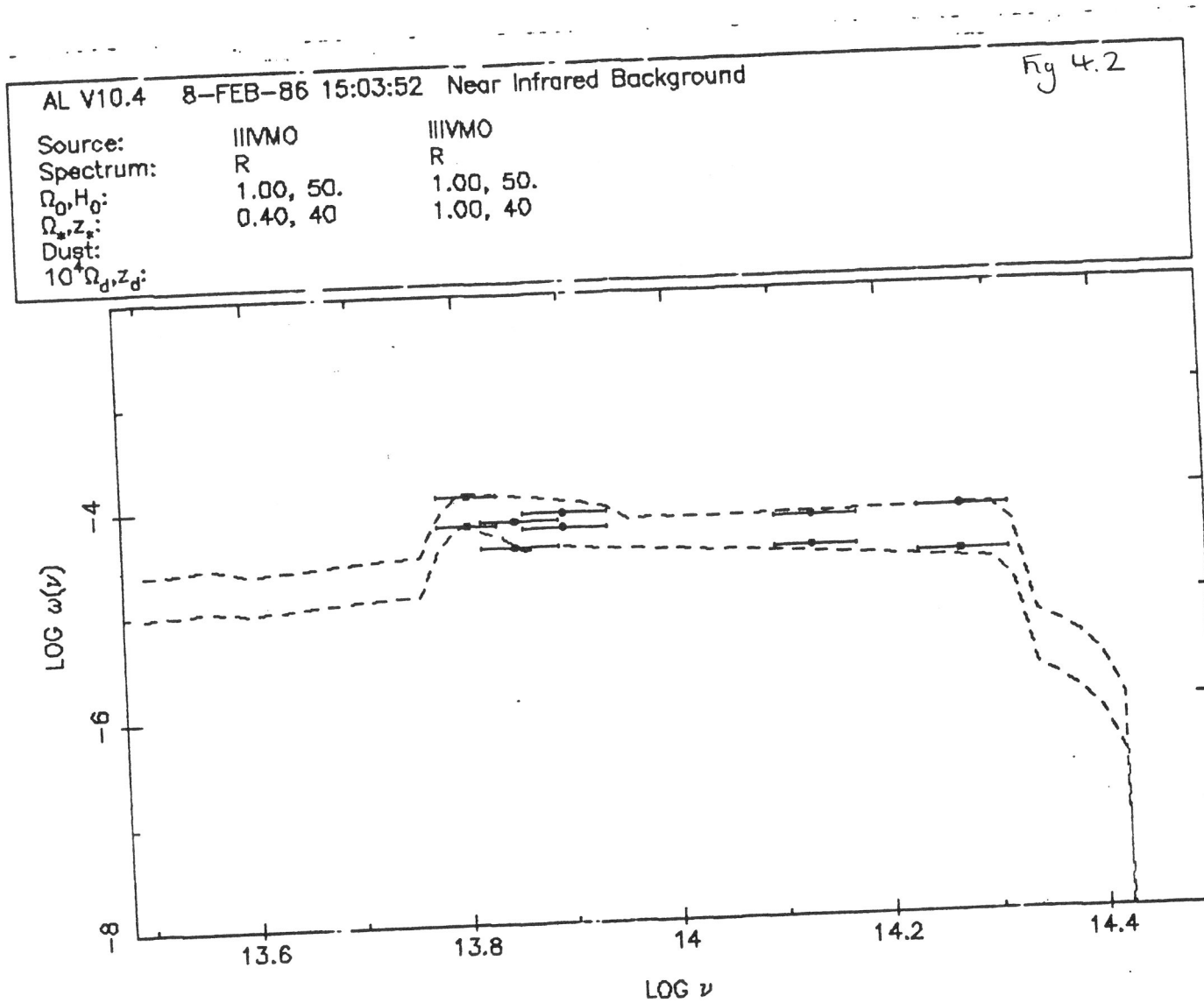
AL V10.4 8-FEB-86 15:03:52 Near Infrared Background
Source: IIIVMO IIIVMO
Spectrum: R R
Ω_0, H_0: 1.00, 50. 1.00, 50.
Ω_*, z_*: 0.40, 40 1.00, 40
Dust:
$10^4\Omega_d, z_d$:
LOG ω(ν)
-4
-6
-8
13.6
13.8
14
14.2
14.4
LOG ν

Fig 4.2

4.3 Accreting black holes and the infrared background

The black hole remnants of pregalactic stars, as well as black holes with no stellar precursors, would inevitably accrete from the background matter. If the holes accrete at the Bondi (1952) rate from gas of density n relative to which they are moving subsonically, and radiate with efficiency ϵ, each should have a luminosity

$$L = 1.1 \times 10^{25} \epsilon M^2 n T_4^{-3/2} \tag{4.3.1}$$

provided that this is less than the Eddington limit. Since the background matter is heated by the radiation from accretion, the evolution of n and T may be very complicated, especially during the period when the holes are surrounded by individual HII regions (Carr 1981a). However, once the universe is ionized, we always have n given by eq (2.2.17b) on average. This corresponds to an accretion rate

$$\dot{M} = 3.4 \times 10^{14} M^2 \Omega_g h_{50}^2 T_4^{-3/2} (1+z)^3 \quad \text{kg/s} \tag{4.3.2}$$

The radiation spectrum from such holes is uncertain, but if they accrete from a disk we may use the standard disk accretion model which, Eardley et al (1978) suggest, results in an approximately black body spectrum at low accretion rates

$$\dot{M} < \dot{M}_{bb} = 10^{13} M^{7/8} \text{kg/s} \tag{4.3.3}$$

This is equivalent to $L/L_{Edd} < 0.02 \epsilon M_6^{-1/8}$, where $M_6 = M/10^6 M_\odot$. In this case, the black body temperature at the inner edge of the accretion disk (where most of the luminosity comes from; taken as $R = 10GM/c^2$) is

$$T_{bb} = 2.1 \times 10^4 (\epsilon \Omega_g h_{50}^2 (1+z)^3)^{1/4} T_4^{-3/8} \text{K} \tag{4.3.4}$$

We note that T is independent of M. The peak of the spectrum is on the low energy side of the Lyman cutoff providing

$$1 + z < 17 (\epsilon \Omega_g h_{50}^2 / 0.01)^{-1/3} T_4^{\frac{1}{2}} \tag{4.3.5}$$

In this case we do not have to worry about absorption by neutral hydrogen, and the spectrum will be unaltered. Of course, it will not be exactly blackbody because of contributions from cooler portions of the accretion disk at larger radii, and the background spectrum will be smeared out due to the range in M and z.

The present energy density and temperature of the blackbody radiation generated by holes at redshift z are respectively

$$\Omega_R = \frac{Lt\Omega_B}{(1+z)Mc^2}$$
$$= 8 \times 10^{-5} \epsilon M_6 \Omega_B \Omega_g \Omega_0^{-\frac{1}{2}} (1+z)^{\frac{1}{2}} T_4^{-3/2} h_{50} \qquad (4.3.6)$$

and

$$T_{obs} = 2.1 \times 10^4 (\epsilon \Omega_g h_{50}^2 (1+z)^{-1})^{1/4} T_4^{-3/8} \mathrm{K} \qquad (4.3.7)$$

(Carr, McDowell and Sato 1983) where t is the expansion time at redshift z (and the approximation of eq (1.5.2) has been used) and Ω_B is the contribution of the black holes to the density parameter. Bond, Carr, and Hogan (1986) consider the case where the gas is clumpy, but I will restrict myself to considering the background gas. T_{obs} is in the range $10^3 - 10^4$K for reasonable values of ϵ,Ω_g, and T_4, and depends on z only weakly.

We now estimate the redshift from which the bulk of the radiation will come. From eq. (4.3.6), this will be the highest redshift at which the holes are radiating with the blackbody spectrum we have assumed, which in this model is the redshift at which the accretion rate drops below that given in eq (4.4). Thus

$$1 + z = 17 M_6^{-3/8} \Omega_g^{-1/3} h^{-2/3} T_4^{\frac{1}{2}} \qquad (4.3.8)$$

The matter temperature T_4 is determined by the balance between heating due to photoionization from the black hole spectrum and cooling due to Compton scattering of electrons off the microwave background and due to recombination line cooling in the gas. Studies of the thermal history of the IGM suggest that T_4 will remain in the range 1-10 while the holes have a soft spectrum, but at higher

redshifts, when the holes would have radiated X-rays, their Compton heating effect could have boosted the temperature to higher values (Carr 1981a).

With the adoption of (4.3.8), z, M and Ω_B are determined once any one of them is specified, if ϵ,Ω_0 and Ω_g are given. The hole mass is

$$M = 4 \times 10^6 \left(\frac{\epsilon}{0.1}\right)^{-1.2} \Omega_B^{-1.2} \Omega_0^{0.6} \Omega_g^{-1.0} h_{50}^{-3.2} T_4^{1.5} \left(\frac{\Omega_R h_{50}^2}{10^{-4}}\right)^{1.2} M_\odot \qquad (4.3.9)$$

We can add an extra constraint by requiring that z be greater than the redshift of galaxy formation z_{gal} This condition implies

$$M < 3 \times 10^7 \left(\frac{\Omega_g}{0.1}\right)^{-0.9} \left(\frac{1+z_{gal}}{10}\right)^{-2.7} h_{50}^{-1.8} T_4^{1.3} M_\odot \qquad (4.3.10)$$

and thus

$$\Omega_B > 0.2 \left(\frac{\epsilon}{0.1}\right)^{-1} \left(\frac{\Omega_g}{0.1}\right)^{-0.1} \left(\frac{1+z_{gal}}{10}\right)^{2.2} h_{50}^{-1.2} T_4^{0.2} \Omega_0^{0.5} \left(\frac{\Omega_R h_{50}^2}{10^{-4}}\right) \qquad (4.3.11)$$

We also impose the condition that $\Omega_B < 1$. This leaves us with a scenario in which M is between 10^7 and 10^8 $M_\odot$, corresponding to precursors in the SMO range, and $\Omega_B > 0.1$, which is sufficient to explain the dark matter problem. The corresponding value of z, the redshift from which the bulk of the radiation comes, is in the range 5-50 even if the holes actually form at much higher redshift. The observed temperature of the spectrum is

$$T_{obs} = 4 \times 10^3 M_6^{0.1} \left(\frac{\epsilon}{0.1}\right)^{1/4} \left(\frac{\Omega_g}{0.1}\right)^{1/3} T_4^{-\frac{1}{2}} h_{50}^{2/3} \mathrm{K} \qquad (4.3.12)$$

The temperature would be smaller if the accretion disks were optically thick, so that their effective radii were increased. The parameter T_4 is also uncertain; if it were as large as 10, a good fit to the data can be obtained with $M = 10^9$ $M_\odot$, $\Omega_B = 1$,$\Omega_g = 0.1$, and z of order 10. If $T_4 = 1$, lower masses can be accommodated, and with $\Omega_g = 0.2$, solutions with M as low as $10^7 M_\odot$ can be consistent.

In conclusion, the infrared background claimed by Matsumoto et al can be explained as the redshifted radiation from pregalactic stars or supermassive black holes, but only if these objects make up a large fraction of the closure density.

5 Background Light Limits for VMOs

5.1 Observational Limits on Extragalactic Background Light

Theoretical interest in a possible cosmological component in the light of the night sky goes back to the paradox of de Cheseaux and Olbers (Olbers 1826). Olbers' paradox, as it is most commonly known, points out that if the universe is infinite and uniformly filled with luminous stars, the night sky would be as bright as a star rather than dark, since any line of sight would encounter the same surface brightness. We now know that the stars are grouped into galaxies, and the distribution of galaxies is not homogeneous even on large scales, but still we should expect to see some radiation from the integrated light from galaxies along our past light cone. In fact, for an infinitely old universe, the radiation density of the universe would diverge even if the expansion and redshifting is taken into account; in the late stages of a recollapsing universe, the sky surface brightness would also become very large. Thus the observation that the night sky is dark is an important cosmological datum. However, the finite amount of emission along a typical line of sight should tell us something about the distribution and formation of galaxies, and the suggestion by Peebles and Partridge (1967) that this emission might contribute to an ultraviolet background stimulated attempts to measure the true brightness of the night sky.

The measurement of an (approximately) isotropic cosmological background is much more difficult than the detection of a faint discrete source, where relative rather than absolute measurements can be made. To estimate the background intensity, all internal (instrumental) backgrounds must be calibrated and as far as possible removed, and the count rate of the instrument must be carefully calibrated in absolute units. The subtraction of other astronomical background sources (zodiacal light, terrestrial atmospheric emission, galactic diffuse emission and the integrated effect of unresolved point sources) introduces errors which are often

difficult to estimate. Nevertheless, broadly consistent data is now available for many regions of the spectrum.

Attempts have been made to observe extragalactic background radiation in nearly every waveband. In this study I consider limits in the region from the far UV to the far IR. The values of the energy density corresponding to the subset of the observations I have adopted to compare with my predicted spectra are listed in table 5.1 as values of the parameter $\omega(\nu)$, the energy density per unit logarithmic frequency interval in units of the critical density. The observations are also plotted in Fig 5.1, together with a 3K blackbody spectrum representing the microwave background. Fig 5.2 is an enlarged copy of Fig 5.1 allowing the individual observational points to be identified; they are labelled with the same reference numbers as in Table 5.1. I have adopted $h_{50} = 1$ in calculating the values of ω. To convert from other units to this 'critical energy density unit' the equivalents are

$$\begin{aligned}\omega(\nu) &= 1.0 \times 10^{2}(\nu i(\nu)/1\text{W m}^{-2}\text{sr}^{-1}) \\ &= 2.0 \times 10^{-9}(f(\lambda)/1 \text{ photon s}^{-1}\text{cm}^{-2}\text{sr}^{-1} \text{ Å }^{-1}) \\ &= 3.0 \times 10^{-4}(\lambda/1\mu\text{m})(i(\nu)/1 \text{ MJy sr}^{-1}) \\ &= 5 \times 10^{-7}(\lambda i(\lambda)/1 S_{10}(V)_{G2V} \text{ at } 4400\text{Å})\end{aligned} \tag{5.1.1}$$

where the S_{10} conversion factor is that quoted by Toller (1983).

In the millimetre and submillimetre range, we are interested in any extra background in addition to the known cosmic microwave background radiation which, for the purposes of this thesis, we assume is the relic radiation from the Big Bang and has an exactly blackbody spectrum with a temperature of 3 K. There is at present no unambiguous evidence for spectral distortions in the 3K background, although Gush (1981) and Woody and Richards (1981) claimed to detect significant distortions. Woody and Richards flew a balloon from Texas in 1977 to a height of 43 km and measured the microwave background spectrum at a

large number of frequencies. I shall not be concerned here with their measurements near the peak, but the observations at higher frequencies, where the signal from the microwave background is small, provide useful upper limits to extragalactic background radiation in the 400 – 700 micron region. The Gush measurement was made using a Nike Black Brant sounding rocket from Fort Churchill in Canada. The observation was of an area in Perseus and the claimed distortion corresponded to $\log \omega(\nu)$=-4 in the 500 – 900 micron range.

De Bernardis *et al.* (1984) flew a balloon payload from Sicily to observe the background in two channels, 150 – 400 microns and a 350 – 3000 micron channel. The wide passband of the low frequency channel makes it difficult to estimate the residual background after galactic emission is subtracted. Ceccarelli *et al.* (1984) use the same data to study dipole anisotropies in the background. This technique has the advantage that any cosmological background will show an anisotropy in the same direction as that of the microwave background, assuming that the latter is due to the motion of the solar system through the rest frame of the background, and the magnitude of the anisotropy depends on the spectrum of the background. The technique can thus measure an extragalactic background without contamination by galactic backgrounds (which will not show the anisotropy). The results are somewhat model-dependent but I adopt a conservative upper limit to the intensity of a background possessing a dipole anisotropy of $\log \omega(\nu)$=-4.0.

The Anglo-US-Dutch IRAS satellite which mapped the sky at 12, 25, 60 and 100 microns in 1983 was designed to observe point sources, but attempts have been made to estimate the possible contribution from diffuse emission. Hauser et al (1984) presented the preliminary results and discussed the dependence of the data on ecliptic latitude and galactic latitude. The interplanetary dust component has already been discussed in chapter 4. Rowan-Robinson (1985) suggests that the 100 micron measurements represent a detection of an extragalactic background with substantial energy density; the calibration of the data is still uncertain, and

it remains possible that all of the 100 μm flux could be due to galactic emission. 10 MJy/sr is a safe upper limit at 100 microns, and 5 MJy/sr is a more reasonable estimate. I adopt the more conservative estimate for now. At 12, 25 and 60 microns I adopt the values tabulated by Hauser *et al.* of 18, 33 and 7 MJy/sr respectively. In the near infrared Hoffmann and Lemke (1978) reported results from a 1972 balloon flight from Palestine, Texas which measured an upper limit to the background at 2.4 microns. The sounding rocket results of Matsumoto et al (1983) were discussed in chapter 4.

There is at present no useful limit on background light in the red part of the visible spectrum, the only constraint being the zodiacal light brightness at the ecliptic pole which is orders of magnitude brighter than limits at nearby wavebands. This region of the spectrum is very important for studies of light redshifted from the early universe, and ultimately observations from space probes at large heliocentric distances will yield useful results in this area.

The best optical limits are those of Dube *et al.* (1979) and Toller (1983). The Dube *et al.* observations were made with a photometer and a narrow band filter from the 91 cm telescope at Kitt Peak; the filter was centered at 5115 A and thus gives a limit corresponding roughly to the V band. Toller's observations at B (4400 A) were made from beyond the asteroid belt (using a photometer on board the Pioneer 10 probe) and should be free of most solar system background light. Both studies obtain an upper limit of approximately 4 S_{10}, or a brightness equivalent to four 10th magnitude solar type stars per square degree. Their estimates are similar to most other attempts to measure the visible light of the night sky; the early work of Roach and Smith (1968) obtained a value of $5S_{10}$, while Spinrad and Stone (1978) also get $5S_{10}$ at 4000Å from photometry on the 90 cm telescope at Lick.

Measurements of the UV background in the past decade have been the subject of some controversy. In 1972 Henry *et al.* (1978) observed the background

with a UV spectrometer on board the spaceship *Apollo 17* during its trans-Earth coast from the Moon. Their result, which may be contaminated by geocoronal Lyman α radiation, was the positive detection of a probably extragalactic background with a peak intensity of 300 photon s^{-1} $cm^{-2}sr^{-1}Å^{-1}$ at 1450 Å , in the form of a feature 400 Å wide, with declining flux toward the edge of the 1180 – 1680 Å bandpass. Later observations have not confirmed this feature, although some have detected a flat spectrum of the same magnitude. Pitz *et al.* (1980) launched a 16 cm telescope with 3 photometers covering the range 1600 – 2800 Å on a Skylark rocket from Spain in 1975 to an altitude of 250 km. This 'Astro-7' mission was mainly intended to study the zodiacal light, and detected large residual signals equivalent to $\log\omega(\nu)$=-5.3 which are probably galactic in origin. Large signals were also detected by the Berkeley EUV telescope (Paresce *et al.* 1979) on board the *Apollo-Soyuz Test Project* spaceship in a 250 km orbit in July 1975. They report patchy UV emission with a minimum value of 300 photon s^{-1} $cm^{-2}sr^{-1}Å^{-1}$, consistent with the Henry *et al.* value, although in some fields the emission was much greater. Limits in the near UV (1500 – 3300 Å) come from the work of Maucherat-Joubert *et al.* (1980) who used photometers on the French D2B ('Aura') satellite which was placed in low Earth orbit in 1976. Results from a spectrometer on board the Soviet Prognoz-6 magnetospheric research satellite were reported by Severny and Zverezda (1983). The spectrometer covered the region 1400-1800Å , and observations were made from a distance of 200,000 km from Earth.

Other observations have tended to reduce the estimates of extragalactic ultraviolet background light. Feldman *et al.* (1981) flew an Aries rocket from White Sands, New Mexico in Jan 1977, to an apogee of 350 km. The payload was a spectrometer covering the range 1200 to 1670 Å and from a total signal of 300 photon s^{-1} $cm^{-2}sr^{-1}Å^{-1}$ they removed several galactic emission lines leaving a fairly constant background of 150 ± 50 photon s^{-1} $cm^{-2}sr^{-1}Å^{-1}$. Jakobsen

et al. (1984) launched a large (95 cm) telescope to 250 km on another Aries flight in 1982. The payload included 3 photometers covering the range 1450 - 2420 Å . The limits they obtained (500 to 1000 photon s^{-1} $cm^{-2}sr^{-1}Å^{-1}$) were weaker than the Feldman *et al.* results. The shortest wavelength point is that of Weller (1983), who observed with a 1220 – 1500 Å photometer on the US Navy Solrad 11B satellite, 100000 km from the Earth. Weller quotes a minimum flux of 180 photon s^{-1} $cm^{-2}sr^{-1}Å^{-1}$ with no quoted error; adopting the claimed 30% accuracy of the experiment's agreement with earlier calibrations, I will adopt an upper limit of $\log \omega(\nu)$=-6.30.

Future measurements of the ultraviolet background are due to be carried out with 'Getaway Special' payloads on the Space Shuttle (Feldman, private communication). Major improvements in our understanding of the universe at high redshift may be possible with the launch of the Cosmic Background Explorer (COBE) from the Shuttle at the end of the decade. COBE (Mather, 1982) will study the diffuse infrared and microwave backgrounds with a 10 band photometer (1 to 300 μm), a far infrared spectrometer (100 μm to 1 cm) and a differential microwave radiometer which will measure deviations from a 3K blackbody in the microwave region.

Table 5.1 Observational limits

The parameter $w(\nu)$ is the energy density per logarithmic frequency interval in units of the critical density needed to close the universe. The values are tabulated for H =50 km/s/Mpc.

Wavelength (μ) Eff.	Bandwidth	Log ν	Log ω_ν	Ref
650	625-665	11.66	-4.3	(1)
590	570-610	11.71	-4.3	(1)
500	490-510	11.78	-4.3	(1)
500	350-3000	11.78	-4.0	(3)
425	415-435	11.85	-4.3	(1)
200	150-400	12.18	-4.36	(2)
100	80-120	12.48	-4.52	(4)
60	40-80	12.70	-4.46	(4)
25	19-30	13.08	-3.40	(4)
12	8-15	13.40	-3.35	(4)
4.7	4.4-5.0	13.81	-3.92	(5)
4.2	3.8-4.5	13.85	-4.17	(5)
3.8	3.4-4.1	13.90	-4.10	(5)
2.4	2.35-2.45	14.10	-3.84	(6)
2.2	2.0-2.4	14.13	-4.19	(5)
1.6	1.45-1.75	14.27	-4.14	(5)

Wavelength (Å) Eff.	Bandwidth	Log ν	Log ω_ν	Ref
5115	5070-5160	14.77	-5.59	(7)
4400	3950-4850	14.83	-5.70	(8)
3100	2850-3350	14.99	-5.60	(9)
2200	2000-2400	15.13	-6.24	(9)
1790	1690-1890	15.22	-6.22	(10)
1690	1520-1860	15.25	-5.82	(9)
1680	1580-1780	15.25	-6.05	(10)
1550	1500-1650	15.29	-6.40	(11)
1450	1400-1500	15.32	-6.40	(11)
1350	1300-1400	15.35	-6.40	(11)
1250	1220-1500	15.38	-6.30	(12)

REFERENCES

(1) Woody and Richards (1981)
Balloon flight, Texas

(2) De Bernardis et al (1984)
Balloon flight, Sicily

(3) Ceccarelli et al (1984)
Dipole anisotropy limit on data of (2)

(4) Hauser et al (1984)
IRAS satellite, low Earth orbit

(5) Matsumoto et al (1983)
Kappa-9M Rocket flight, Japan

(6) Hoffmann and Lemke (1978)
Balloon flight, Texas

(7) Dube et al (1979)
Kitt Peak, Arizona

(8) Toller (1983)
Pioneer 10 space probe, beyond the asteroid belt

(9) Maucherat-Joubart et al (1980)
Aura satellite, low Earth orbit

(10) Severniy and Zverezda (1983)
Prognoz-6 satellite, cislunar space

(11) Feldman et al (1981)
Aries rocket, White Sands, New Mexico

(12) Weller (1983)
Solrad 11B satellite, cislunar space

Fig 5.1

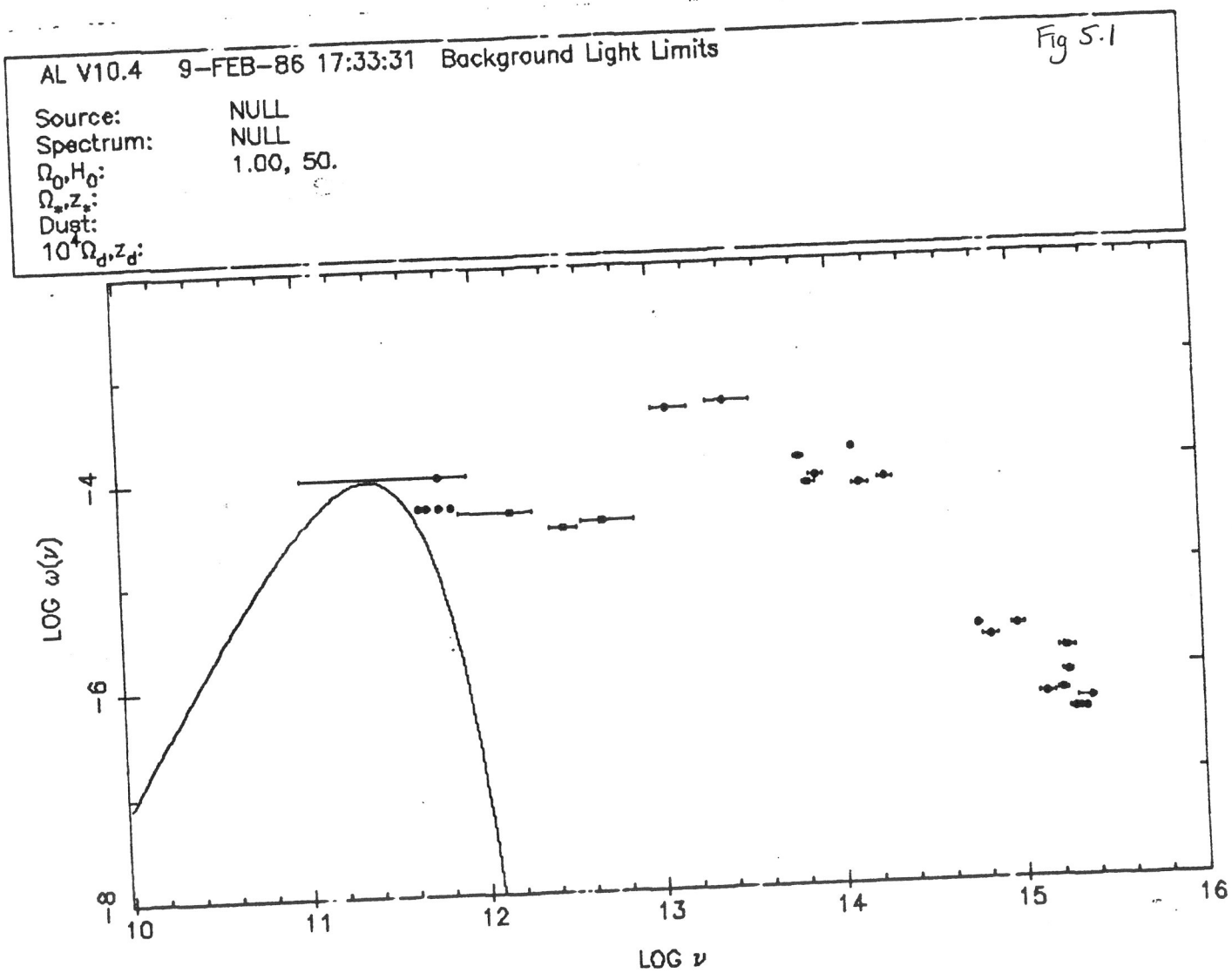
AL V10.4 9-FEB-86 17:33:31 Background Light Limits
Source: NULL
Spectrum: NULL
Ω_0, H_0: 1.00, 50.
Ω_*, z_*:
Dust:
$10^4\Omega_d, z_d$:
LOG $\omega(\nu)$
-4
-6
-8
10
11
12
13
14
15
16
LOG ν

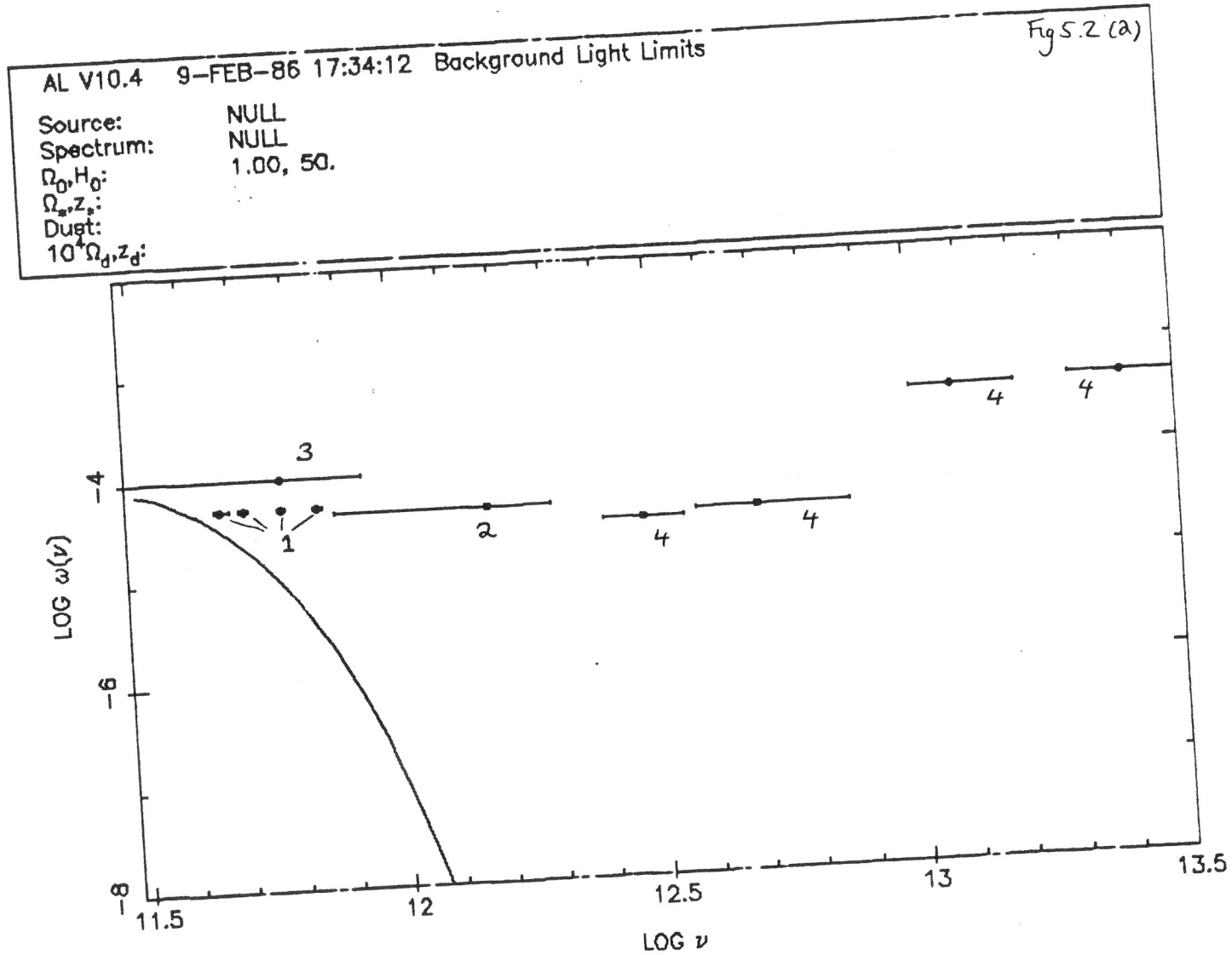
AL V10.4 9-FEB-86 17:34:12 Background Light Limits
Source: NULL
Spectrum: NULL
Ω_0, H_0: 1.00, 50.
Ω_*, z_*:
Dust:
$10^4\Omega_d, z_d$:
LOG $\omega(\nu)$
LOG ν
-4
-6
-8
11.5
12
12.5
13
13.5
1
2
3
4
4
4
4

Fig 5.2 (a)

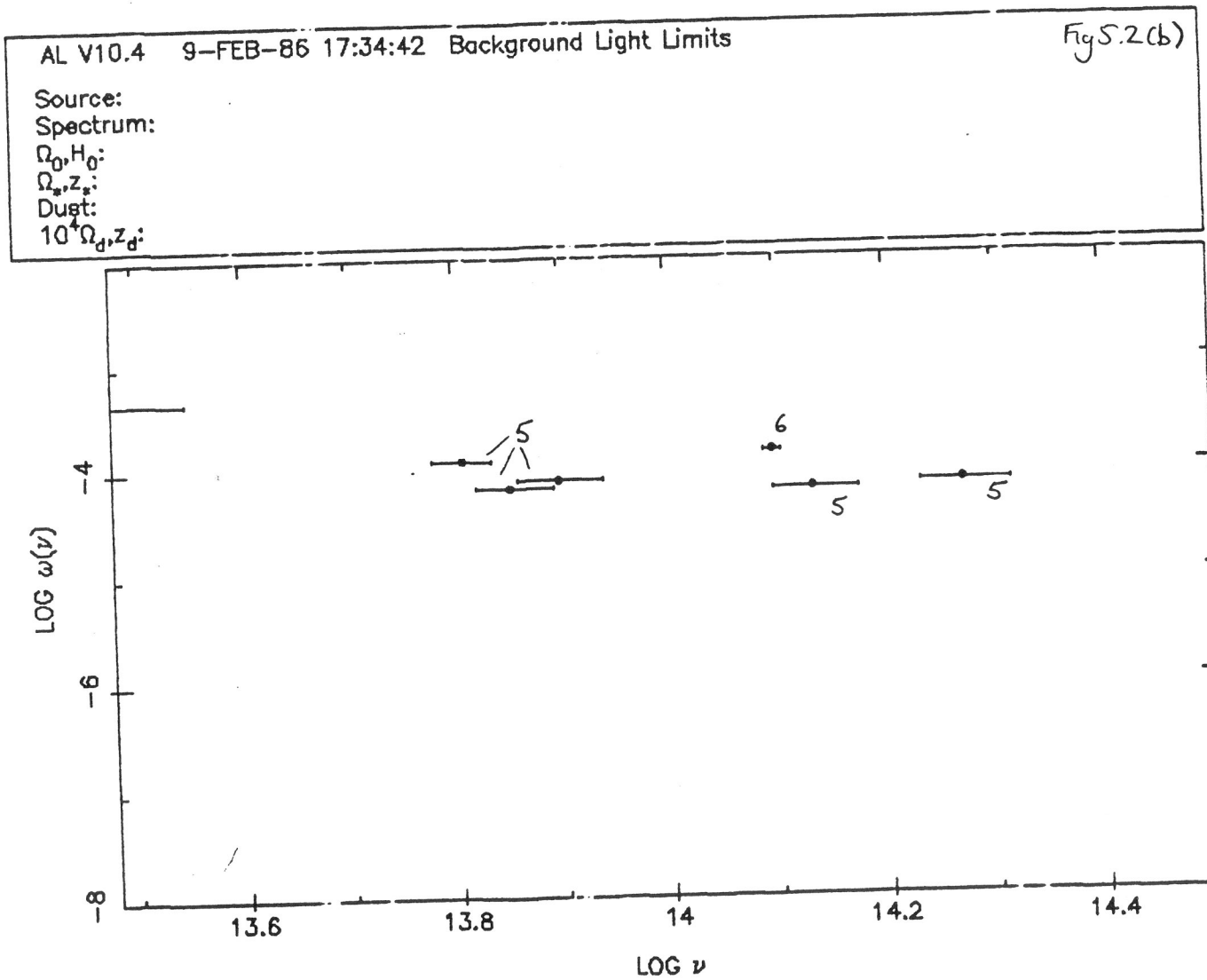
AL V10.4 9-FEB-86 17:34:42 Background Light Limits
Source:
Spectrum:
Ω_0, H_0:
Ω_*, z_*:
Dust:
$10^4\Omega_d, z_d$:
LOG $\omega(\nu)$
-4
-6
-8
13.6
13.8
14
14.2
14.4
LOG ν
5
6
5
5

Fig 5.2(b)

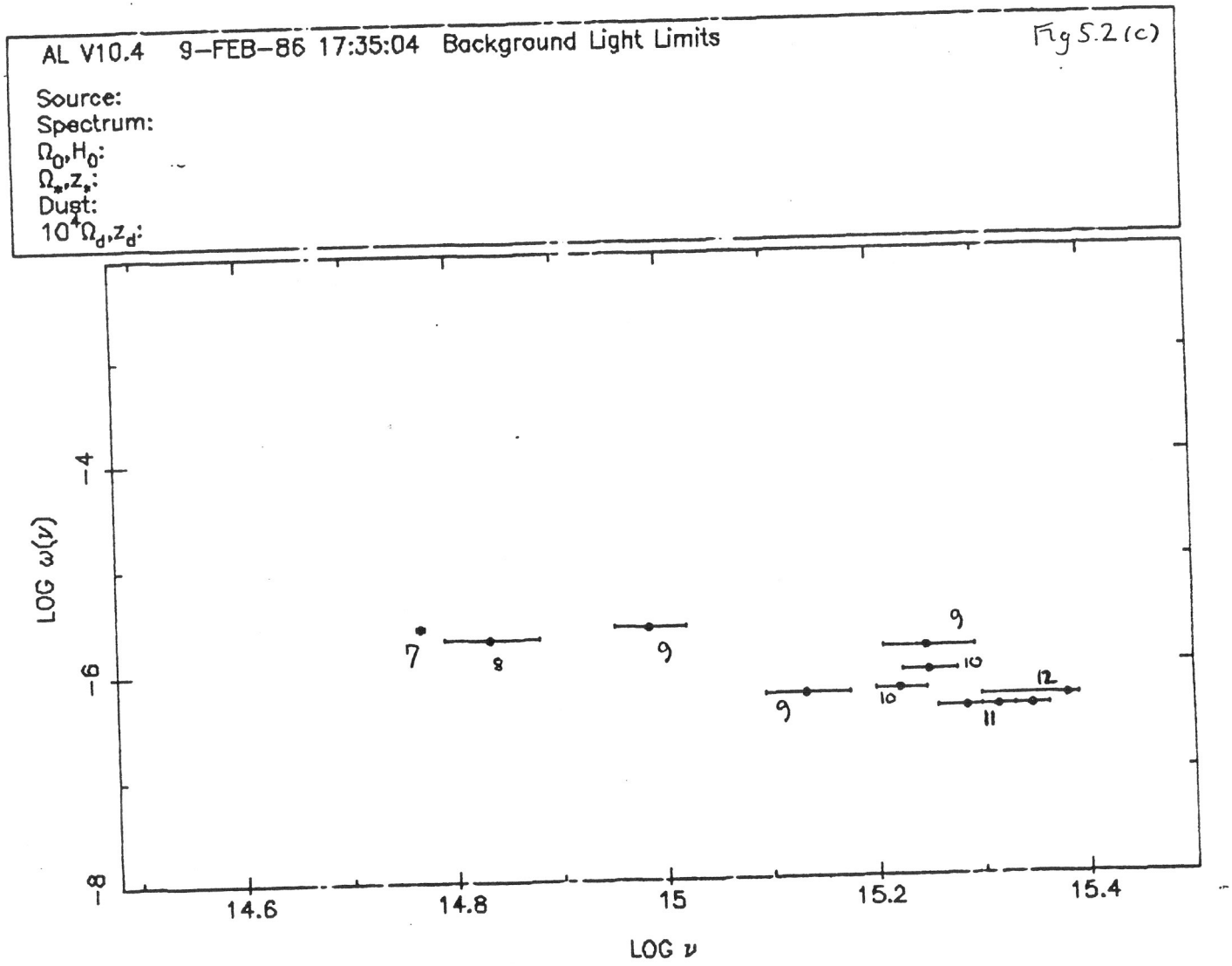
AL V10.4 9-FEB-86 17:35:04 Background Light Limits
Source:
Spectrum:
Ω_0, H_0:
Ω_*, z_*:
Dust:
$10^4\Omega_d, z_d$:
LOG $\omega(\nu)$
-4
-6
-8
14.6
14.8
15
15.2
15.4
LOG ν
7
8
9
9
9
10
10
11
12

Fig 5.2 (c)

5.2 Limits on VMO density as a function of redshift

I now compare the predicted spectra of chapter 3 with the observational limits of section 5.1. To compare a given predicted spectrum with a particular observational limit, I estimate the average value of $\omega(\nu)$ within the estimated bandpass of the observation (after first subtracting the microwave background if appropriate); the bandpass transmission is modelled as a simple box function between the two values of $\log\nu$ defining the bandwidth. In some cases a triangular transmission function might have been a better model but the simple rectangular model was adopted for simplicity and uniformity. The shape of the transmission function of the observational data will only be important for the R model spectrum, where the strong Lyman α line may give a strong observed signal even if it is far from the effective wavelength of the observation. In this context it is worth noting that many of the observations are quite broadband ones. Once the estimated value of $\omega(\nu)$ has been evaluated, it can be compared with the value in Table 5.1. Since the flux is proportional to Ω_* , the ratio of the two values immediately gives the maximum value of Ω_* consistent with the observations. (Actually, one might worry that this may be false in some of the models with dust. If the dust temperature is dominated by the microwave background radiation at small Ω_* , but by the stars at large Ω_* , the dust emission spectrum will not be simply proportional to Ω_* . This should be a minor effect except for very small Ω_* .)

For each spectrum I repeat this procedure for each of the observational limits, and take the smallest limit on Ω_* from any of the observational points. Which point gives the best limit will depend on the assumed star formation redshift z_*; lower redshifts will mean that the spectra peak at higher frequencies and so the points giving the most sensitive limit will be the high frequency ones.

To illustrate the form of the results, Fig 5.3 shows the derived upper limits on Ω_* for a single observational point, the 4400Å point of Toller (1983). The limits displayed are for all four spectral models (BB, H, He, and R) in a dust-free

universe. The limits are strongest where the peak of the spectrum is redshifted to the wavelength of the observation. For the BB model the limits are weak at low z because the observation probes the Rayleigh-Jeans tail of the spectrum; the high z limits are weak because the bulk of the spectrum has been redshifted past the visible into the infrared if the redshift is high. The stellar atmosphere models H and He provide stronger constraints at higher redshifts because the corresponding spectrum is harder than a blackbody one. The R model gives a very strong limit for the redshift range in which the Lyman α line lies within the bandpass of the observation, but gives no constraint at redshifts large enough that the Lyman cutoff is redward of the observed wavelength (Carr, Bond and Arnett 1984).

The corresponding diagrams for other observational points are similar in form. Since the combination $\nu(1+z)$ enters into the spectrum, the curves corresponding to an observation with higher ν will vary more rapidly with z, while the curves from infrared observations will be almost flat. In Fig 5.4 and succeeding figures I present the results from all the observational limits listed in Table 5.1 simultaneously, plotting only the strongest limit at any given redshift.

The first results I present are those for a dust-free universe. The combined limits on Ω_* as a function of redshift are plotted in Fig 5.4 for three of the spectral models, and in Fig 5.5 for the R model. The limits presented in Fig 5.4 are significantly weaker than the approximate limits plotted in Fig. 4 of Carr, Bond and Arnett (1984). The redshift dependence of the R model limits is complicated because of the different redshift ranges corresponding to the Lyman line being redshifted into different observational bands. The limits are quite good for the redshift ranges where this occurs, but where there are gaps in the observational coverage the limits are from the continuum and are much poorer. In a more realistic model the finite extent in redshift of the Population III era should smooth out most of these gaps.

To summarize the data I define a redshift $z(\Omega_*)$ below which a model is

excluded; the star density can only be as much as Ω_* if the stars form at a redshift greater than $z(\Omega_*)$. I tabulate $z(\Omega_*)$ for Ω_* =0.01, 0.1 (the minimum density usually postulated for the dark matter) and 1 (closure density). If z were as large as the value given by eq (3.1.2) for some model, then that model could be completely ruled out. In practice this is not the case with current observational limits, but very modest improvements in the observations would rule out many of the no-dust models (Table 5.2).

Fig 5.6 and Table 5.3 show the results obtained for the blackbody spectral model for varying dust abundances, under the assumption that the dust and the stars formed at the same epoch. As the dust abundance increases, the limit on dark matter Population III stars becomes much weaker, as it depends only on the weak far IR limits. The limit on a closure density of stars does not show this behaviour, and is actually stronger than in the dust free case. This is because the spectra of the high redshift dust emission models become narrower in frequency range as the redshift increases, leaving the peak energy relatively constant even though the total energy decreases. The limit does not, therefore, weaken with redshift in the usual way. The limits for the unabsorbed model are particularly weak as the peak of the redshifted blackbody spectrum lies in an unobserved region of the near infrared.

The models with dust at low redshift (z=3,5) and maximum dust abundance (Fig. 5.7, Table 5.4) give only a slightly stronger constraint for z(0.1). The constraint in these models at high redshift is the 200 μm limit on the intensity of the reradiated emission from dust. It should be noticed that the Woody and Richards and the IRAS points give a constraint which is weaker by a factor of 5, so the 200 micron point is important and more observations in this region would be very useful.

Tables 5.5 and 5.6 show that the results obtained above for dust absorption of the blackbody spectrum are not very sensitive to the input spectrum (Table

5.5, H and He models) or the assumed opacity law (Table 5.6, linear and D3 laws of Section 3.4).

Fig 5.8 shows the results for dusty universes with an R model input spectrum. The limits are similar to those for the other models for redshifts above 5.

The results of this chapter can be summarized as follows. If $h_{50} = 1$, and the universe contains Population III VMOs which ionize the universe but little ($\Omega_d < 10^{-6}$) dust, then the stars must have formed before a redshift of 60 if they close the universe, or a redshift of 35 if they make up one tenth of closure density. These limits are stronger if the Hubble constant is more than 50. If the universe is not ionized (i.e the gas is very clumpy), the radiation from stars making up one-tenth of closure density would remain undetected in the near infrared even if they were burning as recently as z=4.

The limits on a closure density of stars are equally strong if the universe is opaque at high frequency due to dust absorption, but if there is a large dust abundance ($\Omega_d \sim 10^{-4}$) there may be an extragalactic infrared background at a wavelength of a few hundred microns originating from the reprocessing by dust of radiation from Population III stars with $\Omega_* = 0.1$ burning at a redshift of 5 or more.

Finally, I note that the radiative efficiency of supermassive stars prior to their collapse is at least a factor ($M/10^5 M_\odot$) smaller than for VMOs (Carr, Bond and Arnett 1984). The limits for SMOs are hence weaker by at least this factor, but limits on accretion by discrete sources in our galaxy will be stronger (Lacey and Ostriker 1985, and Chapter 7). As emphasized by Bond, Carr and Hogan (1986) and Negroponte (1986), attempts to observe extragalactic background light in the red, near infrared, and far (100-500 μm) infrared may shed crucial light on the history of the universe at high redshift.

Tables 5.2 to 5.6 list values of $z(\Omega_*)$, the smallest redshift at which the model in question exceeds the observational limits.

Table 5.2 Models with no dust

H0=50

Spec: \ Ω_*	0.01	0.1	1
BB	13	29	40
H	18	43	76
He	14	36	64
R	3.5	3.5	20

H0=100

Ω_*	0.01	0.1	1
	23	36	180
	32	65	150
	28	50	210
	4.7	5.9	42

Table 5.3 Blackbody model with varying dust abundance

H0=50

Ω_d \ Ω_*	0.01	0.1	1
0	13	29	40
1.E-6	11	24	81
1.E-5	7.5	11	76
1.E-4	2.3	5.5	62

H0=100

Ω_*	0.01	0.1
	23	36
	-	-
	3.5	25
	5.6	9.0

Table 5.4 Blackbody model with dust forming more recently

H0=50

z_d \ Ω_*	0.01	0.1	1
3	2.4	18	32
5	2.3	5	46
100	2.3	5.5	62
10	2.3	5.3	65

Table 5.5 Dusty models with different source spectra

H0=50, Ω_d=1.E-4

Spec: \ Ω_*	0.01	0.1	1
BB	2.3	5.5	62
H	2.0	5.5	62
He	2.1	5.5	61
R	3.5	3.6	60

H0=50, Ω_d=1.E-5

Spec: \ Ω_*	0.01	0.1	1
BB	7.5	11	76
H	8,5	13	75
He	8.1	12.5	77
R	3.5	4.7	77

Table 5.6 Effect of different opacity laws

H0=50, BB model

Ω_*	0.01	0.1	1
DOA	2.0	5.3	61
D2	2.3	5.5	62
D3	2.0	4.5	62

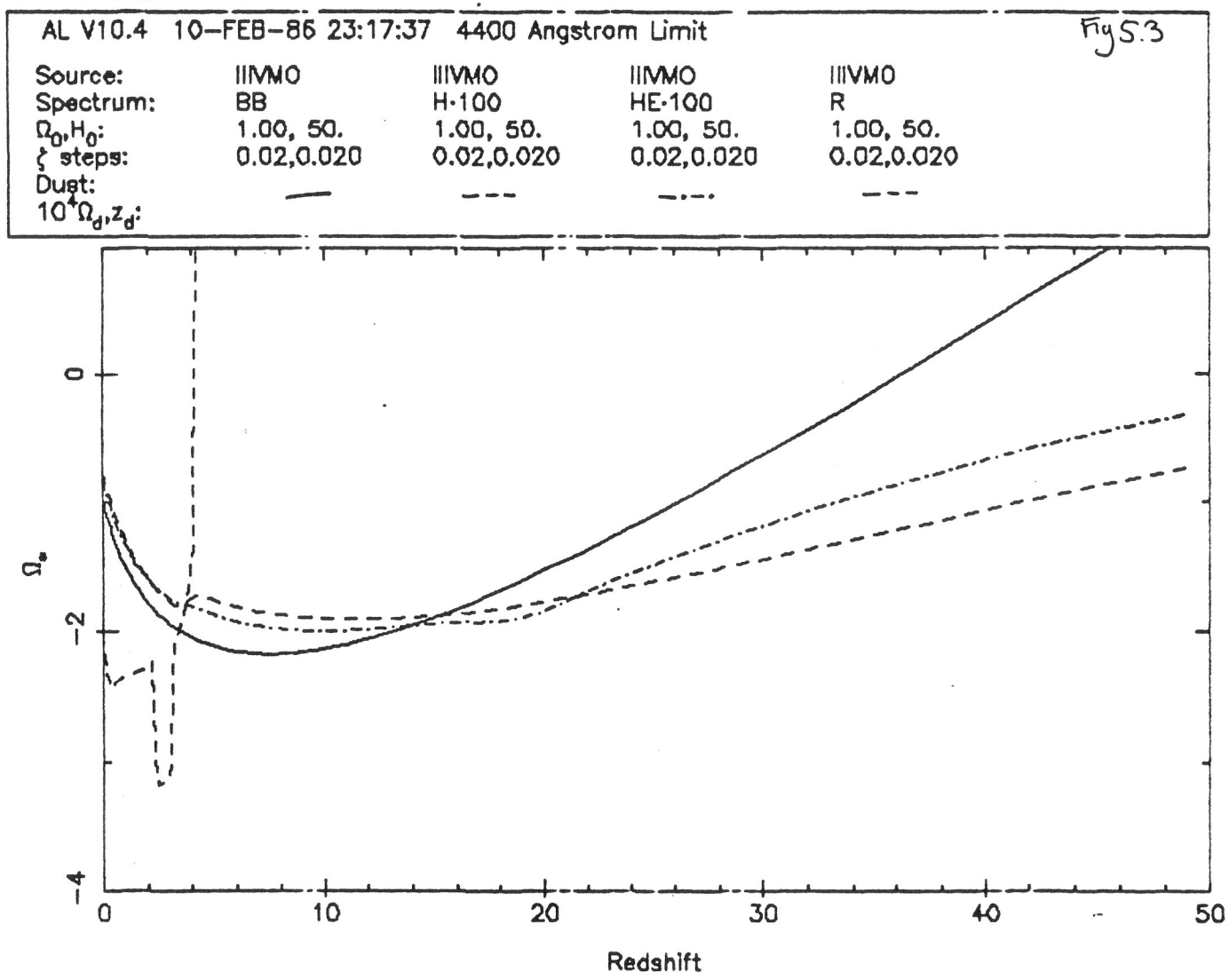
AL V10.4 10-FEB-86 23:17:37 4400 Angstrom Limit
Fig 5.3
Source: IIIVMO IIIVMO IIIVMO IIIVMO
Spectrum: BB H-100 HE-100 R
Ω_0, H_0: 1.00, 50. 1.00, 50. 1.00, 50. 1.00, 50.
ζ steps: 0.02,0.020 0.02,0.020 0.02,0.020 0.02,0.020
Dust:
$10^4\Omega_d, z_d$:
Ω_*
0
-2
-4
0
10
20
30
40
50
Redshift

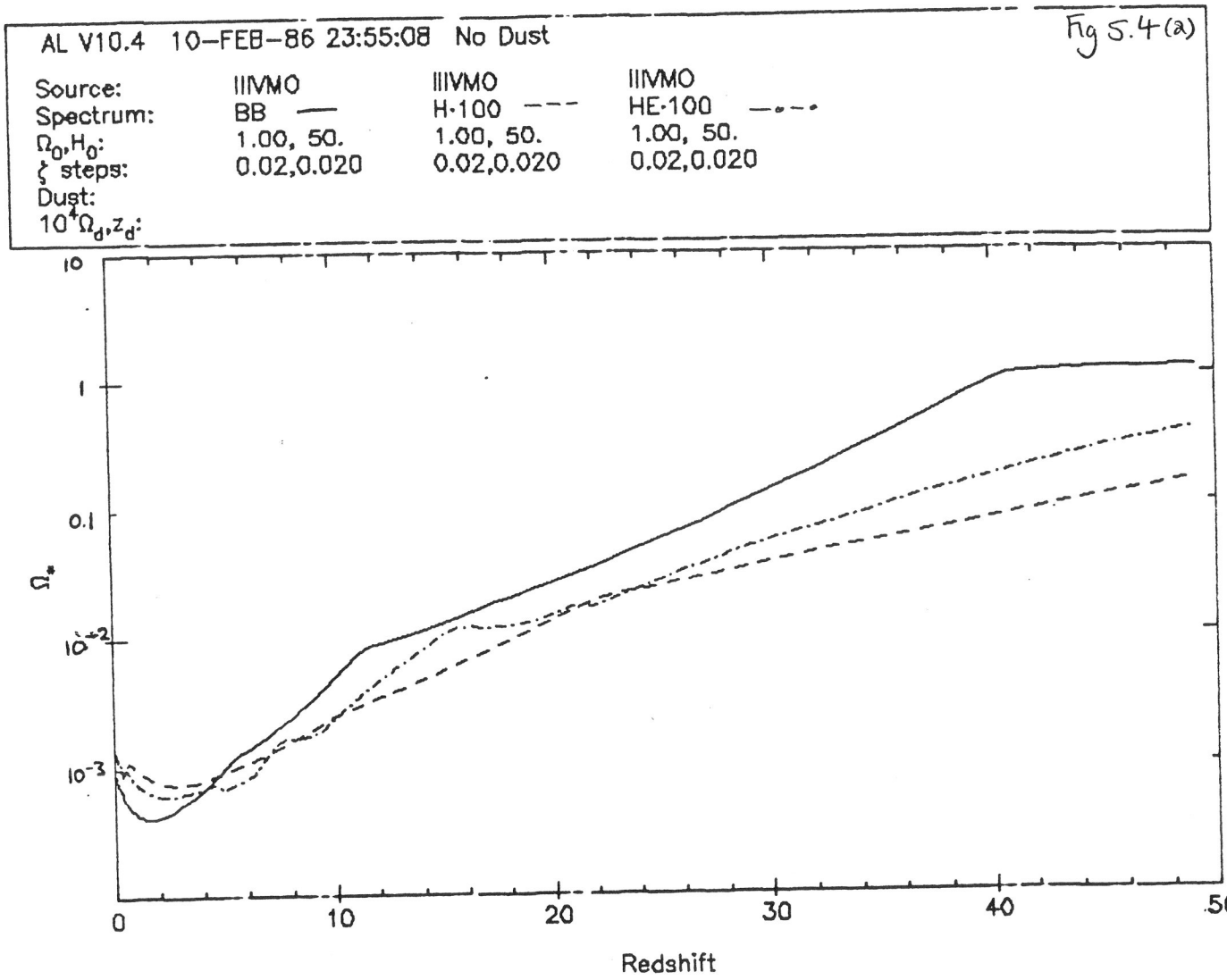
AL V10.4 10-FEB-86 23:55:08 No Dust
Source: IIIVMO IIIVMO IIIVMO
Spectrum: BB H-100 HE-100
Ω_0, H_0: 1.00, 50. 1.00, 50. 1.00, 50.
ζ steps: 0.02,0.020 0.02,0.020 0.02,0.020
Dust:
$10^4\Omega_d, z_d$:
10
1
0.1
10^{-2}
10^{-3}
Ω_*
0
10
20
30
40
50
Redshift

Fig 5.4(a)

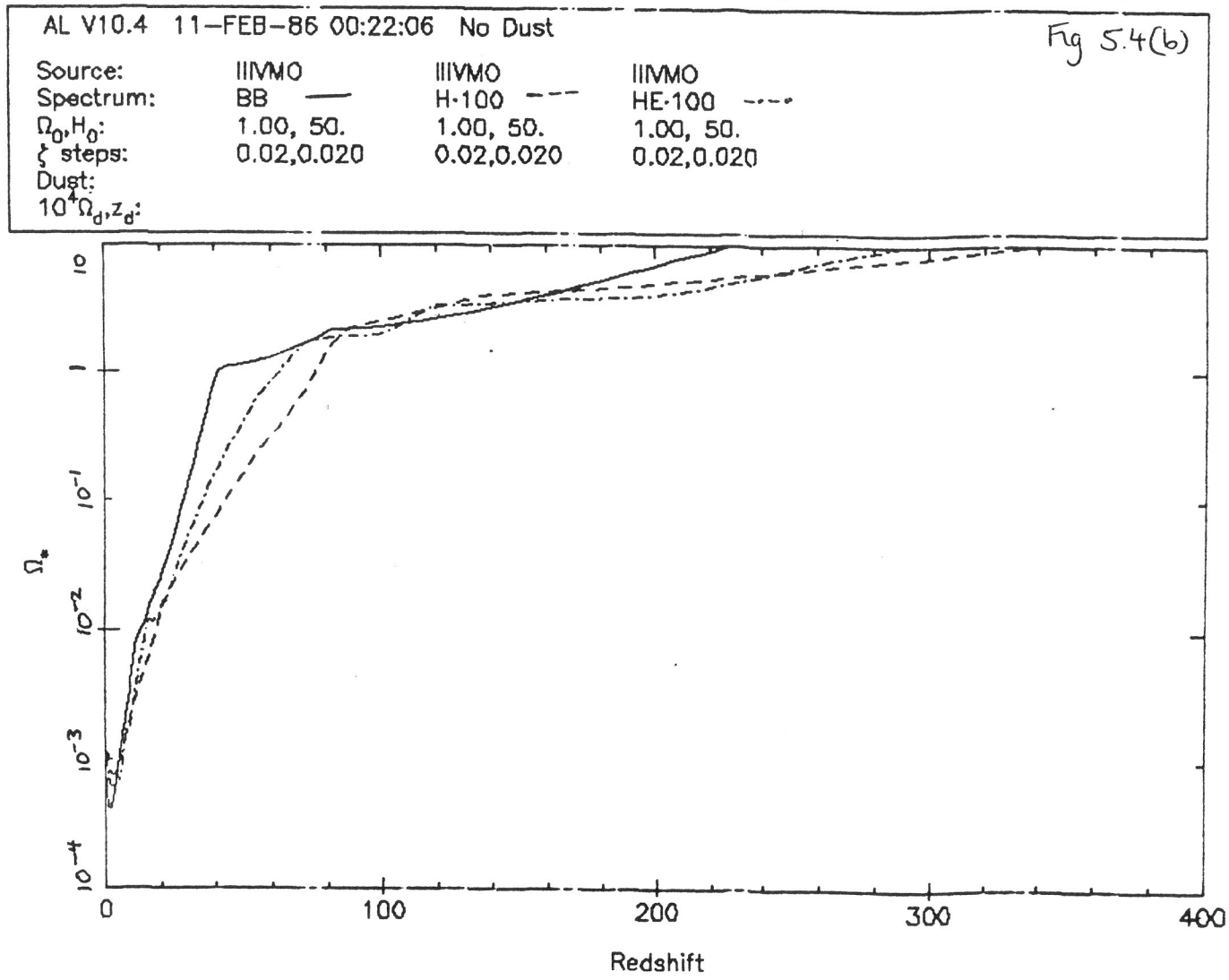
AL V10.4 11-FEB-86 00:22:06 No Dust
Source: IIIVMO IIIVMO IIIVMO
Spectrum: BB H-100 HE-100
Ω_0, H_0: 1.00, 50. 1.00, 50. 1.00, 50.
ζ steps: 0.02,0.020 0.02,0.020 0.02,0.020
Dust:
$10^4\Omega_d, z_d$:
Ω_*
1
10^{-1}
10^{-2}
10^{-3}
10^{-4}
0
100
200
300
400
Redshift

Fig 5.4(b)

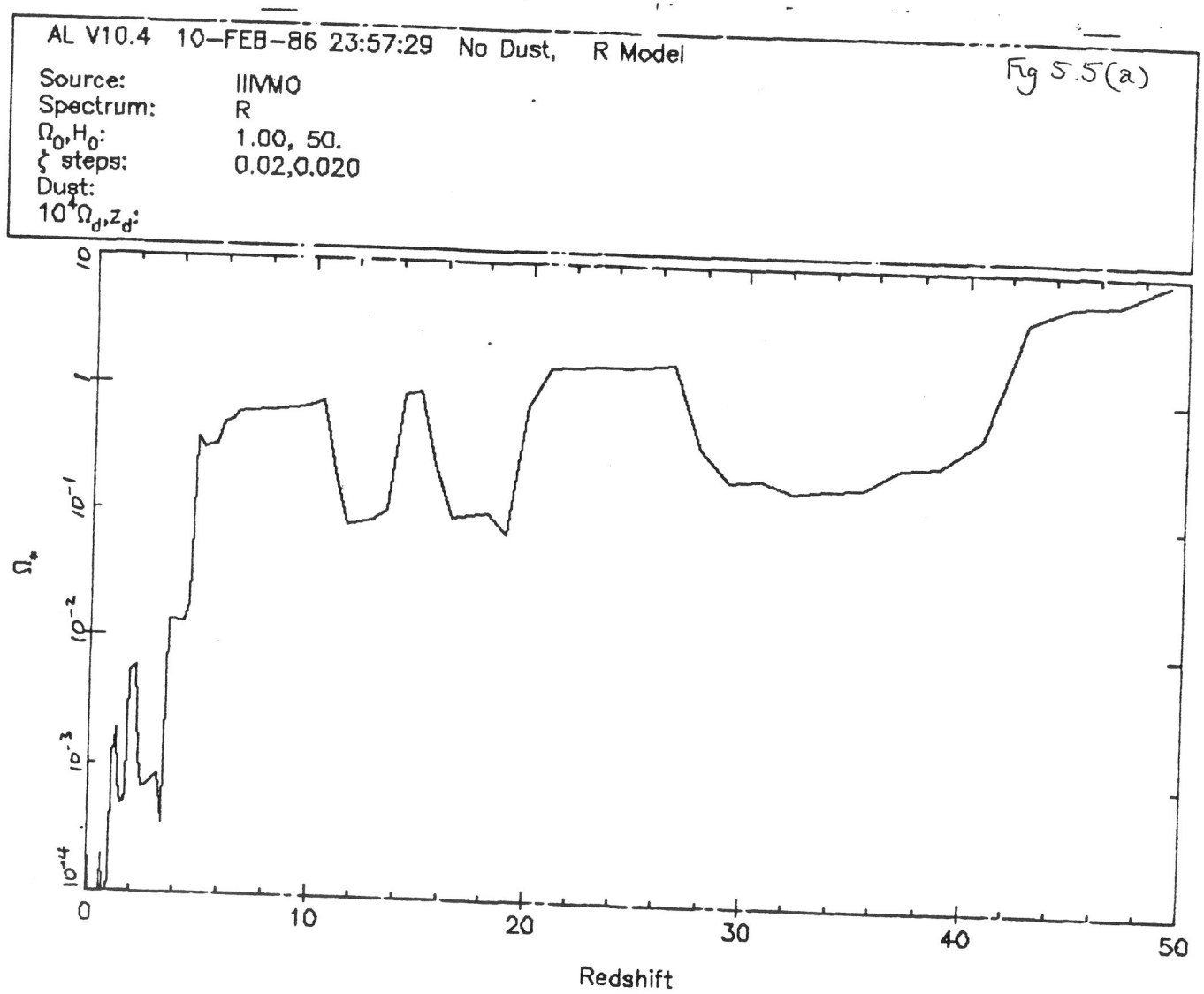
AL V10.4 10-FEB-86 23:57:29 No Dust, R Model
Source: IIIVMO
Spectrum: R
Ω_0, H_0: 1.00, 50.
ζ steps: 0.02,0.020
Dust:
$10^4\Omega_d, z_d$:
Ω_*
10
1
10^{-1}
10^{-2}
10^{-3}
10^{-4}
0
10
20
30
40
50
Redshift

Fig 5.5(a)

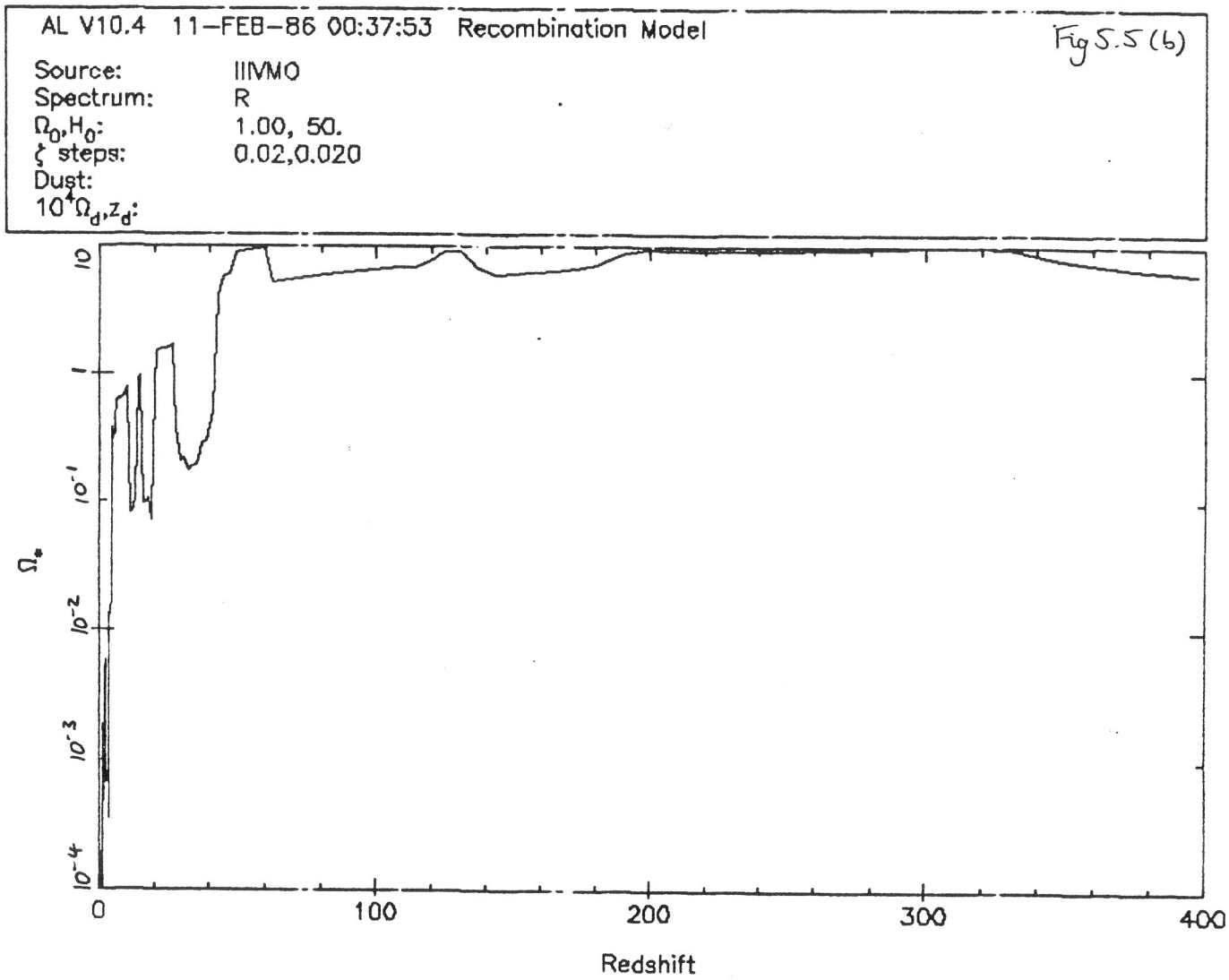
AL V10.4 11-FEB-86 00:37:53 Recombination Model
Source: IIIVMO
Spectrum: R
Ω_0, H_0: 1.00, 50.
ζ steps: 0.02,0.020
Dust:
$10^4\Omega_d, z_d$:
Ω_*
10
1
10^{-1}
10^{-2}
10^{-3}
10^{-4}
0
100
200
300
400
Redshift

Fig 5.5 (b)

Fig 5.6

AL V10.5 27-FEB-86 10:00:18 Fig 5.6 Dusty Universe Limits

Source:	IIIVMO	IIIVMO	IIIVMO	IIIVMO
Spectrum:	BB	BB	BB	BB
Ω_0, H_0:	1.00, 50.	1.00, 50.	1.00, 50.	1.00, 50.
ζ steps:	0.02,0.020	0.02,0.020	0.02,0.020	0.02,0.020
Dust:	D·2	D·2	D·2	D·2
$10^4\Omega_d, z_d$:	1.00,100.0	0.10,100.0	0.01,100.0	0.00,100.0

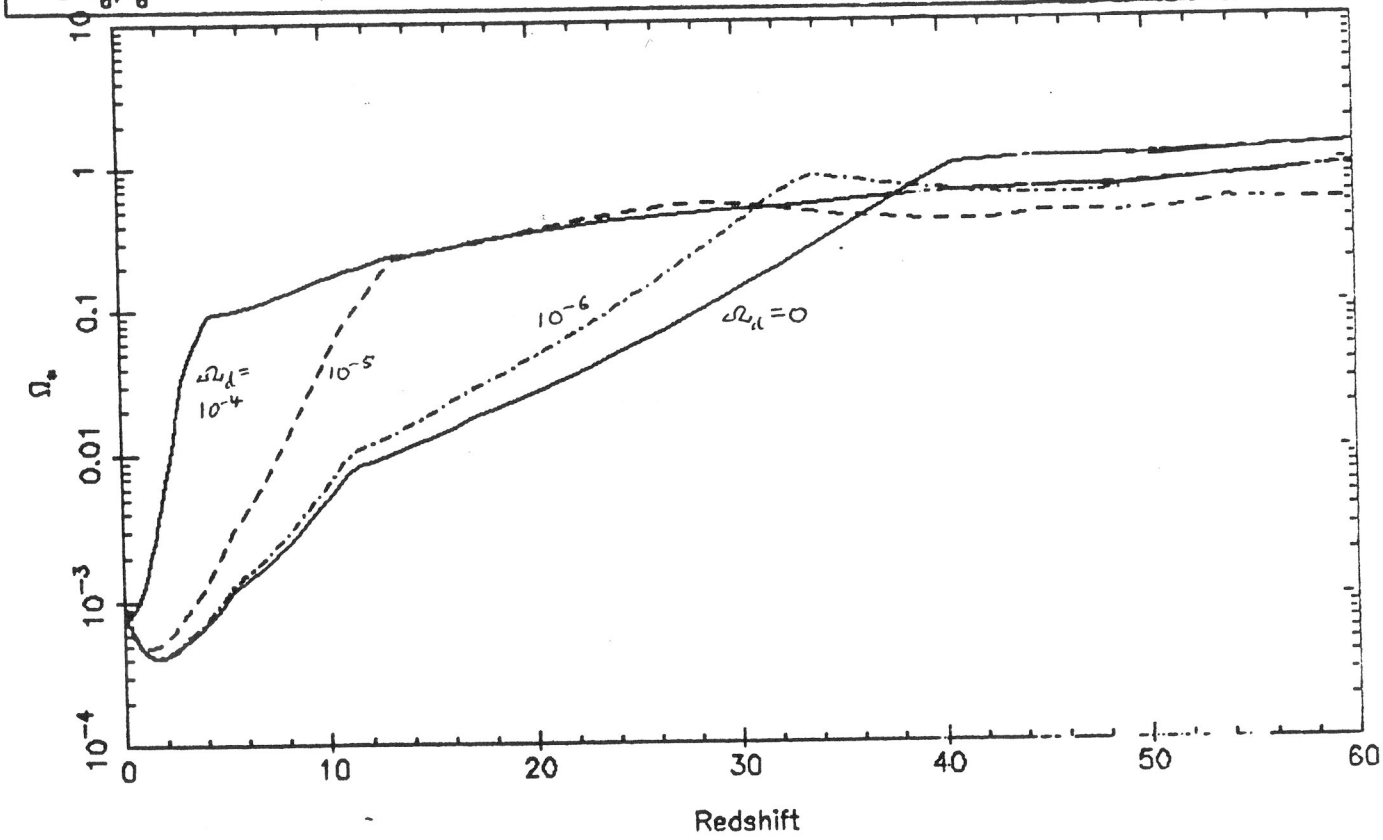

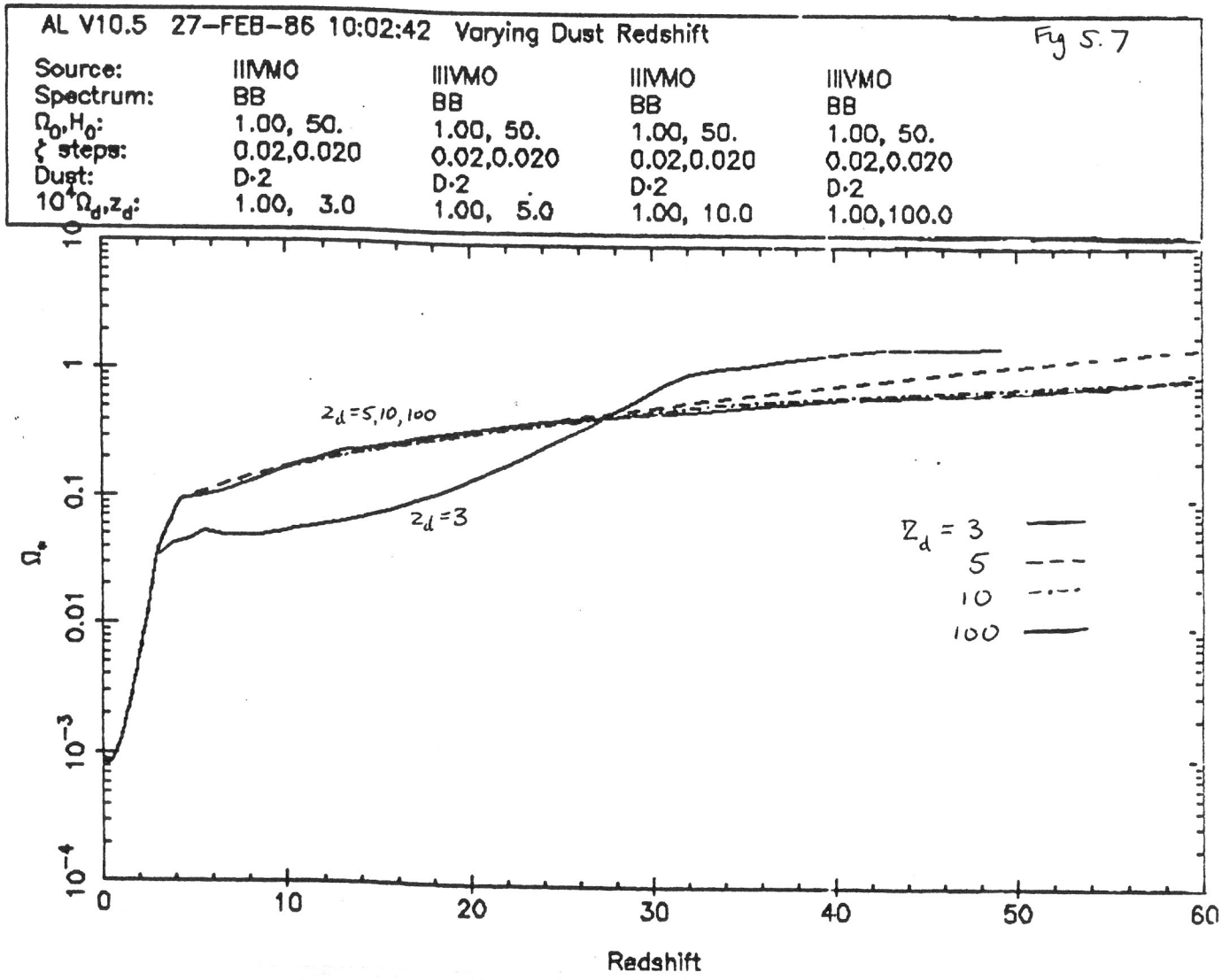
AL V10.5 27-FEB-86 10:02:42 Varying Dust Redshift
Source: IIIVMO IIIVMO IIIVMO IIIVMO
Spectrum: BB BB BB BB
Ω_0, H_0: 1.00, 50. 1.00, 50. 1.00, 50. 1.00, 50.
ζ steps: 0.02,0.020 0.02,0.020 0.02,0.020 0.02,0.020
Dust: D·2 D·2 D·2 D·2
$10^4\Omega_d, z_d$: 1.00, 3.0 1.00, 5.0 1.00, 10.0 1.00,100.0
Fig 5.7
$z_d = 5, 10, 100$
$z_d = 3$
z_d = 3
5
10
100
Ω_*
1
0.1
0.01
10^{-3}
10^{-4}
0
10
20
30
40
50
60
Redshift

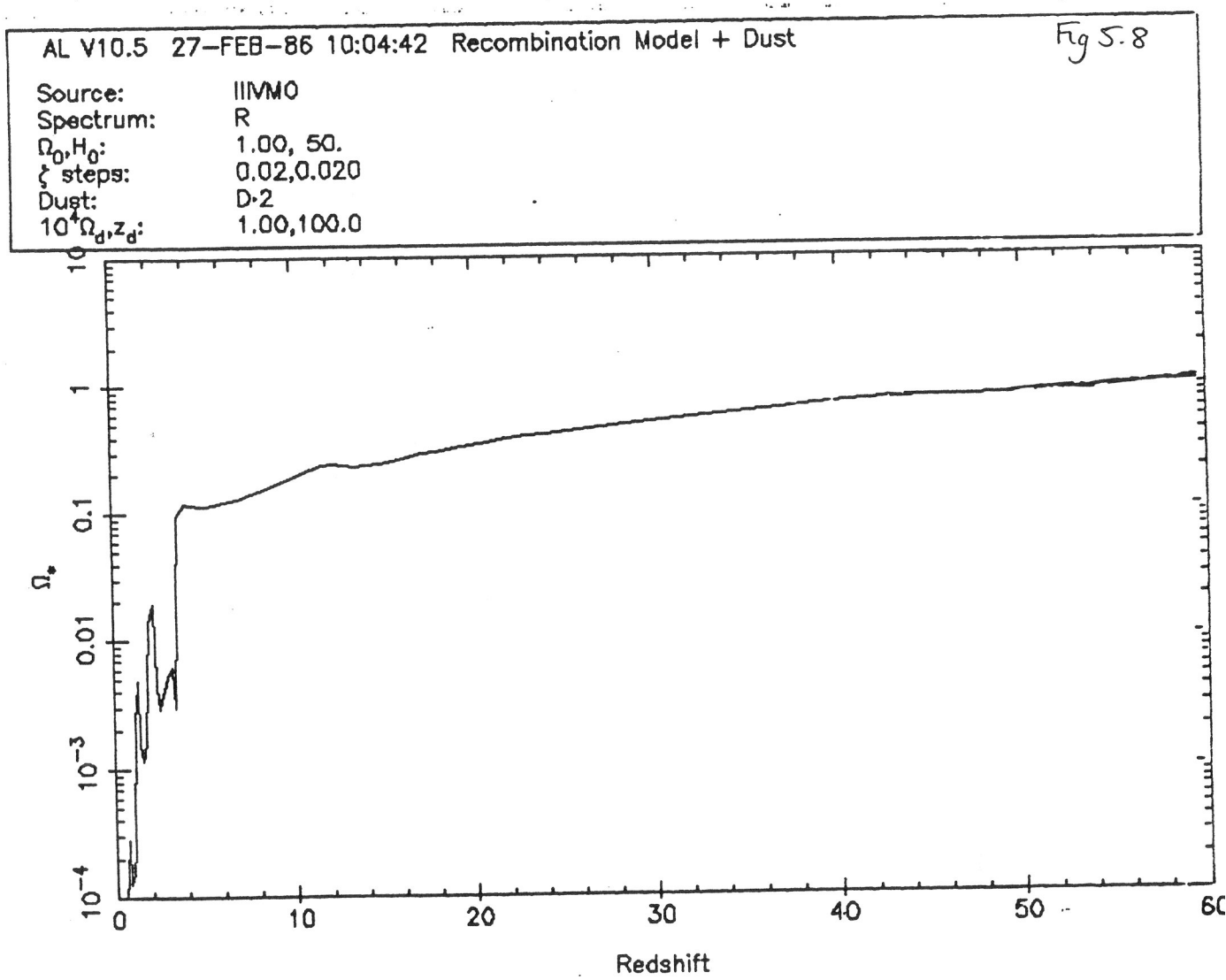
AL V10.5 27-FEB-86 10:04:42 Recombination Model + Dust
Source: IIIVMO
Spectrum: R
Ω_0, H_0: 1.00, 50.
ζ steps: 0.02,0.020
Dust: D·2
$10^4\Omega_d, z_d$: 1.00,100.0
Ω_*
10
1
0.1
0.01
10^{-3}
10^{-4}
0
10
20
30
40
50
60
Redshift

Fig 5.8

5.3 Limits on radiation from accreting remnants

In Section 4.3 I discussed the radiation from accreting black hole remnants in the context of the near infrared background. I now consider accretion by the Population III remnants in a more general context.

The black holes will contribute a larger fraction of the density parameter if they can accrete a mass comparable to their own after their formation. If, as suggested in section 4.3, the radiation from this accretion ionizes the surrounding gas and heats it so that the background the hole is accreting from becomes the cosmological background with density as given in eq (2.2.17b) with $\delta = 1$, then we can work out the maximum fractional mass increase by integrating the Bondi accretion rate with respect to time. If we ignore the decrease in Ω_g due to the accretion, this is

$$\frac{\delta M}{M}(1+\frac{\delta M}{M})^{-1} = 9.6 \times 10^{-11}\Omega_g M((1+z)^{3/2}-1) \qquad (5.3.1)$$

which is always small for masses in the VMO range and formation redshifts less than 400. Hence the VMO remnants can only accrete a significant amount of mass if they do it from dense clumped gas around them.

At the high accretion rates this would entail, the radiative efficiency will be in the range 0.01 to 0.1 (Ch. 7) and the radiation will be either in the UV or the X-rayregions of the spectrum. If it is in the UV, it is obvious that the limits on the total Ω_* will be stronger than with no accretion (since ϵ is larger for accretion than for stellar burning). If the holes are X-ray sources, we can use the limit found by Carr (1980):

$$\Omega_B \lesssim (M\epsilon)^{-1/3} = 0.2\left(\frac{\epsilon}{0.1}\right)^{-1/3} M_2^{-1/3} \qquad (5.3.2)$$

Detailed comparison with the X-ray background would require solving for the coupled density evolution of gas and holes; the luminosity is a complicated function of redshift. I plan to carry out this calculation in the future.

6. Background Light Limits for ordinary stars

6.1 Stellar models for ordinary stars

In this chapter I apply the code described in chapters 3 and 5 to obtain background light limits for stars of masses below the VMO range. In general I have used Population II stellar models and atmospheres. Wagner (1974) suggests that low mass Population III stars evolve considerably more slowly than Population II stars because of their smaller metallicity, but for most masses the difference in the Population II and III main sequences should have only a small effect on the results, to judge from the Population III models that are available. The results I present below are therefore relevant to the light that must have been produced by the bulk of the stars that made the initial metal abundance, whether their composition was Population II or Population III.

My grid of models, tabulated in Table 6.1, covers the masses 0.1, 0.15, 1, 3, 5, 8, 10, and 20 $M_{\odot}$. The stellar parameters have been interpolated from various stellar evolution models. Very low mass stars have been discussed by Grossman, Hays and Graboske (1974), D'Antona and Mazzitelli (1985), and VandenBerg *et al.* (1983). Stars of a half to a few solar masses have been studied by Wagner (1974), Guenther and Demarque (1983), VandenBerg (1983), and Mengel et al (1983). Low metallicity stars in the mass range 1 – 10 $M_{\odot}$ have been studied by Tornambe and Chieffi (1985). For the 10 and 20 $M_{\odot}$ models I have used the same values as Thorstensen and Partridge (1975).

I have adopted stellar atmosphere spectra from Kurucz (1979), using log g =5.0 which is a good approximation for all the models. Spectra for the low mass stars come from Mould (1976) and Carbon *et al.* (1969). The spectra are plotted in Fig 6.1.

Table 6.1

Stellar models.

M ($M_\odot$)	ϵ	t_{ms} (Myr)	T_e (K)	
0.1	t_{ms}/ϵ =	1.6×10^{10}	2500	
0.15	t_{ms}/ϵ =	10^{9}	3500	
1	6×10^{-4}	4700	6500	
3	7×10^{-4}	320	16000	
5	8×10^{-4}	100	25000	
8	8×10^{-4}	40	30000	
10	1×10^{-3}	24	40000	
20	1.5×10^{-3}	9.2	50000	
50	3×10^{-3}	4.4	90000	(Pop III)
100	3.4×10^{-3}	3.4	100000	(Pop III)

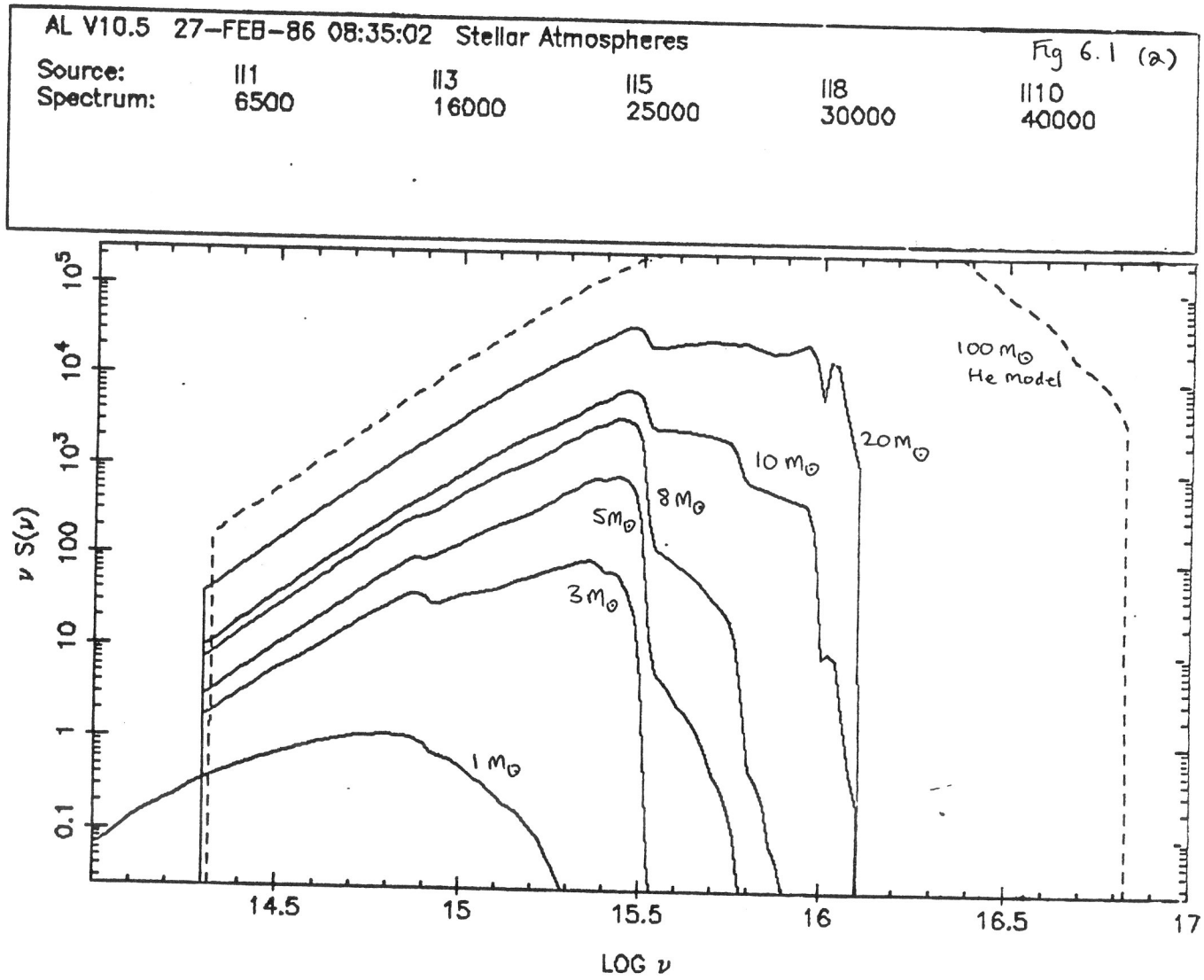
AL V10.5 27-FEB-86 08:35:02 Stellar Atmospheres
Fig 6.1 (a)
Source: 111 113 115 118 1110
Spectrum: 6500 16000 25000 30000 40000
100 M⊙ He model
20 M⊙
10 M⊙
8 M⊙
5 M⊙
3 M⊙
1 M⊙
ν S(ν)
0.1
1
10
100
10^3
10^4
10^5
14.5
15
15.5
16
16.5
17
LOG ν

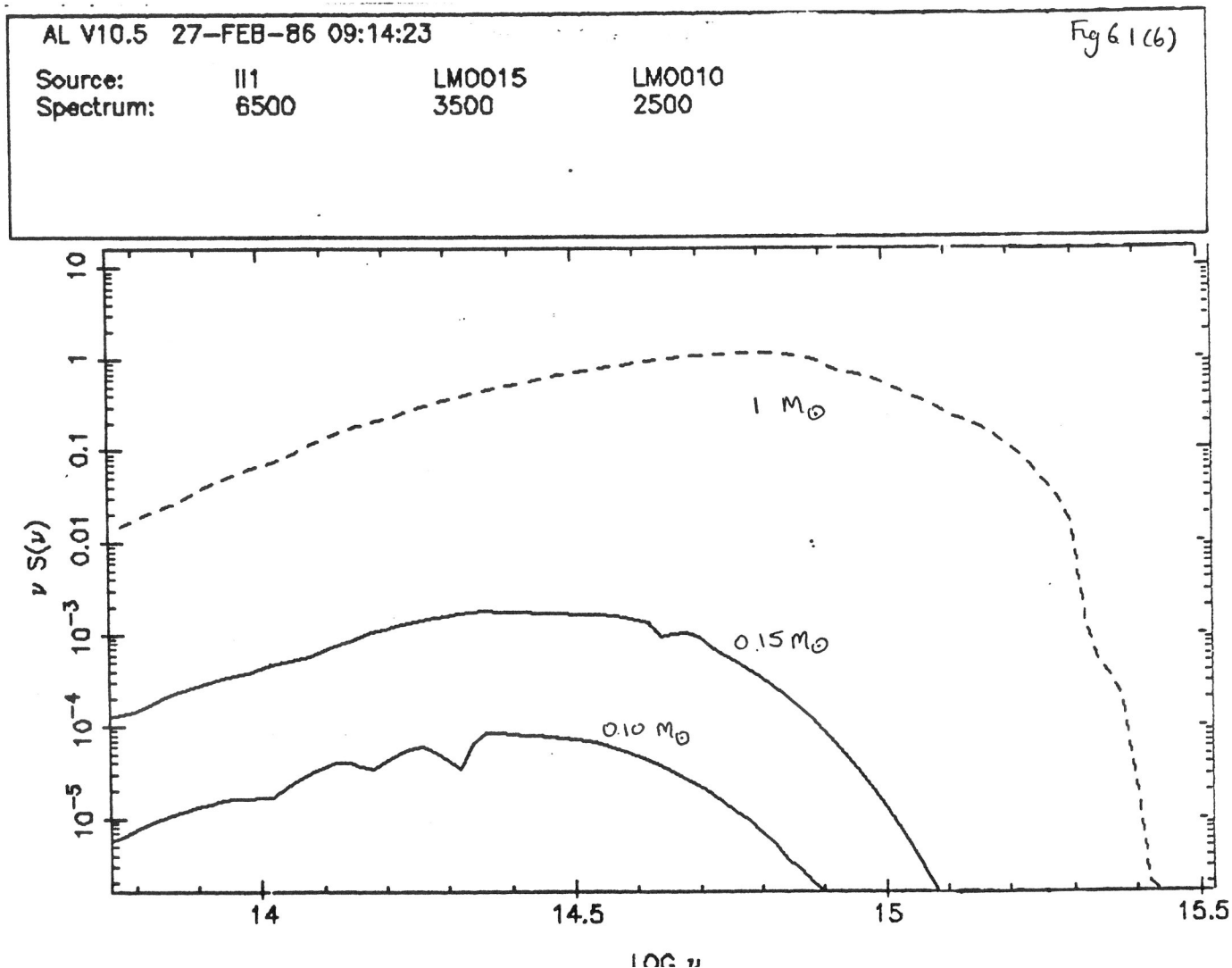
AL V10.5 27-FEB-86 09:14:23
Source: I11 LM0015 LM0010
Spectrum: 6500 3500 2500
Fig 6.1(6)
1 M⊙
0.15 M⊙
0.10 M⊙
ν S(ν)
10
1
0.1
0.01
10^-3
10^-4
10^-5
14
14.5
15
15.5
LOG ν

6.2 Background Light Limits for ordinary stars

All the evolutionary models mentioned in section 6.1 for stars of mass above 1 $M_\odot$ predict radiative efficiencies ϵ equal to 10^{-3} with a variation of about 50 per cent; I have therefore adopted this value consistently for all the masses. This means that the Population II stars discussed here are less well constrained by the background light limits, since they emit less energy per unit mass. The light constraints in the visible allow intermediate mass stars above a redshift of 5 or 6 to close the universe, although enrichment constraints (Carr et al 1984) exclude this possibility. Solar mass stars, however, are more strongly constrained; they cannot close the universe at all and could only make up the dark matter if their lifetime is comparable to the Pop II prediction of 4700 Myr (Wagner 1974), in which case they can complete burning by a redshift of 1. If they are Pop III stars with a much longer lifetime of 19000 Myr (Wagner 1974), they are still burning today and cannot have more than $\Omega_* = 0.025$.

Very low mass stars are only weakly constrained by the data; the stellar luminosity drops of steeply below 1 $M_\odot$. The two low mass models I have adopted give $\Omega_* < 5$ ($.015M_\odot$) and $\Omega_* < 30$ ($.01M_\odot$). Hence the integrated light from a closure density of very low mass stars would escape detection by as much as an order of magnitude. The predicted background spectrum for a closure density of the $0.1M_\odot$ stars is plotted in Fig 6.2 for a set of different formation redshifts. The curves are labelled by redshift.

I illustrate the limits as a function of mass in Fig 6.3 and list them in Table 6.2 for several different formation redshifts. Since the background from the lower mass stars is dominated by the recent epoch, their limits do not vary with redshift. The limits become generally stronger for higher masses. Fig 6.3 is generally similar to Fig. 3 of Carr, Bond and Arnett (1984), which was obtained with simple analytic fits to the source parameters. In Fig 6.4 I construct the diagram of allowed mass versus formation time introduced by Thorstensen and Partidge (1975). The

dotted line shows the constraint for Ω_0 =1 obtained by TP from the optical limit. It is in good agreement with my limit which is based on the optical and near infrared. Regions of the (M,z) plane to the right of the contour are excluded. The near IR limit also excludes a separate region of the (M,z) plane for the 5 and 8 $M_\odot$ models. Two other contours in Fig 6.4 illustrate the allowed regions for Ω_0 =0.1 and Ω_0 =0.01.

Table 6.2

Limits on $\Omega_*(M, z)$

M \ z	0.1	1	5	10	50	100
0.10	60	30	30	30	30	30
0.15	10	5	5	5	5	5
1 (III)	.02	.02	.02	.02	.02	.02
1 (II)	.01	.02	.13	.16	.23	.23
3	6×10^{-4}	2.5×10^{-3}	0.016	1.3	2.5	2.8
5	5×10^{-4}	1×10^{-3}	8×10^{-3}	1.0	3.0	3.8
8	5×10^{-4}	1×10^{-3}	8×10^{-3}	1.0	3.0	
10	5×10^{-4}	1×10^{-3}	8×10^{-3}	0.25	3.2	13
20	6×10^{-4}	1×10^{-3}	2×10^{-3}	0.03	4.0	7.6
50	3×10^{-4}	6×10^{-4}	2.5×10^{-3}	0.02	2.3	4.5
100	1×10^{-3}	7×10^{-4}	7×10^{-4}	2.4×10^{-3}	0.38	2.0

The table gives the maximum allowed value of Ω_* for the given mass and formation redshift.

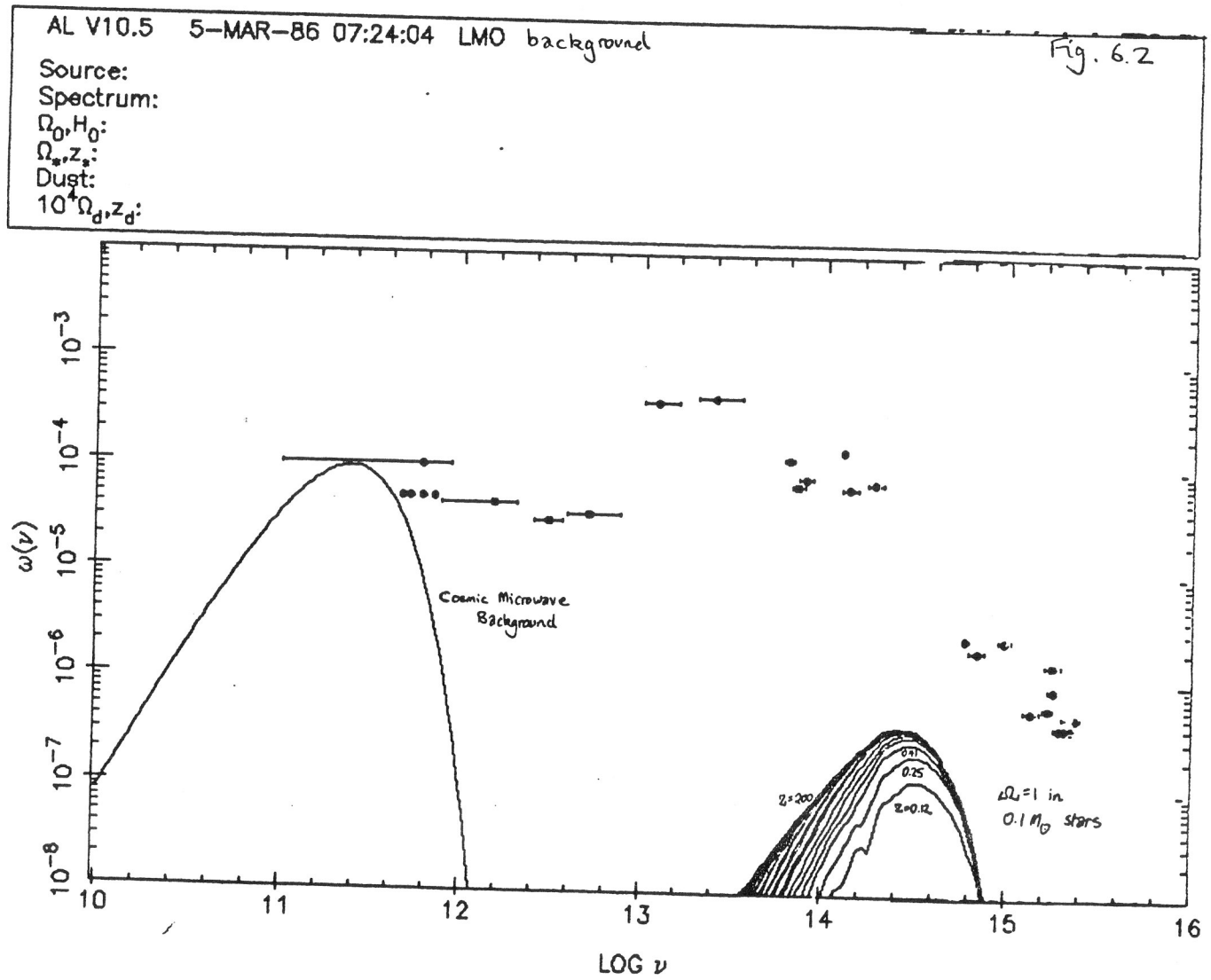
AL V10.5 5-MAR-86 07:24:04 LMO background
Source:
Spectrum:
Ω_0, H_0:
Ω_*, z_*:
Dust:
$10^4\Omega_d, z_d$:
$\omega(\nu)$
10^{-3}
10^{-4}
10^{-5}
10^{-6}
10^{-7}
10^{-8}
Cosmic Microwave Background
$z=200$
0.91
0.25
$z=0.12$
$\Omega_* = 1$ in $0.1\ M_\odot$ stars
10
11
12
13
14
15
16
LOG ν

Fig. 6.2

Fig 6.3 Limit on Ω_* as a function of mass

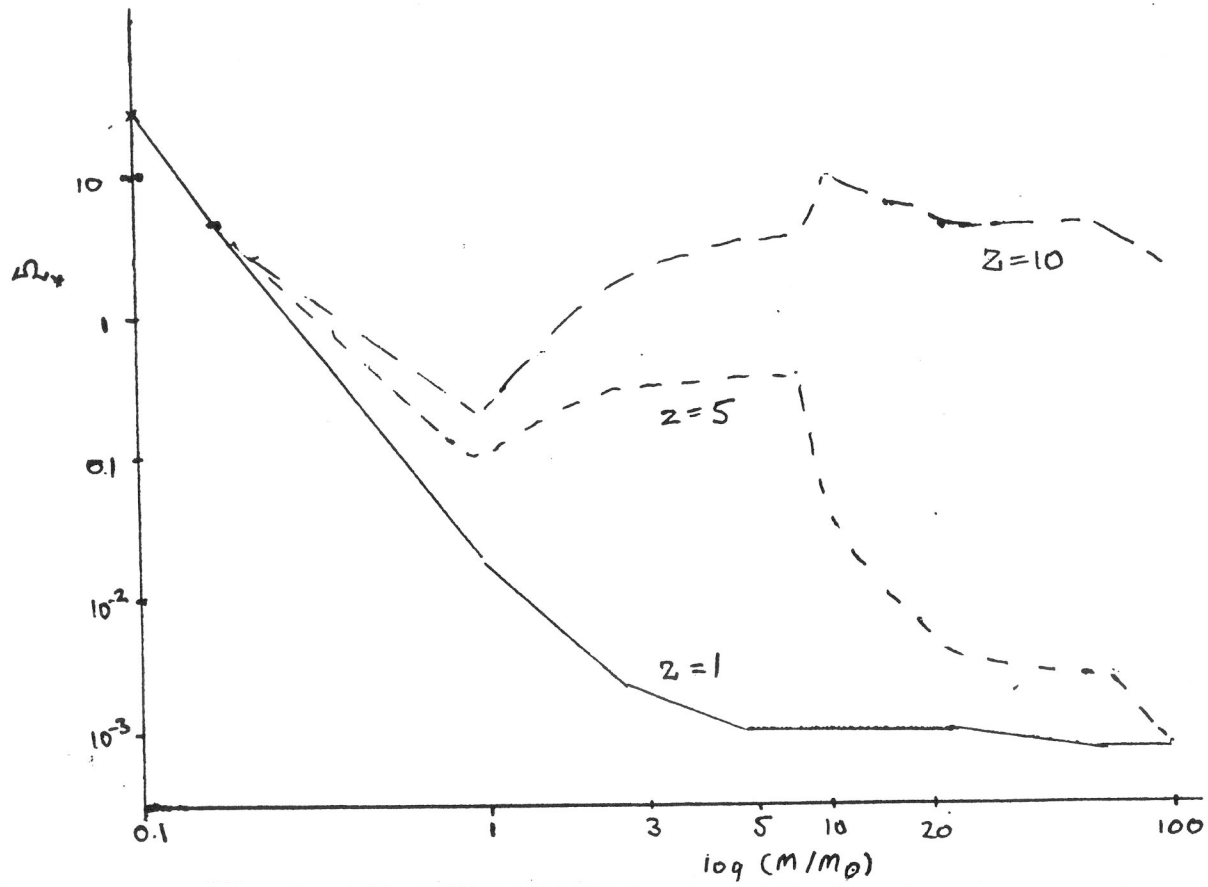

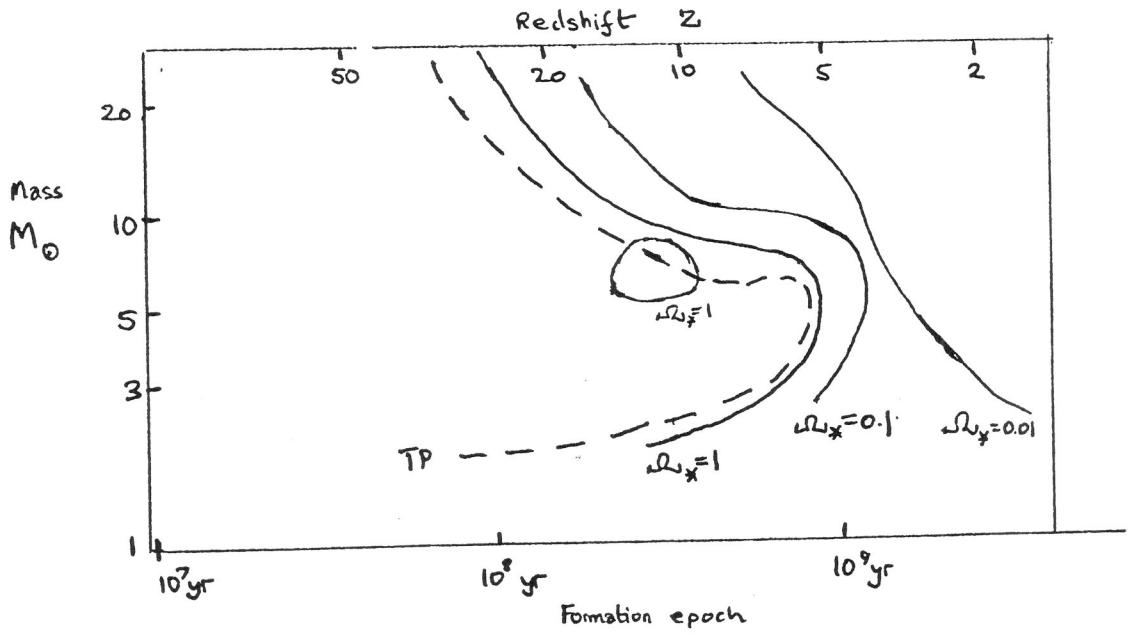

Fig 6.4 Contours of allowed Ω_* as a function of M and z

7. Accretion radiation from nearby isolated black holes

7.1 Black Holes Traversing the Galactic Disc

Recent work attempting to establish the presence of dark matter in the solar neighbourhood has led to renewed interest in the search for the nature of this matter. Bahcall et al. (1985) attempt to exclude large ($\geq 2M_{\odot}$) objects by considering their tidal effect on wide binaries. Here I provide independent constraints on such dark massive objects, if they are black holes, by the requirement that their radiation due to accretion from the ISM should not make the nearest ones directly observable as optical objects. I also predict the expected infrared brightness. Halo holes also traverse the disk. Ipser and Price (1977) have studied the observability of very massive ($10^5 M_{\odot}$) pregalactic black holes in our galactic halo. Their more recent accretion model calculations allow such constraints to be evaluated for lower mass holes .

I investigate accretion radiation limits for three different possible populations of holes. First, I consider the scenario studied by Ipser and Price (1977), in which the galaxy has a massive halo made of black holes which are the remnants of massive pregalactic stars. Lacey (1984) and Lacey and Ostriker (1985) show that such halo holes must have a mass of less than $10^6 M_{\odot}$ to avoid heating up the galactic disc. These holes would traverse the disk of our galaxy rapidly (about 300 km/s), and their luminosity would therefore be small unless the hole mass was at the upper end of the range. I show that the holes must have mass less than about 100 $M_{\odot}$. Secondly, I investigate the possibility that the local 'Oort limit' missing mass is made up of black holes, possibly stellar remnants of a first generation of galactic stars. According to Bahcall (1984) these objects must have a mean velocity of less than 100 km/s relative to the disc to be consistent with the dynamical data. I adopt this maximum value, which gives the lowest luminosity. Fitchett (1984) discusses a gravitational recoil mechanism which could give the black holes

velocities of this size. I derive a limit of $M < 10M_{\odot}$ for this scen ario. These limits all depend on the assumptions I have made about the radiation spectrum. Due to the uncertainties in black hole accretion physics, the results cannot therefore be regarded as conclusive. Thirdly, I attempt to constrain stellar evolution theory by estimating whether the black hole remnants of ordinary massive stars in the disk should have been detected. Even if black holes do not make up the dark matter, they are expected to be present in the disk as remnants of massive stars. In section 7.6 I show that the failure to detect such holes so far is not in conflict with their presence provided the minimum mass M_{BH} of their progenitors is more than 10 $M_{\odot}$. More detailed analysis and improved observations could set more useful constraints on M_{BH}, and, if the holes do exist some of them should be bright enough to be discovered and observed. Shapiro and Teukolsky (1983) calculate that there should be of order 10^8 holes of $\geq 10M_{\odot}$ left in the galactic disc as remnants of the ordinary stellar evolution of massive stars. They assume that all stars above $10M_{\odot}$ collapse into holes with no mass loss, so their calculations almost certainly lead to an overestimate of the density of such holes. I attempt to calculate a more probable estimate.

In all cases, the limits from integrated background light (Carr 1979) are weaker and only exclude holes of larger mass than considered here. Hegyi, Kolb and Olive (1986) also constrain the existence of black holes by both accretion and nucleosynthetic arguments.

7.2 The Local Interstellar Medium

Recent work has somewhat clarified the nature of the interstellar medium in the solar neighbourhood. The old standard picture of a homogeneous ISM with density of $1cm^{-3}$and temperature 10^4K is no longer valid. For some time theorists have suggested the possible existence of multiple phases in the ISM (see, e.g., McKee and Ostriker, 1977). In the past decade there have been many advances in observational techniques with the use of ultraviolet and X-ray spaceborne telescopes to study the ISM. It is indeed clumpy, and locally very underdense, with much of the volume within 50 pc of the sun filled with hot thin ($n=4 \times 10^3 cm^{-3}$) gas that may be the result of recent supernova explosions. This means that the nearest black holes will not accrete as much as more distant ones. The ISM also contains a warm (10^4K), thin (0.1 cm^{-3}) component together with many small cooler clouds. These clouds were detected by Knude (1979), who observed reddening along the lines of sight to a large number of F stars whose distances can be relatively accurately determined; they have a mean density of 30 $cm^{-3}$and a mean size of 4 pc. Their filling factor is somewhat uncertain but is probably about 2 per cent, at least in the region beyond 50 pc. I will adopt these values, since most of our results depend on the ISM at a distance of 50-150 pc, which is the regime studied by Knude.

There is also at least one denser nearby cloud of low optical depth, the Reigel-Crutcher HI cloud at about 125 pc in the direction of the galactic centre, with a density of 100 cm^{-3}(Crutcher and Lien,1984). At its eastern end it merges into the Aquila Rift molecular cloud, and it may be connected with the Scorpius-Ophiuchus complex. We estimate the HI cloud's volume to be at least $10^4 pc^3$. There may be a comparable cloud toward the anticenter in the ϵ Per region, and there is a small amount of gas in the Pleiades cluster. Paresce (1984) gives maps of column density based on observations of Lyman α absorption along the line of sight to nearby stars. I have radially differentiated this map to give a schematic map of the typical number densities in the local interstellar medium. (Fig 7.1).

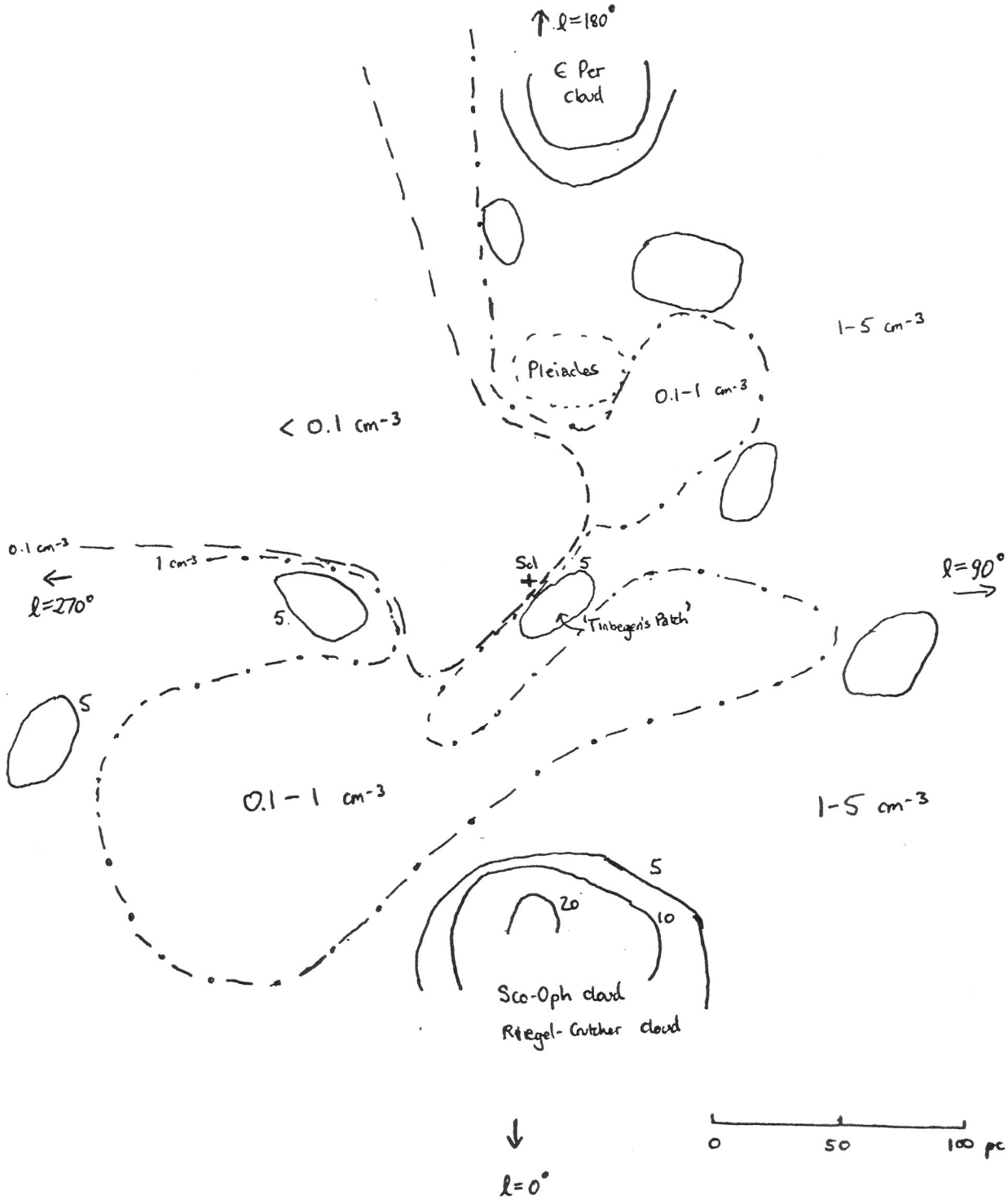

Fig 7.1 The Local Interstellar Medium

7.3. Black Hole Accretion in the Interstellar Medium

The accretion rate of gas onto black holes depends sensitively on the relative velocities of holes and gas and also on the gas density. Typically stars, which are not dissipative, have a higher velocity dispersion than the gas, which is dissipative. Indeed, n-body effects tend to increase the velocity dispersion of the stars systematically. Typical peculiar stellar velocities in the galactic disk are of the order of tens of km/s, so if we restrict ourselves to the warm and cool components of the ISM, with temperatures less than 10^4K, stellar remnant holes will be at least transonic and usually supersonic. Halo holes passing through the disk will be highly supersonic (v=300 km/s). Since the halo gas and the hot phase of the disk ISM are of such low density, the accretion rate in these regions is very small and will not be considered. For a hole moving with velocity v, in gas of number density n and sound speed c_s, the Bondi (1952) accretion rate is

$$\dot{M} = 4\pi\mu \left(\frac{GM}{u^2}\right)^2 m_H n u \qquad (7.3.1)$$

where

$$u^2 = v^2 + c_s^2 \qquad (7.3.2)$$

and μ is an 'accretion eigenvalue' of order unity. The distance GM/u^2 represents an 'accretion radius' within which gas is captured onto the hole. Note that this is just a factor $(c/u)^2$ times the Schwarzschild radius of the hole, so the accretion radius is much larger than the size of the inner region of the potential well where most of the energy release will occur, provided only that the holes are non-relativistic. To describe the accretion flow, it is convenient to adopt the accretion parameter $\mathcal{J}$ used by Schmid-Burgk (1978) and Ipser and Price (1982), which in our notation is

$$\mathcal{J} = 0.016\mu \left(\frac{n}{1\ \mathrm{cm}^{-3}}\right) \left(\frac{u}{100 km/s}\right)^{-3}. \qquad (7.3.2)$$

Therefore

$$\dot{M} = 2.3 \times 10^7 M^2 \mathcal{J}\ \ \mathrm{kg/s} \qquad (7.3.3)$$

$$= 3.6 \times 10^{-16} M^2 \bar{g}\ M_\odot\ /\mathrm{yr}$$

where M is measured in solar masses.

If a Maxwellian distribution is assumed for the holes, with velocity dispersion v_0, then the fraction of them moving slower than v is $0.3(v/v_0)^3$ for $v \ll v_0$. Since the accretion rate also scales as the cube of the velocity down to the sonic value (below which it is independent of v), I obtain a limit for the nearest object better by a factor (v_0/v) by considering the small number of objects with sonic or subsonic velocity and thus maximum luminosity ; the nearest such object will be brighter than the much closer but less luminous high-velocity objects. In practice, though, I must consider the whole range of velocities, as I am interested in the radiation in specific wavebands rather than in total luminosities. Also, the above analysis assumes that the distance of the object is not large compared with the ISM scale height.

The luminosity of the hole depends also on the efficiency ϵ with which the infalling mass-energy is converted into radiation. This, and the spectrum of the radiation from the hole, depend in turn on the angular momentum of the accreting gas. If the gas particles have enough angular momentum to keep them in orbit around the hole, accretion proceeds from a disk in which viscosity slowly removes this angular momentum by transferring most of it outward to a small fraction of the matter. For this 'disk accretion' scenario I adopt the analysis of Shakura and Sunyayev (1973) to predict the spectrum.

It is often suggested that, while ϵ may be as large as 0.1 for disc accretion, it should be very small for an isolated hole accreting low angular momentum gas 'spherically' from the interstellar medium. However, the work of Meszafos (1975) showed that, if the dissipation of magnetic energy is taken into account in the heating of the gas, high temperatures and quite respectable efficiencies are achieved. Ipser and Price (1982) performed detailed calculations which showed that, for low accretion rates, ϵ is also proportional to the accretion parameter $\bar{g}$

and the mass, reaching a maximum value of 0.01 for higher accretion rates. In this case, the brightness of a hole depends on the square of the gas density, so it is much easier to detect accreting holes in a clumpy interstellar medium. Accretion in the halo would be very weak indeed, and our calculations for halo holes are based on the radiation from holes accreting as they pass through the disk of the Galaxy near to the Sun. We emphasize that our results depend on the assumption that the spherical accretion flow involves the dissipation of magnetic field energy in reconnection; if this did not occur, the Ipser and Price results would not be applicable and the luminous efficiencies would be much lower.

Following Ipser and Price (1977), let us examine the assumption of spherical accretion, assuming that the angular momentum of the gas derives from turbulence in the ISM. The turbulent velocity scales with length scale l as $v_{turb} \sim l^q$, where $q = \frac{1}{3}$ for a Kolmogorov spectrum but may lie in the range 0.5 to 1 for the ISM. Observations indicate (Kaplan and Pil'kener 1970, Ipser and Price 1977) that

$$\omega = v_{turb}/l = 3 \times 10^{-15}(l/80pc)^{q-1}\text{rad/s} \qquad (7.3.4)$$

In this case, l is the Bondi radius $r_B = 2GM/u^2$. Ipser and Price derive the criterion for a disk assuming q=3/4:

$$u < 6\left(\frac{M}{M_\odot}\right)^{0.2} \quad \text{km/s.} \qquad (7.3.5)$$

The limits I will consider in sections 7.5 are all for holes with speeds above this admittedly rather uncertain value. Disk accretion may also occur due to the inhomogeneity of the ISM; Lacey and Ostriker (1986) suggest that gradients similar to those present in the clouds I am considering will cause the formation of a disk.

We must check that the hole's radiation itself does not disrupt the accretion flow. If the hole radiates the infalling mass-energy with efficiency ϵ, its luminosity is

$$L = \epsilon \dot{M} c^2 \qquad (7.3.6)$$
$$= 8 \times 10^{21}\epsilon\left(\frac{M}{M_\odot}\right)^2\left(\frac{u}{100km/s}\right)^{-3}\left(\frac{n}{1\ \text{cm}^{-3}}\right) \quad \text{W}$$

We require that this be less than the Eddington luminosity,

$$L_{Edd} = 4\pi cGMm_p/\sigma_T \qquad (7.3.7)$$
$$= 1.3 \times 10^{31} \left(\frac{M}{M_\odot}\right) \quad \text{W},$$

at which the radiation would drive away the infalling matter. Since

$$L/L_{Edd} = 6 \times 10^{-10} \epsilon \left(\frac{M}{M_\odot}\right) \left(\frac{n}{1\ \text{cm}^{-3}}\right) \left(\frac{u}{100 km/s}\right)^{-3}, \qquad (7.3.8)$$

the radiation is sub-Eddington for the range of parameters that we will consider.

7.4 Model Accretion Spectra

7.4.1 Disk accretion

First, I have calculated disk accretion spectra adopting the standard accretion disk theory of Shakura and Sunyayev(1973) and Novikov and Thorne (1973). In these models, the flux generally emerges in the unobserved far ultraviolet and the limits obtainable from the small flux emitted at optical and X-ray frequencies are comparable with the limits obtained below using spherical accretion models.

Define a dimensionless radius parameter R in units of the radius

$$r_g = GM/c^2 \tag{7.4.1}$$

(recall the Schwarzschild radius is at $R = 2$, and the extreme Kerr horizon is at $R = 1$). The flux from the disk at the radius R is

$$\begin{aligned} F(R) &= \frac{3}{8\pi}\frac{\dot{M}c^2}{r_g^2}R^3 I(R) \\ &= 1.1 \times 10^{17} g\, R^{-3} I(R) \text{ W m}^{-2} \end{aligned} \tag{7.4.2}$$

where

$$I(R) = 1 - \sqrt{\frac{6}{R}} \tag{7.4.3}$$

The Rosseland opacities in the centre of the disk to free-free and electron scattering become equal at a radius given implicitly by

$$R_m = 0.3(Mg\, I(R))^{2/3}. \tag{7.4.4}$$

The ratio of the opacities outside this radius is

$$\frac{\kappa_{ff}}{\kappa_{es}} = 2.5 M^{-\frac{1}{2}} g^{-\frac{1}{2}} R^{3/4} I(R)^{-\frac{1}{2}}. \tag{7.4.5}$$

The density in the disk is

$$n_{28} = 1.6\alpha^{-\frac{7}{10}} M^{-3/20} g^{11/20} R^{-15/8} I(R)^{11/20} \tag{7.4.6a}$$

for $R > R_m$ and

$$n_{28} = 2.2\alpha^{-7/10} M^{-3/10} \bar{g}^{\,2/5} R^{-33/20} I(R)^{2/5} \qquad (7.4.6b)$$

for $R < R_m$, where $n_{28} = n/(10^{28} \quad \mathrm{m}^{-3})$ and α is a dimensionless viscosity parameter of order unity. To obtain the spectrum, an approximation at a general point in the disk is (Felten and Rees, 1972)

$$F(\nu) = \sqrt{\frac{\kappa_{ff}(\nu)}{\kappa_{ff}(\nu) + \kappa_{es}}} B(\nu) \qquad (7.4.7)$$

where $B(\nu)$ is the Planck spectrum at the surface temperature T_s at that point. The opacities must also be calculated for the surface temperatures rather than the central ones; the surface temperature is therefore determined implicitly by the requirement that the integral of (7.4.7) over frequency must equal the value of F as given by (7.4.2). If I adopt (7.4.6) as an adequate approximation for the density at the surface, then I can find T_s at each radius and hence the contribution to the spectrum from (7.4.7). The frequency-dependent opacity ratio is

$$\frac{\kappa_{es}}{\kappa_{ff}(\nu)} = 1.6 \times 10^{-3} n_{28}^{-1} T_6^{7/2} \frac{x^3}{1 - e^{-x}} = \lambda \frac{x^3}{1 - e^{-x}}. \qquad (7.4.8)$$

where $T_6 = T_s/10^6\mathrm{K}$, $x = h\nu/kT_s$, and λ is defined by this equation. I then find T_6 by solving

$$F(R) = 0.154\sigma T_s^4 \int_0^\infty \frac{x^3}{e^x - 1} (1 + \lambda \frac{x^3}{1 - e^{-x}})^{-\frac{1}{2}} dx \qquad (7.4.9)$$

Rewriting T_s in terms of λ and using (7.4.2), this becomes

$$0.008 n_{28}^{-8/7} \bar{g}\, R^{-3} I(R) = f_{MBB}(\lambda) \qquad (7.4.10)$$

I have evaluated the integral

$$f_{MBB}(\lambda) = \lambda^{8/7} \int_0^\infty \frac{x^3}{e^x - 1} (1 + \lambda \frac{x^3}{1 - e^{-x}})^{-\frac{1}{2}} dx \qquad (7.4.11)$$

by approximating piecewise by power laws $I = A\lambda^m$; λ and T_6 can then be found explicitly as follows:

$$\lambda = \begin{cases} 0.54f^{14/9} & f > 3.0 \\ 0.72f^{1.30} & 0.22 < f < 3.0 \\ 0.53f^{1.10} & 0.027 < f < 0.22 \\ 0.32f^{0.96} & 2.5 \times 10^{-3} < f < 0.027 \\ 0.19f^{7/8} & f < 2.5 \times 10^{-3} \end{cases} \tag{7.4.11}$$

and

$$T_6 = 6.3 n_{28}^{2/7} \lambda^{2/7}, \tag{7.4.12}$$

For small f_{MBB} this reduces to

$$T_2 = 1.6(\dot{g}\, R^{-3} I(R))^{1/4} \tag{7.4.13}$$

which is the standard blackbody temperature. For large f_{MBB} the modified blackbody temperature is

$$T_6 = 0.6 M^{-1/15} \dot{g}^{\,16/45} R^{-17/10} I(R)^{16/45} \tag{7.4.14}$$

The spectrum is given by

$$\nu F(\nu) = 2.4 \times 10^{23} M^2 T_6^4 \int_2^{R_{max}} R \frac{x^4}{e^x - 1} \left(1 + \lambda \frac{x^3 e^x}{e^x - 1}\right)^{-\frac{1}{2}} dR \quad \text{W} \tag{7.4.15}$$

where x depends on R via T_e.

7.4.2 Spherical accretion

For the black hole spherical accretion spectra, I adopt the models calculated by Ipser and Price (1982). They present a grid of model spectra calculated for masses $\log(M/M_\odot) = 1, 3$, and 5, and accretion parameters $\log \dot{g} = -4, -3, -2, -1, 0, 1, 2$. These spectra are rather flat and peak in the far infrared for low $\dot{g}$ and in the visible for high $\dot{g}$.

They assume that the gas contains at least some small interstellar magnetic field, so that flux freezing within the collapsing gas leads to magnetic energy

density exceeding thermal energy density well outside the horizon. In this inner region reconnection of the field lines must occur, resulting in dissipation of magnetic energy. Ipser and Price assume that this occurs in such a way as to ensure approximate equipartition between magnetic, thermal, and gravitational energy densities. This assumption, together with the assumption that the electron and proton temperatures in the gas are equal, enables the radial temperature distribution and the spectrum to be calculated. The main contribution to the spectrum is synchrotron radiation by thermal electrons. Free-free cooling is found to be unimportant. For low accretion rates ($M\dot{g} < 20$) they show that synchrotron cooling is small compared with the heating due to dissipation, and derive the temperature distribution

$$(T/10^{10}\mathrm{K}) = T_{10} = 90R^{-1} + 4.1R^{-2/3} \qquad (7.4.16)$$

For

$$20\dot{g}^{-1} < M < 10^3\dot{g}^{-\frac{27}{81}} \qquad (7.4.17)$$

synchrotron cooling is important but self-absorption is not. The temperature is given in this case by

$$T_{10} = 184(M\dot{g})^{-\frac{1}{2}}\tanh\left(0.16(M\dot{g})^{\frac{1}{2}}\left(R^{-1}+A\right)\right) \qquad (7.4.18)$$

where the normalization constant A is set by fitting to $T_{10} = 0.3$ at $R = 400$. (I have adopted the same parameter choices, in particular $\beta_d = \frac{1}{2}$, as Ipser and Price, to allow comparison with their numerical results.) Above the accretion rate given by the upper limit in inequality (7.4.17) both synchrotron selfabsorption and Comptonization become important. The details of the spectrum are uncertain because of the effects of Comptonization. Fig 7.2 shows the different regimes of the spectrum in the (M,$\dot{g}$) plane.

Adopting these analytic estimates of the temperature distribution, I then calculate the emergent synchrotron spectrum using the approximate prescription of Ipser and Price. My results are in good agreement with theirs for the models I

have compared. Their evaluation scheme for the spectrum involves angle-averaging over the emerging radiation, taking into account the shrinking of the light cone. Their solution involves the direction cosine

$$\mu = \sqrt{1 - 27\frac{z_g}{R^2}} \tag{7.4.19}$$

where $\mu < 0$ for $R < 3$. The spectrum is

$$F(\nu) = \int_2^{400} x I_p(x) j(R) L(R) dR \tag{7.4.20}$$

where the frequency parameter

$$x = \frac{\nu}{\nu_c}\frac{z_d}{z_g} \tag{7.4.21}$$

depends on the synchrotron frequency,

$$\nu_c = 1.1\bar{g}^{\frac{1}{2}} R^{-1/8} T_{10}^2(R) \quad \text{THz}, \tag{7.4.22}$$

and the gravitational and Doppler redshift factors,

$$z_g = 1 - 2/R \tag{7.4.23}$$

and

$$z_d = 1 - (\mu - 1)/(2R)^{\frac{1}{2}}. \tag{7.4.24}$$

The synchrotron function $I_p(x)$ is tabulated in Pacholzyk (1970) and the other two functions in the integral are

$$j(R) = (2.2 \times 10^{-7} \text{W Hz}^{-1} \text{ sr}^{-1} \text{ m}^{-3})\bar{g}^{3/2} R^{-11/4} \tag{7.4.25}$$

which normalizes the synchrotron luminosity, and

$$L(R) = 8\pi^2 r_g^3 (1 + \mu) R^2 z_g z_d^{-2} \tag{7.4.26}$$

which takes care of the volume factor.

In figs 7.3 to 7.5 I plot calculated disk and spherical accretion spectra for masses 3, 10, 100, and 1000 $M_\odot$, and $\bar{g}$ =0.02, 0.5, 60. The values of $\bar{g}$ correspond to velocities 300, 100, and 20 km/s in a cloud of density 30cm^{-3}.

Fig 7.2 Spherical Accretion Regimes

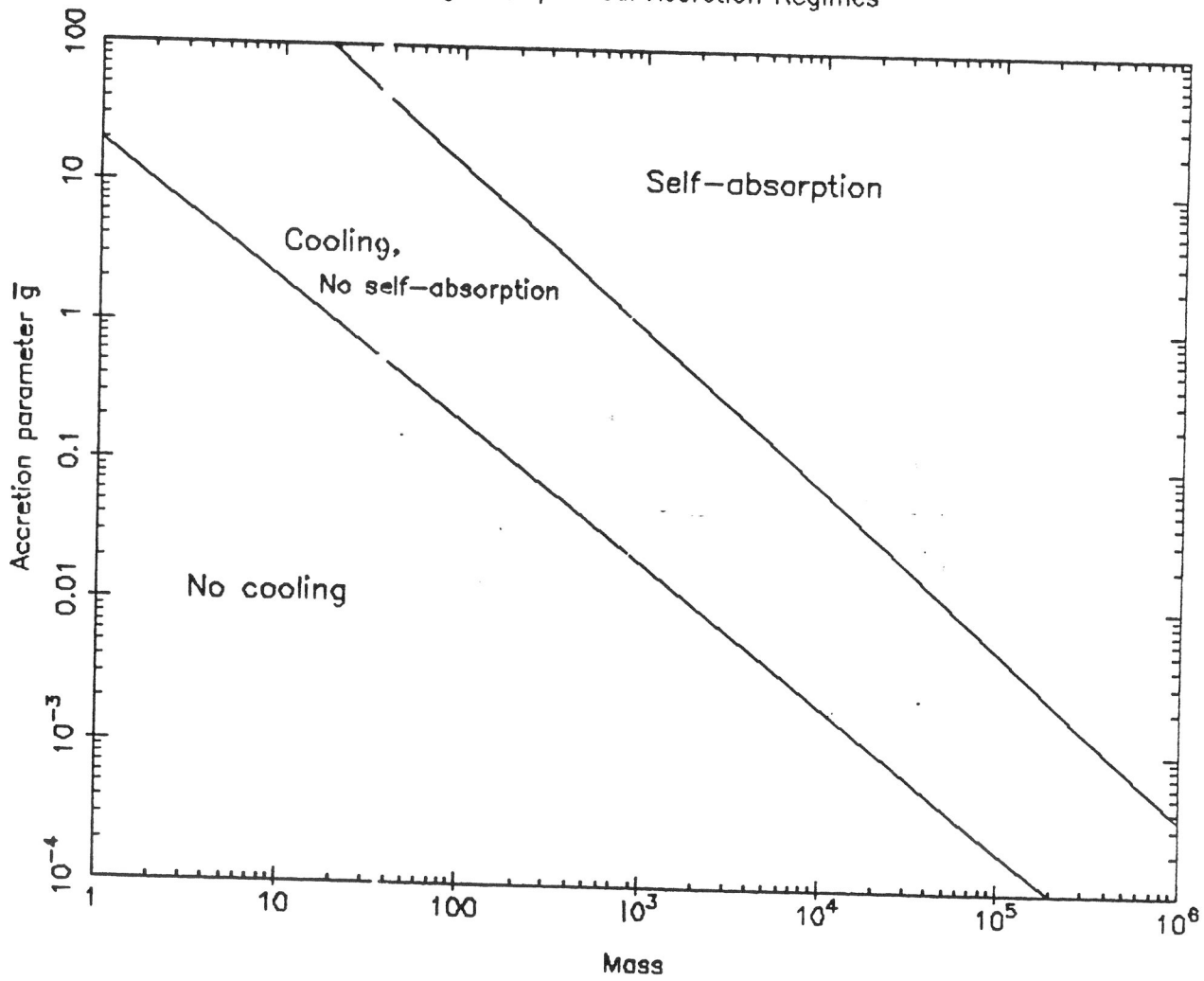

7.5 Limits on nearby black holes

7.5.1 The nearest black holes

To assess the detectability of the brightest accreting holes, I estimate their apparent brightness in the V band (0.55μ) and in IRAS band 4 (100μ). Brightnesses in the K (2.2μ) and IRAS 12μ bands have also been calculated but are not as useful. I perform the calculations for 5 masses: 3, 10, 10^2, 10^3 and $10^5 M_\odot$. Fig. 7.3 shows spectra adopted for different masses for the case of holes moving at 300 km/s in a cloud of density 30 cm^{-3}which is appropriate for typical halo holes traversing clouds in the disk. Fig. 7.4 shows the spectra for holes moving at 100 km/s, or β =0.5, corresponding to the disk dark matter holes. Finally, Fig 7.5 shows the spectra if v=20 km/s. Spherical accretion spectra are shown as solid lines, and disk accretion spectra are shown as dotted lines, are included for the high mass cases for comparison.

The apparent brightness that such sources would have is discussed below for the three scenarios mentioned above. To use these predictions to set constraints is more difficult. It should be noted that the IRAS catalogue should contain all objects down to 1 Jy, and Luyten's proper motion surveys will contain almost all nearby objects with proper motion above 0.2"/yr down to visual magnitude 17 over about half the sky and magnitude 14 over the whole sky (Luyten, 1981). Whether such objects would have already attracted attention if they were toward the faint end of such surveys is unclear. However, the detection of other faint unusual objects such as the double QSOs implies that it is not impossible that 14th magnitude objects with unusual properties would have been noticed, even if there are only a handful in the sky.

We need to estimate the distance of the nearest hole. If we assume that the holes are uniformly distributed with number density n, the probability that there

is no hole within a volume V is

$$\lim_{\delta V \to 0} (1 - n\delta V)^{\frac{V}{\delta V}} = e^{-nV} \tag{7.5.1}$$

and so the expectation value of the distance of the nearest hole is

$$\begin{aligned} \langle r \rangle &= \int_0^\infty 4\pi n r^3 e^{-\frac{4}{3}\pi n r^3} dr \\ &= \left(\frac{3}{4\pi n}\right)^{\frac{1}{3}} \Gamma(\frac{4}{3}) \\ &= 0.55 n^{-1/3} \end{aligned} \tag{7.5.2}$$

The distance within which there is a probability p that there is a hole is

$$r(p) = \left(\frac{3}{4\pi n}\right)^{\frac{1}{3}} \ln(\frac{1}{1-p}) \tag{7.5.3}$$

If we take the logarithmic term to be unity we see that there is a hole within the mean separation $r = 0.62 n^{-1/3}$ with probability 0.63. For predicted distances much larger than the cloud scale height (which I take to be 100 pc for definiteness) the disklike geometry of the galaxy must be taken into account. The distance r estimated from spherical geometry is corrected to $r' = (\sqrt{r/140})r$, corresponding to the same volume in a disklike geometry.

7.5.2 Black holes in the galactic halo.

Suppose the galactic dark halo is composed of black holes with $v_0 = 300$km/s, and mass density $10^{-2} M_\odot$ pc^{-3} locally (Bahcall and Soneira 1980). Then if the typical mass of such a hole is M solar masses, the nearest one will be at $r = 3M^{\frac{1}{3}}$ pc. The nearest hole with a speed of v or less will on average be $1.5(v_0/v)$ times further away. The best limits, presented in Table 7.1, come from the nearest hole in a cloud or a more distant but slow one also in a cloud. The radiation from closer holes in the intercloud medium is always much smaller. For each mass, Table 7.1 shows the distance r of the nearest hole travelling at or below

speed v , the V magnitudes predicted for the disk and spherical accretion models, the corresponding IRAS band 4 flux for the spherical accretion model, and an estimate of the typical proper motion calculated from the speed and distance. For the spherical accretion models, the V-K colours are mostly about +4, except for the $10^5 M_\odot$ case which has a predicted K magnitude of 3, clearly excluding this case. The 1000 $M_\odot$ holes with V=15 should have been picked up in the proper motion surveys, but 100 $M_\odot$ holes might just have escaped detection; if the rare slow ones at V=14 exist, they would be easy to miss. The disk accretion spectra set similar limits; in this case it is the most numerous, rapidly moving holes which set the best limit. Supermassive holes of mass of the order of a million solar masses may radiate X-rays; Lacey and Ostriker (1985) use this band and a similar model for the ISM to exclude such holes. We conclude that holes of mass above 100 $M_\odot$ cannot constitute the suggested halo dark matter, thus improving the constraint set by Ipser and Price (1977) and Lacey and Ostriker (1985).

7.5.3 Black Holes as the missing mass in the disk.

The analyses by Bahcall (1984) of the dynamical evidence that $0.1 M_\odot\ pc^{-3}$ of dark matter is required to make up the Oort limit have renewed interest in the local missing mass. The claim by Bahcall et al (1984) to exclude dark objects of mass above 2 $M_\odot$ depends upon the existence of very wide binaries in the galaxy. Since the evidence for these objects rests on a rather small number of candidates, it is still interesting to exclude massive dark objects by independent constraints. Following Bahcall, we assume a velocity dispersion of 100 km/s for the objects, and also assume that a small fraction of the objects are moving slowly , as predicted by a Maxwellian velocity distribution.

The results are presented in Table 7.2, in the same format as Table 7.1. Holes of mass of or greater than 100 $M_\odot$ are clearly excluded, and, provided the low velocity tail of the Maxwellian is populated down to velocities of order 20 km/s,

even 5 $M_\odot$ objects can be excluded if the spherical accretion calculations are adopted. The disk accretion spectra give slightly fainter V magnitudes but still constrain the mass to be about 10 $M_\odot$ or less. Even the low velocity 3 $M_\odot$ holes are not far outside the proper motion survey limits, and a large proper motion survey to fainter magnitudes could pick them up. (The fast-moving limit, V=20 and μ=2".4/yr, should not be taken seriously because of the lack of nearby clouds.)

It is interesting to note the limits set by the RC HI cloud alone; for 100 $M_\odot$ there should be 10 objects, just in the proper motion survey, at V=14, and one of V=11. For 10 $M_\odot$, the cloud should contain 100 objects ,all brighter than magnitude 20, with the brightest predicted to be magnitude 13; for 3 $M_\odot$ the predicted numbers are 3 times larger than this and the brightness 4 mag fainter.

I conclude that, if black holes make any significant contribution to the local missing mass, they must be of low mass ($< 5 - 10 M_\odot$) , and even then their existence might be subject to observational confirmation , particularly by faint proper-motion surveys targeted on nearby HI clouds.

Table 7.1

Halo Dark Matter Holes

M	v(km/s)	r (pc)	μ ("/yr)	V(disk)	V(sph.)	100μ
10^5	300	1000		4	10	400 Jy
1000	300	100	0.5	11	15	0.2 Jy
	100	1000		12	13	50 mJy
500	300	110		12	17	
	100	550		14	13	
200	100	330		15	14	
100	300	50		14	20	1 mJy
	20	2000		18	14	
50	300	50		15	23	
	100	160		16	16	
10	200	60	0.5	18	24	
	60	160		19	17	

Best limits on halo dark matter holes passing through clouds in the disk. The assumed velocity dispersion is 300 km/s; for some masses the results for smaller values of v are also presented, as holes in the slowly moving tail of the Maxwellian distribution accrete more matter and give a better limit in many cases.

V magnitudes are given for the disk and spherical accretion models, with 100 micron fluxes also given for some of the spherical accretion models, and estimated typical proper motion where this is large.

Table 7.2

Disk Dark Matter Holes

M	v(km/s)	r (pc)	μ ("/yr)	V(disk)	V(sph.)	100μ
10^5	100	300	0.1	1	5	10 Jy
1000	100	50	0.3	8	7	30 Jy
100	100	25	0.7	11	12	.4 Jy
	20	250	0.0	13	19	60 mJy
10	100	10	1.7	15	17	5 mJy
	20	100	0.0	17	12	3 mJy
	10	145		17	11	
8	100	14		15	18	
	20	67		17	12	
	10	130		18	12	
5	100	12		16	19	
	20	60		18	13	
	10	115		19	12	
3	100	7	2.4	16	20	
	20	60	0.1	18	15	

Best limits on nearby disk dark matter holes in clouds, as for Table 7.1. The assumed velocity dispersion is 100 km/s. The cases with r less than 50 are suspect since clouds are thought to be underabundant in the immediate solar neighbourhood.

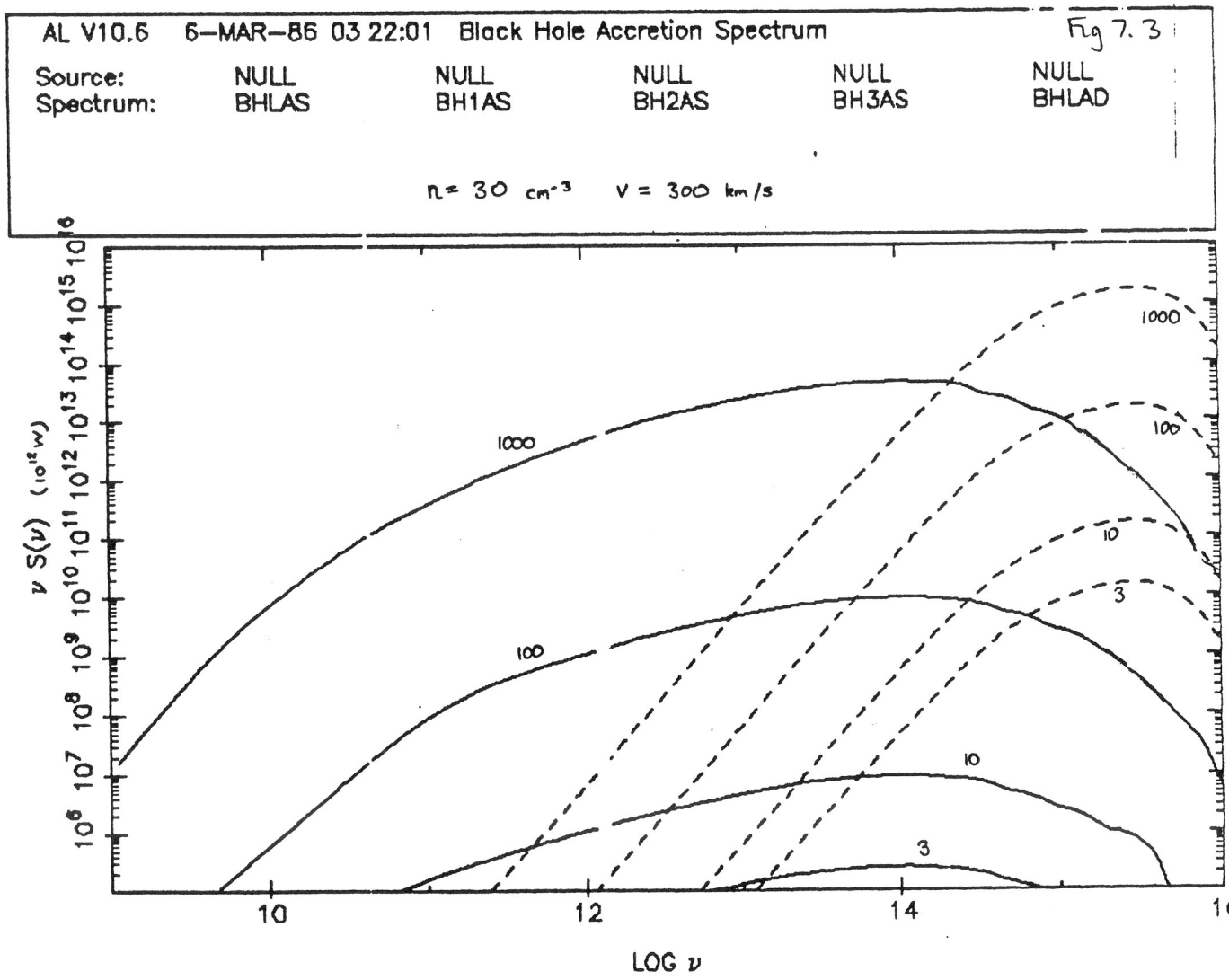
AL V10.6 6-MAR-86 03 22:01 Black Hole Accretion Spectrum
Fig 7.3
Source: NULL NULL NULL NULL NULL
Spectrum: BHLAS BH1AS BH2AS BH3AS BHLAD
n= 30 cm⁻³ V = 300 km/s
ν S(ν) (10¹² w)
10⁶ 10⁷ 10⁸ 10⁹ 10¹⁰ 10¹¹ 10¹² 10¹³ 10¹⁴ 10¹⁵ 10¹⁶
1000
100
10
3
LOG ν
10
12
14
16

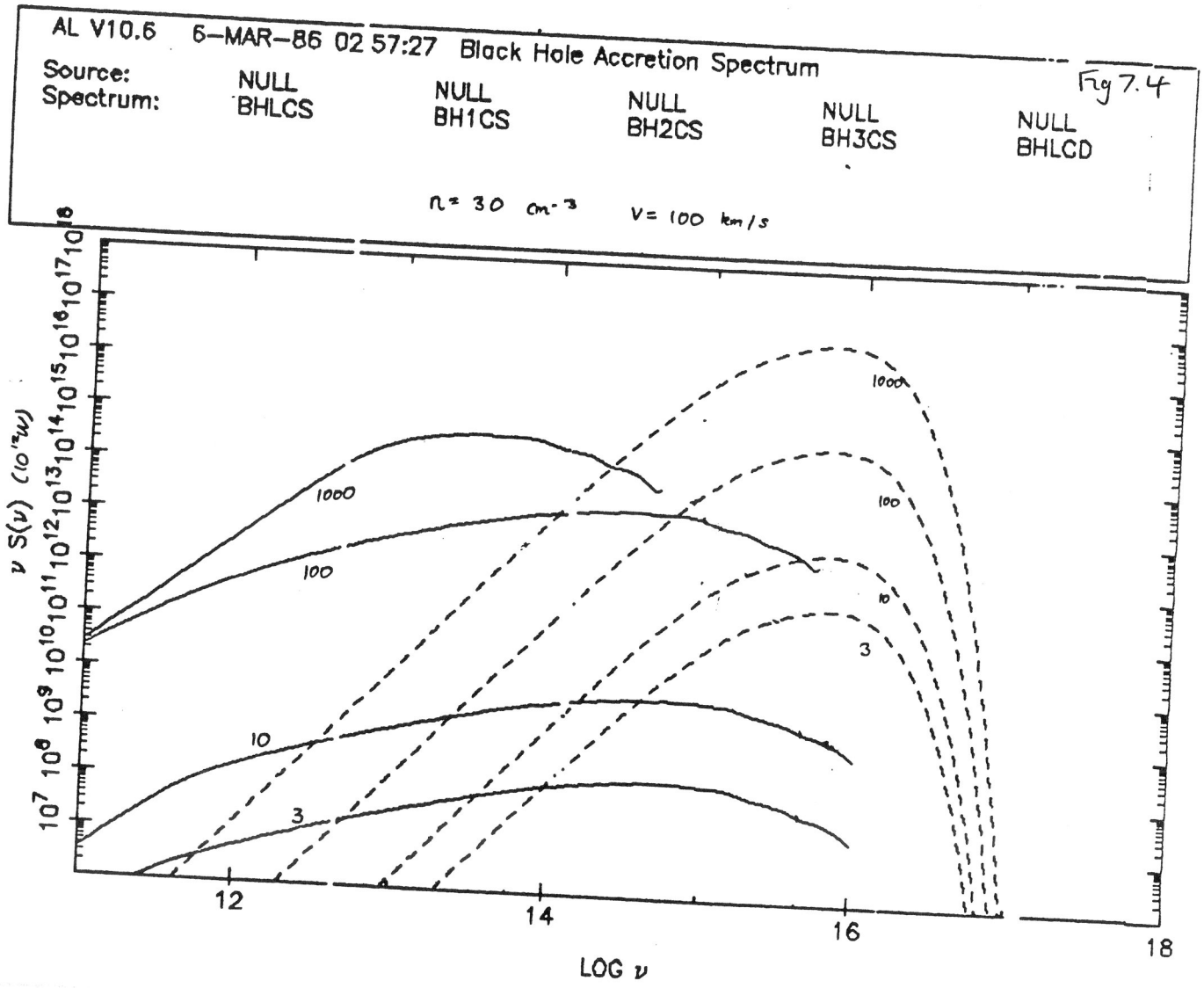
AL V10.6 6-MAR-86 02 57:27 Black Hole Accretion Spectrum
Source: NULL NULL NULL NULL NULL
Spectrum: BHLCS BH1CS BH2CS BH3CS BHLCD
n= 30 cm-3 V= 100 km/s
ν S(ν) (10^-23 W)
LOG ν
1000
100
10
3
12
14
16
18

Fig 7.4

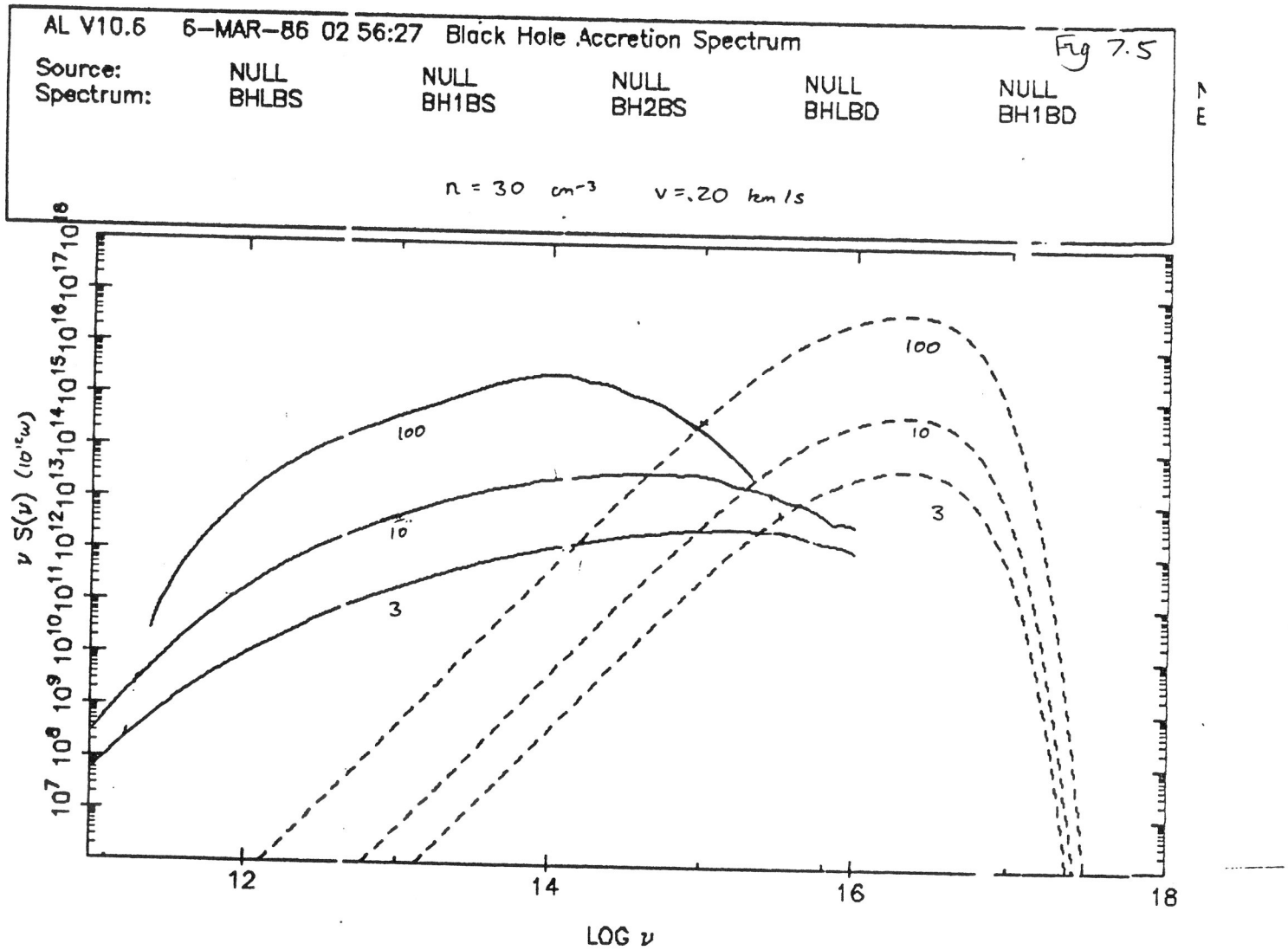
AL V10.6 6-MAR-86 02 56:27 Black Hole Accretion Spectrum
Source: NULL NULL NULL NULL NULL
Spectrum: BHLBS BH1BS BH2BS BHLBD BH1BD
n = 30 cm⁻³ v = 20 km/s
ν S(ν) (10^ν ω)
LOG ν
100
10
3
100
10
3
12
14
16
18

Fig 7.5

7.6. Black Hole Remnants of Massive Population I Stars

At the end of their evolution, many massive stars leave at least some of their mass in a compact imploded remnant. In many cases this remnant is a neutron star and may be detectable as a radio or X-ray pulsar. If the collapsing core is more massive than the maximum stable mass for a neutron star, the remnant will be a black hole. We can therefore expect that at least some ordinary massive stars in our part of the galaxy have left black hole remnants. An attempt to estimate the number density of such remnants in the solar neighbourhood is beset with two uncertainties: we do not yet know from stellar evolution theory either the mass range of progenitor stars that leads to black hole formation or the mass of the final remnants of such stars. Let us assume that all stars of initial mass M above some critical mass $M_{BH} \geq 10M_{\odot}$ end up as black holes of mass ϕM. For simplicity we will assume ϕ is independent of M; this reflects our lack of understanding of mass loss in massive stars. The number density of remnants of stars of mass M is

$$N(M) = n_*(M)\frac{t_0}{t_{ms}}\frac{h_1}{h_2} \tag{7.6.1}$$

where n_* is the number density of presently shining stars, h_1 and h_2 are the scale heights of the young stars and of the old remnant population respectively, and (t_0/t_{ms}) is the ratio of the age of the Galaxy to the lifetime of the stars. We also assume that the star formation rate is roughly constant over the life of the galaxy. We use the initial mass function for massive stars derived by Miller and Scalo (1979) for n_* which gives

$$N(M)dM = AM^{-\alpha}dM = 0.16M^{-3.3}dM \quad (\mathrm{pc}^{-3}) \tag{7.6.2}$$

for $M > 10M_{\odot}$.

I have calculated the V magnitudes for the Ipser and Price accretion models for a variety of parameters and obtained a crude analytic fit. I define a psuedo-flux $F(V) = 10^{-0.4V}$, in terms of which this fit is

$$F(V) = \begin{cases} 16(\phi M)^3 n^2 v^{-6} r^{-2} & (v > 4(\phi M n)^{\frac{1}{3}}) \\ 0.22(\phi M)^2 n v^{-3} r^{-2} & (v < 4(\phi M n)^{\frac{1}{3}}) \end{cases} \tag{7.6.3}$$

where n,v, and r are gas density in cm^{-3}, hole velocity in km/s and hole distance in pc respectively. The break is due to the saturation of ϵ discussed in section 7.3, which has been fitted by

$$\epsilon = \min\ (4.7 \times 10^{-5} M\dot{g}, 0.01) \tag{7.6.4}$$

I will describe holes with velocities below the break as 'bright accretors' and holes with velocities above the break, radiating with lower efficiency, as 'dim accretors'. Since I will be considering the motion of the holes through the dense clouds discussed in chapter 7, the motion will always be supersonic, so the further break in brightness in the transsonic regime will be ignored. (At even lower velocities, eq(7.3.5) would imply that disks form, but despite their totally different luminosities and spectra, the visual magnitudes calculated from the standard disk model are coincidentally within a magnitude of the spherical accretion models for the parameter range of interest; we therefore ignore the uncertain question of disk versus spherical accretion in this section.)

With this approximation, assuming a Maxwellian distribution with the velocity dispersion of σ =30 km/s expected for such a population and the interstellar cloud model used above, with n = 30$cm^{-3}$and filling factor f_C = 0.02, we can estimate the number density of objects above a given absolute magnitude by integrating the number moving slowly enough to be seen at a given mass over the mass distribution. We hence calculate the number of holes as a function of apparent visual magnitude in a given distance range, which we choose to be 50-150 pc to coincide with the range in which the clouds are known to exist (Knude 1979,1983).

We approximate the cumulative Maxwellian distribution by a power low, giving the fraction of the objects travelling at velocity less than v as

$$f(v) = \min(0.27(v/\sigma)^3, 1) \tag{7.6.5}$$

This approximation ignores the tail of the Maxwellian by assuming that all objects travel more slowly than $v = 1.5\sigma$. More precisely, holes travelling faster than this

are treated as if they had exactly this velocity. I will refer to holes travelling as rapidly as this as 'fast' holes. The number of objects with apparent magnitude greater than V is then

$$N(<V) = \int dr 4\pi r^2 f_C \int_{M_{BH}}^{\infty} N(M) f(v(F(V)))dM \qquad (7.6.6)$$

Evaluating the integral over mass and distance is complicated because of the different breaks in f(V). Suppose that we consider a hole to be 'visible' if it is brighter than some given apparent magnitude V. Then for given hole mass and distance there are several possibilities: For large enough masses, $M > M_F(r)$, all the holes are visible. For small enough masses, $M < M_D(r)$, only some of the 'bright' holes are visible. In some intermediate mass range all of the 'bright' holes and only some of the 'dim' holes are visible. This range may not exist since above a mass

$$M_B = 0.05\sigma^3/n\phi, \qquad (7.6.7)$$

all of the holes are 'bright' accretors (in our approximation that no hole travels faster than 1.5σ). Hence there is a distance

$$r_A = 0.07\sqrt{\frac{\phi M_B}{F(V)}} \qquad (7.6.8)$$

beyond which any hole of small enough mass and large enough velocity to be accreting dimly is too faint. If $r < r_A$,

$$M_F(r) = M_F^D(r) = (r/1.3F(V)^{-\frac{1}{2}}\phi^{3/2}n\sigma^{-3})^{2/3} \qquad (7.6.9)$$

and

$$M_D(r) = (r/0.07F(V)^{-\frac{1}{2}}\phi^{\frac{1}{2}})^2; \qquad (7.6.10)$$

while, if $r > r_A$,

$$M_F(r) = M_F^B(r) = (r/0.29F(V)^{-\frac{1}{2}}\phi n^{\frac{1}{2}}\sigma^{-3/2}) \qquad (7.6.11)$$

I rewrite f(V) as

$$f(V) = \begin{cases} 1 & M > M_F(r) \\ (M/M_F^D(r))^{3/2} & M_F(r) > M > M_D(r) \\ (M/M_F^B(r))^2 & M < M_D(r) \end{cases} \qquad (7.6.12)$$

Since we are integrating only for $M > M_{BH}$, some of the above mass ranges may not contribute to the integral at all values of r. Within a radius $r_B = (M_{BH}/M_B)^{\frac{1}{2}} r_A$, the term in the mass integral corresponding to the brightly accreting holes vanishes because $M_{BH} > M_D$. This radius is always less than r_A for the parameter ranges of interest. Within $r_C = (M_{BH}/M_B)^{3/2} r_A$, $M_{BH} > M_F$ and all the holes in the clouds are bright enough to be visible. The radii r_A, r_B, r_C lie within the integration range $r_{min} = 50$ pc to $r_{max} = 150$ pc for some apparent magnitudes in the range of interest, so the integral has to be split up into the different ranges. To summarize the complicated array of mass and radius scales that I have introduced, I have plotted the different regimes in Fig. 7.6. In regions 1, 2, and 3 some of the holes are dimly accreting, while in regions 4 and 5 all of them are bright. In regions 3 and 5 even the fastest holes are visible. In region 2 some of the dim holes are too faint to be seen, and in regions 1 and 4 some of the bright holes (and all of the dim ones) are too faint.

The integral can be expressed as

$$N(<V) = 4\pi f_C A M_{BH}^{1-\alpha} r_A^3 T(r_{min}, r_{max}, r_A, r_B, r_C) \qquad (7.6.13)$$

where T is a complicated function of its arguments. I have calculated the cumulative distribution $N(<V)$ and hence the differential distribution $N(V)$ for several sets of values of ϕ and M_{BH}.

Shapiro and Teukolsky (1983) take $M_{BH} = 10M_\odot$ and $\phi = 1$ and, using the Salpeter mass function get $n = 8 \times 10^{-4} pc^{-3}$. We take $\phi = 0.3$ to make a more reasonable minimum remnant mass of 3 $M_\odot$, or just above the neutron star maximum mass, and we adopt the Miller-Scalo IMF. We calculate that the brightest hole in this case would be 11th magnitude. The integral over mass

and distance is dominated by the contribution from slowly moving (20 km/s) low mass, distant objects. The distribution of holes as a function of apparent magnitude is shown in Fig. 7.7 as model 'A'. The total number of holes in this volume is predicted to be 2000, of which 100 will be in clouds. The apparent magnitude distribution peaks at 19th mag. For a more pessimistic model, we take $M_{BH} = 50M_{\odot}$, as suggested by empirical evidence presented by Schild and Maeder (1985), and $\phi = 0.1$. This model is labelled 'B' in Fig. 7.7. In this case the brightest object would be only magnitude 16. In fact, there are only predicted to be 2 objects in clouds in this distance range. Varying M_{BH} changes the number of progenitors and hence the expected number of holes, while varying ϕ changes the final remnant masses and hence the typical brightness of the holes. If M_{BH} is as high as $50M_{\odot}$, it may be more practical to search for holes in the intercloud medium, although the distribution for this model peaks at around 25th magnitude. Some results for other parameter choices are presented in Table 7.3.

In this simple model the results are much more sensitive to the mass loss parameter ϕ than to M_{BH}, and so an attempt to estimate the minimum allowed M_{BH} from this model would have little meaning, but it does seem that M_{BH} must be much larger than 10 $M_{\odot}$ to explain the fact that no accreting holes have been observed. Conversely, these calculations indicate that if M_{BH} is 50 $M_{\odot}$ or lower, it may eventually be possible to detect and observe unambiguously identifiable black holes. An isolated hole accreting from the ISM could be less ambiguous than the current binary star candidates, because the inner regions would be less obscured, and could provide a cleaner laboratory to study relativistic astrophysics.

The best hope for their detection is a study of high proper motion objects in the optical, combined with improved mapping of the local ISM to locate nearby regions of high density. We cannot yet constrain stellar evolution theory by the non-observation of black holes, but the results presented here suggest that such a constraint is possible, and that, if black holes are really a normal endpoint of

massive star evolution, it should eventually be possible to discover them.

Table 7.3

V		9	10	11	12	13	14	15	16	17	18	19	20
∅	M_{BH}												
1	10	1	1	2	4	9	15	18	18	17	10	0	0
.3	10	0	0	1	1	3	4	7	8	12	15	19	17
.3	20	0	0	0	1	2	2	3	3	4	3	1	0
.3	30	0	0	0	1	1	1	2	1	1	0	0	0
.3	50	.1	.1	.2	.4	.4	.5	.4	.1	0	0	0	0
.1	50	0	0	0	.1	.2	.2	.3	.3	.4	.5.	3	0

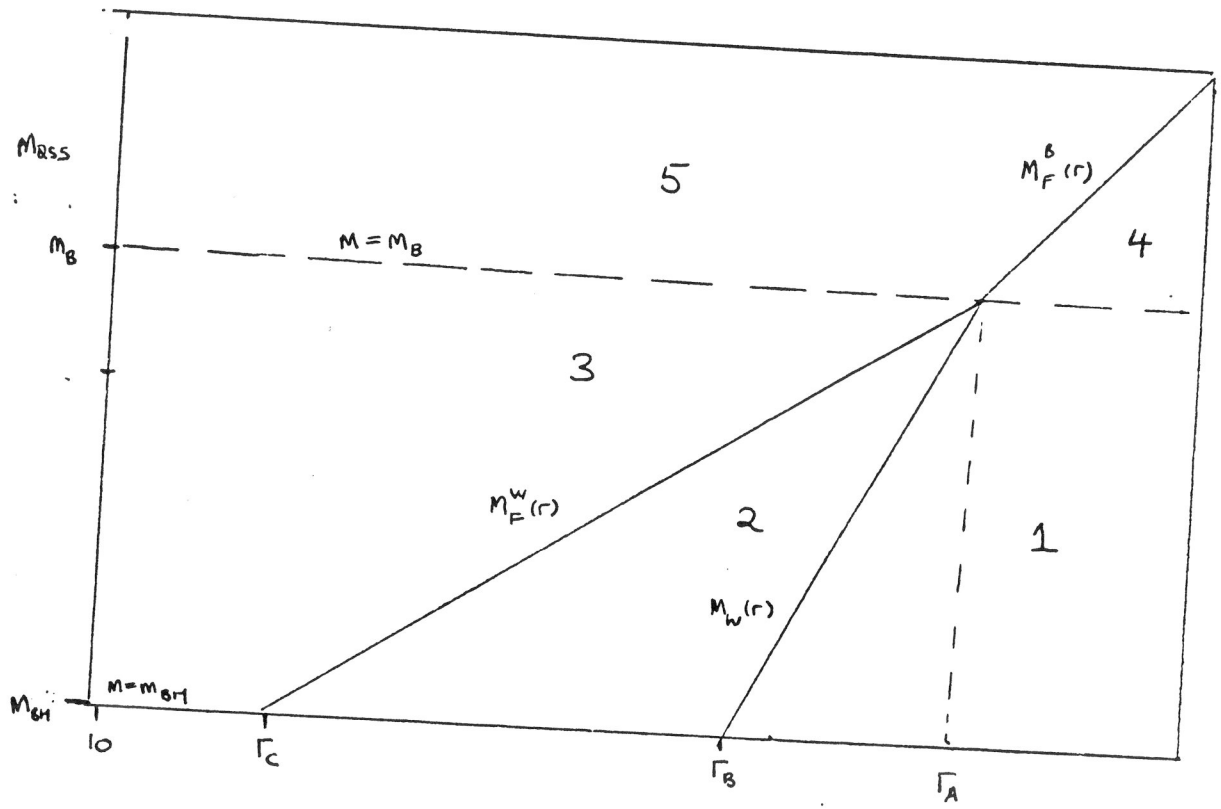

Fig 7.6 Mass regimes in equation (7.6.6.)

Fig 7.7 Apparent Magnitude Distribution of Nearby Holes

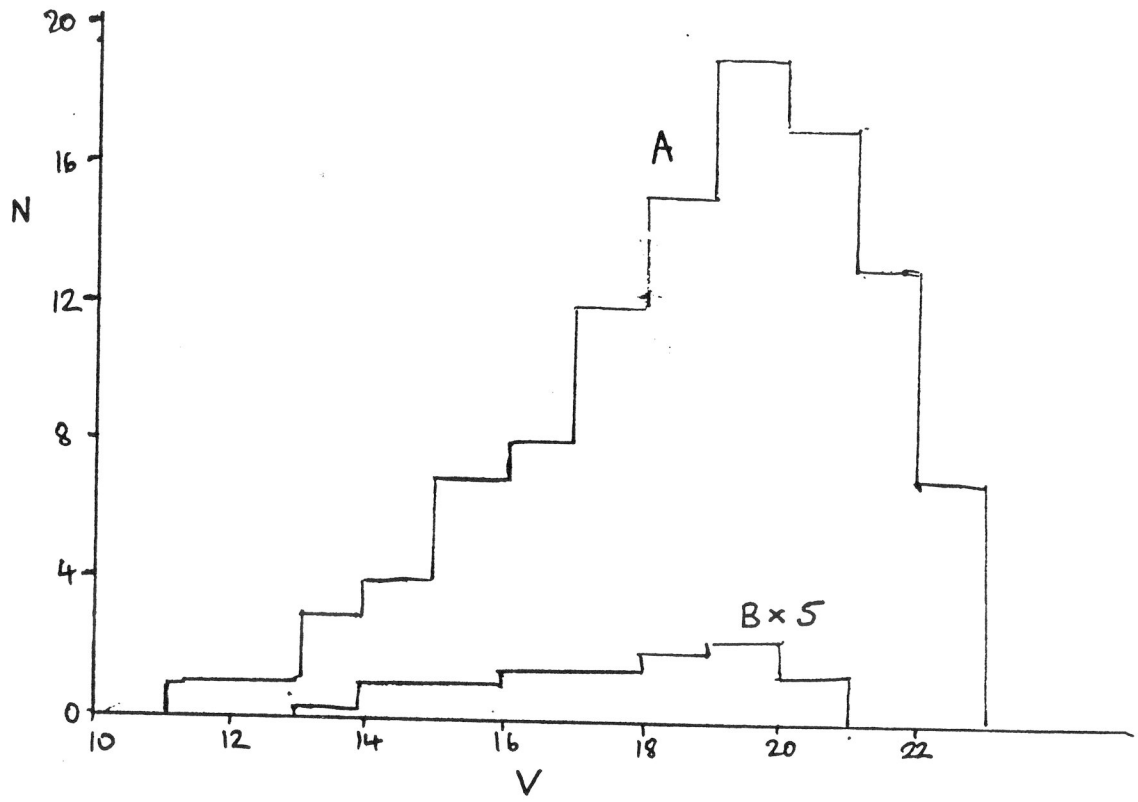

8. Conclusion

It is surely of great importance to astrophysicists to have some idea of the basic physical constituents of the universe. As I explained in Chapter 1, the bulk of present evidence suggests that much of the matter in the universe is dark and so far unidentified. In this thesis I have investigated one obvious astrophysical candidate, black hole stellar remnants. I have developed and constrained this scenario both by studying the radiation from the stellar precursors of such black holes and by studying the radiation that would be produced today by the holes themselves. The background light limits on redshifted starlight cannot rule out the scenario but constrain the redshift of the stars. The local accretion limits on individual sources are very strong but the uncertainties about the accretion models means that these bounds are not conclusive. Black holes remain a viable candidate for the halo dark matter provided that their precursors formed at redshifts of more than 4 and that they do not radiate efficiently when traversing clouds in the disk.

If there is a present day cosmological density of black hole stellar remnants, their most likely progenitors are Population III Very Massive Objects (VMOs). In Chapter 2 I reviewed previous results on VMO properties, discussed the probable stellar spectrum of VMOs, and extended work on their effects on their surroundings, calculating the expected spectrum from the gas surrounding the VMOs in the case where they fail to ionize the universe. About half of the energy in this spectrum is found to be in recombination line radiation. The stars will only fail to ionize the universe if they contain much less mass than the gas or if the gas density is larger than normal in regions of star formation. This work could be extended by more detailed treatment of dynamical effects in the HII region around the VMO, and by including the effects of helium in the recombination spectrum of the nebula.

In Chapter 3 I discussed the isotropic background spectrum produced by Population III VMOs. The extragalactic background may be our only source

of information on the universe in the pregalactic era between recombination at z=1500 and the era of active galaxies at redshifts of a few. I show that if VMOs make up a significant fraction of the mass of the universe, they will ionize the universe unless the gas in the universe is clumpy with overdensities of order $10^5/\Omega_*$ or more. In this latter case, the recombination spectrum calculated in chapter 2 will be a better approximation to the spectrum. It is possible that the universe is opaque at high redshifts because of dust either in an intergalactic medium or in galaxies (for redshifts at which the latter cover the sky). I have estimated the magnitude of this effect, and calculated the predicted background spectrum in the far infrared, using a cosmological radiative transfer code. The results show that current infrared limits are close to the expected signal from dust heating at high redshift. The code does not yet include the effects of hydrogen absorption in the universe and will be extended to include this in the future.

In Chapter 4 I compare my dust-free background radiation predictions with a near-infrared observation of a postulated extragalactic background signal. I conclude that redshifted Lyman α radiation from Population III stars with $\Omega_* = 0.4$ to 1 forming over an extended redshift range of z=10 to 40 can explain the observations.

The status of other observational limits on the extragalactic background light was reviewed in Chapter 5. I have compared my predicted spectra with limits from the IR to the UV and hence derived a set of constraints on the allowed density of VMOs as a function of formation redshift and intergalactic dust abundance. In a dust-free universe in which the gas is insufficiently clumped to prevent ionization, the VMOs can make up one-tenth of closure density only if they formed at a redshift of more than about 35. Observations are urgently needed of the extragalactic background light in the region 0.6-10 microns and 100-500 microns. These two wavelength ranges offer our best hope for a window onto the universe at high redshift.

Background light limits do not yet constrain the possibility that low mass stars make up the dark matter. The constraints on stars of around one solar mass are stronger, but limits in the range 2-50 $M_{\odot}$ are weaker than the limits on VMOs because of the lower efficiencies of such stars. Chapter 6 summarized these limits, which improve on previous such limits by using stellar atmosphere model spectra rather than simple blackbodies as the input to the background radiation code. At, present the dearth of evolutionary models and model atmospheres for very low mass stars makes it difficult to determine the mass below which the constraints become weak, but it is somewhat less than 1 $M_{\odot}$.

An alternative approach to constraining the cosmological density of black holes is to search locally for the nearest ones. Black holes become visible by accreting from the interstellar medium. By using recent models of spherical accretion onto black holes and a multi-component model for the ISM, I have shown that, if the black holes making up the halo dark matter are more massive than 100 $M_{\odot}$, then the brightest ones will have a visual apparent magnitude brighter than 14. Holes making up the local disk dark matter will have V=14 or brighter even if their mass is as low as 5-10 $M_{\odot}$. It is possible that such objects may have escaped detection, but objects a factor of 10 more massive are several magnitudes brighter and would surely have been noticed.

The same technique can be applied to black holes which are expected to be present as the remnants of Population I stars. In this case we believe we know the initial mass function of the progenitors, so I have performed a more detailed calculation to derive the expected apparent magnitude distribution of the holes in the visible. The results are dependent on the assumed progenitor mass but the brightest such black holes may have V between 11 and 17. Future work on the problem of local black holes will involve more study of the observations of the local interstellar medium and attempts to better define the best observational constraints.

References

Aaronson, M., and Olzewski, E., 1986. *IAU Symposium 117*, in press

Abramowicz, M., and Stegun, I.A., 1965. *Handbook of Mathematical Functions* (Dover, N.Y.)

Bahcall, J.N., 1984. *Astrophys. J.* **287**,926

Bahcall, J.N., Hut, P., and Tremaine, S., 1985. *Astrophys. J.* **290**,15

Bahcall, J.N., and Soneira, R.M., 1980. *Astrophys. J. Suppl.* **44**,73

Baker, J.G., Menzel, D.H., and Aller, L.H., 1938. *Astrophys. J.* **88**, 422.

Blitz, L., Fich, M., and Kulkarni, S., 1983. *Science*,**220**,1233

Bond, J.R., Arnett, W.D., and Carr, B.J., 1984. *Astrophys. J.* **280**,825

Bond, J.R., Carr, B.J., and Arnett, W.D., 1983. *Nature*,**304**,514.

Bond, J.R., Carr, B.J., and Hogan, C., 1985. Preprint.

Bond, J.R., and Szalay, A., 1983. *Astrophys. J.* **274**,443.

Bond, H.E., 1981. *Astrophys. J.* **248**,606.

Bondi, H., 1952. *Mon. Not. R. astr. Soc.* **112**,195

Bosma,A, 1978. Ph.D Thesis, Groningen. *The Distribution and Kinematics of Neutral Hydrogen in Spiral Galaxies of various Morphological Types*

Boughn, S.P., Saulson, P.R., and Seldner, M., 1981. *Astrophys. J.* **250**,L15.

Burstein, D., Rubin, V.C., Ford, W.K., and Thonnard, N. ,1982. *Astrophys. J.* **253**,70.

Cameron, A.G.W., and Truran, J., 1971.*Astrophys. Space Sci.***14**,179

Carbon, D., Gingerich, O.J., and Latham, D.W., 1969. in *Low Luminosity Stars* (ed: S. Kumar),p. 435.

Carnigan, C., and Freeman, K.C., 1985. *Astrophys. J.* **294**,494

Carr, B.J., 1977. *Astr. Astrophys.* **56**,377.

Carr, B.J., 1978. *Comments Ap.***7**,161

Carr,B.J., 1979 *Mon. Not. R. astr. Soc.* **189**,123.

Carr, B.J., 1980. *Nature***284**,326

Carr, B.J., 1981a. *Mon. Not. R. astr. Soc.* 194,639

Carr, B.J., 1981b. *Mon. Not. R. astr. Soc.* 195,669.

Carr, B.J., 1985. *Observational and Theoretical Aspects of Relativistic Astrophysics and Cosmology*, (eds. L. Sanz, L.J. Goicoechea), p. 1.

Carr,B.J., Bond, J.R., and Arnett, W.D.,1984. *Astrophys. J.* 277,445

Carr, B.J., and Glatzel, W., 1985. Preprint.

Carr, B.J., and Lacey, C.G., 1986. In preparation.

Carr,B.J., McDowell,J.C., and Sato,H., 1983. *Nature* ,306,666

Carr, B.J., and Rees, M.J., 1984a. *Mon. Not. R. astr. Soc.* 206, 315

Carr, B.J., and Rees, M.J., 1984b. *Mon. Not. R. astr. Soc.* 206, 801

Ceccarelli, C., et al, 1983. *Astrophys. J.* 275,L39.

Chamberlain, J.W., 1953. *Astrophys. J.* 117,387.

Chandrasekhar, S., 1931.*Astrophys. J.* 74,81

Couchman, H.M.P. , 1985. *Mon. Not. R. astr. Soc.* 214, 137

Cox, D.P., and Matthews,W.G. 1969*Astrophys. J.* 155,859

Crutcher, R.M. and Lien, D.J., 1984. in *Proc. IAU Colloqium 81* , NASA CP-2345, p.117

D'Antona, F., and Mazzitelli, I., 1985. *Astrophys. J.* 296,502.

Davis, M., Efstathiou, G., Frenk, C., and White, S.D.M., 1985. *Astrophys. J.* 292,371.

De Bernardis, P., Masi, S., Melchiorri, B, Melchiorri, F., and Moreno, G., 1984. *Astrophys. J.* 278,150.

Draine, B.T., and Lee, H.M., 1984. *Astrophys. J.* 285,89

Dube, R.R., Wicks, W.C., and Wilkinson, D.T., 1979. *Astrophys. J.* 232,333

Eardley, D.M., Lightman, A.P., Payne, D.G., and Shapiro, S.L., 1978. *Astrophys. J.* 224,53

Eichler, D., and Solinger, A., 1976. *Astrophys. J.* 203, 1

Einstein, A, 1916. *Annalen der Physik* 49, 769

El Eid, M.F., Fricke, K.J., and Ober, W.W., 1983 *Astr. Astrophys.* **119**,54

Ezer, D., and Cameron, A.G.W., 1971. *Astrophys. Spa. Sci.* **14**,399

Faber, S.M., and Gallagher, J.S., 1979. *A. Rev. Astr. Astrophys.* **17**,135.

Fabian, A.C., Arnaud, K.A., and Thomas, P.A., 1985. Preprint.

Fabian, A.C., Nulsen, P.E.J., and Canizares, C., 1982. *Mon. Not. R. astr. Soc.* **201**,933.

Fabian, A.C., and Guilbert, P., 1986, preprint.

Fall, S.M., 1979. *Rev. Mod. Phys.***51**,21.

Fabricant,D, and Gorenstein, P, 1983. *Astrophys. J.* **267**,535

Feldman, P.D., Brune, W.H., and Henry, R.C., 1981.*Astrophys. J.* **249**,L51

Felten, J., and Rees, M.J., 1972.*Astr. Astrophys.* **17**,226

Fitchett, M.J., 1984. Ph.D. thesis, University of Cambridge.

Forman, W., *et al.* , 1976. *Astrophys. J.* **208**,849.

Fowler, W.A., 1966. *Astrophys. J.* **144**,180.

Freeman, K.C., 1970. *Astrophys. J.* **160**,811

Frenk, C.S., and White, S.D.M., 1982. *Mon. Not. R. astr. Soc.* **198**,173.

Fricke, K.J., 1973. *Astrophys. J.* **183**,941

Fuller, G.M., Woolsley, S.E., and Weaver, T.A., 1985. Preprint.

Gilmore, G., and Hewett, P.C., 1983. *Nature*,**306**,669.

Glatzel, W., El Eid, M.F., and Fricke, K.J., 1986. *Astr. Astrophys.* , in press.

Grossmann, H.S., Hays, D., and Graboske, H.C., 1974. *Astr. Astrophys.* **30**,95.

Guenther, D.B., and Demarque, P. 1983. *Astr. Astrophys.* **118**,262.

Gush, H., 1981. *Phys. Rev. Lett.*, **47**,745.

Guth, A., 1981. *Phys. Rev. D*,**23**,347.

Hartquist, T.W., and Cameron, A.G.W., 1977. *Astrophys. Spa. Sci.* **48**,145

Hartwick, F.D.A., and Sargent, W.L.W, 1978, *Astrophys. J.* **221**,512

Hauser, M., et al., 1984. *Astrophys. J.* **278**,L15

Hawking, S.W., 1971. *Mon. Not. R. astr. Soc.* **152**,75

Hawkins, M.R.S., 1986. Preprint.

Hegyi, D.J., 1981. *Proc. Moriond Astrophys. Meeting* (Frontiers, Dreux), p. 321.

Hegyi, D.J., and Olive, K., 1983. *Phys. Lett.*126B,28.

Hegyi, D.J., Kolb, E.W., and Olive, K., 1986. *Astrophys. J.* 300,492.

Heisler, J., Tremaine, S., and Bahcall, J.N., 1985. *Astrophys. J.* 298,8.

Henry, R.C., Feldman, P.D., Fastie, W.G., Weinstein, A, 1978. *Astrophys. J.* 223,437

Hoffmann, W., and Lemke, D., 1978.*Astr. Astrophys.* 68,389

Hogan, C., 1983. *Mon. Not. R. astr. Soc.* 202,1101.

Howarth,I.,1983 *Mon. Not. R. astr. Soc.* 203, 301.

Hoyle,F., Solomon,P.M., and Woolf, N.J., 1973. *Astrophys. J.* (Letters),185,L89.

Husfeld,D., Kudritzi, R.P., Simon, K.P., and Clegg, R.E.S., 1984. *Astr. Astrophys.* 134,139.

Ikeuchi, S., 1981. *Publ. Astr. Soc. Japan*,33,211.

Ipser, J.R., and Price, R.H., 1977. *Astrophys. J.* 216, 578

Ipser,J.R., and Price,R.H., 1982. *Astrophys. J.* 255,654.

Jakobsen, P., Bowyer, S, Kimble, R., Jelinsky, P., Grewing, M., Kramer, G., and Wulf-Mathies, C., 1984. *Astr. Astrophys.* 139,481

Kaplan, S.A., and Pikel'ner, S.B., 1970. *The Interstellar Medium*, (Harvard University Press).

Katz, N., and Richstone, D.O., 1984. *Astr. J.* 89,975

Kent, S.M., and Gunn, J.E., 1982. *Astr. J.* 87,945.

Kerr, R.P., 1963.*Phys. Rev. Lett.*11,237

Knude, J, 1979. *Astr. Astrophys. Suppl.* 38,407

Knude, J., 1983. *Astr. Astrophys.* 126,89

Kurucz, R, 1979. *Astrophys. J. Suppl.* 50,1

Lacey, C.G. , 1984., in *Formation and Evolution of Galaxies and Large Structures in the Universe*, eds. J. Audouze and J. Tran Thanh Van (Reidel,

Dordrecht).

Lacey, C.G., and Ostriker, J.P., 1985. *Astrophys. J.* **299**,633.

Laplace, P.S., 1795. *Le Systeme du Monde, II*, Paris.

Laplace, P.S., 1799. *Allgemeine geographische Ephemeriden, 8vo Weiner, IV, Bd. 1 St. 1799*, (in Hawking, S.W., and Ellis, G.F.R., 1973, *The Large Scale Structure of Space-Time*, CUP.)

Larson, R., 1985. Preprint.

Layzer, D., and Hively, R.M., 1973. *Astrophys. J.* **179**,361.

Lin, D.N.C., and Faber, S.M., 1983. *Astrophys. J.* **266**,L21.

Linde, A.D., 1982. *Phys. Lett*, **108B**,39.

Luyten,W.J.,1981. Proper Motion Survey with the 48" Schmidt, LVII. (Minnesota)

Lynden-Bell,D., Cannon, R., Godwin, P.J., 1983. *Mon. Not. R. astr. Soc.* **204**,87P

Lynden-Bell, D., and Pineault, S., 1978. *Mon. Not. R. astr. Soc.* **185**,679.

Mather, J.C., 1982. *Optical Engineering*,**21(4)**,769

Matsumoto, T., Akiba, M., and Murakami, H., 1984. *Adv. Space Res.***3**,469.

Maucherat-Joubart ,M., Deharveng,J.M, and Cruvellier, P., 1980. *Astr. Astrophys.* **88**,323

McCarthy, D.W., Probst, R.G., and Low, F.J., 1985. *Astrophys. J.* **290**,L9.

McDowell, J.C.,1985,*Mon. Not. R. astr. Soc.* **217**,77

McDowell, J.C., and Godwin, P.J., 1986., *Observatory*, **106**, no. 1070, p.19.

Mengel *et al.* , 1978. *Astrophys. J. Suppl.* **40**,733

Meszaros, P., 1975.*Astr. Astrophys.* **44**,59.

Michell, J., 1784. *Phil. Trans. R. Soc. Lond.***74**,35

Miller, G.E., and Scalo, J.M., 1979. *Astrophys. J. Suppl.* **41**,513

Mould, J., 1976 *Astr. Astrophys.* **48**,443

Negroponte, J., 1986. Preprint.

Negroponte,J., Rowan-Robinson,M. and Silk, J. ,1981 *Astrophys. J.* **248**,58

Novikov, I.D., and Thorne, K.S., 1973.,in *Black Holes*,eds. De Witt, B., (Gordon and Breach, New York).

Olbers, H.W.M., 1826. *Bode Jahrbuch*,110.

Oort, J., 1960. *Bull. Ast. Inst. Neth*, **15**,45.

Oppenheimer, J.R., and Snyder, H 1939. *Phys. Rev.*,**56**,455

Osterbrock, D.E., 1974. *Astrophysics of Gaseous Nebulae.* (Freeman, San Fransisco.)

Ostriker, J.P., and Cowie, L.L., 1981. *Astrophys. J.* **243**,L127.

Ostriker, J.P., and Heisler, J., 1984. *Astrophys. J.* **278**,1.

Pacholczyk, A.G., 1970. *Radio Astrophysics* (San Francisco, Freeman). Paresce, F., 1984 *Astr. J.* **89**,1022

Paresce, F, Margon, B., Bowyer, S., and Lampton, M., 1979. *Astrophys. J.* **230**,304

Peebles, P.J.E., 1974. *Astrophys. J.* **189**,L51.

Peebles, P.J.E., 1984. *Astrophys. J.* **284**, 439

Peebles, P.J.E., and Partridge, R.B., 1967. *Astrophys. J.* **148**,377

Peterson, R.C., 1985. *Astrophys. J.* , **297**,309

Pitz, E., Leinert, C, Schulz, A., and Link, H., 1979. *Astr. Astrophys.* **72**,92

Probst, R.G., 1983. *Astrophys. J.* **274**,237.

Puget, J.L., and Heyvaerts,J., 1980. *Astr. Astrophys.* **83**,L10

Radford, G., 1976. Ph.D. thesis, University of Cambridge

Ramadurai, S., and Rees, M.J., 1985. *Mon. Not. R. astr. Soc.* **215**,53P.

Rees,M.J., 1978. *Nature*,**275**,35

Rees, M.J., 1985. ıProc. R. Soc. Lond. A, 400,183. Reid, I.N., and Gilmore, G., 1982. *Mon. Not. R. astr. Soc.* **201**,73.

Reid, I.N., and Gilmore,G., 1984. *Mon. Not. R. astr. Soc.* **206**,19

Roach, F.E., and Smith, L.L., 1968. *Geophys. J. R. A.S.*,**15**,1

Rood, H.J., 1981. *Rep. Prog. Phys.***44**,1077.

Rowan-Robinson, M., 1985a. Preprint.

Rowan-Robinson, M., 1985b. Preprint.

Rowan-Robinson, M, Negroponte, J, and Silk, J., 1979. *Nature*281, 635.

Rubin, V.C., Ford, W.K., and Thonnard,N. ,1980. *Astrophys. J.* 238,471.

Sandage, A. R., 1972. *Astrophys. J.* 178,1

Savage, B.D., and Mathis, J.S., 1979. *A. Rev. Astr. Astrophys.* 17,73

Schild, H., and Maeder, A., 1985. *Astr. Astrophys.* 143,L7.

Schmid-Burgk, J. 1978. *Astrophys. Spa. Sci.* 56,191.

Schmidt, M., 1963. *Astrophys. J.* 137,758

Schwarzchild, K., 1916. *Sitzungsber. Dtsch. Akad. Wiss. Berlin, Kl. Math. Phys. Tech.*, 189.

Schwarzchild, M., and Spitzer, L., 1953. *Observatory*,73,77

Severniy,A., and Zverezda,A., 1983. *Ap.Lett.*23,71.

Shakura, N., and Sunyaev, R.A, 1973. *Astr. Astrophys.* 24,337

Shapiro,S. L., and Teukolsky,S.A. , 1983.*Black Holes, White Dwarfs and Neutron Stars*,(New York, Wiley)

Silk, J., 1983. *Mon. Not. R. astr. Soc.* 205,705

Silk, J., and Stebbins, A., 1983. *Astrophys. J.* 269,1.

Sparke, L.S., 1986. *Mon. Not. R. astr. Soc.* , in press

Spinrad, H., and Stone, R.P.S., 1978. *Astrophys. J.* 226,609

Spitzer, L., 1978. *Physical Processes in the Interstellar Medium*, (New York, Wiley).

Stecker, F.W., 1985. Preprint.

Talbot, R.J., and Arnett, W.D., 1971. *Nature*229,250.

Tarbet, P., and Rowan-Robinson, M., 1982. *Nature*298,19.

Thorstensen,J.R. and Partridge, R.B., 1975. *Astrophys. J.* 200,527.

Tohline, J. ,1980. *Astrophys. J.* 239,417

Toller,G., 1983. *Astrophys. J.* 266,L79

Toor, A., 1977. *Astrophys. J.* **215**,L57.

Tornambe, A., and Chieffi, A., 1985. ESO preprint.

Turner, E., 1986. *IAU Symposium 117* , in press

Tyson,J., *et al.* , 1986. *IAU Symposium 117* , in press

Valtonen, M.J., Innanen, K.A., Huang, T.Y., and Saarinen, S., 1985, *Astr. Astrophys.* **143**, 182

VandenBerg,D, 1981. *Astrophys. J. Suppl.* **51**,29

Vandenberg, D., Hartwick, F.D.A., Dawson, P., and Alexander, D.R., 1983. *Astrophys. J.* **266**,747.

Wagner, R, 1974. *Astrophys. J.* **191**,173.

Weller, C.S., 1983. *Astrophys. J.* **268**,899

Wesemael,F. ,Auer,L.H., Van Horn,H.M., Savedoff, M.P. 1980. *Astrophys. J. Suppl.* **43**,159

Wheeler, J.A., 1968. *American Scientist***56**,1

White,S.D.M. and Rees, M.J., 1978. *Mon. Not. R. astr. Soc.* **183**,341

Woody, D.P., and Richards, 1981. *Astrophys. J.* **248**,18.

Wright, E.L., 1981. *Astrophys. J.* **250**,1.

Yahil, A., Walker, D., and Rowan-Robinson, M., 1985, preprint.

Yang, J., Turner, M.S., Steigman, G., Schramm, D.N., and Olive, K.A., 1984. *Astrophys. J.* **281**,493

York, D.G., and Frisch, P.C., 1984, in *Proc. IAU Coll. 81,* NASA CP-2345, p.51.

Zwicky, F., 1933. Helvetica Phys. Acta **6**,110.